Scanning Photoelectrochemical Microscopy and Its Application to Living Cells

Nikita Maria Thomas

A thesis submitted to the Faculty of Graduate Studies of

The University of Manitoba

in partial fulfilment of the requirements of the degree of

Doctor of Philosophy

Department of Chemistry

University of Manitoba

Winnipeg, Manitoba, Canada

© Nikita Maria Thomas, 2025, All rights reserved

Abstract

Living cell electrochemistry enables the non-invasive qualitative and quantitative measurement of metabolite and biomarker flux from individual or groups of cells. Scanning electrochemical microscopy (SECM) is an electroanalytical technique that allows for real-time detection of species flux from living cells. This thesis emphasizes the importance of maintaining optimal physiological conditions during SECM and explores the advancement of SECM to scanning photoelectrochemical microscopy (SPECM) for studying living cells. The first part of this thesis investigates the effects of experimental parameters such as temperature, media composition, and light on cellular electrochemical signals. It is shown that maintaining ideal physiological conditions is crucial for reliable SECM and SPECM data. Studies on Adenocarcinoma cervical cancer (HeLa) cells across different temperature ranges reveal inconsistent cellular electrochemical reactivity with small deviations from physiological temperature. However, HeLa cells demonstrate enhanced and stable electrochemical signals when cultured in serum-free media under constant light exposure.

To advance SECM to SPECM, the integration of optical fiber (OF) probes is explored to enhance both electrochemical and spectroscopic capabilities. A new, easy-to-fabricate micro-optical ring electrode (MORE) is introduced, with its functionality assessed through electrochemical analysis, numerical modeling, scanning electron microscopy (SEM), and spectroelectrochemistry. The MORE, integrated into SPECM, is used for localized irradiation and as an electrochemical sensor for quantitative analysis of single algal cells. This proof-of-concept demonstrates the potential of applying SPECM to mammalian cells. SPECM is further applied to skin cells for the detection of reactive oxygen species (ROS) and melanin production, which are elevated in response to external stimuli. Overall, a comprehensive exploration of the application of SPECM to mammalian cell studies is investigated with suggestions for future research, highlighting its potential in diverse applications.

Acknowledgements

The completion of this thesis work has stretched my limits and showed me that I'm capable of much more than I'm aware of. Thank you, God, for your grace has brought me this far. *"I can do all things through Christ who strengthens me." Philippians 4:13*. My sincere appreciation goes to the following people who have been my cheerleaders throughout this journey.

My deepest gratitude goes to my supervisor, Dr. Sabine Kuss, for being so welcoming and teaching me electrochemistry. Over the years, you have encouraged me to be an independent researcher and to think about solutions to problems wisely. I'm grateful for the opportunities you gave me in mentoring students, communicating science, and learning valuable life lessons. Thank you for being so understanding in my personal life. I would also like to extend my sincere thanks to my committee, Dr. Gregg Tomy, Dr. Sean McKenna, Dr. Aleeza Gerstein, and Dr. Zhifeng Ding (former), your insightful comments, suggestions, and discussions have allowed me to grasp knowledge and wisdom from different perspectives.

I'm extremely grateful for the scholarships, UMGF and NSERC PGSD, which kept me financially sound during my PhD study. Special thanks to all the members of the Department of Chemistry, the Faculty of Science, and the Faculty of Graduate Studies at the University of Manitoba who have been instrumental in helping me to prepare the application and achieve this success. I'm also thankful for the several departmental and faculty of science awards.

Dr. Vikram Singh and Dr. Dhésmon Lima, thanks for being such wonderful postdocs. Thanks for the discussions and encouragement during challenging experiments. Thanks for being all ears during my rants. Your friendship and humor made the lab environment so enjoyable. I'm thankful for the time you took to train me in electrochemistry and in writing manuscripts. Dr. Ana Carolina Mendes Hacke, though we have not worked together, thank you for being so entertaining and joyous during our lunch and coffee breaks.

Dr. Frank Wang and Dr. Dao Trinh, thanks for being my most valuable collaborators. I have learnt a great amount of electrochemistry from you. I'm thankful for your time and patience. Many thanks

to Dr. John Sorenson, Dr. Evan Booy, and Dr. Ravinder Sidhu for being so generous with your time and the laboratory equipment.

A big thanks to the present and past graduate and undergraduate students of both (Dr. Sabine Kuss and Dr. Christian Kuss) the Kuss labs. I loved the time we spent together as a group. I'm grateful for the memorable conversations we have had not just about science but also about life experiences. I'm thankful for the things I have learnt from each one of you and wish you all the best in your professional and personal lives.

To my amazing parents, T. M. Thomas. and Geena Thomas, my brother, Neville Thomas, my brother and sister-in-law, Nithin Thomas and Kimsuka Ramesh, and my sister-in-law and brother-in-law, Neethu Varghese and Rohit Kaushal, your prayers, actions, and words of support have been my pillars of strength. My lovely parents-in-law, K.P.Varghese. and Ancy Varghese, I appreciate your unwavering prayers and love.

To my forever love, my husband, Nithin Varghese, I'm deeply indebted to you for your love, encouragement, and support throughout my PhD. This would not have been possible without you. Thank you for believing in me. Thanks for the wonderful meals you made and are still making, it is as heartwarming as you. I'm thankful for our lovely son, Ethan, for being my happiness, motivating me every day to achieve my dream.

My long-time friends, Anne Rosalind Samuel, Alka Singh, Jithu Alin Varghese, Jeslyn Stephen, Angel Abraham, and Laavanya G. R., though miles apart, thank you for the fun filled phone calls which bought me to reality. Thank you to my friends in Winnipeg for planning trips and parties which kept me lighthearted.

Lastly, my sincere thanks to everyone who has been a helping hand throughout these years.

Dedicated to my dearest parents

Thank you for your love and sacrifices.

Table of contents

List of Figures

List of tables

List of Abbreviations and Acronyms

$^{\bullet}OH$	Hydroxyl radical
2D	Two Dimensional
3D	Three Dimensional
A431	Human epidermal carcinoma
A498	Human kidney epithelial cell
AC	Alternating Current
AFM	Atomic Force Microscopy
Ag	Silver
AgCl	Silver chloride
$AgNO_3$	Silver nitrate
APTES	(3-Aminopropyl) triethoxysilane
Au	Gold
BCC	Basal Cell Carcinoma
BHF	Buffered Hydrogen Fluoride
$BiVO_4$	Bismuth vanadate
Br_2	Bromine
C	Carbon
CA	Chronoamperometry
$CaCl_2$	Calcium chloride
carboxy-H_2DCFDA	5-(and-6)-carboxy-2′,7′-dichlorodihydrofluorescein diacetate
Cd	Cadmium
CE	Counter electrode
CHO	Chinese Hamster Ovary
CO_2	Carbon dioxide
Co_3O_4	Cobalt(II,III) oxide
COS-7	African green monkey kidney fibroblast-like cell line
CP	Conducting polymer
CPCC 127	Eremosphaera viridis

Cu	Copper
CV	Cyclic Voltammetry
CVD	Chemical Vapor Deposition
DC	Direct Current
DMEM	Dulbecco's Modified Eagle Medium
$DMEM^{FBS}$	Dulbecco's Modified Eagle Medium + 10% Fetal Bovine Serum
DNA	Deoxyribonucleic acid
EAB	Electroactive biofilm
ECL	Electrochemiluminescence
ECM	Extracellular matrix
EDC	1-(3-Dimethyl-aminopropyl)-3-ethylcarbodiimide hydrochloride
EDL	Electrical Double Layer
EGFR	Epidermal Growth Factor Receptor
ELISA	Enzyme Linked Immunosorbent Assay
EMCCD	Electron Multiplying Charge-Coupled Device
EMEM	Eagle's Minnimum Essential Medium
F	Fluorine
FBS	Fetal Bovine Serum
$FcCH_2OH$	Ferrocenemethanol
Fe	Iron
$Fe(NO_3)_3$	Iron(III)nitrate or ferric nitrate
Fe_2O_3	Iron(III) oxide or ferric oxide
FEM	Finite Element Model
FeS	Iron sulfide
FTO	Fluorine doped tin oxide
GC	Gas Chromatography
GeO_2	Germanium (IV)oxide or Germanium dioxide
GFP	Green Fluorescence Protein
GIPC-1	Tumor growth promoting protein
Gox	Glucose Oxidase
GSH	Glutathione (reduced)

GSSG	Glutathione disulfide (oxidized)
H_2	Hydrogen
H_2O	Water
H_2O_2	Hydrogen Peroxide
H_2SO_4	Sulfuric acid
HCHO.	Formaldehyde
HCV	Hepatitis C Virus
HCV-E2	Hepatitis C virus host receptor binding protein
HEKa	Human Epidermal Keratinocyte Cell
HeLa	Adenocarcinoma Cervical Cancer Cell
HEMa	Human Epidermal Melanocyte Cell
HF	Hydrogen Fluoride
IFEs	Fluorescence-based imaging fiber electrodes
IHP	Inner Helmholtz Plane
In_2O_3/SnO_2	Indium oxide/ Tin oxide
IPD	Immediate Pigment Darkening
ITO	Indium Tin Oxide
$K_3[Fe(CN)_6]$	Potassium ferricyanide
KBr	Potassium bromide
KCl	Potassium chloride
KH_2PO_4	Potassium dihydrogen phosphate
L012	Luminol
LED	Light Emitting Diode
LSV	Linear Sweep Voltammetry
ME	Microelectrode
$MgSO_4$	Magnesium sulfate
MMF	Multimode Fiber
Mo	Molybdenum
MORE	Micro-Optical-Ring Electrode
MoS_2	Molybdenum disulfide
MPS	3-(mercaptopropyl)-trimethoxysilane

MRP1	Multidrug Resistance Associated protein
MS	Mass Spectrometry
NA	Numerical Aperture
Na_2HPO_4	Disodium Hydrogen Phosphate or sodium phosphate dibasic
Na_2SO_3	Sodium sulfite
$Na_3Au(SO_3)_2$	Sodium gold (I) sulfite
NaCl	Sodium chloride
NaOH	Sodium hydroxide
Ne	Neon
NH_4F	Ammonium Fluoride
Ni	Nickel
NiFe	Nickel-Iron alloy
Ni-P	Nickel phosphorus
NP	Nanoparticle
NSOM	Nearfield Scanning Optical Microscopy
O_2	Oxygen
$O_2^{\bullet}$	Superoxide radical
OER	Oxygen Evolution Reaction
OF	Optical Fiber
OFCS	Optical Fiber Corrosion Sensor
OHP	Outer Helmholtz Plane
OM	Optical Microscopy
Os	Osmium
PAAH	Polyacrylic acid
PAH	Polycyclic aromatic hydrocarbon
PANI	Polyaniline
PBS	Phosphate Buffered Saline
PC	Polycarbonate
PC12	Rat adrenal medulla tumor cell
PCBS	poly{1-[4-((3-carboxy-4-hydroxyphenyl) azo)-benzenesulfonamido]-1,2-ethanediyl, sodium salt}

PCS	Polymer clad silica
Pd	Palladium
PDE	Partial Differential Equations
PEC	Photoelectrochemical
PEDOT	Poly(3,4-ethylenedioxythiophene)
PEM	Photoelectrochemical Microscopy
PLL	Poly L-Lysine
PMT	Photomutiplier Tube
PPD	Persistent Pigment Darkening
PPy	Polypyrrole
PS-1	Photosystem-1
PS-2	Photosystem-2
Pt	Platinum
QA	Plastoquinone
RBITC	Rhodamine B isothiocyanate
RC	Redox competition
RE	Reference Electrode
RFMRE	Radial flow micro-ring electrode
RG	Dimensionless Radius of Glass
RNA	Ribonucleic Acid
ROS	Reactive Oxygen Species
Ru(bpy)	tris (2,2'-bipyridyl) ruthenium (II)
RuHex	Hexaaminеruthenium (III) chloride
SCC	Squamous Cell Carcinoma
Se	Selenium
SEAP	Secreted embryonic alkaline phosphatase protein
SECCM	Scanning Electrochemical Cell Microscopy
SECM	Scanning Electrochemical Microscopy
SEM	Scanning Electron Microscopy
SERS	Surface Enhanced Raman Spectroscopy
SG/TC	Substrate Generation/ Tip Collection

SGECM	Scanning Gel Electrochemical Microscopy
Si	Silicon
SICM	Scanning Ion Conductance Microscopy
SiO_2	Silicon dioxide
SK-MEL-28	Melanoma cell
SMF	Single Mode Fiber
Sn	Tin
SPECM	Scanning Photoelectrochemical Microscopy
SPM	Scanning Probe Microscopy
SPR	Surface Plasmon Resonance
SSE	Stainless Steel Electrode
STA	Standing Approach
STM	Scanning Tunneling Microscopy
T24	Human Bladder Epithelial Cell
TFBG	Tilted Fiber Bragg Grating
TG/SC	Tip Generation/ Substrate Collection
Nb:TiO_2	Niobium-Doped Titanium Dioxide
Ti	Titanium
TiO_2	Titanium Dioxide
TLR4	Toll-like receptors
TMPD	N,N,N′,N′-tetramethyl-para-phenylene-diamine
UME	Ultramicroelectrode
UV	Ultraviolet
V_b	Valence band
VFT	Vogel-Fulcher-Tammann
VSM	Voltage Switching Mode
W	Tungsten
WE	Working electrode
WNV	West Nile Virus
Xe	Xenon
Xe-Hg	Xenon-Mercury

XPS	X-ray Photoelectron Spectroscopy

List of Symbols

Symbol	Description	Units
A	Electrode Surface	m^2
C	Concentration	mol cm^{-3} or mol/l
C_i	Concentration of species i	mol/l or M
$\partial\phi(x)/\partial x$	Potential gradient	V/m
$\partial C_i(x)/\partial x$	Concentration gradient of species i	mol cm^{-4}
$\partial C_o(x)/\partial x$	Concentration gradient of species o	mol cm^{-4}
D_i	Diffusion coefficient of species i	cm^2/s or m^2/s
D_o	Diffusion coefficient of species o	m^2/s
D_T	Temperature dependent Diffusion coefficient	m^2/s
E_f	Final electrode potential	V
E_i	Initial electrode potential	V
E_{pa}	Anodic electrode potential	V
E_{pc}	Cathodic electrode potential	V
F	Faraday Constant (96485)	C/mol
i_p	Peak current	A
I_{pa}	Anodic peak current	A
I_{pc}	Cathodic peak current	A
i_{ss}	Steady state current	A
$J_i(x)$	Flux of species i at distance x from the surface	mol/(m^2s)
$J_o(x,t)$	Flux of species o at distance x and time t	mol/(m^2s)
k_0	Apparent heterogeneous rate constant	m/s
k_B	Boltzmann constant ($1.380\ 649 \times 10^{-23}$)	J/K
n	Number of electrons	
η	Dynamic viscosity	N.s/m^2 or Pa s
Ps	Shear Peclet number	
R	Universal Gas Constant (8.314472)	J/Kmol
r	Radius of Active Material	m or cm

T	Temperature	K or °C
T	Time	s
μ	Electrical Mobility	m^2/ V s
$v_{(x)}$	Scan Velocity of Electrode	m/s
z_i	Charge of species i	C

Author Contributions

The work presented here is the result of collaborative research involving multiple authors. The following section outlines each publication and highlights the contributions made by each collaborator.

Chapter 2: Optical fibers in analytical electrochemistry: Recent developments in probe design and applications

Published in 2021 in the journal of Trends in Analytical Chemistry, Volume 136, https://doi.org/10.1016/j.trac.2021.116196

As the first author of this manuscript, NT was responsible for gathering all literature for this review article. NT and VS both contributed to writing the manuscript, with NT taking the lead in drafting the introduction (Section 2.1), probe design advancements for scanning applications (Section 2.3.1), characterization of surface corrosion materials (Section 2.3.3), and biological applications (Section 2.3.4). Dr. Vikram Singh (VS) contributed to the sections on optical fiber electrodes (Section 2.2) and photoactive electrodes for energy applications (Section 2.3.2). While majority of the figures were obtained from the corresponding references, Figure 2.1 was prepared by NT, and Figure 2.7A was adapted by NT from the reference cited, while VS adapted Figure 2.2 from the mentioned reference. Table 2.1 was compiled by NT and reviewed by VS and SK. The conclusion was written by NT and edited by VS. The completed manuscript was reviewed and edited by SK (corresponding author), and all co-authors agreed to the submission.

Chapter 3: Temperature Effect on the Electrochemical Current Response during Scanning Electrochemical Microscopy of Living Cells

Published in 2023 in the journal of Analytical Chemistry, Volume 95, Issue 49, Pages 17962 to 17967, https://doi-org.uml.idm.oclc.org/10.1021/acs.analchem.3c03716

All experimental work involving cell culture and electrochemical measurements was designed and performed by Nikita Thomas (NT). Data analysis and treatment of the experimental results were conducted by NT (Figures 3.1 experimental, 3.2, 3.3, A1.2, A1.3, and A1.4), providing the basis

for numerical modeling. Dr. Dao Trinh (DT) performed numerical modeling on the experimental data using COMSOL, producing Figures 3.1 simulation, 3.4, A1.1, and A1.5. Dr. Dhésmon Lima (DL) reviewed the original manuscript draft prepared by NT, offering scientific insight and comments. Dr. Sabine Kuss (SK) provided expertise, contributed to experimental design and discussions, and reviewed the manuscript. All corrections requested by co-authors DL, DT, and SK (supervisor and corresponding author) were incorporated by NT, finalizing the manuscript for submission.

Chapter 4: Effects of Media Composition and Light Exposure on the Electrochemical Current Response during Scanning Electrochemical Microscopy Live Cell Imaging

Published in 2024 in the journal of Analyst, Volume 149, Issue 22, Pages 5555 to 5562, https://doi-org.uml.idm.oclc.org/10.1039/D4AN01075B

As a shared first-author article, the design and performance of all experiments, along with data analysis, were conducted by NT (Figures 4.1, 4.2b, 4.3a, 4.4, 4.5, and Scheme 4.1) and Mengzhen Lyu (ML) (Figures 4.2a, 4.3b-d, A2.1, A2.2, A2.3, A2.4, and A2.5). Jadon Khouv (JK) performed experimental replicates of the light exposure studies (Figures A2.6 and A2.7). NT organized all collaborations and wrote the manuscript to the co-authors. DL and SK (corresponding author) contributed to experimental design and discussions, as well as reviewing the manuscript.

Chapter 5: Single Cell Scanning Photoelectrochemical Microscopy using Micro-Optical-Ring Electrodes

Published in 2022 in the journal of Biosensors and Bioelectronics, Volume 217, https://doi.org/10.1016/j.bios.2022.114658

All experimental work involving the fabrication and characterization of MOREs (Scheme 5.1 and Figure 5.1), as well as the culturing and immobilization of algae (Figure 5.4), was designed and performed by NT. VS contributed to the spectroscopy and spectroelectrochemistry experiments (Figures 5.2b-d and Figure 5.3). Numerical modeling of the MOREs was carried out by DT (Figures 5.2a, A3.1, A3.3, and A3.4). Nafisa Ahmed (NA) and VS contributed to the fabrication of MOREs, ensuring the repeatability of the procedure. All co-authors, NT, VS, NA and SK

(supervisor and corresponding author) reviewed and provided feedback on the manuscript, contributing to the final version.

Chapter 1

Introduction

1.1 Background, Motivation, and Scope of Thesis

Over the past two decades, the field of biosensors has evolved into a multidisciplinary domain encompassing micro- and nanotechnology, electronics, basic sciences, biomedicine, and electrochemistry. The first true biosensor was developed by Professor Leland C. Clark in 1956. His oxygen probe, known as the Clark electrode,[1,2] was made of platinum and covered with a cellophane membrane, allowing for the measurement of ambient oxygen partial pressure in whole blood.[3] In 1962, Clark further advanced biosensor technology by introducing "intelligent" electrochemical sensors that used enzymes as recognition elements for detecting specific analytes. His most notable contribution was the glucose biosensor.[4] This innovation was an extension of the oxygen electrode, where a layer of glucose oxidase (GOx) enzyme was immobilized between a polyethylene dialysis membrane. The GOx enzyme catalyzes the conversion of glucose into hydrogen peroxide (H_2O_2), and the resulting H_2O_2 concentration correlates with the glucose levels in the sample.[5,6] Clark's glucose sensor technology was later commercialized by Yellow Springs Instrument Company, leading to the development of the first glucose analyzer for whole blood measurements.[5] The glucose biosensor remains one of the most commercially successful electrochemical sensors, sparking significant research in electrochemical biosensors during the 1980s.[5]

Electrochemical biosensors primarily focus on detecting specific analytes by binding them to a biorecognition element, which in turn generates a signal detected by a transducer (usually an electrode) and processed by a data analysis system.[7,8] While traditional electrochemical biosensors are designed to detect biomolecules in biological fluids, probe electrochemistry combines electrochemical sensing with microscopy to examine the electrochemical activity and efflux of molecules from samples, such as living cells. This approach, often referred to as

"bioelectrochemistry," applies electrochemical techniques to study living cells and biomolecules.[9] Electrodes play a critical role in both electrochemical biosensors and probe electrochemistry, as they are electron conductors that facilitate the transfer of charge through an ionic conductor. Based on size, electrodes are classified as macroelectrode (dimensions in millimeter, centimeter, or meter), microelectrode (ME) (dimensions between 25µm and 1 mm), ultramicroelectrode (UME) (dimensions between 10 nm and 25µm), and nanoelectrodes or nanodes (smaller than 10 nm).[10,11] The dimensions of electrodes can refer to various tip geometries and combinations such as disk, ring, conical, hemispherical, etc.[10–14] MEs and UMEs play a major role in sensing applications *in-vivo* and *in-vitro*. *In-vivo* electrochemistry focuses mainly on the central nervous system for electroanalysis of complex neurochemistry.[14] Whereas *in-vitro* electrochemistry focuses exploring living cells through analytical detection of biochemical messengers/ molecules being fluxed within cells or extracellularly. [14]

UMEs are beneficial *in-vitro* to study cells closely and to understand cellular processes at the microscopic or nanoscopic level. (Figure 1.1) They enable us to monitor cells at the molecular level to analyze metabolic activities pertaining to growth, respiration, cell to cell communication, and reproduction. UMEs, apart from their dimensions in the range of nm to 25 µm which enables detection of electrochemically active molecules in small volumes and imaging of objects or living cells with smaller dimensions have several advantages such as (A) Quick response time implying that oxidation and reduction of redox active species can be monitored in nanoseconds. (B) Decreased *iR* drop due to small electrode surface area enabling measurements even in solutions without electrolyte. (C) Improved signal to noise ratio due to the hemispherical diffusion.[14]

UMEs have been used to examine various cellular pathological mechanisms.[13–16] Studying and understanding various diseases such as Alzheimer's,[17] diabetes,[18] cystic fibrosis,[19] Parkinson's,[20] kidney disease,[21] genetic disorders,[22] cancer,[23] etc., which only involve treatment plans and therapies, though single cell studies are more essential than ever. Single cell analyses are more advantageous than using populations of cells where heterogeneities exist leading to differences in cellular mechanisms, cell to cell communication in turn resulting in inaccurate interpretation of biochemical or chemical pathways.[24] Cellular heterogeneity is an inevitable feature of living cells.[25–27] Heterogeneity allows cells to respond or adapt to distinct environmental features.[27] Cell

population-based studies give an insight into understanding complex signaling networks, it can be based on averages from large number of cells or mathematical averages over distributions of single cells. Further, it is also known that population averages often amplify the most dominant cellular mechanism within individual cells in a population.[27] Though population studies are easier than capturing minor variations in individual cells, the understanding on which variation to avoid or not plays a crucial role in exploring disease mechanisms. The minor variations in cell expressions which have been tagged as unimportant has been challenged by researchers, which led to significant scientific milestones.[27] For instance, cancer being a very complex and heterogeneous disease, the therapeutics which work for one patient may not work for another patient with the same cancer due to cell heterogeneities.[25,26] Thus, single cell analysis is very important, as these minor heterogeneities in cells may get activated during unexpected cellular stresses.[27] Analyzing cells at the single cell level or in groups of two or three allows us to gain an in-depth understanding of intracellular dynamics and enables the quantification of molecules. Currently, single cell analysis is performed by various molecular biology techniques and fluorescence methods.[24] However, these methods are time consuming and require labels which can interfere with the metabolism of the target analyte in the cell.

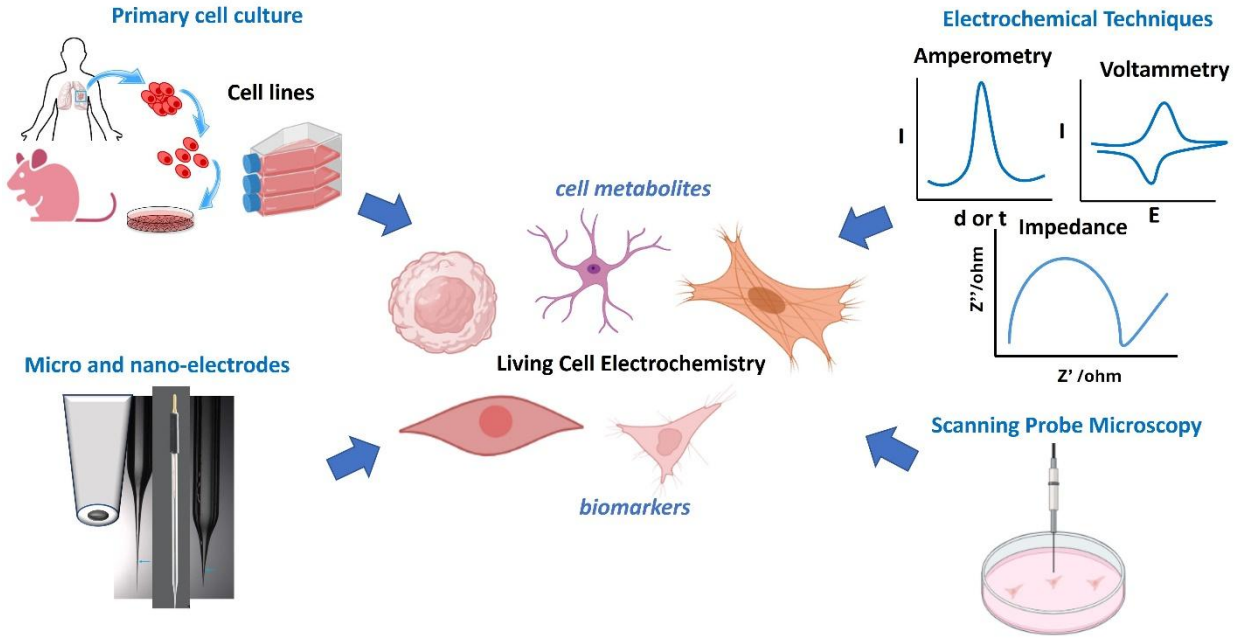

Figure 1.1 *Illustration of living cell electrochemistry showcasing cells harvesting through primary cell culture and applying electrochemical techniques through micro/nano probes integrated in scanning probe microscopy.*

Analyzing biomarkers/ biomolecules through classical biological methods from cells involves processing cells, separating cellular components, and treating them with several specific reagents, used in substantial volumes, is time consuming and requires expert personnel.[28] Electrochemical methods for investigating cells are cost effective, time efficient, and fast. Techniques often employed in electrochemistry to study biological samples are voltammetry, amperometry, and impedance to quantify cell metabolites and biomarkers in response to cell stimulation[13] (Figure 1.1). These methodologies measure with precision and are non-invasive. Hence, cellular pathologies can be examined at the microscopic level with high spatiotemporal resolution.

Micro and nano scale resolution is essential for exploring cellular electrochemical flux. High resolution imaging is an important characteristic of scanning probe microscopy (SPM).[29] It was the invention of Scanning Tunneling Microscope (STM), which measures the electrical current between the tip and the specimen, by Binning and Rohrer in 1981 that made a significant impact for surface characterization of materials.[29] Later, Atomic Force Microscope (AFM) was developed measuring electrostatic force between the tip and substrate. The invention of STM and AFM, brought about a new class of instrumentation, SPM. It was the development of UME by Wightman and Fleishman that led to the integration of electrochemistry to scanning probe techniques, later, SPM integrated with electrochemical techniques gained attention.[30–32] It was the discovery of scanning electrochemical microscopy (SECM) by Allen J Bard which led to its popularity among various fields to understand electrochemical reactivity of substrates[31,33]. It has a characteristic movable electrode positioned near the cell, measuring current for spatially resolved electrochemical signals.[33] Over time, SECM, has found its niche in studying surface reactions of homogeneous[34,35] and heterogeneous materials[36,37], sustainable energy[38] involving solar cells[39,40] and hydrogen fuel cells[41,42], corrosion[43,44], and biomedical applications[45,46].

1.2 Diverse Applications of SECM to Biological Systems

SECM is used to understand different facets of cellular activity in mammalian cells. It has been used for electrochemical imaging, metabolic profiling, protein expression, biomarkers detection, drug delivery, nanoparticle interactions, and cell membrane dynamics to name a few. Several

review papers highlight the various applicability of SECM towards not only human cells but also other mammalians.[12,47–49] The application of SECM towards cultured mammalian cells was first introduced by the research group of Dr. Tomokazu Matsue, where Yasukawa *et al.* measured the extracellular oxygen concentration around human colon cancer cells.[50] The electrochemical imaging revealed lower oxygen concentrations around the cell. They also observed that cyanide lowered cellular activity by hindering the electron transport in respiration. Kaya *et al.*, from the Matsue lab, monitored the cellular activity of HeLa cells in the presence of cyanide, ethyl alcohol, and antibiotic drug, Antimycin A using SECM and compared the results with fluorescence microscopy.[51] It was observed that SECM allowed analysis on the respiratory mechanism of Adeno HeLa cell whereas fluorescence measurement with Calcein AM showed drug action on cellular membrane. Their research was extended into bovine embryos, Shiku *et al.* analysed the metabolic activity of single embryos by monitoring their oxygen consumption in cone shaped microwells *vs.* flat bottom dishes. It was observed that metabolic processes of the cells are depended on the geometries of the culture vessel.[52]

Apart from understanding cellular respiration, Matsue's research lab also carried out SECM for monitoring protein expression. They measured alkaline phosphatase (ALP) in MCF7 cells, mouse embryoid bodies and HeLa cells.[53] Takahashi *et al.*, detected epidermal growth factor receptor (EGFR), a cancer biomarker protein, in normal Chinese Hamster Ovary (CHO) cells, EGFR-overexpressing CHO cells, and human epidermoid carcinoma (A431) cells.[54,55] They were able to observe differences in the expression levels in all the three cell lines and demonstrated that SECM is a non-invasive technique for monitoring protein expression. Further, Takahashi *et al.* obtained electrochemical images of boar sperm cell, rat adrenal medulla tumor (PC12) cell line, A431 cell line and rat cardiac myocyte.[56] The authors also performed Voltage Switching Mode (VSM)-SECM for topographical and electrochemical imaging of EGFR on A431 cell line and neurotransmitter transmitter release in PC12 cell lines.

The research group of Dr. Micheal V. Mirkin observed significant differences in the redox activity of non-transformed human breast epithelial cells, motile breast cells and highly metastatic breast cancer cells.[57] The authors demonstrated electrochemical mapping of transmembrane charge transfer rates and validated that single cell SECM measurements provide valuable information

which cannot be provided by averaged signal from population of cells. Feng *et al.* and Susan *et al.*, further used SECM in combination with optical and fluorescence, for cancer detection by generating a spatially resolved redox map of individual cells when both malignant and non-transformed cells were combined in a single culture plate.[58,59]

While Mirkin's research was focused on cancer detection, the research group of Dr. Zhifeng Ding investigated the release of reactive oxygen species (ROS) from single cells. ROS production in single human bladder (T24) and kidney (A498) epithelial cells on stimulation with heat-killed uropathogenic Escherichia coli GR-12.[60] It was observed that T24 cells showed ROS release unlike A498 cells due to presence and absence of toll-like receptors (TLR4) respectively. The authors showed that SECM technique can be used to image biochemical reactions, also emphasizing the *in-vitro* measurement of ROS as inflammatory response to infection. Further, Ding's group measured hydrogen peroxide in T24[61] and COS-7[62] cells by SECM. The authors demonstrated that H_2O_2 profiling by SECM provides understanding of single cell physiology and pathology. Zhang *et al.*, performed time-lapse SECM to monitor the extracellular ROS from T24 cells and observed that the ROS generation increased in cisplatin induced apoptosis of T24 cells.[63] Additionally, the authors also investigated cell permeability changes in T24 with the induction of cisplatin.[64,65] This study showed that SECM could be used for understanding the mechanism of anti-cancer drugs based on single cell response in real time. Further, Li *et al.* used SECM to investigate membrane permeability in T24 cells by using heavy metal cadmium along with three different redox mediators, ferrocenecarboxylate, 1'1-ferrocene dicarboxylate, and hexaaminеruthenium.[66–68] It was found that these hydrophilic molecular probes are essential to be used in SECM while measuring toxins, as they destroy cell membrane integrity. Similarly, the authors also studied the impact of chromium on membrane permeability and viability.[69–71]

Cytotoxicity research using SECM was also performed by the research group of Dr. Allen J. Bard. Mauzeroll *et al.*, measured thiodione efflux from single human liver cells after undergoing oxidative stress due to menadione exposure.[72] Li and Bard demonstrated using SECM that ferrocene methanol can be used to monitor cellular activity in HeLa cells.[73] It was also observed that culture media containing silver ion did not impact the activity of HeLa cells. Koley and Bard performed SECM experiments to explore the effects of Triton X-100 on HeLa cell morphology,

membrane permeability, and viability.[74] The authors demonstrated that SECM is an indispensable tool for measuring not only cell viability but also quantitative measure of membrane permeability.

Fei Li's research group monitored the effect of extracellular matrix (ECM) stiffness on the functional activity of multidrug resistance associated protein (MRP1).[75] The studies were conducted by performing SECM measurements on an engineered *in-vitro* cancer cell model showcasing the benign, malignant and advanced stages of cancer. It was found that increased ECM stiffness increased the functional activity of MRP1. Similarly, SECM was used to understand how the stiffness of extracellular matrix impacted the function of cardiomyocyte.[76,77] It was found that the mechanical microenvironment of the cell has a significant impact on the redox state of the cell. Furthermore, they explored the impact of electrical stimulation on cardiac tissue using SECM and found that the tissues had increased oxygen consumption and increased membrane permeability for electrical energy over 0.001 J.[78]

Dr. Wolfgang Schuhmann's group, used SECM for visualizing the respiration activity in PC12 cells.[79] The authors demonstrated that combining redox competition mode SECM with shear force-based constant distance mode is more advantageous than constant-distance mode SECM. It was observed that the electrochemical current due to oxygen concentration at the tip of the electrode was impacted not only by the oxygen consumption of the cells, but also due to dissolved oxygen in solution, and oxygen released through membrane permeation.[79] Reinforcing this, recently, Professor Patrick R. Unwin's research group, validated that measuring single cell oxygen consumption rate using SECM is challenging avoiding the disruption of cell's function.[80]

With SECM being used to delve deeper into the complex intricacies of mammalian cells, the most common challenge that researchers face is providing the ideal physiological environment for cells without compromising the cell's functioning. Cellular microenvironments which include temperature, media, and light exposure are important considerations for ideal mechanistic functioning of cells and sustainable bioelectrochemical analyses. Literature on SECM for mammalian cells, consists of over one hundred research articles since 1996. It is observed (Figure 1.2) that 76% and 69% of research experiments were performed in room temperature and using buffer solutions, respectively, demonstrating that experimental conditions were inconsistently

considered among various research groups. This poses a challenge to the scientific community in comparing research findings and validating electrochemical analyses of same cell lines performed in different research labs. In addition, the accurate measurement of biomolecules under non-ideal experimental conditions may compromise the integrity of results. This thesis presents a thorough investigation of experimental parameters for the analysis of living cells by SECM. The effect of temperature on the cellular electrochemical current signal has been successfully examined in Chapter 2, and the effect of cell media composition and light on the electrochemical current is investigated in Chapter 3.

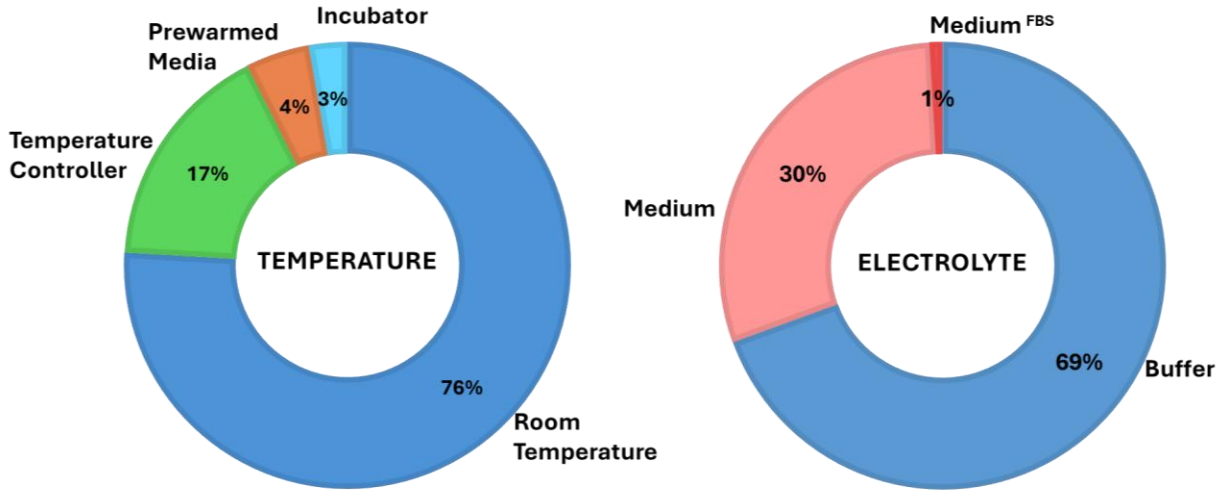

Figure 1.2 *Depictions of temperature setups and electrolyte solutions used in the literature pertaining to SECM for mammalian cells from 1996 to 2024.*

With the versatility and non-invasive feature of SECM, several variants such as Scanning Ion Conductance Microscopy (SICM)[81], Scanning Electrochemical Cell Microscopy (SECCM)[82], and Scanning Gel Electrochemical Microscopy (SGECM)[83] have emerged over the years through developments in electrode design. Apart from these variants, hybrid SECM techniques were developed to increase data output and reliability beyond electrochemical characteristics.[84,85] Combination techniques have gained attention mainly due to the development of sophisticated probes beyond microelectrodes/ UMEs.[85] Combination SECM techniques have the advantage of analyzing data from different perspectives, comparing and reasoning data relativity. SECM has been combined with AFM for applications in battery and material sciences.[86–88] NSOM-SECM

has been used to study various optically active substrates.[89–91] SICM-SECM is used to understand Li-ion battery technology.[92] Further, SECM has been hyphenated with other technologies such as electrochemical quartz microbalance, mass spectrometry, surface plasmon resonance, Raman and IR.[93] This has expanded its horizons in various interdisciplinary fields of nanotechnology, engineering, battery, and biomedical research. Combination of SECM with various techniques improves experimental validation and reliability through quantitative and qualitative data analysis.

The presented research in this thesis combines SECM with spectrophotometry. This is possible through specialized electrodes known as micro-optical ring electrodes (MOREs). These multi-functional probes consist of a gold coated OF (optical fiber) enclosed in a glass capillary. MOREs can irradiate light onto a sample (here cells), simultaneously performing electrochemical imaging and collecting photons, thus, advancing SECM to scanning photoelectrochemical microscopy (SPECM). This research is discussed in Chapters 2, 5 & 6. Chapter 2 gives an insight into different types of optical fiber probes that are used in analytical chemistry and their importance for various research applications. Chapter 5 elaborates on the fabrication methodology of MOREs, their integration into SECM forming SPECM measurements and their application to a light sensitive biological model system. In Chapter 6, SPECM was applied to investigate ROS and melanin production in skin cells.

The following section of this chapter discusses the fundamental principles of electrochemistry and SECM/SPECM which is the basis of the electrochemical analyses presented throughout this work.

1.3 Electrochemistry Principles

1.3.1 Electrochemical Cell

Electrochemical processes involve the movement of electrons at the interface of different conducting phases producing a measurable current or potential. The electrochemical cell is the core component of an analytical electrochemistry experiment where reactions occur. The three-electrode system is the traditional and most used setup for electrochemical analyses. It comprises the working electrode (WE), reference electrode (RE), and counter electrode (CE) immersed in an electrolyte solution and connected to data acquisition through a potentiostat (Figure 1.3). In

sensing applications, the redox reaction of the analyte or molecule of interest occurs at the WE surface. Inert materials such as gold, platinum, carbon, graphite etc. are used as WE material. These materials for WE are chosen based on their conductivity, robustness, and their ability to remain unaffected by the electrolyte and chemical reactivities. The potential applied to the WE is referenced to a standard potential using a RE, avoiding deviations from the set value. All through this thesis a Ag/AgCl pseudo/quasi RE is used instead of a commercial Ag/AgCl. This is attributed to the fact that a commercial Ag/AgCl RE consists of silver wire with AgCl coating placed inside a capillary filled with saturated KCl and a ceramic frit at the end is not well suited for miniaturized electrochemical setups like the SECM. In contrast, a pseudo RE is preferred for its compact and practical nature. Furthermore, since all electrochemical measurements in this thesis are conducted in chloride-rich buffer system or biological media, the pseudo RE maintains a stable and reproducible potential in respect to the chloride-dependent equilibrium of Ag/AgCl redox system This ensures its non-polarizability and consistent potential, making it a reliable RE. The pseudo-Ag/AgCl RE used here is fabricated by immersing a silver wire in a saturated solution of potassium chloride (3 M KCl) and applying a potential to electrochemically deposit AgCl on its surface. The prepared electrode is stored in 3 M KCl to retain its surface integrity and long-term potential stability. Apart from maintaining the potential of the WE, the potential of the RE is maintained during high current experiments by introducing a CE. The CE allows charge to flow through it, keeping a charge balance in the system. Platinum wires with a large surface area, stability under various conditions, and conductivity are widely chosen as CE material.

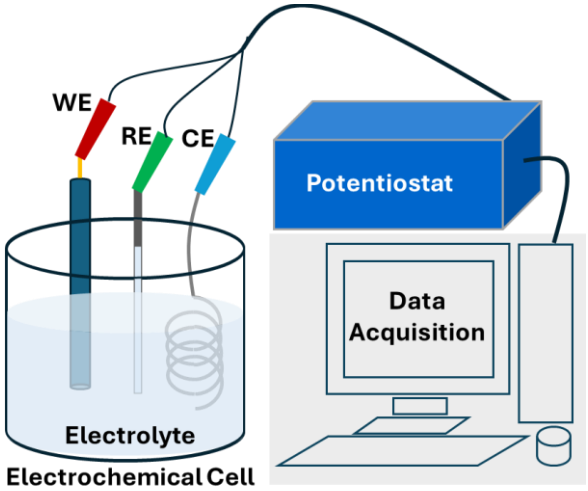

Figure 1.3 *Basic electrochemical workstation with the WE (red), RE (green), and CE (blue) placed in an electrochemical cell, coupled with a potentiostat and data acquisition system.*

1.3.2 Faradaic and Non-Faradaic Currents

When an electrode is immersed in solution, two types of chemical processes occur at its surface. The phenomenon that involves oxidation and reduction due to electron transfer between the electrode-solution interface resulting in a current is known as Faradaic process. This reaction is governed by the Faraday's Law where the amount of chemical reaction due to the flow of charge is proportional to the current produced. Processes at the electrode surface which generate a transient current and the change in potential occur without charge transfer are known as non-Faradaic processes. Electrode reactions such as adsorption, desorption or surface charging due to ionic species in solution contribute to non-faradaic currents. Though faradaic currents are of utmost importance in sensing applications, non-faradaic currents cannot be neglected during electrochemical analyses to obtain charge-transfer information.

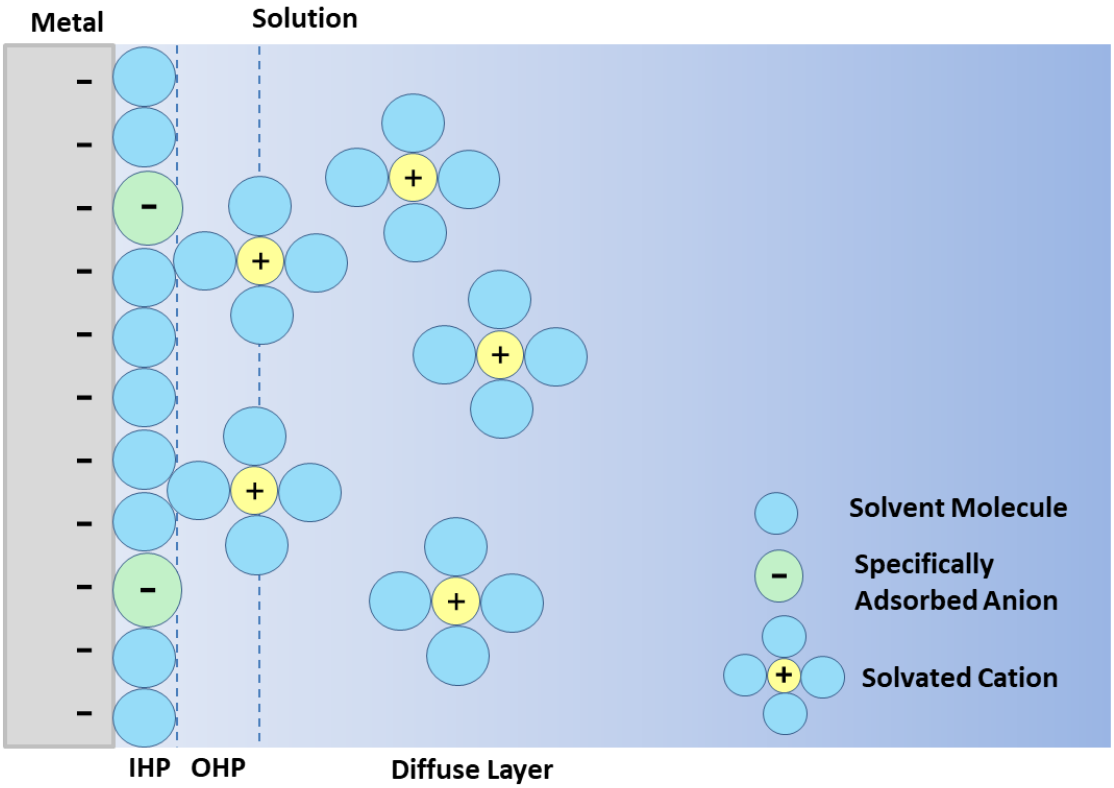

Figure 1.4 *Schematic representation of the Electrical Double Layer showcasing the inner and outer Helmholtz planes with the adsorbed charged ions and solvent molecules, extending further into the bulk solution through diffuse layer of mobile ions.*

Non-faradaic processes, which involve surface charging at the electrode-solution interface, are closely related to the Electrical Double Layer (EDL) (Figure 1.4). The EDL consists of layers of charges formed to maintain electrical neutrality at the interface. At the electrode surface, a layer of specifically adsorbed ions or oriented solvent molecules forms the Inner Helmholtz Plane (IHP). Beyond the IHP, solvated ions that are not specifically adsorbed form the Outer Helmholtz Plane (OHP) through long range electrostatic interactions. These ions are distributed further into the diffuse layer, where their concentration gradually approaches the bulk solution concentration. The reaction rate of faradaic processes depends on heterogenous electron transfer kinetics and mass transport of the analyte to the electrode surface.

1.3.3 Mass Transport

The flux/ movement of analyte molecules towards the electrode surface is governed by three terms of mass transport: diffusion, migration and convection. (Figure 1.5)

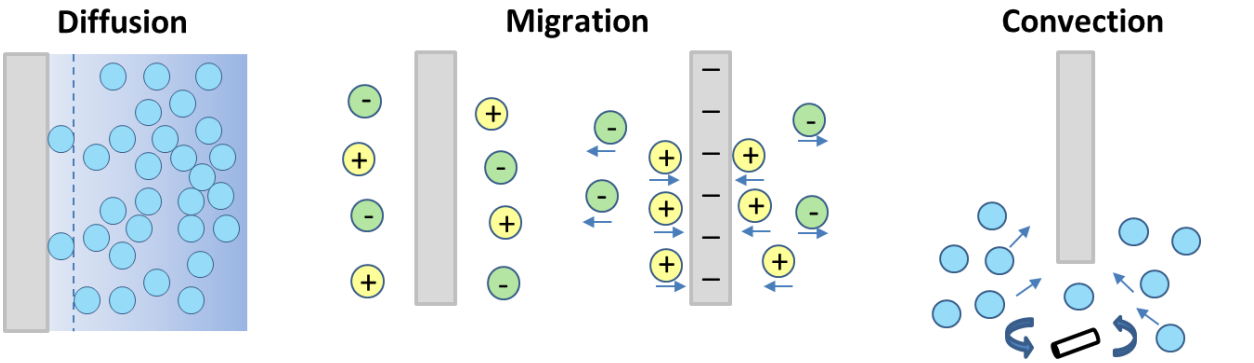

Figure 1.5 *Illustration of the different modes of mass transport. Diffusion: movement of species due to concentration gradient, Migration: movement of species due to an electric field, and Convection: movement of species due to fluid motion.*

Diffusion occurs due to a concentration gradient where the molecules move from the solution bulk to a region of lower concentration. This relates to Fick's law of diffusion[94], given by the equation

$$-J_o(x,t) = D_o \frac{\partial C_o(x)}{\partial x} \tag{1.1}$$

Where $J_o(x,t)$, the flux of species o at distance x and time t is proportional to $\partial C_o(x)/\partial x$, the concentration gradient, and D_o is the diffusion coefficient. Migration takes place due to the presence of a local electric field resulting in the movement of charged particles across a potential gradient. Convection happens due to a density gradient resulting in the flow of charged particles. Convection can also be caused by stirring or hydrodynamic transport. The total movement of analyte to the electrode is governed by the sum of contributions from diffusion, migration and convection. However, in most electrochemical systems with a supporting electrolyte (suppresses migration) and without stirring or flow (avoids convection), diffusion is the most dominant form of mass transport. The overall mass transport considers all three terms and is given by the Nernst-Planck Equation[94]

$$J_i(x) = -D_i \frac{\partial C_i(x)}{\partial x} - \frac{z_i F}{RT} D_i C_i \frac{\partial \phi(x)}{\partial x} + C_i \upsilon(x) \tag{1.2}$$

where flux of species i at distance x from the surface is given by $J_i(x)$ *(mol* s^{-1} cm^{-2}*)*, diffusion coefficient is given by D_i *(*cm^2/s*)*, concentration gradient at distance x is $\partial C_i(x)/\partial x$,$\partial\phi(x)/\partial x$ is the potential gradient, z_i is the charge and C_i represents concentration (mol cm^{-3}) of species i, and $\upsilon(x)$ is the velocity *(cm/s)*.

1.4 Electroanalytical Chemistry

Electroanalytical chemistry is a branch of analytical chemistry where the analyte of interest in an electrochemical cell can be quantitatively studied by a direct measure of current or potential. Electroanalytical techniques are classified into potentiometry: measures the potential across the WE and RE immersed in a solution containing the analyte (pH meter), coulometry: measures the total charge required for the redox conversion of the analyte (electrolysis), and voltammetry: measures current based on the potential applied in a solution of the analyte. Voltammetric techniques of Cyclic Voltammetry and Chronoamperometry have been used in chapters 2, 3, & 5. An overview of these two techniques is presented here.

1.4.1 Cyclic Voltammetry

Cyclic Voltammetry (CV) is a potential sweep technique where current is measured as a function of a linearly applied potential. Electron transfer kinetics of the analyte are studied when an analyte reacts with the electrode at a specific potential. The intensity of the faradaic current at a specific potential during the potential sweep gives a quantitative (concentration) value of the redox active analyte. The potential is swept between two values as a function of time, *t*, represented as a triangular waveform (Figure 1.6). The forward scan starts at E_i and is reversed at E_f and swept back to E_i. The slope of the graph indicates the scan rate.

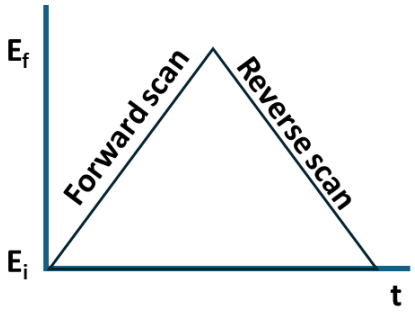

Figure 1.6 *Potential sweep with respect to time indicating the forward and reverse scan*

The current plotted as a function of voltage represents a cyclic voltammogram. The diffusion of analyte towards the surface of a macroelectrode is commonly described as either linear or planar. The cyclic voltammogram of a macroelectrode is shaped as shown in Figure 1.7.

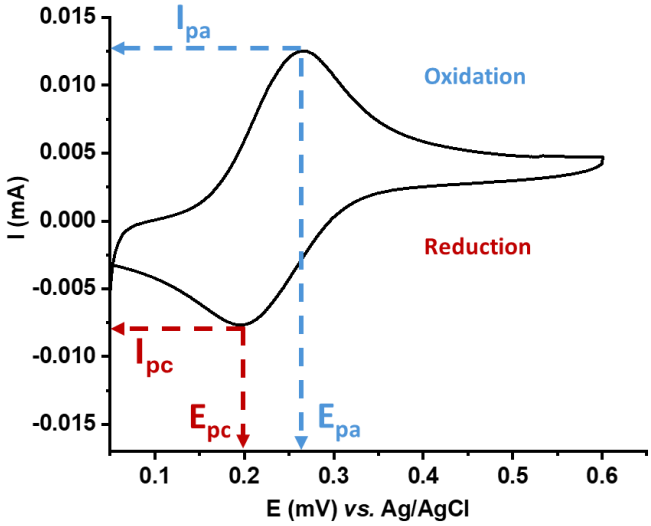

Figure 1.7 *Cyclic voltammogram of 1 mM $FcCH_2OH$ at 80 mv/s. I_{pa} and E_{pa} are anodic peak currents and peak potentials. I_{pc} and E_{pc} are cathodic peak currents and peak potentials.*

This plot can be characterized as follows:

$$i_p = 0.4463nFAC\sqrt{\left(\frac{nF\upsilon D}{RT}\right)} \tag{1.3}$$

Equation 1.3 is the Randles- Sevcik equation where the peak current i_p *(A)* is proportional to the square root of scan rate, υ *(V/s)*. *n* is the number of electrons, *F* is the Faraday constant *(C mol^{-1})*, *A* is the electrode area *(cm^2)*, *C* is the concentration *(mol/cm^3)*, *R* is the gas constant *(JK^{-1}mol^{-1})* and *T* is the temperature in *K*. At 25℃,

$$i_p = 2.69\,x10^5\,AC\,n^{3/2}D^{1/2}\upsilon^{1/2} \tag{1.4}$$

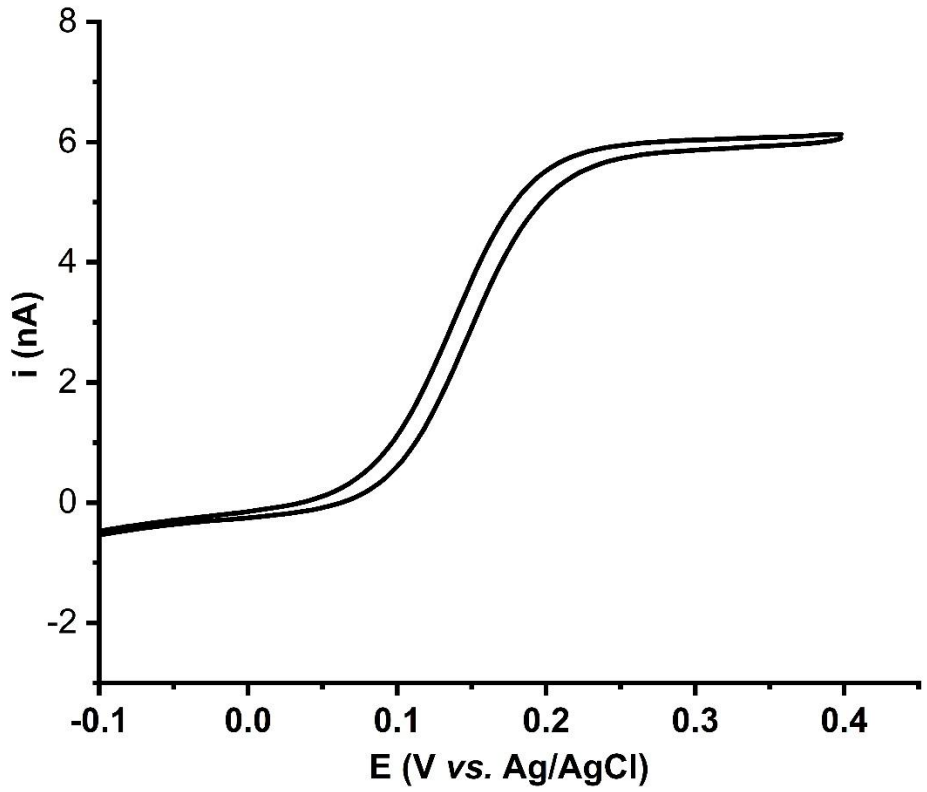

Figure 1.8 *Cyclic voltammogram of a microelectrode in 1 mM $FcCH_2OH$ at 50 mV/s showing a steady state current region.*

The diffusion at a disk microelectrode surface is radial owing to its surface dimension (diameter) smaller than that of the diffusion layer. The cyclic voltammogram of a microelectrode/ UME has a sigmoidal shape (Figure 1.8), unlike a macroelectrode, showing a constant current known as steady state current, i_{ss} and is given by the equation:

$$i_{ss} = 4nFDCr \tag{1.5}$$

where *n* is the number of electrons, *F(sA/mol)* is the Faraday constant, *D(cm^2/s)* is the diffusion coefficient, *C(M)* is the concentration of the redox mediator and *r(cm)* is the radius of the microelectrode. Microelectrodes offer an improved limit of detection compared to macroelectrodes due to their higher signal-to-noise ratio. Their smaller surface area minimizes capacitive and background currents, reducing noise and enhancing the precision of electrochemical current measurements.

1.4.2 Chronoamperometry

Chronoamperometry (CA) is a potential step technique where the current is measured as a function of time following a sudden step change in applied potential (Figure 1.9 a). In an electrochemical cell, when the potential is stepped to a value to drive an electrochemical reaction, a redox active species is oxidized or reduced at the electrode. This causes a depletion of reactant at the electrode surface, leading to a diffusion of species from the bulk to the electrode. As the distance from the electrode increases, the electrochemically active species decreases in concentration. (Figure 1.9 c) The faradaic current, *i(t)* is diffusion limited and is an exponential decrease is observed (Figure 1.9 b) which is given by Cottrell equation:

$$i(t) = \frac{nFAC_o{D_o}^{1/2}}{\pi^{1/2}t^{1/2}} \tag{1.6}$$

where the number of electrons is given by *n*, Faraday constant is *F (sA/mol)*, area of the electrode is *A (cm^2)*, concentration of the redox mediator is C_O *(M)*, Diffusion coefficient is given by D_O *(cm^2/s)*, and time is *t (s)*.

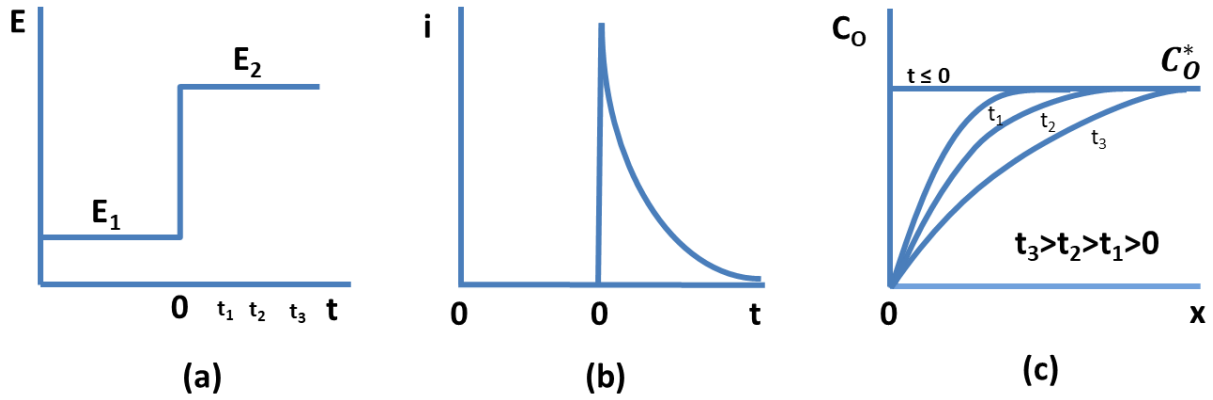

Figure 1.9 *Basic potential step. (a) Potential step experiment waveform where the species O is electrochemically inactive at E_1 and is reduced by the diffusion limited current at E_2. (b) Current inversely proportional to time due to limited diffusion of species to electrode (c) concentration profile of the species O at different time intervals, C^*_o is the bulk concentration.*

1.5 Scanning Electrochemical/ Photoelectrochemical Microscopy

Scanning Electrochemical Microscopy (SECM) is an advanced electroanalytical technique to understand substrates at the micro or nanoscale. Engstrom and Bard introduced SECM in the 20th century, which led to various interdisciplinary applications. SECM has advanced over the years in terms of instrumental development leading to high resolution signal output. Many companies have now commercialized the instrument due to its wide acceptance as a surface analytical technique. The following section gives an introduction on the basic principle of SECM/SPECM.

1.5.1 Principle and Instrumentation

SECM is a scanning probe technique where the microelectrode as a probe is the key component. SECM measures electrochemical reactivity and surface topography of a substrate based on current or potential response. The signal output and resolution are highly dependent on the probe characteristics. The SECM setup for a three-electrode system electrochemical cell used throughout this thesis is shown in Figure 1.10. It consists of the WE which is also known as the SECM tip with dimensions in the micro/nanoscopic range. A biopotentiostat which is connected to the working, counter, and reference electrodes applies a potential and measures currents in close

proximity to the substrate. A three-dimensional (3D) positioning system with piezo motors enables movement of the WE in the z direction. The sample stage with the electrochemical cell moves in the x-y direction. Another component which is essential in SECM pertaining to biological applications is the inverted optical microscope, equipped with a camera for monitoring samples in real time. The WE, bipotentiostat, sample position system, and microscope are integrated to a data acquisition system for coordinated signal measurement. The SECM instrument is placed in a faraday cage to avoid external electrical influence.

With respect to SPECM, in addition to the SECM components, a spectrophotometer and light source are present (Figure 1.10), which can be interchangeably connected either to the WE (illumination and spectroscopy through the electrode) or to the optical microscope.

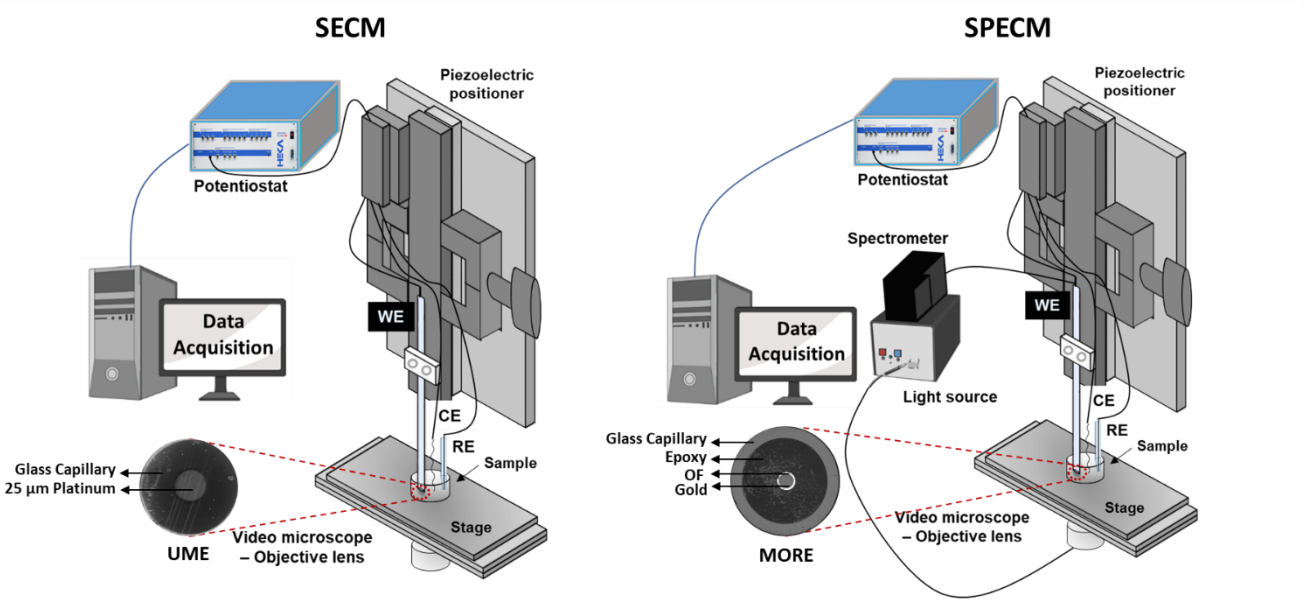

Figure 1.10 *Schematic representation of SECM with UME tip and SPECM with MORE tip*

1.5.2 Modes of Operation

SECM and SPECM are available for electroanalytical surface analysis in different operating modes: substrate generation/ tip collection (SG/TC), tip generation/ substrate collection (TG/SC), redox competition (RC), and feedback mode.

In SG/TC mode, the redox active species is generated at the substrate and collected at the SECM biased tip (Figure 1.11 a). The current is measured at both the substrate and the tip. In this mode a large substrate is required, and a steady state current is not attained due to the continuous regeneration of species from the substrate. In TG/SC mode, the redox active species is generated at the tip and collected at the substrate (Figure 1.11 b). The current is measured at the substrate; eventually steady state current is attained with time and as the distance between the tip and substrate decreases. In RC mode, the SECM tip and substrate are both biased with potential and compete for the electroactive species, but the current is measured only at the tip (Figure 1.11 c). To increase sensitivity and reduce depletion of the electroactive mediator, the substrate is biased at the reduction potential and the SECM tip is biased at a reductive potential pulse. A decreased current is measured at SECM tip during substrate reduction activity.

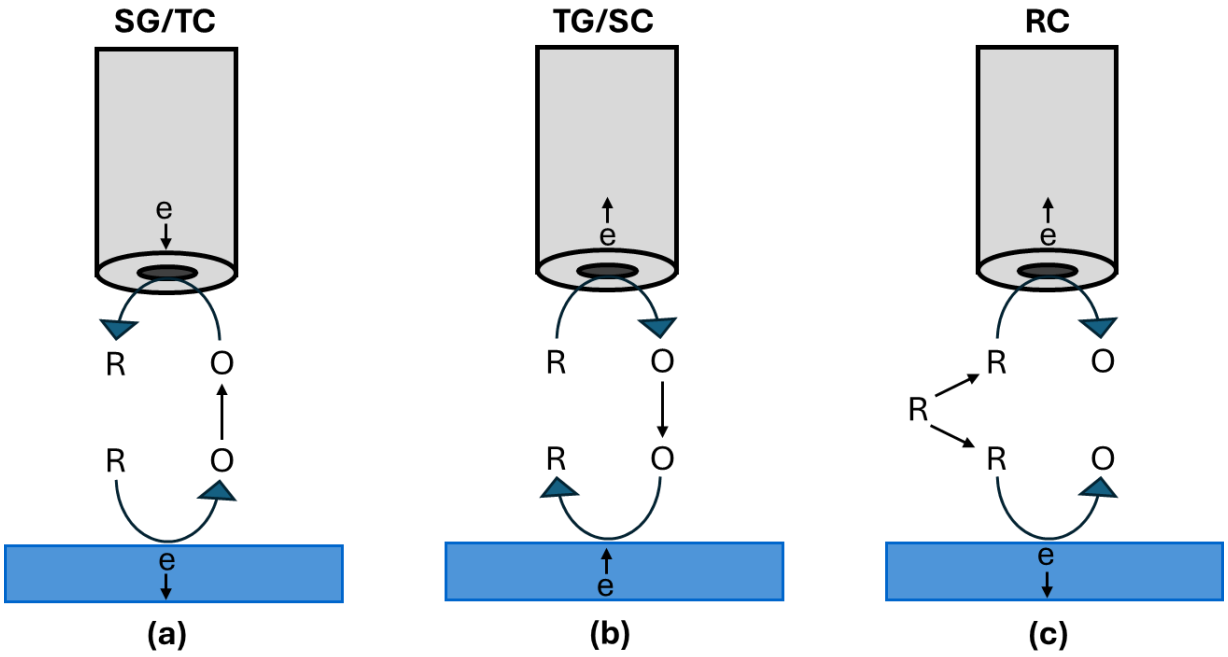

Figure 1.11 *Modes of SECM. (a) SG/TC (b) TG/SC (c) RC*

The SG/TC, TG/SC, and RC modes of SECM have not been explored in this thesis. However, the SC/ TG mode is important for corrosion[95] and enzymatic applications[96], TG/SC mode is invaluable for kinetics[97–99] and substrate modifications[100] studies, and RC mode plays an important role for catalytic applications.[101,102] SECM feedback mode is the prime focus in the presented research.

1.5.2.1 SECM Feedback Mode

The feedback mode in SECM is widely used and applied in various fields of study. In this mode, the SECM tip is biased at a potential, the current attained as the SECM tip approaches the substrate is due to the oxidation of the electroactive species. This current is influenced by the topography and the electrochemical reactivity of the substrate. In the bulk solution, the faradaic current is a measure of the diffusion-controlled flux of the redox mediator. When the biased SECM tip is approaching a fully insulating substrate, hindered diffusion is observed, resulting in a decrease of current. This is known as negative feedback (Figure 1.12 a). However, when the tip is approaching a true conductor, the measured current increases, due to the regeneration of the redox species resulting in an increase in current known as positive feedback (Figure 1.12 b).

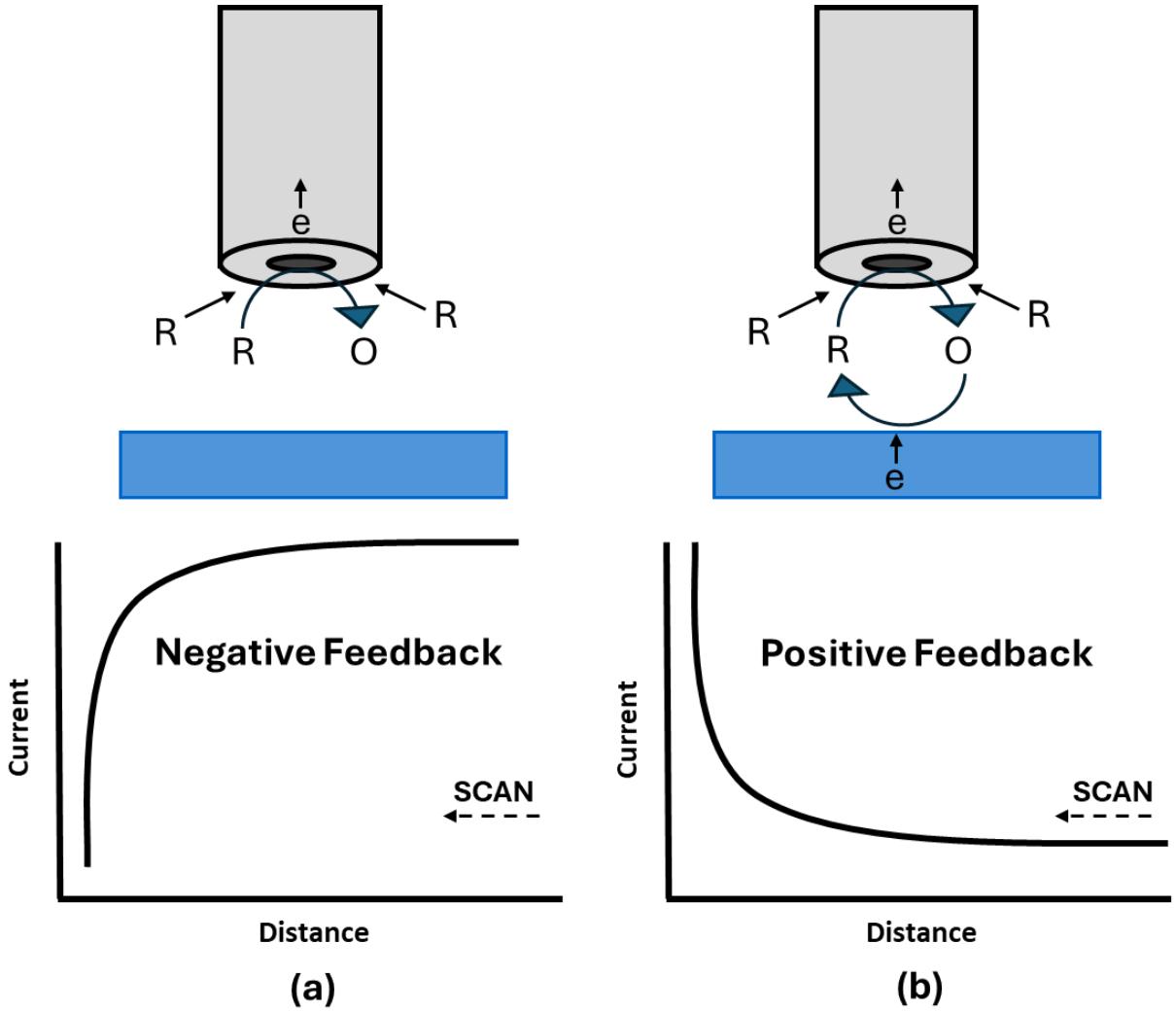

Figure 1.12 *Feedback mode SECM. (a) Negative feedback and the respective current profile (b) Positive feedback and the respective current profile.*

1.6 Thesis Outline

The main focus of this thesis is the understanding and the optimization of fundamental experimental parameters during SECM of living mammalian cells and the advancement of SECM to SPECM, which was applied to biological samples. This thesis strives to understand the impact of experimental parameters such as temperature, media and light exposure towards cellular electrochemical current signal. Additionally, SECM is advanced to SPECM. This includes creating a standardized fabrication methodology for MOREs and exploring their applicability to living cells. The thesis is organized into the following chapters (Figure 1.13).

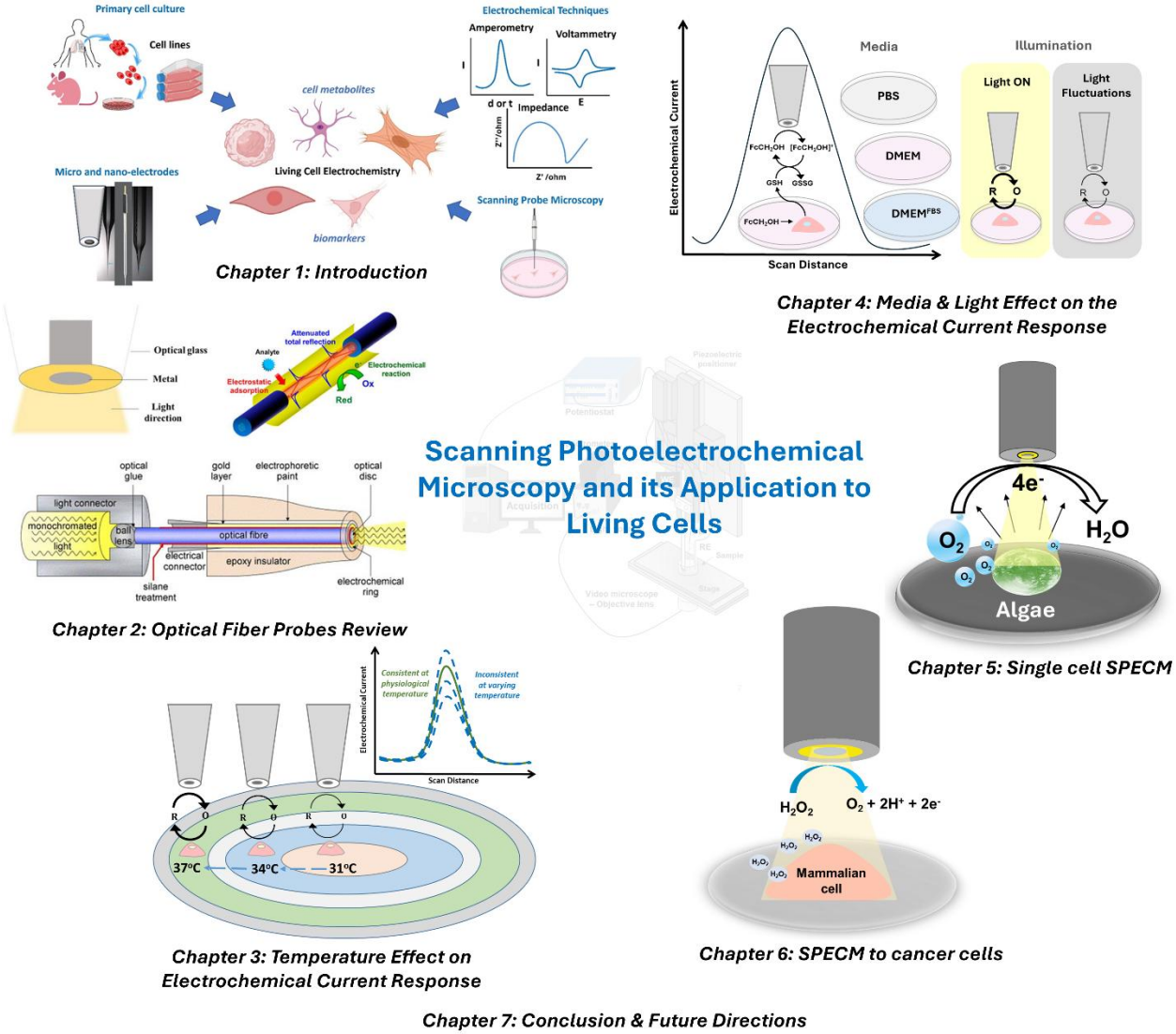

Figure 1.13 *Illustration of thesis outline*

Following the **introductory Chapter 1**, **Chapter 2** reviews the literature on different types of optical fibers (OF) used in electrochemistry which is essential for advancing SECM to SPECM. The past and current fabrication procedures of OF-electrodes are discussed. Further, a complete outlook on the application of these electrodes in fields of energy, corrosion, and biological applications are elaborated. This literature review brings together more than 100 research articles over 40 decades and is beneficial to interdisciplinary researchers focusing on biosensing using photoactive materials or surfaces. This literature study served as a precursor for developing a user-friendly fabrication methodology for micro-optical-ring electrodes which is elaborated in Chapter 5.

Chapter 3 investigates the relationship between temperature and the electrochemical current signal during SECM imaging of adenocarcinoma cervical cancer (HeLa) cells. Here, temperature and diffusion coefficient were seen as directly proportional to each other. Furthermore, placing HeLa cells at different temperature zones with temperatures varying from 30 to 37-degree Celsius showed temperature-depended electrochemical reactivity of cells, which was validated through numerically simulation data. This chapter highlights that temperature is an essential parameter to be considered while performing SECM on living cells.

Building on findings on the effect of temperature on the electrochemical current signal of HeLa cells, **Chapter 4** extends the investigation of experimental parameters to media and light exposure on HeLa cells during SECM imaging. The electrochemical current signal from HeLa cells is compared and analyzed in phosphate buffered saline (PBS), Dulbecco's Modified Eagle's Medium (DMEM), and DMEM + 10% fetal bovine serum (FBS). It was found that DMEM without FBS at physiological temperatures was essential for monitoring real time electrochemical current signals. Furthermore, consistent light exposure in combination with media and temperature control, provided stable electrochemical measurements during HeLa cell imaging.

On understanding the importance of maintaining experimental conditions during SECM of mammalian cells, **Chapters 5, and 6** focus on advancing SECM to SPECM. **Chapter 5** illustrates the fabrication process and applicability of MOREs in SPECM. MOREs were fabricated in a time efficient manner, and they were characterized electrochemically, optically, and through numerical

modelling. Integrating MOREs into SPECM, spectro-electrochemistry of N, N, N, N'-Tetramethyl p-phenyl-enediamine (TMPD) was performed while optimizing the tip-to-substrate distance. The absorption spectra of its oxidized and reduced forms were obtained simultaneously while varying the MORE tip potential. Additionally, the applicability of SPECM to live cell imaging was verified by monitoring the electrochemical oxygen production in living algae, *Eremosphaera viridis* in the absence and presence of localized illumination.

Chapter 6 combines the application of knowledge obtained from chapters 2 through 5. Experimental conditions were maintained at optimal parameters while monitoring reactive oxygen species in Human Epidermal Keratinocytes (HEKa), Human Epidermal Melanocytes (HEMa), and Melanoma (SK-MEL-28) electrochemically. Results were verified through fluorescence microscopy. Additionally, melanin production in HEMa and melanoma was electrochemically detected, and the impact of UV irradiation on the melanin production in melanoma was investigated. This chapter presents the potential of SPECM towards mammalian cell studies.

The final **Chapter 7** is an overall summary and in-depth discussion of conclusions across the thesis. A discussion on the impact of the research findings is presented and placed into the context of the research field. Suggestions for future research are presented with emphasis on SPECM towards probe development, different modes and other cell lines. Applications with electrochemiluminescence, biomaterials, and agriculture are also discussed.

1.7 References

(1) Palchetti, I.; Mascini, M. Biosensor Technology: A Brief History. *Lecture Notes in Electrical Engineering*; **2010**, 50, 15–23. https://doi.org/10.1007/978-90-481-3606-3_2.

(2) Bhalla, N.; Jolly, P.; Formisano, N.; Estrela, P. Introduction to Biosensors. *Essays Biochem* **2016**, *60* (1), 1–8. https://doi.org/10.1042/EBC20150001.

(3) Severinghaus, J. W.; Astrup, P. B. Historical Review: History of Blood Gas Analysis IV. Leland Clark's Oxygen Electrode. *J Clin Monit* **1986**, 2, 125-139

(4) Clark, L. C.; Lyons, C. Electrode systems for continuous monitoring in cardiovascular surgery. *Ann N Y Acad Sci* **1962**, *102* (1), 29–45. https://doi.org/10.1111/j.1749-6632.1962.tb13623.x.

(5) Wang, J. Glucose Biosensors: 40 Years of Advances and Challenges. *Electroanalysis* **2001**, *13* (12), 983–988. https://doi.org/10.1002/1521-4109(200108)13:12<983::AID-ELAN983>3.0.CO;2.

(6) Clark, L. C.; Duggan, C. A. Implanted Electroenzymatic Glucose Sensors. *Diabetes Care* **1982**, *5* (3), 174–180.

(7) Abdulbari, H. A.; Basheer, E. A. M. Electrochemical Biosensors: Electrode Development, Materials, Design, and Fabrication. *ChemBioEng Reviews* **2017**, 92–105. https://doi.org/10.1002/cben.201600009.

(8) Wu, J.; Liu, H.; Chen, W.; Ma, B.; Ju, H. Device Integration of Electrochemical Biosensors. *Nature Reviews Bioengineering* **2023**, *1* (5), 346–360. https://doi.org/10.1038/s44222-023-00032-w.

(9) Suprun, E. V.; Budnikov, H. C. Bioelectrochemistry as a Field of Analysis: Historical Aspects and Current Status. *Journal of Analytical Chemistry* **2022**, 643–663. https://doi.org/10.1134/S1061934822060168.

(10) Bozal-Palabiyik, B.; Selcuk, O.; Uslu, B. Development of Nanoparticle-Modified Ultramicroelectrodes and Their Electroanalytical Application. *Handbook of Nanobioelectrochemistry* **2023**, 861–879. https://doi.org/10.1007/978-981-19-9437-1_39.

(11) Bard, A. J., Inzelt, G., Scholz, F., Eds.; Electrochemical Dictionary; Springer Berlin Heidelberg: Berlin, Heidelberg, **2012**.

(12) Beaulieu, I.; Kuss, S.; Mauzeroll, J.; Geissler, M. Biological Scanning Electrochemical Microscopy and Its Application to Live Cell Studies. *Anal Chem* **2011**, *83* (5), 1485–1492. https://doi.org/10.1021/ac101906a.

(13) Adams, K. L.; Puchades, M.; Ewing, A. G. In Vitro Electrochemistry of Biological Systems. *Annual Review of Analytical Chemistry*. **2008**, 329–355. https://doi.org/10.1146/annurev.anchem.1.031207.113038.

(14) Schulte, A.; Schuhmann, W. Single-Cell Microelectrochemistry. *Angewandte Chemie - International Edition*. **2007**, 8760–8777. https://doi.org/10.1002/anie.200604851.

(15) Wightman, R. M. Probing Cellular Chemistry in Biological Systems with Microelectrodes. *Science (1979)* **2006**, *311* (5767), 1570–1574. https://doi.org/10.1126/science.1120027.

(16) Kita, J. M.; Wightman, R. M. Microelectrodes for Studying Neurobiology. *Curr Opin Chem Biol* **2008**, *12* (5), 491–496. https://doi.org/10.1016/j.cbpa.2008.06.035.

(17) Passeri, E.; Elkhoury, K.; Morsink, M.; Broersen, K.; Linder, M.; Tamayol, A.; Malaplate, C.; Yen, F. T.; Arab-Tehrany, E. Alzheimer's Disease: Treatment Strategies and Their Limitations. *International Journal of Molecular Sciences.*, **2022**. https://doi.org/10.3390/ijms232213954.

(18) Sugandh, F.; Chandio, M.; Raveena, F.; Kumar, L.; Karishma, F.; Khuwaja, S.; Memon, U. A.; Bai, K.; Kashif, M.; Varrassi, G.; Khatri, M.; Kumar, S. Advances in the Management of Diabetes Mellitus: A Focus on Personalized Medicine. *Cureus* **2023**, *15* (8), e43697. https://doi.org/10.7759/cureus.43697.

(19) Linnemann, R. W.; Friedman, D.; Altstein, L. L.; Islam, S.; Bach, K.-T.; Georgiopoulos, A. M.; Moskowitz, S. M.; Yonker, L. M. Advance Care Planning Experiences and Preferences among People with Cystic Fibrosis. *J Palliat Med* **2019**, *22* (2), 138–144. https://doi.org/10.1089/jpm.2018.0262.

(20) Kobylecki, C. Update on the Diagnosis and Management of Parkinson's Disease. *Clin Med (Lond)* **2020**, *20* (4), 393–398. https://doi.org/10.7861/clinmed.2020-0220.

(21) Chen, T. K.; Knicely, D. H.; Grams, M. E. Chronic Kidney Disease Diagnosis and Management: A Review. *JAMA* **2019**, *322* (13), 1294–1304. https://doi.org/10.1001/jama.2019.14745.

(22) Grosse, S. D.; Schechter, M. S.; Kulkarni, R.; Lloyd-Puryear, M. A.; Strickland, B.; Trevathan, E. Models of Comprehensive Multidisciplinary Care for Individuals in the United States with Genetic Disorders. *Pediatrics* **2009**, *123* (1), 407–412. https://doi.org/10.1542/peds.2007-2875.

(23) McCorkle, R.; Ercolano, E.; Lazenby, M.; Schulman-Green, D.; Schilling, L. S.; Lorig, K.; Wagner, E. H. Self-Management: Enabling and Empowering Patients Living with Cancer as a Chronic Illness. *CA Cancer J Clin* **2011**, *61* (1), 50–62. https://doi.org/10.3322/caac.20093.

(24) Zhang, J.; Zhou, J.; Pan, R.; Jiang, D.; Burgess, J. D.; Chen, H. Y. New Frontiers and Challenges for Single-Cell Electrochemical Analysis. *ACS Sensors*. **2018**, 242–250. https://doi.org/10.1021/acssensors.7b00711.

(25) Elsasser, W. M. Outline of a Theory of Cellular Heterogeneity. *Proc. Natl. Acad. Sci. USA* **1984**, *81*, 5126–5129.

(26) Rubin, H. Early Origin and Pervasiveness of Cellular Heterogeneity in Some Malignant Transformations. *Proc. Nati. Acad. Sci. USA* **1984**, *81*, 5121–5125

(27) Altschuler, S. J.; Wu, L. F. Cellular Heterogeneity: Do Differences Make a Difference? *Cell* **2010**, *141*, 559–563. https://doi.org/10.1016/j.cell.2010.04.033.

(28) Chen, Y.; Zhu, Z.; Yu, Y. Novel Methodologies in Analysis of Small Molecule Biomarkers and Living Cells. *Tumor Biol* **2014**, *35*, 9469–9477.

(29) Salapaka, M. V.; Salapaka, S. M. Scanning Probe Microscopy. *IEEE Control Syst* **2008**, *28* (2), 65–83. https://doi.org/10.1109/MCS.2007.914688.

(30) Wightman, R. M. Microvoltammetric Electrodes. *Anal Chem* **1981**, *53* (9), 1125A-1134A. https://doi.org/10.1021/ac00232a791.

(31) Daniele, S., Denuault, G. From Microelectrodes to Scanning Electrochemical Microscopy. In *Developments in Electrochemistry* **2014**, 223–244. https://doi.org/10.1002/9781118694404.ch12.

(32) Brina, R.; Pons, S. Ultramicroelectrodes Sensors and Detectors. *J. Electroanal. Chem* **1988**, *244*, 81–90.

(33) Bard, A. J.; Fan, F. R. F.; Kwak, J.; Lev, O. Scanning Electrochemical Microscopy. Introduction and Principles. *Anal Chem* **1989**, *61* (2), 132–138. https://doi.org/10.1021/ac00177a011.

(34) Zhou, F.; Unwin, P. R.; Bard, A. J. Scanning Electrochemical Microscopy. 16. Study of Second-Order Homogeneous Chemical Reactions via the Feedback and Generation/Collection Modes. *J. Phys. Chem.* **1992**, *96* (12), 4917–4924.

(35) Shea, T. V.; Bard, A. J. Digital Simulation of Homogeneous Chemical Reactions Coupled to Heterogeneous Electron Transfer and Applications at Platinum/ Mica/ Platinum Ultramicroband Electrodes. *Anal. Chem* **1987**, *59* (17), 2101–2111.

(36) Wipf, D. O.; Bard, A. J. Scanning Electrochemical Microscopy: VII. Effect of Heterogeneous Electron-Transfer Rate at the Substrate on the Tip Feedback Current. *J. Electrochem. Soc.* **1991**, *138*, 469–474.

(37) Johnson, L.; Niaz, A.; Boatwright, A.; Voisey, K. T.; Walsh, D. A. Scanning Electrochemical Microscopy at Thermal Sprayed Anti-Corrosion Coatings: Effect of Thermal Spraying on Heterogeneous Electron Transfer Kinetics. *Journal of Electroanalytical Chemistry* **2011**, *657*, 46–53. https://doi.org/10.1016/j.jelechem.2011.03.009.

(38) Bertoncello, P. Advances on Scanning Electrochemical Microscopy (SECM) for Energy. *Energy and Environmental Science*. **2010**, 1620–1633. https://doi.org/10.1039/c0ee00046a.

(39) Martin, C. J.; Bozic-Weber, B.; Constable, E. C.; Glatzel, T.; Housecroft, C. E.; Wright, I. A. Using Scanning Electrochemical Microscopy to Examine Copper(I) Sensitizers for Dye-Sensitized Solar Cells. *Journal of Physical Chemistry C* **2014**, *118* (30), 16912–16918. https://doi.org/10.1021/jp500409c.

(40) Martin, C. J.; Bozic-Weber, B.; Constable, E. C.; Glatzel, T.; Housecroft, C. E.; Wright, I. A. Development of Scanning Electrochemical Microscopy (SECM) Techniques for the Optimization of Dye Sensitized Solar Cells. *Electrochim Acta* **2014**, *119*, 86–91. https://doi.org/10.1016/j.electacta.2013.11.172.

(41) Kucernak, A. R.; Chowdhury, P. B.; Wilde, C. P.; Kelsall, G. H.; Zhu, Y. Y.; Williams, D. E. Scanning Electrochemical Microscopy of a Fuel-Cell Electrocatalyst Deposited onto Highly Oriented Pyrolytic Graphite. *Electrochim Acta* **2000**, *45*, 4483–4491.

(42) Ahmed, S.; Ji, S.; Petrik, L.; Linkov, V. M. Scanning Electrochemical Microscopic Study of Hydrogen Oxidation and Evolution at Electrochemically Deposited Pt Nanoparticulate Electrode Incorporated in Polyaniline. *Analytical Sciences* **2004**, *20*, 1283–1287.

(43) Traxler, I.; Singewald, T. D.; Schimo-Aichhorn, G.; Hild, S.; Valtiner, M. Scanning Electrochemical Microscopy Methods (SECM) and Ion-Selective Microelectrodes for Corrosion Studies. *Corrosion Reviews* **2022**, *40* (6), 515–542. https://doi.org/10.1515/corrrev-2021-0104.

(44) Org, W. E.; Izquierdo, J.; González, S.; Souto, R. M. Application of AC-SECM in Corrosion Science: Local Visualization of Heterogeneous Chemical Activity in AA2024 Surfaces. *Int. J. Electrochem. Sci* **2012**, *7*, 11377–11388.

(45) Zhou, Y.; Takahashi, Y.; Fukuma, T.; Matsue, T. Scanning Electrochemical Microscopy for Biosurface Imaging. *Curr Opin Electrochem* **2021**, *29*. https://doi.org/10.1016/j.coelec.2021.100739.

(46) Soldà, A.; Valenti, G.; Marcaccio, M.; Giorgio, M.; Pelicci, P. G.; Paolucci, F.; Rapino, S. Glucose and Lactate Miniaturized Biosensors for SECM-Based High-Spatial Resolution Analysis: A Comparative Study. *ACS Sens* **2017**, *2* (9), 1310–1318. https://doi.org/10.1021/acssensors.7b00324.

(47) Polcari, D.; Dauphin-Ducharme, P.; Mauzeroll, J. Scanning Electrochemical Microscopy: A Comprehensive Review of Experimental Parameters from 1989 to 2015. *Chem Rev* **2016**, *116* (22), 13234–13278. https://doi.org/10.1021/acs.chemrev.6b00067.

(48) Filice, F. P.; Ding, Z. Analysing Single Live Cells by Scanning Electrochemical Microscopy. *Analyst* **2019**, *144* (3), 738–752. https://doi.org/10.1039/c8an01490f.

(49) Conzuelo, F.; Schulte, A.; Schuhmann, W. Biological Imaging with Scanning Electrochemical Microscopy. *Proceedings of the Royal Society A: Mathematical, Physical and Engineering Sciences* **2018**, *474* (2218). https://doi.org/10.1098/rspa.2018.0409.

(50) Yasukawa, T.; Kondo, Y.; Uchida, I.; Matsue, T. Imaging Cellular Activity of Single Cultured Cells by SECM. *Chem Lett* **1988**.

(51) Kaya, T.; Torisawa, Y. S.; Oyamatsu, D.; Nishizawa, M.; Matsue, T. Monitoring the Cellular Activity of a Cultured Single Cell by Scanning Electrochemical Microscopy (SECM). A Comparison with Fluorescence Viability Monitoring. *Biosens Bioelectron* **2003**, *18* (11), 1379–1383. https://doi.org/10.1016/S0956-5663(03)00083-6.

(52) Shiku, H.; Shiraishi, T.; Aoyagi, S.; Utsumi, Y.; Matsudaira, M.; Abe, H.; Hoshi, H.; Kasai, S.; Ohya, H.; Matsue, T. Respiration Activity of Single Bovine Embryos Entrapped in a Cone-Shaped Microwell Monitored by Scanning Electrochemical Microscopy. *Anal Chim Acta* **2004**, *522* (1), 51–58. https://doi.org/10.1016/j.aca.2004.06.054.

(53) Arai, T.; Nishijo, T.; Matsumae, Y.; Zhou, Y.; Ino, K.; Shiku, H.; Matsue, T. Noninvasive Measurement of Alkaline Phosphatase Activity in Embryoid Bodies and Coculture Spheroids with Scanning Electrochemical Microscopy. *Anal Chem* **2013**, *85* (20), 9647–9654. https://doi.org/10.1021/ac401824q.

(54) Takahashi, Y.; Miyamoto, T.; Shiku, H.; Asano, R.; Yasukawa, T.; Kumagai, I.; Matsue, T. Electrochemical Detection of Epidermal Growth Factor Receptors on a Single Living Cell Surface by Scanning Electrochemical Microscopy. *Anal Chem* **2009**, *81* (7), 2785–2790. https://doi.org/10.1021/ac900195m.

(55) Matsumae, Y.; Takahashi, Y.; Shiku, H.; Matsue, T. Quantitative Real-Time Monitoring of Antibody-Induced Internalization of Epidermal Growth Factor Receptor on Single Living Mammalian Cells Using Scanning Electrochemical Microscopy. *ChemElectroChem* **2018**, *5* (20), 3096–3101. https://doi.org/10.1002/celc.201800563.

(56) Takahashi, Y.; Shevchuk, A. I.; Novak, P.; Babakinejad, B.; Macpherson, J.; Unwin, P. R.; Shiku, H.; Gorelik, J.; Klenerman, D.; Korchev, Y. E.; Matsue, T. Topographical and Electrochemical Nanoscale Imaging of Living Cells Using Voltage-Switching Mode Scanning Electrochemical Microscopy. **2012**. https://doi.org/10.1073/pnas.1203570109/-/DCSupplemental.

(57) Liu, B.; Rotenberg, S. A.; Mirkin, M. V. Scanning Electrochemical Microscopy of Living Cells: Different Redox Activities of Nonmetastatic and Metastatic Human Breast Cells. *Proc Natl Acad Sci U S A* **2000**, *97* (18), 9855–9860. https://doi.org/10.1073/pnas.97.18.9855.

(58) Feng, W.; Rotenberg, S. A.; Mirkin, M. V. Scanning Electrochemical Microscopy of Living Cells. 5. Imaging of Fields of Normal and Metastatic Human Breast Cells. *Anal Chem* **2003**, *75* (16), 4148–4154. https://doi.org/10.1021/ac0343127.

(59) Rotenberg, S. A.; Mirkin, M. V. Scanning Electrochemical Microscopy: Detection of Human Breast Cancer Cells by Redox Environment. *J Mammary Gland Biol Neoplasia* **2004**, *9* (4), 375–382. https://doi.org/10.1007/s10911-004-1407-7.

(60) Zhao, X.; Lam, S.; Jass, J.; Ding, Z. Scanning Electrochemical Microscopy of Single Human Urinary Bladder Cells Using Reactive Oxygen Species as Probe of Inflammatory Response. *Electrochem commun* **2010**, *12* (6), 773–776. https://doi.org/10.1016/j.elecom.2010.03.030.

(61) Zhao, X.; Zhang, M.; Long, Y.; Ding, Z. Redox Reactions of Reactive Oxygen Species in Aqueous Solutions as the Probe for Scanning Electrochemical Microscopy of Single Live T24 Cells. *Can J Chem* **2010**, *88* (6), 569–576. https://doi.org/10.1139/V10-051.

(62) Zhao, X.; Zhu, R.; Anikovskiy, M.; Wu, Q.; Ding, Z. Profiling H2O2 from Single COS-7 Cells by Means of Scanning Electrochemical Microscopy. *Biosens Bioelectron* **2023**, *227*. https://doi.org/10.1016/j.bios.2023.115123.

(63) Zhang, M. N.; Ding, Z.; Long, Y. T. Sensing Cisplatin-Induced Permeation of Single Live Human Bladder Cancer Cells by Scanning Electrochemical Microscopy. *Analyst* **2015**, *140* (17), 6054–6060. https://doi.org/10.1039/c5an01148e.

(64) Zhang, M. M. N.; Long, Y. T.; Ding, Z. Cisplatin Effects on Evolution of Reactive Oxygen Species from Single Human Bladder Cancer Cells Investigated by Scanning Electrochemical Microscopy. *J Inorg Biochem* **2012**, *108*, 115–122. https://doi.org/10.1016/j.jinorgbio.2011.11.010.

(65) Zhang, M.-N.; Ding, Z.; Long, Y.-T. Sensing Cisplatin-Induced Permeation of Single Live Human Bladder Cancer Cells by Scanning Electrochemical Microscopy. *Analyst* **2015**.

(66) Filice, F. P.; Li, M. S. M.; Henderson, J. D.; Ding, Z. Mapping Cd2+-Induced Membrane Permeability Changes of Single Live Cells by Means of Scanning Electrochemical Microscopy. *Anal Chim Acta* **2016**, *908*, 85–94. https://doi.org/10.1016/j.aca.2015.12.027.

(67) Li, M. S. M.; Filice, F. P.; Henderson, J. D.; Ding, Z. Probing Cd2+-Stressed Live Cell Membrane Permeability with Various Redox Mediators in Scanning Electrochemical Microscopy. *Journal of Physical Chemistry C* **2016**, *120* (11), 6094–6103. https://doi.org/10.1021/acs.jpcc.6b00453.

(68) Li, M. S. M.; Filice, F. P.; Ding, Z. A Time Course Study of Cadmium Effect on Membrane Permeability of Single Human Bladder Cancer Cells Using Scanning Electrochemical Microscopy. *J Inorg Biochem* **2014**, *136*, 177–183. https://doi.org/10.1016/j.jinorgbio.2014.02.009.

(69) Henderson, J. D.; Filice, F. P.; Li, M. S. M.; Ding, Z. Tracking Live-Cell Response to Hexavalent Chromium Toxicity by Using Scanning Electrochemical Microscopy. *ChemElectroChem* **2017**, *4* (4), 856–863. https://doi.org/10.1002/celc.201600783.

(70) Filice, F. P.; Li, M. S. M.; Wong, J. M.; Ding, Z. The Effects of Long Duration Chronic Exposure to Hexavalent Chromium on Single Live Cells Interrogated by Scanning Electrochemical Microscopy. *J Inorg Biochem* **2018**, *182* (January), 222–229. https://doi.org/10.1016/j.jinorgbio.2018.02.009.

(71) Filice, F. P.; Henderson, J. D.; Li, M. S. M.; Ding, Z. Correlating Live Cell Viability with Membrane Permeability Disruption Induced by Trivalent Chromium. *ACS Omega* **2019**, *4* (1), 2142–2151. https://doi.org/10.1021/acsomega.8b02113.

(72) Mauzeroll, J.; Bard, A. J.; Owhadian, O.; Monks, T. J. Menadione Metabolism to Thiodione in Hepatoblastoma by Scanning Electrochemical Microscopy. *Proc Natl Acad Sci U S A* **2004**, *101* (51), 17582–17587. https://doi.org/10.1073/pnas.0407613101.

(73) Li, X.; Bard, A. J. Scanning Electrochemical Microscopy of HeLa Cells - Effects of Ferrocene Methanol and Silver Ion. *Journal of Electroanalytical Chemistry* **2009**, *628* (1–2), 35–42. https://doi.org/10.1016/j.jelechem.2009.01.002.

(74) Koley, D.; Bard, A. J. Triton X-100 Concentration Effects on Membrane Permeability of a Single HeLa Cell by Scanning Electrochemical Microscopy (SECM). *Proc. Natl. Acad. Sci. USA.* **2010**, *107* (39), 16783–16787. https://doi.org/https://doi.org/10.1073/pnas.1011614107.

(75) Kuermanbayi, S.; Yang, Y.; Zhao, Y.; Li, Y.; Wang, L.; Yang, J.; Zhou, Y.; Xu, F.; Li, F. In Situ Monitoring of Functional Activity of Extracellular Matrix Stiffness-Dependent Multidrug Resistance Protein 1 Using Scanning Electrochemical Microscopy. *Chem Sci* **2022**, *13* (35), 10349–10360. https://doi.org/10.1039/d2sc02708a.

(76) Li, Y.; Lang, J.; Ye, Z.; Wang, M.; Yang, Y.; Guo, X.; Zhuang, J.; Zhang, J.; Xu, F.; Li, F. Effect of Substrate Stiffness on Redox State of Single Cardiomyocyte: A Scanning Electrochemical Microscopy Study. *Anal Chem* **2020**, *92* (7), 4771–4779. https://doi.org/10.1021/acs.analchem.9b03178.

(77) Lang, J.; Li, Y.; Ye, Z.; Yang, Y.; Xu, F.; Huang, G.; Zhang, J.; Li, F. Investigating the Effect of Substrate Stiffness on the Redox State of Cardiac Fibroblasts Using Scanning Electrochemical Microscopy. *Anal Chem* **2021**, *93* (14), 5797–5804. https://doi.org/10.1021/acs.analchem.0c05284.

(78) Ye, Z.; Li, Y.; Zhao, Y.; Zhang, J.; Zhu, T.; Xu, F.; Li, F. Effect of Exogenous Electric Stimulation on the Cardiac Tissue Function In Situ Monitored by Scanning Electrochemical Microscopy. *Anal Chem* **2023**, *95* (10), 4634–4643. https://doi.org/10.1021/acs.analchem.2c04758.

(79) Nebel, M.; Grützke, S.; Diab, N.; Schulte, A.; Schuhmann, W. Microelectrochemical Visualization of Oxygen Consumption of Single Living Cells. *Faraday Discuss* **2013**, *164*, 19–32. https://doi.org/10.1039/c3fd00011g.

(80) Cremin, K.; Meloni, G. N.; Valavanis, D.; Soyer, O. S.; Unwin, P. R. Can Single Cell Respiration Be Measured by Scanning Electrochemical Microscopy (SECM)? *ACS Measurement Science Au* **2023**, *3* (5), 361–370. https://doi.org/10.1021/acsmeasuresciau.3c00019.

(81) Perry, D.; Paulose Nadappuram, B.; Momotenko, D.; Voyias, P. D.; Page, A.; Tripathi, G.; Frenguelli, B. G.; Unwin, P. R. Surface Charge Visualization at Viable Living Cells. *J Am Chem Soc* **2016**, *138* (9), 3152–3160. https://doi.org/10.1021/jacs.5b13153.

(82) Snowden, M. E.; Güell, A. G.; Lai, S. C. S.; McKelvey, K.; Ebejer, N.; O'Connell, M. A.; Colburn, A. W.; Unwin, P. R. Scanning Electrochemical Cell Microscopy: Theory and

Experiment for Quantitative High Resolution Spatially-Resolved Voltammetry and Simultaneous Ion-Conductance Measurements. *Anal Chem* **2012**, *84* (5), 2483–2491. https://doi.org/10.1021/ac203195h.

(83) Liu, L.; Etienne, M.; Walcarius, A. Scanning Gel Electrochemical Microscopy for Topography and Electrochemical Imaging. *Anal Chem* **2018**, *90* (15), 8889–8895. https://doi.org/10.1021/acs.analchem.8b01011.

(84) Kranz, C.; Christophe Demaille, C. HYBRID SCANNING ELECTROCHEMICAL TECHNIQUES: METHODS AND APPLICATIONS.; p 608.

(85) Kranz, C. Recent Advancements in Nanoelectrodes and Nanopipettes Used in Combined Scanning Electrochemical Microscopy Techniques. *Analyst* **2013**, *139* (2), 336–352. https://doi.org/10.1039/c3an01651j.

(86) Izquierdo, J.; Eifert, A.; Kranz, C.; Souto, R. M. In Situ Investigation of Copper Corrosion in Acidic Chloride Solution Using Atomic Force—Scanning Electrochemical Microscopy. *Electrochim Acta* **2017**, *247*, 588–599. https://doi.org/10.1016/j.electacta.2017.07.042.

(87) Mahankali, K.; Thangavel, N. K.; Reddy Arava, L. M. In Situ Electrochemical Mapping of Lithium-Sulfur Battery Interfaces Using AFM-SECM. *Nano Lett* **2019**, *19* (8), 5229–5236. https://doi.org/10.1021/acs.nanolett.9b01636.

(88) Shi, X.; Qing, W.; Marhaba, T.; Zhang, W. Atomic Force Microscopy - Scanning Electrochemical Microscopy (AFM-SECM) for Nanoscale Topographical and Electrochemical Characterization: Principles, Applications and Perspectives. *Electrochimica Acta*. Elsevier Ltd February 1, 2020. https://doi.org/10.1016/j.electacta.2019.135472.

(89) Hsu, J. W. P. *Near-Field Scanning Optical Microscopy Studies of Electronic and Photonic Materials and Devices*.

(90) Lee, Y.; Bard, A. J. Fabrication and Characterization of Probes for Combined Scanning Electrochemical/Optical Microscopy Experiments. *Anal Chem* **2002**, *74* (15), 3626–3633. https://doi.org/10.1021/ac015705d.

(91) Takahashi, Y.; Hirano, Y.; Yasukawa, T.; Shiku, H.; Yamada, H.; Matsue, T. Topographic, Electrochemical, and Optical Images Captured Using Standing Approach Mode Scanning Electrochemical/Optical Microscopy. *Langmuir* **2006**, *22* (25), 10299–10306. https://doi.org/10.1021/la0611763.

(92) Lipson, A. L.; Ginder, R. S.; Hersam, M. C. Nanoscale in Situ Characterization of Li-Ion Battery Electrochemistry via Scanning Ion Conductance Microscopy. *Advanced Materials* **2011**, *23* (47), 5613–5617. https://doi.org/10.1002/adma.201103094.

(93) Izquierdo, J.; Knittel, P.; Kranz, C. Scanning Electrochemical Microscopy: An Analytical Perspective. *Analytical and Bioanalytical Chemistry*. Springer Verlag January 1, 2018, pp 307–324. https://doi.org/10.1007/s00216-017-0742-7.

(94) Bard, A. J.; Faulkner, L. R. *Electrochemical Methods Fundamentals and Applications*, 2nd ed.; Wiley.

(95) Madhan Kumar, A. The Utilization of Scanning Electrochemical Microscopic (SECM) Technique in Corrosion Monitoring. In *Recent Developments in Analytical Techniques for Corrosion Research*; Springer International Publishing: Cham, 2022; pp 51–90. https://doi.org/10.1007/978-3-030-89101-5_4.

(96) Morkvenaite-Vilkonciene, I.; Kisieliute, A.; Nogala, W.; Popov, A.; Brasiunas, B.; Kamarauskas, M.; Ramanavicius, A.; Linfield, S.; Ramanaviciene, A. Scanning Electrochemical Microscopy: Glucose Oxidase as an Electrochemical Label in Sandwich Format Immunoassay. *Electrochim Acta* **2023**, *463*. https://doi.org/10.1016/j.electacta.2023.142790.

(97) Fernández, J. L.; Bard, A. J. Scanning Electrochemical Microscopy 50. Kinetic Study of Electrode Reactions by the Tip Generation-Substrate Collection Mode. *Anal Chem* **2004**, *76* (8), 2281–2289. https://doi.org/10.1021/ac035518a.

(98) Cannan, S.; Cervera, J.; Steliaros, R. J.; Bitziou, E.; Whitworth, A. L.; Unwin, P. R. Scanning Electrochemical Microscopy (SECM) Studies of Catalytic EC′ Processes: Theory and Experiment for Feedback, Generation/Collection and Imaging Measurements. *Physical*

Chemistry Chemical Physics **2011**, *13* (12), 5403–5412. https://doi.org/10.1039/c0cp02530e.

(99) Zhang, Q.; Ye, Z.; Zhu, Z.; Liu, X.; Zhang, J.; Cao, F. Separation and Kinetic Study of Iron Corrosion in Acidic Solution via a Modified Tip Generation/Substrate Collection Mode by SECM. *Corros Sci* **2018**, *139*, 403–409. https://doi.org/10.1016/j.corsci.2018.05.021.

(100) Hynek, D.; Zurek, M.; Babula, P.; Adam, V.; Kizek, R. Monitoring of the Surface Modification of Nanoparticlesby Electrochemical Measurements Using Scanning Electrochemical Microscope. In *Modern Electrochemical Methods in Nano, Surface and Corrosion Science*; InTech, 2014. https://doi.org/10.5772/57203.

(101) Eckhard, K.; Chen, X.; Turcu, F.; Schuhmann, W. Redox Competition Mode of Scanning Electrochemical Microscopy (RC-SECM) for Visualisation of Local Catalytic Activity. *Physical Chemistry Chemical Physics* **2006**, *8* (45), 5359–5365. https://doi.org/10.1039/b609511a.

(102) Karnicka, K.; Eckhard, K.; Guschin, D. A.; Stoica, L.; Kulesza, P. J.; Schuhmann, W. Visualisation of the Local Bio-Electrocatalytic Activity in Biofuel Cell Cathodes by Means of Redox Competition Scanning Electrochemical Microscopy (RC-SECM). *Electrochem commun* **2007**, *9* (8), 1998–2002. https://doi.org/10.1016/j.elecom.2007.05.015.

Chapter 2

Optical fibers in analytical electrochemistry: Recent developments in probe design and applications

While Chapter 1 gives us an outlook on the technique and biological applications of SECM, this chapter serves as an introduction to the advancement of SECM to SPECM. Optical fiber probe is a key component in SPECM, and reviewing their development and progress in analytical electrochemistry is essential to understanding their versatility. Optical fiber probes have been utilized by researchers since the 1980s in a variety of applications, including materials science, energy, biomedical research, and scanning probe instrumentation.

This chapter provides a comprehensive literature review on the different types of optical fiber probes and fabrication methodologies developed over the years. It highlights how these probes have been modified to meet the specific needs of various scientific applications, such as sensing and scanning. The review also covers research that has employed optical fiber probes in SPECM for illumination and probing photoelectrochemical reactions. Furthermore, it discusses future possibilities for optical fiber probes in distinct interdisciplinary fields.

This chapter has been published in the TrAC Trends in Analytical Chemistry and is reproduced from: *Thomas, N., Singh, V., Kuss, S. (2021) Optical Fibers in Analytical Electrochemistry: Recent Developments in Probe Design and Applications. TrAC Trends in Analytical Chemistry, 136, 116–196.* *https://doi.org/10.1016/j.trac.2021.116196*. As specified by the journal and as an author of this Elsevier article, I'm not required permission to include it in the thesis.

NT and VS contributed to the literature review, writing the manuscript, and preparing figures and tables. SK provided guidance on writing, editing, finalizing the figures, and bringing the manuscript to completion.

2.1 Abstract

The integration of optical fibers into electroanalytical instrumentation enables the sensitive detection and quantification of micro- and nanoscopic processes by photoelectrochemistry. This review provides a comprehensive literature overview on the design and fabrication of different types of optical fiber probes for scanning probe techniques, such as scanning electrochemical microscopy and scanning photoelectrochemical microscopy. Optical fiber probes have been classified into single optical electrodes, comprising of disk, ring and lateral surface electrodes, and multi- electrode systems, including optical fiber arrays. Fiber optics technology has influenced probe design and fabrication for scanning probe microscopy techniques, surface characterization of photoactive materials and corrosion films, and moreover bioelectrochemical sensing and imaging of living cells. Underlying principles and the implementation of optical fibers into these applications are discussed in detail and recent developments and future prospects are highlighted.

2.2 Introduction

Optical fibers (OFs) gained significant attention in electroanalytical chemistry over the last decade, as they become increasingly useful for imaging of micro- and nanoscopic surfaces in a variety of industrial and biological processes (Figure 4.1). The use of OFs in combination with micro- and nanoelectrodes enables the quantification of various processes down to a resolution at the nanoscale. OFs consist of an inner core, surrounded by cladding of a lower refractive index than the core material, followed by a buffer and jacket.[1,2] OFs function based on the principle of total internal reflection.[1,2] Depending on the light path, there are two kinds of OFs: single mode fibers (SMF, core diameters of 5 or 10 µm) and multi-mode fibers (MMF, core diameter of 50 to 62.5 µm).[2] In the literature, OFs have also been classified based on structure, refractive index profile, dispersion and signal processing ability.[2]

Transmitting light through glass rods was first achieved by scientists in the 19th century. Robert Maurer, Donald Keck, and Peter Schultz designed "Optical Waveguide fibers,"[3] which revolutionized the telecommunication system in the 20th century.[4] The term "fiber optics" was mentioned first in 1967 by Narinder Singh Kapany for the design and application of OFs.[5]

Advantages, such as high sensitivity, lack of electromagnetic interference, small size, light weight, robustness, and the cost effective nature of OFs has made them widely employed for developing sensors of various kinds .[6] Today, OF sensor measurements are based on absorbance, reflectance, luminescence (fluorescence, phosphorescence, chemiluminescence), reflective index change or light scattering.[6] Specifically, Surface Enhanced Raman Spectroscopy (SERS), based on OF probes, made significant contribution in nano-sensing applications.[7]

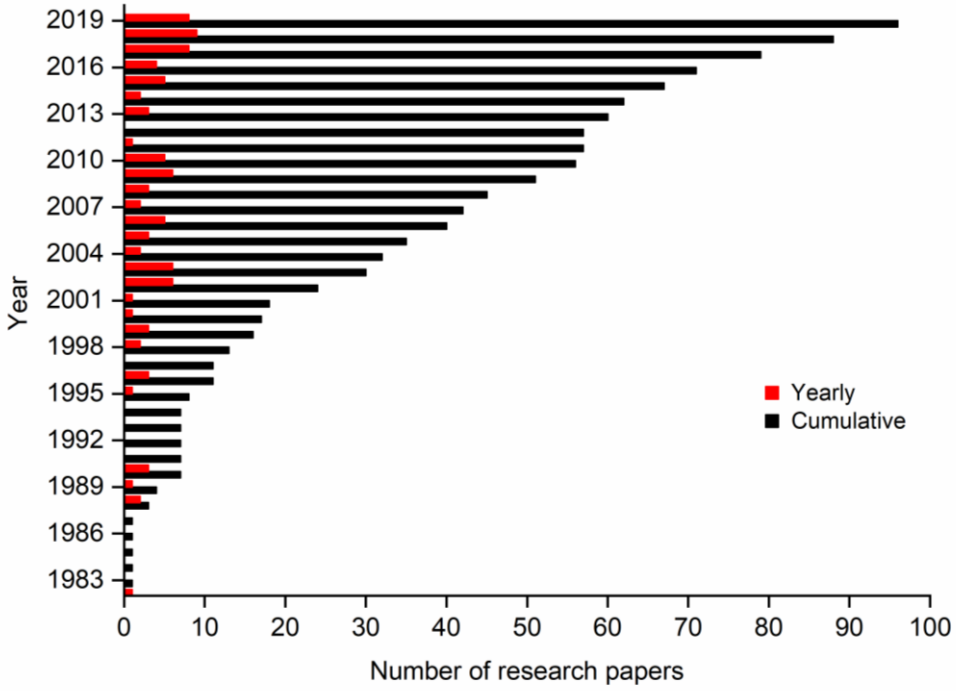

Figure 2.1 *Graphical representation of yearly and cumulative appearance of research articles published from 1982 to 2019.*

Beyond sensing applications, the development of ultramicroelectrodes (UMEs) played a significant role in the emergence of optoelectrodes for scanning applications. It led to the development of scanning tunneling microscopy (STM) by Binnig and Rohrer,[8] which thereafter gave rise to scanning probe microscopy (SPM) techniques, primarily for imaging purposes.[9–11] Among various SPM techniques, the invention of scanning electrochemical microscopy (SECM) by Allen J. Bard in 1989 paved the path for high resolution electroanalysis of a sample's topography as well as reactivity.[12] A daughter technique of SECM, which gained popularity during the most recent years is scanning photoelectrochemical microscopy (SPECM), which facilitates

simultaneous imaging and photocurrent measurements. OF UMEs are widely used in SPECM as a waveguide for illuminating a specimen and to probe local photoelectrochemical reactions, simultaneously.

The fabrication of OFs in electrochemistry has been explored and reviewed in the literature.[13–15] For example, a concept of electrogenerated chemiluminescence at ultramicroelectrode was proposed by Bard et al in 1998.[16] Later, in 2003 by Szunerits and co-authors summarizes the developments in micro optical ring electrode arrays for fluorescence and electrochemiluminescence imaging.[17] The authors describe the fabrication of an optoelectrochemical microring array, where the OFs are coated with gold via electro-less gold deposition (see Section 2.3.2) for simultaneous electrochemical and optical measurements. Thirteen years later in 2016, Tuan Guo reviewed the advantages of using metal coated tilted fiber Bragg grating (TFBG) OFs using Surface Plasmon resonance in biochemical and electrochemical sensors.[18] However, a comprehensive literature review about state-of-the-art OF probes and their application in electroanalytical chemistry is missing. The presented review covers various types of OF electrodes, focusing on the design and fabrication of probes for electrochemical sensing of photoactive materials in research fields ranging from energy applications to surface corrosion to biological sciences. More than 100 research articles have been published since 1982 (Figure 2.1), indicating the importance of a critical review on the implementation of OFs in analytical electrochemistry. This review reports on principles, such as electrode structure and surface modification, but also highlights the combination of photoelectrochemistry and scanning electrochemical microscopy to benefit analytical chemists, interdisciplinary researchers and quantitative bioelectrochemistry researchers.

2.3 Optical Fiber Electrodes

This section covers advancements in the designing and fabrication of OF electrode. Nowadays, electrodes have been designed for cost-effective and environment-friendly scanning probe microcopy applications at high resolution. In the following we discuss different types of available electrode, including single optical electrodes, optical arrays and optical ring electrodes. Detailed

fabrication approaches are presented, followed by a review of applications in various fields to investigate the electrode/electrolyte interface at the micro/nanometer scale.

2.3.1 Single Optical Electrodes

To understand microscopic phenomena occurring at the electrode/electrolyte interface using photo-electrochemical visualization, various shapes (disk, ring and lateral) of OF microelectrodes have been developed.[19] Typically, all optical electrode consists of three essential components, which include the OF, a metal as a conductive sensor and insulating coating. Depending upon the shape of the metal component, optical electrode can be classified as disk, ring or lateral shaped electrode (Figure 4.2 A-C). In order to fabricate these optical electrode, various methodologies have been explored to optimize the tip of the optical electrode and its ability to visualize important processes, such as photoelectrocatalytic water splitting[20–22], single cell imaging[23,24], and corrosion[25–27]. Over the past decade, it was shown that the shape and size of the optical electrode play a crucial role to accurately estimate the electron transfer and evaluate the related processes at heterogeneous interfaces.[28] OF electrodes not only serve as light guide, but also to function as micro/nanoelectrode, and therefore enables the simultaneous collection of both electrochemical and photochemical response with exceptional resolution and selectivity over the submicron surface. In this section, we present several fabrication methodologies developed.

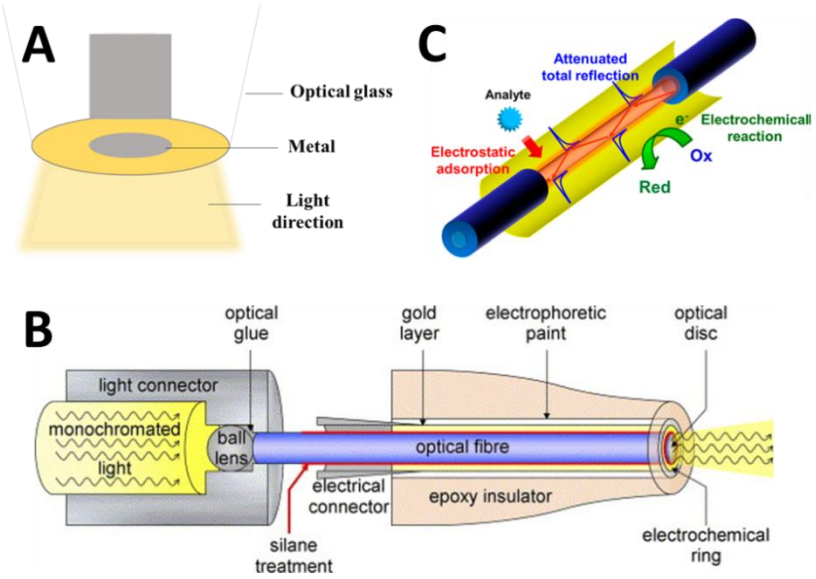

Figure 2.2 *Structural representation of various optical electrode (A) disk-shaped, (B) ring-shaped and (C) lateral-shaped respectively. B and C are taken from reference*[29,30]

2.3.1.1 Optical Disk Electrodes

Towards the development of optical disk electrode, Samina S. Khan and co-authors discovered the concept of electrochemically modulated, fluorescence-based imaging fiber electrodes (IFEs).[19] In short, an IFE was fabricated using a silica fiber with a diameter of 350 µm, which is composed of 6000 individually cladded OFs of 3 µm in diameter (Figure 2.3A). Prior to use, the distal end of the fiber was cleaned using acetone and polished with various grades of lapping film. In order to coat the gold film on an imaging fiber, initially, silanization was performed by placing the fiber in an aminated solution using 3-(mercaptopropyl)-trimethoxysilane (MPS).[31] The fiber was rinsed several times with isopropanol and water and then kept in a drying oven for 8 minutes at 105°C. The semi-transparent gold layer was coated on top of the MPS-silanized fiber using a sputtering coater. Nafion coating was then achieved by vertically placing the gold containing IFE onto a spinner mixer-head. The Nafion coating was dried at room temperature. In order to prepare a rhodamine B isothiocyanate (RBITC) and IFE conjugate (RBITC-IFCP), the Nafion-modified IFE, was immersed into a 0.25 mM RBITC/PBS solution for 2 hours, which resulted in the formation of fully functional RBITC-IFCPs for the detection of peroxide (H_2O_2) with high regeneration ability (95%). This was accomplished by monitoring the change in fluorescence of the immobilized fluorescent redox dye as a result of homogeneous and heterogeneous electron transfer reactions when the electrode was kept in PBS containing H_2O_2 (Figure 2. 3 A-B).

Most recently in 2020, Bobo Du and co-workers utilized plasmonic nanostructures that find application in various fields, such as nanophotonics, photochemistry, and chemical sensing, to functionalize IFEs.[32] Plasmonic fiber sensors were developed, by utilizing a gold nanomembrane attached to the fiber end face by epoxy and MoS_2 coating on the gold membrane (Epoxy/Au/MoS_2) (Figure 2.3 C). A template transfer methodology was adopted using a Si-template of a hexagonal nanohole-array with 200 nm in diameter and 700 patterns using electron beam lithography. Subsequently, a 100 nm thin layer of gold was coated over the Si-template. Epoxy was applied to the gold coated Si-template using 1 µm thermal-curing for 4 hours. The Si-template was detached carefully which leaves behind the nanohole array. The authors determined an epoxy layer thickness of 100 µm, which counterbalances the light coupling from the fiber core to the gold membrane. A monolayer of MoS_2 was then grown on top of the expoxy/Au nanostructure by chemical vapor deposition (CVD) using a polystyrene and toluene mixture. A water droplet was then placed on

top of the obtained sample, which results in the formation of Polystyrene/MoS_2 composite, which is sequentially transferred to the fiber end facet (Figure 2.3C). Achieving high selectivity and specificity at room temperature is typically challenging, especially for micro- and nanosensors. However, the OF sensor design by Du *et al* enables the sensitive and selective detection of methanol (gas) at room temperature.[32]

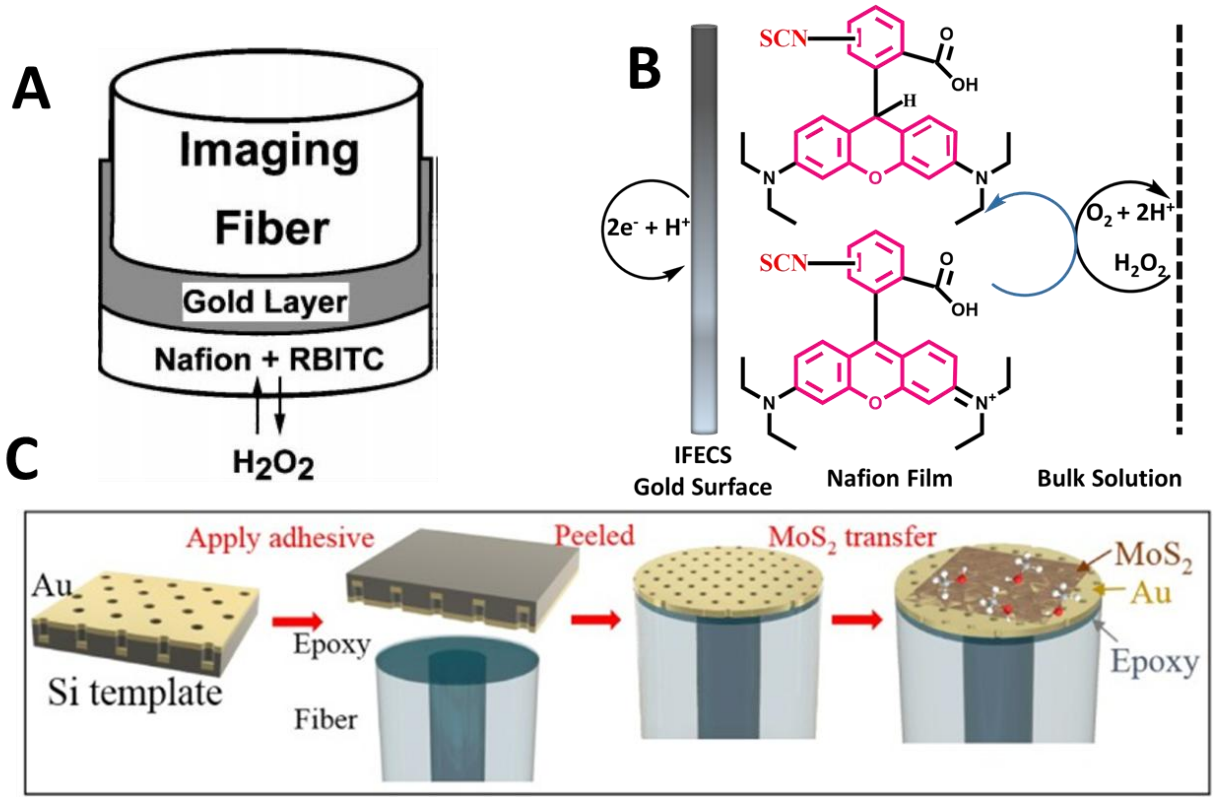

Figure 2.3 *Schematic representation of disk-shaped optical electrode, (A) represents the distal tip of a RBITC-imaging fiber electrode and chemical sensor along with its sensing principle (B).*[19] *(C) Fabrication strategy for the design of Epoxy/Au/MoS_2 fiber-optic gas sensor structure. The dark yellow and brown layer depicts the gold membrane and MoS_2 respectively.*[32] *(B is redrawn based on Ref 19 for clarity).*

2.3.1.2 Optical Ring Electrodes

Early work on the fabrication of micro-optical ring electrodes (MOREs) was increasingly presented in the 1990s[33–35] and researchers explored the effect of geometry as well as radius ratio of ring *vs.* disk. [29,36] The fabrication of micro-optical ring electrodes (MOREs) is similar to the scanning electrochemical microscopy/photoelectrochemical microscopy (SECM/PEM) tip

fabrication procedure developed by Bard *et al* and stepwise includes: heating and pulling of the OF, metal coating, electrical insulation, and exposing the electrode tip.[37]

Typically, an OF with a known diameter is chosen and thoroughly cleaned. After rinsing several times with ethanol, the electrode is dried. The cleaned OF is heated and pulled down to a micro- or nanometer scale of 50 to 100 nm using a CO_2 laser puller. An important point to be considered is that OFs can lose light during illumination by scattering, and therefore a suitable coating is necessary. A suitable coating source is the use of a reflective metal, such as aluminum, which can effectively avert the loss of light during illumination. Other electrode materials, such as Au and Pt, can also be employed owing to the advantages of easy evaporation under vacuum and therefore can serve as both ultramicroelectrode and reflective coated layer. The coating of Au and Pt is performed by placing the OF at an angle of 45° and with a rotation speed of 30 revolutions per minute under vacuum. The metal coated OF tip is then connected to a power source. Before electrochemical measurements can be taken, electrical insulation and exposure of the tip is performed to achieve the desired electrode with suitable size and shape. Generally, the tip of the OF is insulated with anodic electrophoretic paint, which consists of polyacrylic acid (PAAH) in the presence of an excess of a base.[38] The metal-coated OF is immersed into the anodic paint solution and a particular alterative current (AC) or direct current (DC) voltage is applied between the pulled OF and Pt-coil until the current dropped to a stable steady state value. Due to a local decrease in pH, induced by the oxidation of water, water insoluble PAAH deposits onto the metal coated OF. Curing is performed to obtain a sharp and geometrically well-defined end of the fiber by heating the insulated OF at 150 °C for a few minutes, followed by another insulation step in a dilute solution of PAAH. Following this procedure, OFs with outer radii of 100 nm can be achieved, whereby the shape and size of the tip depends strongly on pulling parameters, such as heating power of the instrument, laser spot size, pulling power, pulling velocity and time-delay in reaching the particular pulling velocity to pull it apart. After fabrication, MOREs must be tested for a reproducible electrochemical current response.

In order to overcome challenges associated with inconsistent heating and pulling during fabrication, Xiong and co-worker reported in 2004 a new methodology of etching the OF, which served as a template for the design of selective electrode.[39] Usually, in this approach, GeO_2-doped

SiO_2 core, SiO_2 inner cladding, and F-doped SiO_2 outer cladding was etched in buffered hydrogen fluoride (BHF) solution containing NH_4F (40 wt%)/HF (50 wt%)/H_2O (Figure 2.4 A-B). The etching process was performed several times under controlled conditions at a concentration ratio of X:1:Y (where X = NH_4F, Y = H_2O and 1 for HF) for optimized duration and temperature to obtain the desired nanoelectrode. The coating of metal (Au) was performed over the specifically etched fiber by gold- sputtering with a known thickness at the nanometer scale using anodic electrophoretic paint as described above.[38] This methodology was adopted by various research groups to design optical nanoelectrode with high selectivity and resolution. K. Maruyama and co-workers developed various electrode with tip-shapes, such as protruding, pencil and triple-tapered electrode surfaces.[40] To fabricate pencil-shaped electrode, initially, the authors etched the OFs (Figure 4.4 B-I) followed by preparing its electrode using the above-mentioned approach. Scanning electron microscopy (SEM) was used to characterize the pencil-shaped OFs (Figure 2.4 B-I-III). Importantly, the authors achieved a tip radius scaling down to 5 nm by optimizing the etching parameters (Figure 2.4 B).[40]

Another approach to fabricate MOREs was presented by S. Wu and co-worker, utilizing electroless coating of gold at polycarbonate (PC) rods under ambient conditions (Figure 4.4 C).[41] For this approach, the authors adopted and modified the methodology developed by Chen *et al* for plating gold on a PC plate.[42] Initially, the functionalization of PC rods was achieved by exposing rods to UV-light using a low pressure mercury lamp (k = 254 nm, 30 mW) for about 12 hours. In order to obtain a uniform distribution of the carboxylic groups over the rod surface, rods were continuously rotated by placing it on rotating plate at a gap of 3.5 cm from the UV lamp (Figure 4.4 C). The amination of the obtained functionalized rods was achieved by immersing them into phosphate buffered saline (PBS) at a pH of 7.0, containing 50 mM of 1-(3-Dimethyl-aminopropyl)-3-ethylcarbodiimide hydrochloride (EDC) and 0.36 M ethylenediamine for 3 hours. Consequently, a thin layer of Au-nanoparticles (Au-NPs) was casted over the PC rods, by placing them into a solution comprising of 1 mM $HAuCl_4$ for 2.5 hours, followed by 10 min in 0.1 M $NaBH_4$. The obtained gold thin layer acted as the catalytic center for further growth of Au-nps when the PC rods were immersed in a solution containing $Na_3Au(SO_3)_2$, Na_2SO_3 and HCHO. The oxidation of HCHO results in the deposition of Au-NPs under the given set of conditions and the electrode is

further annealed at 130 °C for 3 hours. A Cu-tape was placed at one end to achieve the electrical contact followed by insulation with a thin layer of melt adhesive (Figure 2.4 C).

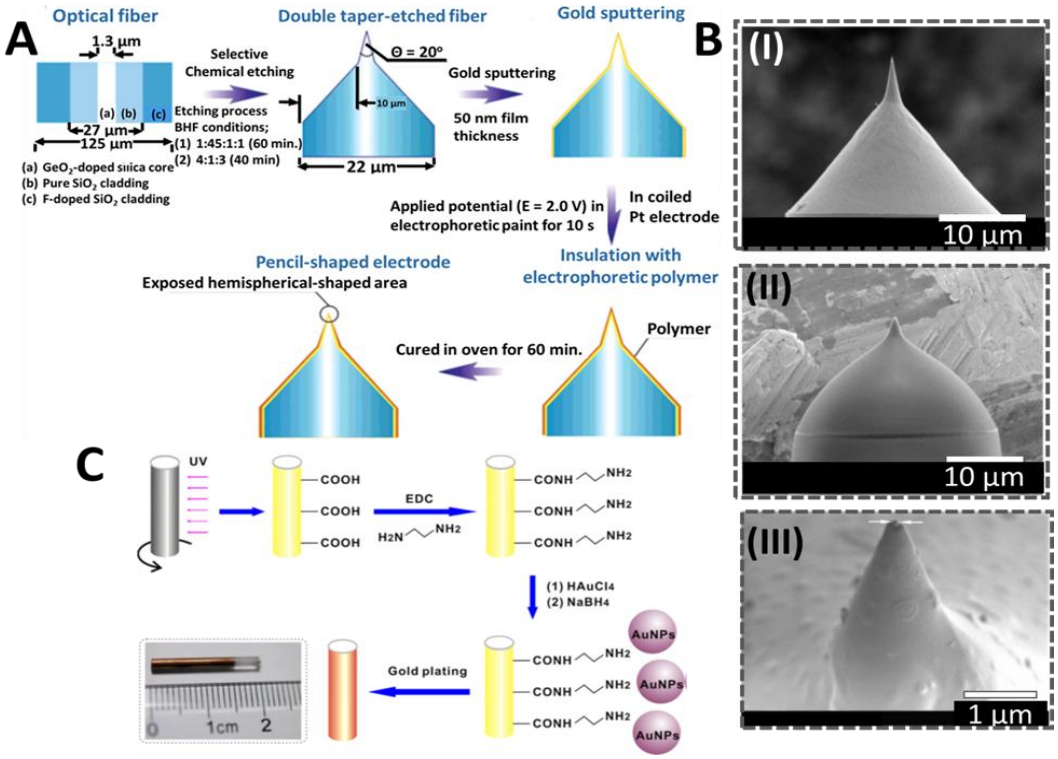

Figure 2.4 *(A) Schematic illustration of the fabrication methodologies developed for designing pencil-shaped MOREs, (B) SEM images of different types of MORE obtained by selective chemical etching under optimized conditions, (I) etched OF, (II) pencil-shaped electrode in front view and (III) top view of pencil-shaped MORE.*[40] *(C) Stepwise representation for designing the microring electrode using PC-rod. The inset shows an optical photograph of the designed electrode.*[41]

In 2005, I. Svir *et al* developed a technique for the fabrication of MOREs using photolithography.[43] Initially, glass wafers were chosen and cleaned with acid, followed by continuous rinsing and washing with Millipore water. The cleaned wafers were dried in a nitrogen flow. A gold microring pattern was created over the wafers by the photolithographic technique using a projection printing system. This step requires a technical drawing software platform to create a scaled black and white sculpture of the microring, which is transferred onto the high resolution millimask negative plates using photographic techniques. A thin layer (app. 5 µm) of photoresist material was obtained using a spin coater and further baked over a hot-plate at 115 °C for 1 minute. The obtained millimask

plates were used to project the UV light source from a maskaligner onto the substrate containing a thin layer of photoresistive material. The bare layer of photoresist was developed using a developer solution to expose the desired photoresist microring pattern. The metal (titanium/gold) coating over the patterned substrate was achieved by a metal evaporator under vacuum. The metal coated substrate was then kept in acetone to remove the photoresist material and to finally reveal the microring pattern. The authors characterized the thickness of the microring to be around 80 nm using atomic force microscopy (AFM).

2.3.1.3 Optical Lateral Surface Electrodes

The use of OFs as lateral electrodes was firstly discovered by Beam and co-workers in 2008.[44] They have utilized the advantage of an optic electroactive fiber chip as a model to fabricate the electrodes and, more importantly, to understand both photo- and electrochemical processes under controlled conditions. The fabrication methodology in this publication initially involved polishing of an OF, mounted on a V-shaped groove to create a planer surface to minimize loss of light (Figure 2.5 A). Typically, an OF with a 50 µm core diameter step-index, MMF, a 125 µm cladding diameter and a numerical aperture (NA) of 0.22, was mounted onto a glass V-groove, using thermally curing epoxy. Further polishing was conducted to expose the fiber core as a waveguide for the spectroelectrochemical measurements. The sensitivity of the exposed area was characterized by monitoring the absorbance using self-assembled polyelectrolyte films. To improve the electroactivity of the optical chip, a uniform and defect free thin (40 nm) coating of Indium-tin oxide (ITO) was achieved using sputter deposition under vacuum. A In_2O_3/SnO_2 (90/10 wt %) 3-inch diameter target was sputtered at 200 W for 4 minutes to produce a 40 nm thick film of ITO. Subsequently, the electroactive optical chip was annealed at 300°C for 10 minutes under vacuum to produce an effective sheet with a resistance of 200 Ω. The thickness of the ITO layer was assessed using AFM measurements. Finally, the electrical connection was established by placing silver paste on the edge of the V-grove and externally connecting to the light source and potentiostat to perform spectroelectrochemical analyses.

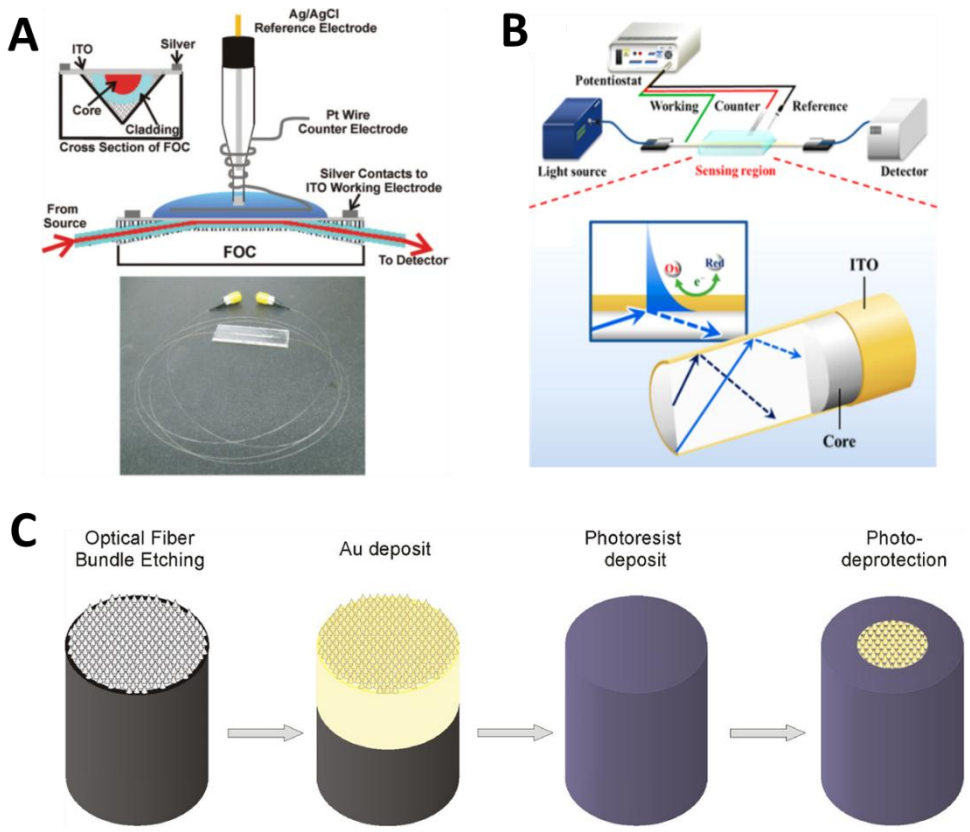

Figure 2.5 *Schematic representation of lateral shaped electrodes with their experimental set-up, working components and principle for an (A) EA-FOC (inset showing cross-section view)* [44]*, and (B) OTE based electrode.*[45] *(C) Schematic visualization of the step-wise design of optical array electrodes.*[46]

In 2015, Kenichiro Imai *et al* developed a spectroelectrochemical fiber optic sensor, which exhibits three modes of operation i.e. electrochemistry, spectroscopy and electrostatic adsorption.[30] The design and fabrication of the proposed sensor is simple and composed of a gold mesh over a multimode fiber, which enables attenuated total reflection as the optical detection mode. The sensing principle is based on the variation in the loss of light intensity passing through the fiber core, accompanying the electrochemical redox processes at the electrode surface. In this fabrication process, a multimode plastic-clad optical silica fiber with a core diameter of 200 µm was chosen (Figure 2.5 B). Prior to use, the optical fiber was cut into small units and plastic cladding was removed to up to 8 cm in length using acetone. An (3-Aminopropyl)triethoxysilane (APTES) immobilized fiber was obtained using a silane coupling reaction. Initially, the exposed 8

cm core of the fiber was activated by placing it in 1 M NaOH for 1 hour, followed by rinsing it several times with Millipore water. Subsequently, the silanization was achieved by placing the activated core fiber in a solution of acetone containing APTES for 1 minute at room temperature. After the silanization, the self-assembled monolayer was applied onto the core of the optical fiber using Polyallylamine hydrochloride (PAH) and poly{1-[4-((3-carboxy-4-hydroxyphenyl)azo)-benzenesulfonamido]-1,2-ethanediyl, sodium salt} (PCBS) polycation and polyanion, respectively. The PCBS layer was obtained on the fiber containing APTES layer by immersing it in a solution containing PCBS (10 mM) at room temperature for 15 minutes. A bilayer of PCBS/PAH with a thickness of 1.5 nm was achieved when the authors placed the PCBS/APTES-fiber in PAH solution under the same conditions. In a most recent study published in 2018 by Takuya Okazaki *et al*, the authors developed a scalable approach by fabricating disposable electrode using ITO over the optic fiber using same methodology described above**.**[45]

2.3.2 Multi-Electrode Systems

The design and fabrication of optical electrodes for their integration into scanning probe techniques is often based on opto-electrochemical arrays composed of a micro-ring as working electrode. This concept finds widespread interest and application to characterize photoelectrochemical processes at the nano- and microscopic level.[47,48] These electrodes possess all necessary advantages of a single optical micro-ring electrode, including the ability to obtain higher currents due to the increased number of working electrodes, quick response time and steady-state behavior.[17,49] The advantages of designing optical array electrodes over a single optical electrode is that in the former, higher currents can be achieved without any change in the micro-/nanoelectrode behavior and therefore, high resolution can be obtained during the photoelectrochemical measurements.Because of these advantages, it is not surprising that various research groups have explored different methodologies for the fabrication of multi-electrode systems.

In the context of designing and utilizing OF arrays, Szunerits and co-workers, developed an interesting methodology for the fabrication of an optical micro-ring electrode array based on the deposition of Au-nanoparticles on OFs via the electro-less approach published in 2002.[17] The authors fabricated an optical micro array with a diameter of 25 µm, consisting of 600 individual OFs, followed by the removal of the insulation and cleaning the system several times using ethanol

and water. Initially, deposition of Sn^{2+} on cleaned OFs was achieved by immersing electrodes in a solution containing Sn^{2+} ions and triflouroacetic acid in a water and methanol mixture (50% v/v) for 20 minutes. The coated OFs were rinsed with methanol several times to remove the excess adsorbed Sn^{2+} particles, followed by immersing them into an ammonical $AgNO_3$ solution for 15 minutes. During this procedure Ag-particles deposit on to the surface of OFs, which is catalyzed by the Sn^{2+} ions. The Ag-coated OFs were then dipped into a solution containing Au-ions, Na_2SO_3 and formaldehyde different concentrations during stirring for 1 hour.[17] The formaldehyde present in the solution chemically oxidizes the Ag-particles, while concurrently Au-ions are reduced and deposited over the surface of the fiber. The gold-nanoparticles containing OFs were washed gently with dilute Nitric acid followed by rinsing with methanol and water several times. The electrode insulation was achieved by placing the gold-coated OFs into ethanolic solutions of 11-mercapto-1-undecanol, followed by curing at 100 °C for several hours. A subsequent study published in 2003 by the same authors, developed a submicron-sized optical array by employing chemical etching of the OF bundle as described above (section 2.1.2).[17] The authors demonstrated a novel opto-electrochemical micro-ring array, which probed electrochemical reactions wherein the chemical compounds emit light upon electrochemical stimulation. To achieve the targeted signal amplification, diffusional overlap was optimized by statistically spacing the individual conducting optoelectrochemical electrodes in the array. This would empower stimulating a target cell amongst a pool of non-target cells by either detecting an optical signal from the target cell followed by delivering electric current to it, to destroy the target cell or *vice-versa i.e.,* detect electrochemically and stimulate optically.

Most recently in 2019, Bombail and co-authors, fabricated a dual electrode for spectroelectrochemical analysis by depositing the gold over optical array (Figure 2.5C).[46] In their fabrication process, a nanotip-array was produced on top of OF bundle under chemical etching conditions, followed by deposition of a gold layer and finally insulated by photolithography (Figure 2.5 C). A 350 µm diameter OF bundle, which is composed of 6000 individually cladded cores, exhibiting an overall diameter of 3-4 µm, was chosen. Chemical etching was performed using the methodology developed by Xiong and co-worker (NH_4F and HF) described above.[40] After etching and drying the fiber bundle, a 40 nm thick gold layer was coated on the sensor using

a magnetron sputtering setup. Finally, a connection was established to the fiber bundle using a Cu-wire and further insulation by a tunable coating of photoresist material was carried out.

2.3.3 Other Approaches

One of the most important advancement in the field of MOREs was reported by Julie V. Macpherson and co-workers in 1998, by developing hydrodynamic optical UMEs by coupling a MORE with a high-speed upright impinging microjet.[50] In this setup, called radial flow micro-ring electrode (RFMRE), the solution flows through a capillary nozzle, which is aligned in close proximity to the substrate with the help of a micro-positioner. The authors explored two operating configurations: The ring electrode material was coated around the microject capillary, or the ring electrode was positioned on the substrate directly underneath the capillary. In both these configurations, the fluid flowing through the capillary is forced into the nozzle/substrate gap generating a radial flow past the ring electrode (Figure 2.6A-B). These hydrodynamic optical electrodes can be characterized by a well-defined and variable mass transport rate under steady state voltammetric conditions. In a subsequent study in 2007, the authors designed hydrodynamic optical electrodes by coupling MOREs with a speed impinging microjet, resulting in a variable thickness of the ring. In this study, the authors designed two types of ring electrodes based on an OF, coating a thin metal film and insulating them either using epoxy resin or glass.[51] Two types of insulating materials were used to fabricate the isolated ring in the hydrodynamic electrodes. In one case, the metal-coated OF was immersed into a cylindrical Teflon mold, containing epoxy resin for 48 hours. In another approach, a coated fiber was inserted into a pulled and sealed borosilicate glass capillary with an outer and inner dimension of 2.0 mm and 1.16 mm, respectively. In order to seal another end of the capillary, a vertical puller was used by heating the coil at a temperature range of 700-800 °C. This step has been considered as the critical step, as metal can form clusters under high temperature during the sealing procedure. Finally, the electrode surface was cleaned using diamond impregnated pads. Upon polishing, thin ring microelectrodes with radii in the range of 100-300 nm were obtained and further characterized by employing an impinging microjet system. Both specifically designed hydrodynamic microelectrodes show an increase in the mass transport-limited current, which was highly dependent upon the flow rate as commonly observed in macro rotating ring-disk electrodes (RRDE).[52,53] More importantly, the authors found that the

glass-sealed microelectrode showed a better electrochemical current response and reproducibility over epoxy resin.

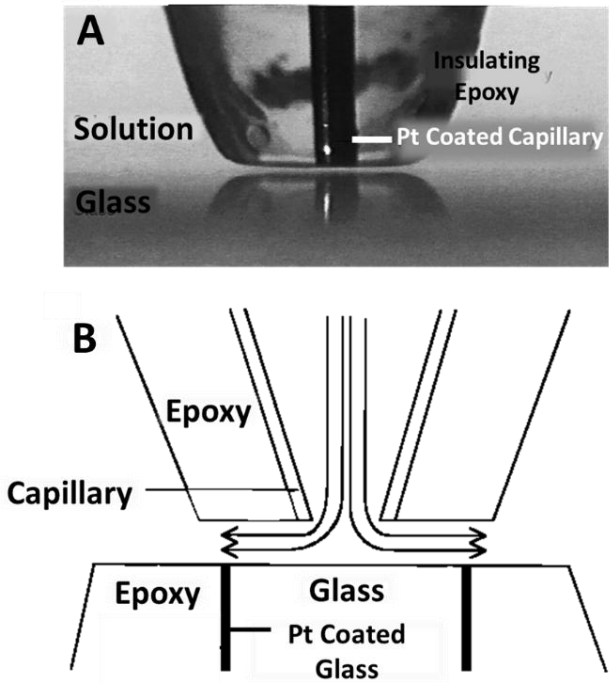

Figure 2.6 *(A) Video microscopy image of the radial flow microring electrode (RFMRE), and (B) represents the schematic representation of cross section of the RFMRE with the ring electrode positioned centrally underneath the capillary nozzle.*[50]

Dual disk-shaped ultramicroelectrodes are another alternative which can be explored to trap various intermediate species independently during the electrochemical process which could be instrumental in mechanistic analysis. The fabrication involves a dual-barrel quartz 'theta' capillary pulled to a sharp point of known diameter using a laser-puller as described above.[21] The designing of such dual electrodes allowed new advancement in the field of electrode fabrication. An example is the work by F. Zhao and co-workers, where the authors traced the partially reduced oxygen species by placing the sensor in close proximity to the substrate.

So far, we have explored various types of electrodes ranging from disk-shaped, ring-shaped to lateral shaped, which were fabricated by different approaches, adopted by the scientific community to investigate the photo- and electrochemical processes simultaneously at the micro/nanometer

scale. These different shaped electrodes have shown remarkable progress by providing spatial and temporal resolution with high selectivity at the nanoscale. Moreover, the behavior of these specifically designed electrodes is highly influenced by the diffusion of active species from the electrolyte solution and therefore, the thickness of the insulating materials is critical. For example, the disk-shaped electrode is characterized by the ratio of electrode radius to the surrounding insulating material (RG value) which was evaluated to be in-between 2 to 10 for an optimal response.[21] Ring-shaped electrodes have an ideal thick-ring electrode configuration of $a/b < 0.91$ (where 'a' and 'b' are the interior and exterior radii).[54] These optimized dimensions offer advantages of high material flux to the electrode surface and therefore facilitate the detection of short-lived intermediate species generated over the substrate. It also enables enhanced collection efficiency of the ring to capture the electroactive species, photo-generated by the concentric optical disk. Therefore, it is desirable to fabricate OF electrodes with an optimized geometry and more importantly at nanometric scale (app. 5 nm).

However, designing and fabricating OF electrodes at the nanoscale with reproducibility is challenging. For instance, methodologies involving a laser-puller can fabricate nanoelectrode with a diameter of ~100 nm with high reproducibility, whereas, selective-chemical etching approaches generate a probe with dimensions down to 5 nm scale.[55] However, the use of hazardous and corrosive etching chemicals such as HF (hydrofluoric acid) hinders its applicability globally due to restricted availability and laboratory equipment. Therefore, desirable future alternatives would either make use of chemical etching under more safe and handy conditions, or be able to decrease the OF size using a laser-puller. In a publication by Mirkin and co-works, the authors fabricated disk-shaped optical electrode by laser puller methodology, exhibiting diameters at the order of 40 nm.[55] The authors were able to achieve high resolution during electrochemical water splitting under photo-electrochemical conditions. This work is definitely an encouragement for future development of OF probes that tackle existing challenges with the current fabrication technologies. The optimization of a defined OF probe enables the imaging of a diverse range of surfaces at the micrometer scale for the mechanistic understanding of various photoelectrochemical processes, as described in the upcoming section.

2.4 Applications

2.4.1 Probe Design Advancements for Scanning Applications

Over the past decade, advancements in probe design facilitated increasingly optical imaging approaches as well as topographical and electrochemical studies in fields ranging from photoactive materials to single live cell studies. STM in combination with light illumination was previously used for various photoelectrochemical (PEC) applications of semiconductors.[56,57] Later on, OFs coupled to a laser source were used for laser spot scanning[58] as well as photoelectrochemical microscopy applications[59]. But it was the upcoming of SPECM, which widely exploited the dual functionality of OF microelectrodes of irradiating substrates and collecting photocurrent, whereby the sensitivity of the SPECM instrument depends greatly on probe characteristics, such as numerical aperture or size of the OF tip.[60] The applicability of OF electrodes during SPECM studies is reported in this section.

In 1995, Casillas and co-workers proposed a technique which combines SECM and SPECM to characterize a Ti/TiO_2 substrate.[33] A 125/50 µm cladding/core diameter quartz OF, coated with a 15 µm thick gold layer and a 10 µm thick outer polyimide probe, was positioned at 40 µm above the substrate and scanned across the sample at 40 µm/s. Initially, the authors conducted experiments, where the SPECM operated in a coupled mode as combined SECM and PEM. It was found that the electrochemical reduction of Br_2 to Br^- was coincident with the rise in photocurrent recorded as the illumination beam moved onto a TiO_2/Ti disk, which was immersed in a solution of 1.0 M KBr and 0.05 M H_2SO_4. It was observed that the reduction current was larger at the centre of the disk than at the edge. Also, the photocurrent and image resolution were low at the edges due to scattering. In the following year, the authors conducted experiments in coupled as well as decoupled mode of SPECM. Coupled mode describes the functioning of the SPECM as both SECM and PEM simultaneously, whereas the decoupled mode refers to the absence of interference between the two techniques.[34] The authors observed that the current response at the microelectrode was prone to an interference of the electro-assisted and photo-assisted reactions in the coupled mode, whereas this was eliminated in the decoupled mode. Different modes of operation of SPECM were demonstrated to study these interferences. (Figure 2.7A) The authors concluded that

this technique was helpful in detecting the precursor sites and studying the photocurrent response with respect to the position of the electrode.

However, the lateral resolution of SECM/ SPECM greatly depends on the geometry of the microelectrode tip, which subsequently plays a role in controlling the tip-to-substrate distance.[39,61,62] In respect to this, Professor Mirkin and coworkers discussed the importance of exposed active tip area at the lowest point of the electrode for increased lateral resolution.[61] OF microelectrodes with well-defined tip geometry was produced by Xiong *et al*[39] and K. Maruyama *et al* [40] as described previously in section 2.1.2. In the former, Xiong and coworkers performed numerical simulations to confirm that the tip-to-substrate distance is dependent not only on the diameter of the insulating layer of the electrode but also on the tip angle. Whereas, in the latter, K. Maruyama and coworkers produced pencil- shaped and triple tapered OF electrodes of nanometer size and demonstrated that with a 105 nm diameter electrode higher electrochemical image resolution was obtained when the probe-to-substrate distance was less than 100nm. Moreover, it was also demonstrated that the feedback effect is minimal with sharper (smaller tip angle) conical electrode.[39,63] Furthermore, improved spatial resolution could only be obtained by modifying the probe throughput and incidence. In regard to this, Avalos-Martinez and co-workers demonstrated that the OF probes with taper tips produced by chemical etching in HF solution with taper angles in the range of 15° to 25°, improved the performance of the SPECM by better light transference.[60] Apart from the taper angle, reducing the overall length of the probe also contributed to improved light transmission through the OF.

A major advancement in electrode design was reported by Zhao and co-workers of the Schuhmann group, where a hydrogen biosensor was incorporated into SPECM as a light source for initiating local photobioelectrochemical reactions. This strategy transformed the OF electrode into an SPECM microbiosensor for the detection of hydrogen in solution, as well as on a bio-photocatalytically active substrate of a redox hydrogel.[64] Here, the microelectrode (Figure 2.7B) was prepared by depositing a thick layer of carbon on the inner wall of a Quartz capillary (inner diameter of 0.9 mm and outer diameter of 1.2 mm) by pyrolysis under inert atmosphere, followed by polishing of the tip and sealing it with carbon paste. This microelectrode tip was then modified by exposing it to a mixture of hydrogenase enzyme and a viologen-based polymer. This construct

was coupled to a Xe-Hg lamp through the top of the glass wall of the microbiosensor for SPECM measurements, which demonstrated a 30-fold increase of the tip current in the modified microelectrode, compared to a bare Pt microelectrode. The Schuhmann group further explored the charge transfer process in a photosystem 1 (PS-1) based solar energy conversion device in 2017 using a similar setup.[65] During SPECM, the biophotoelectrode is a gold or p-doped Si electrode, onto which the authors immobilized PS-1, embedded in an Os-complex modified hydrogel. It was illuminated by coupling a visible light lamp to the top glass wall of the microelectrode. (Figure 4.7 C). Here, SPECM enabled the monitoring of both the photocurrent and the production of reduced charge carriers, which is different from the traditional approach of biophotoelectrochemical half-cell characterization by photocurrent only. Thus, SPECM gives a detailed overview about charge recombination and quenching pathways for developing efficient PS-1 based energy conversion devices.

In 2002, Yougmi and co-authors combined SECM and optical microscopy (OM) to obtain simultaneous topographical and optical images of freshwater diatoms in constant SECM current mode.[15] In this study, the electrode consisted of a gold coated pulled OF core, which was insulated using electrophoretic paint. The OF electrode was mounted on a prong of a quartz crystal tuning fork. The authors discovered that the tuning fork should not be immersed in liquid, and it was concluded that the combination of OFs and SECM shear force constant-current mode maintains the advantages of constant-distance imaging, eliminating strong interaction forces between the tip and the biological sample.

To improve the signal to noise ratio during SPECM, the substrate was microfabricated in such a way that only the photo active spot was exposed to illumination and the electrolyte.[48] The major advantage of this fabrication strategy is the elimination of a background photocurrent and the improvement of the image quality, thereby facilitating efficient studies on photoactive materials. Here, an OF tip coupled to xenon light source was used to probe photoelectrocatalytic reaction on a titaniumdioxide based nanomaterial for solar cells. In this study, the quality of photoelectrocatalytic materials, which are used in sustainable energy resources, was assessed. This is discussed further in the following section.

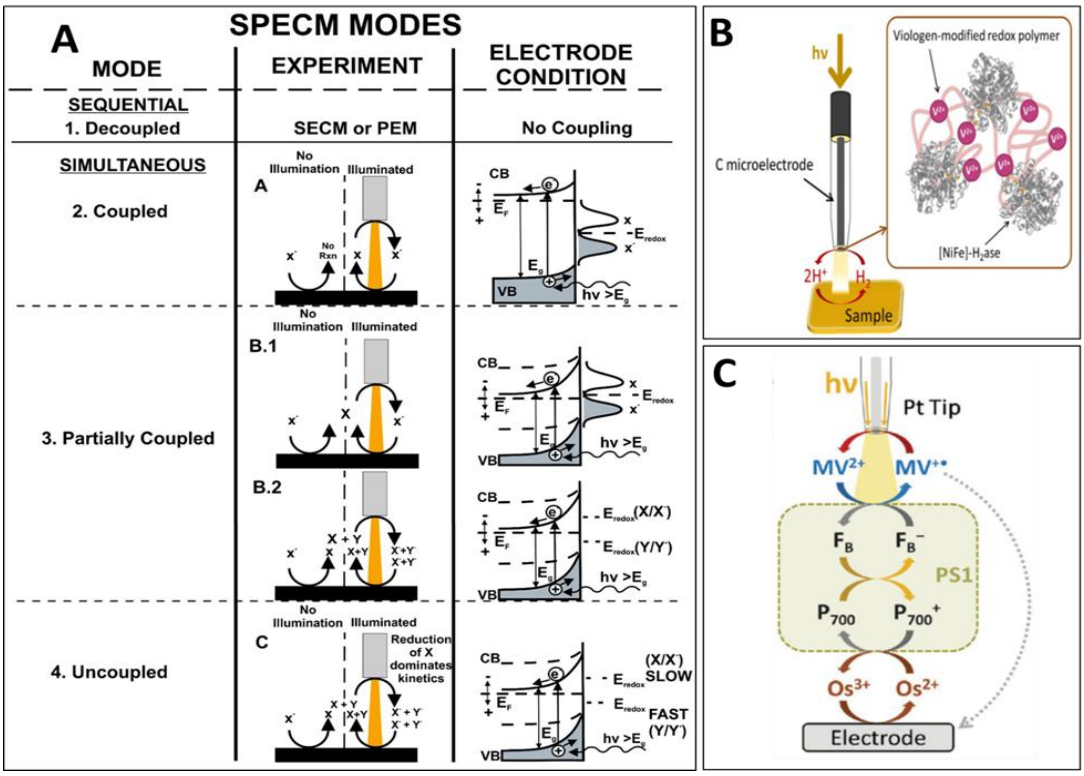

Figure 2.7 *(A) Coupling modes of SPECM,[34] (B) Schematic representation of the [NiFe]-hydrogenase/viologen-based polymer modified hydrogen microbiosensor used as SPECM tip [64] (C) SPECM illustration where the Pt microelectrode is positioned <5µm above the biophotocathode. Osmium (Os)-complexes of the redox polymer provide electrons for the reduction of the photo-oxidized $P700^+$ site, while the MV^{2+} is oxidized to $MV^{+\bullet}$ (methyl viologen radical cation) by electrons from the FB- site of PS1. The charge recombination path is indicated by the grey arrow [65] The 'A' is redrawn based on Ref 34 for clarity.*

2.4.2 Photoactive Electrodes for Energy Applications

This section describes how OF electrodes designed for SPECM instrumentation, have been utilized to understand the photoelectrochemical processes happening at the heterogeneous interface during catalytic turnover conditions. The generation of hydrogen is central towards a renewable and clean fuel by splitting water ($H_2O \rightarrow H_2 + O_2$) using photoelectrochemical micro/nanoelectrodes under light irradiation. Thereby, solar energy can be converted into hydrogen as a clean fuel.[66] For better

understanding a brief introduction about the photoelectrochemical water splitting is provided along with its associated challenges.

Semiconductor based materials have been identified as a key aspect to generate clean and renewable energy by catalyzing water splitting to produce oxygen and hydrogen under UV-visible light irradiation. After the discovery of the concept of photoelectrochemical (PEC) water splitting by Fujishima and co-workers, enormous efforts have been put forth for the production of hydrogen as a clean fuel from abundantly available water and this process has made significant progress in the recent past. [67–69] In general, a PEC water splitting system consists of several important components, which include the photoactive materials as an electrode (photocathode or photoanode) immersed in aqueous electrolyte and a light source. The following sequential steps lead to the splitting of water molecules (Figure 2.8 A)[69]: First, irradiation of a photoelectrode by sunlight occurs, followed by a charge carrier generation as a result of the photoexcitation of electrons in the valence band (V_b) of the photoelectrode material. Second, the separation and transport of charge carriers to the electrode surface is facilitated by the bias applied through the circuit. Third, photo-excited electrons cause the oxidation of water at the photoanode. Instantaneously, the diffusion of H^+ ions from anode to cathode and the transport of photo-excited electrons to the cathode *via* an external circuit occurs, which results in the reduction of H^+ ions to H_2 (gas) at the cathode surface.

Although this procedure is successful to split water molecules and derive fuel, this conversion is challenging due to ineffective charge carrier generation and separation. Furthermore, a high overpotential is needed to drive the reaction and sluggish kinetics of the anodic process (O_2-evolution reaction, OER) are observed. [70,71] In order to tackle these challenges, various photoelectrode materials such as metal oxides[72,73], sulfides[74,75] and their doped variants[76,77] have been designed to mitigate the present energy crisis and to realize the practical applicability of the PEC process. However, none of those examined photocatalysts have yet been found to fulfill all necessary requirements for establishing an industrially viable photoelectrochemical water splitting.[71] Among various semiconductor materials, $BiVO_4$ has been considered as one of the most promising materials, since it is composed of low-cost elements and can effectively utilize the visible light to split water molecules into hydrogen and oxygen. [75] Moreover, $BiVO_4$ has an optimal

bandgap of 2.4 – 2.5 eV with tunable optical and chemical properties just by doping it with the 4th or 5th elements (discussed in the upcoming paragraph). However, shorter carrier diffusion length and substantial recombination of photogenerated electron-hole pairs limit the photoactivity of $BiVO_4$. Besides, the low conversion efficiency (9%) and poor kinetics over its surface also limits its applicability at the industrial scale.[78]

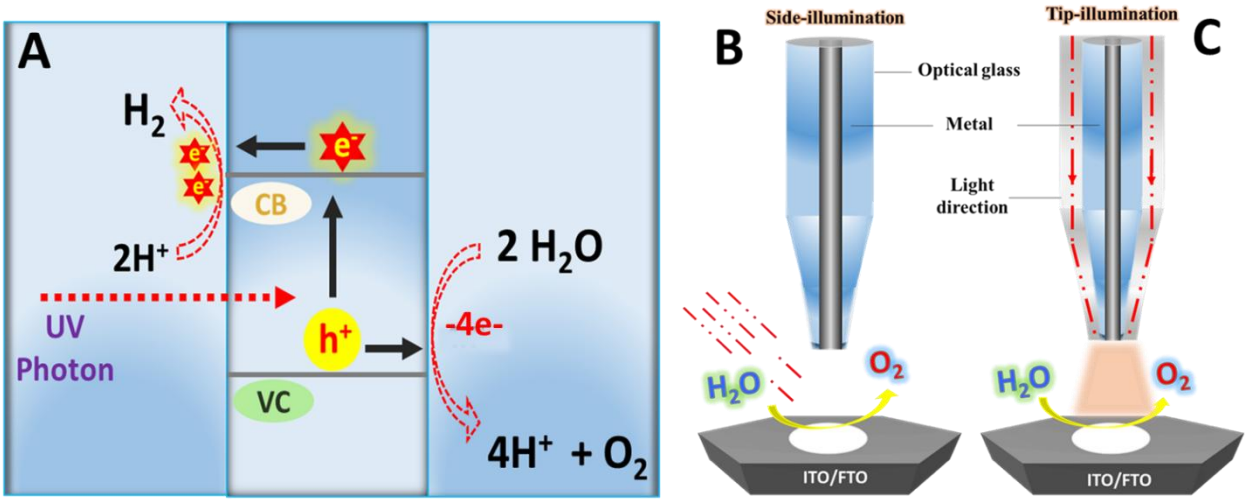

Figure 2.8 *Schematic representation of (A) the photoelectrochemical water splitting mechanism; and two modes of illuminating the surface/catalyst: (B) Side and (C) tip-illumination to facilitate water splitting.*

In the recent past, various strategies were developed by the groups of Prof. Allen J. Bard and Prof. Wolfgang Schuhmann. These approaches aim to improve the efficiency of water-splitting by introducing OFs. Therefore, it is important to understand the interfacial behavior of the designed photocatalyst locally under turnover conditions. The techniques of SPECM and SECM are capable to provide the interfacial information at the photocatalyst surface with exceptionally high resolution, as they enable the local irradiation of the sample with light and monitoring the produced intermediate/final species at the UME by electrochemistry. There are two approaches to irradiate the sample (a) side illumination, and (b) tip illumination. The work of Je Hyun Bae and co- presents the sideway irradiation of a sample (Figure 2.8 B) and the electrochemical collection of the consecutively produced species at the UME.[79] However, this approach suffers from illuminating the entire surface, which results in a higher sample current and thereby hinders local

degradation analysis of the sample and reaction kinetics at the UMEs interface. Irradiating a sample locally through tip illumination (Figure 2.8 C), as shown by Bard and co-workers, enables the exposure of only few micrometers.[80] The locally restricted light exposure during illumination through the tip overcomes the challenges of side illumination. Tip illumination can therefore explore the capability of the catalyst towards water splitting without interference from the background signal. The quantification of intermediate species exhibiting very short lifetimes at the order of nano- or even picoseconds can be performed and thus effectively determines the local concentration of evolved oxygen during the oxidation of water under turnover conditions. H. Ye and co-authors analyzed an array of photocatalysts by SPECM, resulting in the visualization of its photoelectrochemical activity.[80] In this publication, metal salts were casted as a precursor on a FTO/ITO surface, followed by its thermal treatment (calcination) at temperatures above 500 °C to fabricate the desired metal oxide-based photocatalyst. In this study,the authors successfully synthesized Fe_2O_3, $BiVO_4$ catalysts and their variants, by doping other elements such as Co, Zn and Eu in their optimal ratio. In this photocatalytic investigation, high improvement in the photoactivity of the designed catalysts towards splitting water was observed. The authors demonstrated that using this method can not only impart a quick, straightforward and highly reproducible approach of fabricating 300 μm spot size photocatalyst arrays but also results in a highly reliable and rapid electrochemical response.

The advancement of arrays of photocatalysts were continued by the Bard group towards the improvement of the photoelectrochemical activity of Fe_2O_3 by incorporating additional elements, such as Cu, Ni, Sn, Ti and W during the synthesis in a stoichiometric amount.[81] Interestingly, the authors observed both positive and negative effects towards the photocatalytic oxidation of water. However, upon varying the different dopants the authors found the best photoelectrocatalytic activity when 6% of Be and 4% of Sn are doped into the crystal of Fe_2O_3 under SPECM measurements. In another study, Hyun S. Park and co-authors successfully synthesized and evaluated different variants of $BiVO_4$ by incorporating W and Mo under controlled conditions (Figure 2.9 A-C).[82] It was observed that upon doping the 4^{th} or 5^{th} elements (or both together) in the parent crystal of $BiVO_4$, a 6 to 10-fold enhancement in photocatalytic activity was observed towards the photo-oxidation of water (Figure 2.9 B-C). More importantly, the First-Principles Density-Functional Calculation revealed that when W and Mo are incorporated into the crystal of

$BiVO_4$, improvements in the electron-hole separation takes place without a significant change in the bandgap or the material's optical properties. This approach was applied in 2019 by Je Hyun Bae and co-workers to obtain high-resolution photoelectrochemical imaging of the oxidation of ferrocenemethanol and water (oxygen evolution reaction) at the Nb:TiO_2 rutile (110) single crystal surface. The Pt-nano tips were polarized in Sample-Generation/Tip Collection (SG/TC) mode of SECM at a potential of -0.4 V (ferrocenemethanol) and -0.9 V (oxygen reduction potential).[55] This was the first attempt by the authors towards utilization of these Pt-nano probes for SPECM analysis.

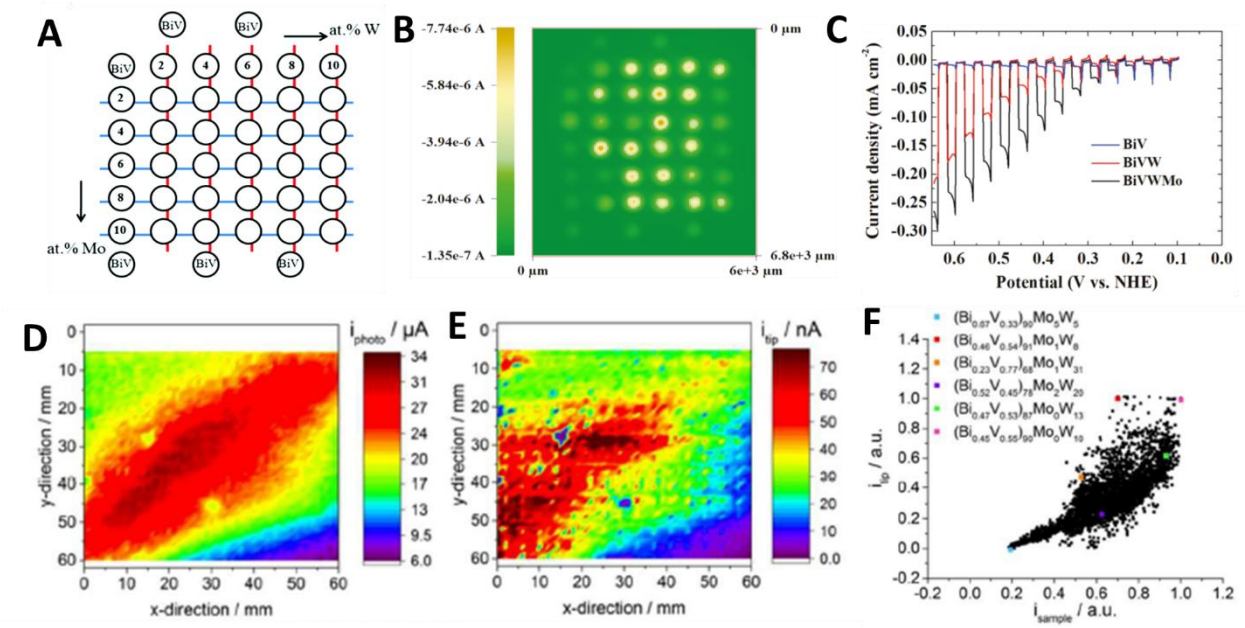

Figure 2.9 *Compositional optimization of metal doped $BiVO_4$ variants and their subsequent effects on water splitting ability. (A) Schematic representation for the atomic composition of the dispensed photoelectrocatalysts on an FTO surface, where each spot consists of 18 drops of the precursors Bi/V (0.1 or 0.02M), W (0.02M), and Mo (0.002 M), respectively in ethylene alcohol; (B) and (C) showing the obtained photoelectrocatalytic activity response towards the splitting of water as analyzed by H.S. Park and co-workers.[82] The photocurrent (D) and tip current (E) of the Mo-W-$BiVO_4$ ML determined by SPECM at 25 µm Pt-microelectrode and connected light fiber in 0.1 M borate buffer, (E) represents the correlation between the tip current and the photocurrent observed at the Bi(V-Mo-W)O_4 ML, as reported by R. Gutkowski and co-workers.[83]*

The design and screening of the photocatalytic material library was advanced by the research group of Prof. Schuhmann. Specifically, R. Gutkowski and co-workers unraveled the compositional effects on the light-induced ability of $Bi(V\text{-}Mo\text{-}X)O_4$ (where X = W, Nb and Ta) towards the oxygen evolution reaction under photo-turnover conditions (Figure 2.9 D-F)[83]. Initially, the authors synthesized a thin film library with well-defined variants of $Bi(V\text{-}Mo\text{-}X)O_4$ by incorporating two additional transition metals with a combination of W-Mo, Mo-Nb and Mo-Ta by combinatorial sputter-co-deposition using a home-made droplet cell. A study under controlled photocatalytic conditions revealed that the deviation from the equiatomic ratio of V:Bi leads to degradation in photocurrent as compared to the pristine $BiVO_4$. However, these effects were controlled by doping with other transition metals and no such significant decrease in photocurrent was observed at 10 atomic % of the transition metal. The authors concluded that an excellent photoactivity with high performance was observed only when the atomic ratio of 70:30 for V:Bi with >10 % of Nb was incorporated into the parent crystal of $BiVO_4$. More importantly, a major highlight of this work is the local *in-situ* detection and local quantification of evolved oxygen by the photocatalyst using UMEs when it is polarized at a fixed potential. The authors calculated the faradaic efficiency using UME by placing it in close vicinity of the semiconductor surface and performing SPECM in SG/TC mode. This has an advantage of in-situ monitoring instead of conventional online analysis by gas chromatography (GC) or mass spectroscopy (MS).[84,85]

In 2018, D. Kimmich and co-workers proposed a combinatorial screening of photoanode materials as a uniform platform for compositional arrays.[86] The authors discovered the new platform for printing metal oxide (Fe_2O_3) using eicosane and glycerol as an effective non-volatile solvent over ITO surfaces. The printer process was optimized using Zn^{2+} and Fe^{3+} ions as salt precursors, followed by calcination at 600 °C under limited supply of oxygen. From the XPS analysis, it was confirmed that no replacement of Zn(II) by Fe(II) was observed, since no significant peaks for Fe^{2+} were recorded in the obtained spectra. Upon performing SPECM measurements, the authors analyzed that the most electroactive spot of the sample was composed of 17 % of Zn^{2+} and 83 % of Fe^{3+} ($Zn_{0.17}Fe_{0.83}O_x$). Moreover, P.S. Shinde and co-authors reported in 2018 the rapid screening of co-incorporated $BiVO_4$ as photoanode material using SPECM over FTO and Ti substrates.[87] The SPECM measurements showed that the most active photocatalyst is composed of 6% Co, incorporated into the pristine $BiVO_4$. The authors concluded that optimal incorporation of Co plays

a crucial role not only to improve the kinetics of the oxygen evolution reaction via formation of Co_3O_4 on the surface of $BiVO_4$, but is also partially due to the enhancement in electronic conductivity of the parent crystal.

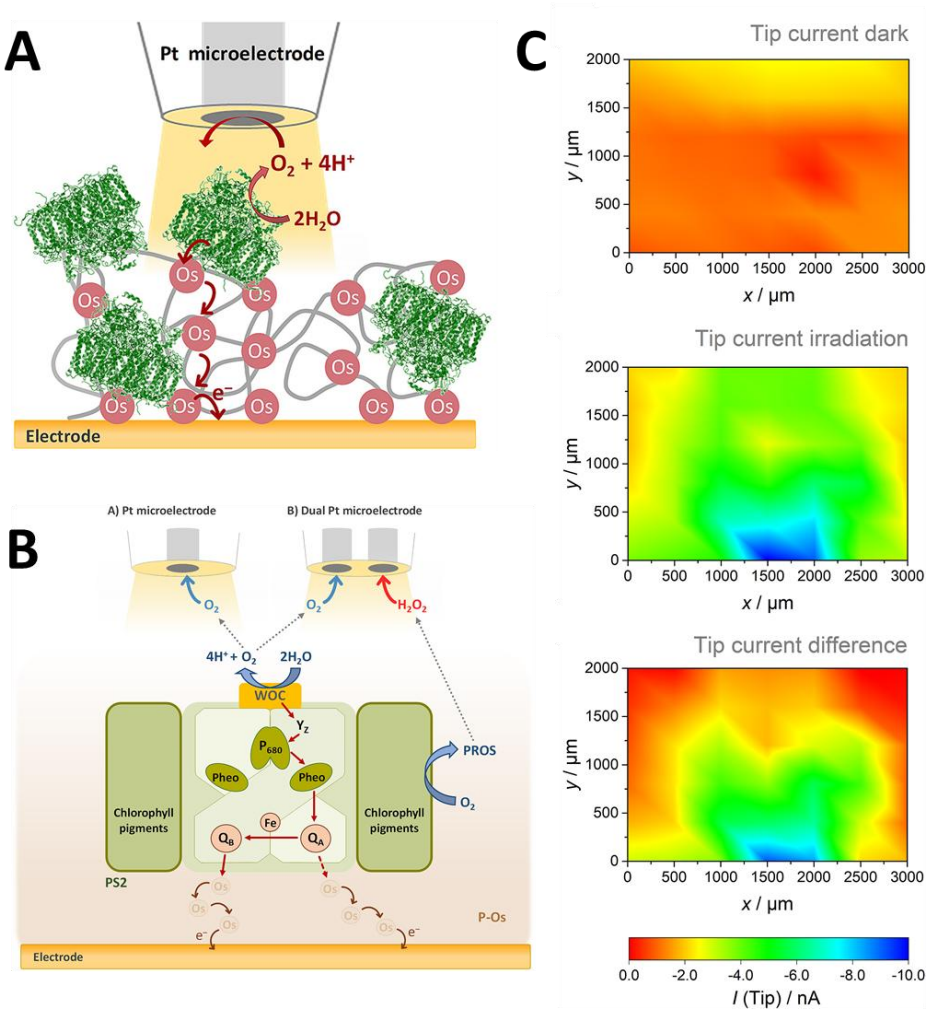

Figure 2.10 *Investigation of the water splitting ability of PS-2. The isolated PS-2 is embedded in the tridimensional redox polymer matrix providing an electron hopping mechanism for the electron transfer from PS-2 to the electrode surface. This enables partial extraction of electrons from the intermediate plastoquinone (QA). (A) Schematic illustration of embedded PS-2 in Os-complex modified redox polymers, (B) SPECM experimental set-up representation to investigate the PS-2/P-Os bio-cathode activity towards understanding water oxidation, (C) SPECM images obtained under dark, localized irradiation. Figure taken from references.*[20]

Besides the industrial importance of water splitting, it becomes important to explore the natural process of water splitting involved in photosynthesis under biological conditions. During natural photosynthesis, PS-1 and photosystem 2 (PS-2) both actively participate to split water molecules by the sequential transfer of electrons under physiological conditions. However, the intermediate generation of partially reduced oxygen species, such as H_2O_2 occurs, which is highly toxic. This causes degradation of proteins present in PS-1 and leads ultimately to a deprivation in activity.[21] Therefore, it becomes necessary to trace and understand the formation, lifetime and kinetics of harmful intermediate species generated during photosynthesis. Very few reports achieved tracing of formed H_2O_2 during artificial photosynthesis at the nano- and micrometer scale. A first attempt was made by Schuhmann and co-workers, evaluating in-depth the PS-1/Os complex-modified redox polymer-based bio cathode towards the generation of H_2O_2 using SPECM.[20,21] The SPECM measurements were performed using a dual disk-shaped Pt-UME in close proximity to the substrate (Figure 4.10 A-C). The dual disk Pt-UME was enclosed in a theta-type borosilicate glass capillary, therefore acting as both light source and electrode for collecting the electrochemical response. One of the two Pt-UMEs was continuously polarized at -600 mV *vs* Ag/AgCl to collect and reduce the formed H_2O_2 species during the consumption of O_2 at the bio-cathode. The other electrode was kept at 600 mV *vs* Ag/AgCl to oxidize the formed H_2O_2 throughout the process. As the bio-cathode (PS-1/Os complex) is irradiated with light, the generation of H_2O_2 as an intermediate species was observed, which was concomitantly collected at the two disk Pt-UME by polarizing them at their respective potentials. A high current response was observed over both Pt-UME when the bio-cathode is irradiated under light. These findings demonstrate that the produced intermediate species was continuously collected over the dual Pt-UME. Various control measurements suggest that the formation of these toxic species cannot be avoided. They were found responsible for the instability of the PS-1 under turnover conditions, which demands more effort.

A subsequent study performed by the same group studied the electron transfer during oxygen evolution at the PS-2 implanted in tri-dimensional Os-complex modified redox polymer using SPECM measurements.[20] In this study, Zhao and co-workers used both a single and dual disk-shaped Pt-UME to simultaneously collect the produced species under photo-irradiation of the bio-photoanode. The single Pt-UME was polarized and positioned in close proximity to the bio-anode

to collect the evolved oxygen, following photochemical splitting of water (Figure 4.10B). On one of the dual disk-shaped Pt-UMEs, partially reduced H_2O_2 was collected and the other monitored the evolved oxygen from the bio-photoanode. The increment in current was observed at all electrodes when the photo-anode is illuminated, this proved the formation of partially reduced H_2O_2 under turnover conditions (Figure 2.10 C). The authors successfully probed multiple electrochemical processes in the immobilized protein complex and its electron transfer with the redox tethers of the polymer matrix.

The aforesaid discussion confirms the crucial role of specifically designed OF probes integrated into UMEs to understand various semiconductor-based material libraries towards the understanding of the kinetically challenged water splitting reaction. From the multitude of studies described above, it has been proven that the doping of 4^{th} and 5^{th} elements in the parent $BiVO_4$ can improve its activity over several folds.[82,88]

Strikingly, the dual disk-shaped electrode eventually became instrumental to trace and understand the formation of partially reduced oxygen species with high resolution. Therefore, these electrodes are now an important tool to identify and even quantify reaction intermediates/products when placed in close proximity to the sample in the SPECM measurements. Apart from these photo-energy applications, such electrodes aided to understand the rate of surface corrosion under different conditions as described in the next section.

2.4.3 Characterization of Surface Corrosion Materials

Corrosion is a major issue in various industries, such as oil, gas, and chemical engineering. Corrosion of equipment in these industries results in health and environmental risks, which has led to the development of corrosion resistant materials and corrosion sensors. Though the success of corrosion resistant materials and sensors remains undecided, it is insight into the local reactions at the substrate-electrolyte level, which will help us to mitigate corrosion. Electrochemical scanning probe techniques using UMEs play a significant role in understanding electrochemical reactions at metallic surfaces.[89] This section discusses how OF have been integrated for forming OF corrosion sensors as well as the role of SECM/SPECM in characterizing surface homogeneities/ heterogeneities in metal/ metal oxide films.

OF corrosion sensors have been developed by various groups for early detection of underlying corrosion processes.[90–92] Abderrahmane and co-authors reported on the development of an optical fiber corrosion sensor (OFCS) [92]. (Figure 2.11 A**)** Here, an uncladded plastic/polymer clad silica (PCS) multimode fiber underwent an electroless deposition of nickel-phosphorus (Ni-P). (Figure 2.11 B) After polishing, the input end of the OF was connected to a laser diode emitting beam at 670 nm, and the light was focused on a silicon photodiode. The Ni-P coated portion of the OF was placed in an aqueous solution with different concentrations of phosphoric acid. (Figure 2.11 C-D**)** The authors reported that the angle of incidence of the light transmitted through the OF varied as the Ni-P coating corroded. It was observed that the numerical aperture, which is a function of angle of incidence of the OF increased as the metallic layer corroded. Similarly, an OFCS with the electroless deposition of copper film on the core of the PCS fiber was developed by Benounis and co-workers. Here, the OF was placed in an experimental set up consisting of a laser diode and silicon photodiode with the metallic portion immersed in an agitated aqueous solution of nitric acid. Alongside, a Ag/AgCl reference and a Pt counter electrode was placed in the aqueous solution to detect the variation in electrochemical potential with changing Cu^{2+} concentration in solution.[93] The aim of the authors was to correlate the optical and electrochemical detection of copper corrosion. It was concluded that the optical signal (angle of inflection) progressively increased with a uniform degradation of the corrosion film. More than 50% of the copper was corroded at the maximum inflection angle of 19.5°. Moreover, the rate of corrosion depends not only on the intensity of the light transmitted, but also on the concentration of the corrosion solution and exposure time.[94] Though these corrosion sensors are advantageous, they have to be shielded from other contaminants as there can be interferences in distinguishing the corroded layer and other contaminations.[93]

To address this challenge, characterizing corrosion films by various surface analytical techniques became a focus research area during the 1990s to understand various corrosion mechanisms. In 1999, Garfias-Mesias and co-workers developed a technique of photoelectrochemical imaging by NSOM (Near-field Scanning Optical Microscope).[27] This study focused on studying corrosion in microelectronic and magnetic storage devices where degradation of metallic structures occurs at small scales. The authors prepared an OF tip of 100 nm diameter by chemical etching and also polycrystalline titanium samples with inclusions of Al and Si and polycrystalline Ti with a

defective oxygen film. This OF nanoelectrode was attached to a quartz crystal tuning fork for a shear-force feedback method of PEM to attain the topography and the photocurrent simultaneously from the Ti sample. NSOM helped in maintaining the nanoelectrode tip-to-sample distance in the range of 10 to 30 nm. It was concluded that the lateral resolution of topography of inclusions exceeds 100 nm and the contrast between the grains is shown by minor changes of 5 pA in photocurrent.

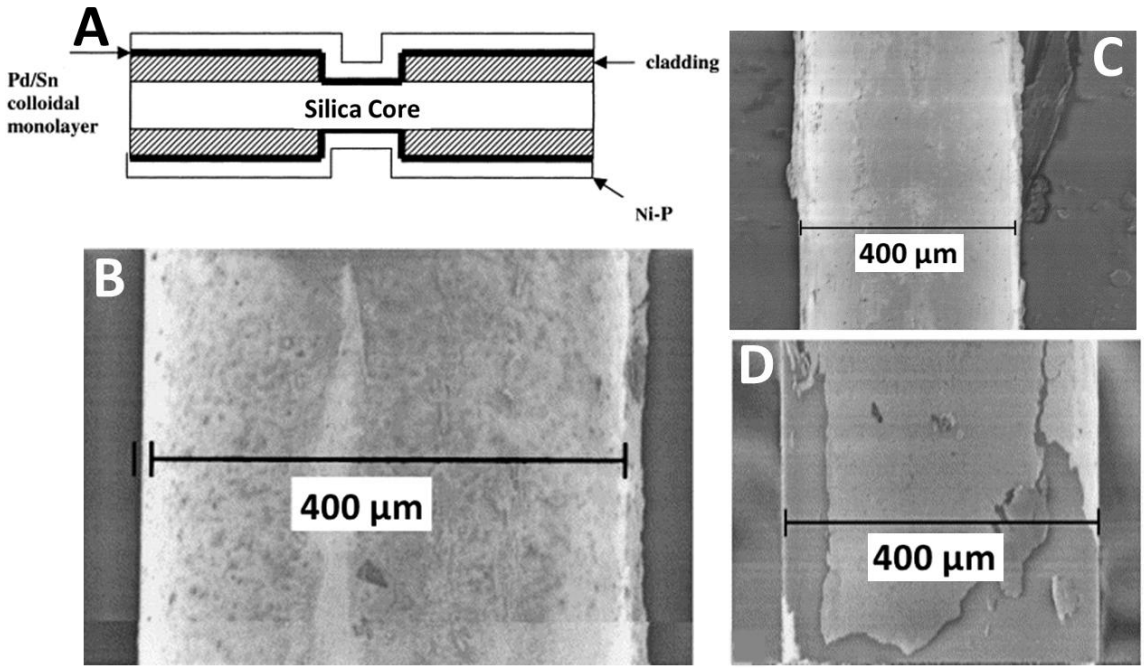

Figure 2.11 *(A) Schematic representation of OF corrosion sensor. SEM image of Ni-P coated OF (B) before and after placing it in (C) 10^{-3} N and (D)10^{-1}N phosphoric acid solution for 1 hour.*[92]

SECM/ SPECM have been employed in studying the electrochemical reactivity, surface kinetics and mass transport at the solid-liquid interface of corroding surfaces.[95] Sosa and co-authors, conducted surface experiments on iron sulfide (Fe_xS_y) films that were grown on a clean carbon steel 1018 electrode.[25] The carbon steel electrode with Fe_xS_y film was placed in sulfide, nitrate, sulfate and borate media for 18 hours for SPECM characterization. A multimode OF with gold coating, insulated in polyimide and positioned at a distance of 25 µm from the sample was biased at a positive potential of 126 mV (*vs.* SSE, stainless steel electrode), while the sample was biased

at a potential of -550 mV (*vs.* SSE) in 0.1M $K_3[Fe(CN)_6]$. SPECM being more advantageous than SECM by providing information on not only the electronic conductivity but also topography and homogeneity, showed that the carbon steel was coated by the corrosion products and this layer underwent a physicochemical modification in different electrolyte solutions. It was observed that the current response in these media were higher than that of the reference Fe_xS_y film (200 nA) prepared electrochemically in a sour media but less than the freshly polished carbon steel surface (2500 nA). Based on the current response and activity, it was found that the film surface became more homogeneous after 18 hours of immersion in nitrate solution in comparison to the reference film. Thus, it was concluded that SPECM gave information about the homogeneity and electronic conductivity of the corrosion films. In a later study by the same group, it was found through SPECM that the composition of the corrosion film changed as a function of electrochemical oxidation time.[26] Through SPECM it was found that corrosion products were heterogeneous, adherent and passivating after 1 minute, whereas after 30 and 60 minutes they were homogeneous and active. Thus, SPECM gives an overview of the physical and chemical characterization of these films which can play a vital role in developing corrosion inhibitors.

Besides sensing and characterizing metal films using OFs, another emerging field of research is the area of biofilms and electroactive biofilms (EABs). Characterizing and sensing biofilms is of utmost importance due to the threat they pose on healthcare and food industry. These biofilms, mainly formed from microbial colonies of bacteria, grow rapidly on implanted biomedical devices and on food processing equipment leading to health risks and corrosion of materials. A review by S. Subramanian and co-authors gives a detailed summary on different microsystems used for their characterization and sensing.[96] Various optical fiber sensors have been developed for monitoring the growth of biofilms. Philip-Chandy and co-workers[97] as well as Zhong and co-authors. [98] developed OF sensors by exposing the sensing area to “declad” and monitoring biofilm growth through evanescent wave spectroscopy in water process systems and photobioreactors, respectively. Though biofilms have their drawbacks, they are also used for valuable purposes, such as sewage treatment and clearing oil spillage. Moreover, EABs are being studied for harvesting energy and for forming useful chemicals from waste. Yong Yuan and colleagues reported in 2016 on the in-situ detection of EABs through electrochemical surface plasmon resonance.[99] Here, a single mode OF was uniformly coated with gold (with a thickness of ~50 nm) and the core was

imprinted with a tilted fiber Bragg grating (TFBG). This uniform gold coating over the TFBG OF allows for highly efficient electrochemical and optical sensing of EABs. Other more strongly bioelectrochemical applications of OFs are discussed in the following section.

2.4.4 Biological Applications

OF electrodes have increasingly been utilized to analyze biological issues. This includes applications in sensing, imaging, therapy and diagnosis over the past two decades.[100] A review paper published by Deiss and co-authors in 2010 highlights the use of nanostructured OF bundles for various biochemical sensing applications.[47] Biosensors using OFs have been extensively exploited in healthcare and environmental chemistry resulting in remarkable outcomes. [47,101,102] These sensors can be miniaturized and require only a small sample volume, enabling high sensitivity and reliable selectivity.[102] OFs employed in biosensors are inert and resistant to strong acids or alkaline solutions, oxidants and other aggressive environments. Furthermore, they have the advantage of improved selectivity, as the fiber surface can be modified with a receptor (eg; antibody, enzyme, DNA, microorganism, cell etc.), specific to an analyte of interest.[102]

The applicability of surface immobilization of OF probes was demonstrated initially by Van Dyke and Hung-Yuan Cheng [49] where the authors fabricated a probe with fused silica OFs embedded in an electrically conductive graphite/ epoxy material with an optical end face. The main aim of the authors here was to create a probe that enables spectroelectrochemical measurements in deep in situ regions of the human body or in small sample volumes. Spectroelectrochemical experiment was performed in a gel matrix containing 0.5 mM ascorbic acid and 0.1 mM dopamine in pH 7.4 phosphate buffer, which resembled a biological tissue consistency. It was recorded that ascorbate underwent depletion after 7 minutes of electrolysis at + 0. 50 V showing a remarkable increase in transmittance at 265 nm. This led to the observation of qualitative similarity in the UV spectrum of ascorbic acid with a standard spectrometer and the spectrum of this depleted ascorbic acid. Additionally, the electrode was coupled with a microsyringe filled with ascorbate solution and inserted into a dog brain with the light reflection maintained at 265 nm. The photocurrent initially increased when 10 μl of ascorbate was released into the brain and then remained stable, indicating either the complete absorption of ascorbate was impossible by the brain tissue, or the brain tissue underwent damages. The authors concluded that the amount of ascorbate in the model gel could

be obtained based on redox modulated optical signal. Moreover, the feasibility of spectroelectrochemical measurement in brain tissue by immobilization of chemical reagents at the OF microelectrode end face was also demonstrated.[49]

Biosensors with surface-modified OFs gained significant attention in the 1990s. For instance, an OF cholesterol biosensor with an oxygen OF electrode transducer was developed by Trettnak and Wolfbels, which facilitates the sensing of cholesterol.[103] In this procedure, cholesterol oxidase enzyme was immobilized on the OF surface through a nylon membrane. OF DNA sensors were developed, where a oligonucleotide is immobilized on an OF probe to facilitate hybridization with a target DNA/RNA.[104–106] Another example of surface immobilization is the non-covalent adhesion of bioluminescent *E.coli* to the OF core for the application of environmental monitoring.[107,108] Thus, biosensors based on OF probes were exploited for discovering promising alternative to conventional, much more time intensive methods. An important achievement of these biosensors is real time analytical detection of infections by being able to detect biomarkers in urine and saliva samples. It also enables the remote sensing of different patient samples from different locations at the same time.[102] These biosensors are also cost effective as they would not require the use of expensive chemicals for carrying out the traditional assay experiments.

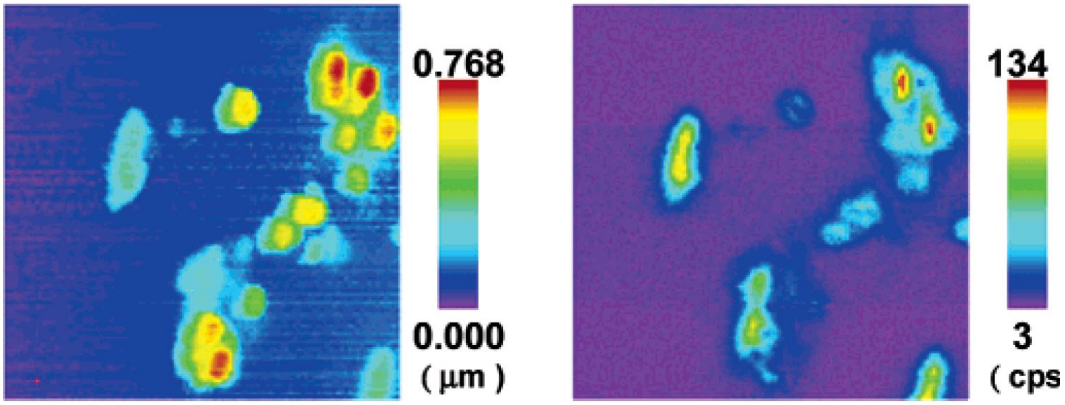

Figure 2.12 *High-resolution SECM using OF. Topographic (right) and fluorescence (left) imaging of GFP-E. coli at a scan range of 20 µm x 20µm.*[23]

Marks and co-workers presented dedicated work on OF biosensors based on chemiluminesence.[108–116] The authors fabricated a microbiosensor for the diagnosis of the hepatitis C virus by surface modifications of the OF.[116] Here, electrically inert doped silica OFs were modified by depositing a thin layer of indium tin oxide through rf-sputtering. For attaching a biological receptor to the OF tip, the electroconductive surface was further modified by an electrochemically polymerized poly(pyrrole-benzophenone) film. This allows the photoimmobilization of the HCV-E2 envelope protein (hepatitis C virus host receptor binding protein) antigen by biotin-avidin linkage. The electroactivity of the polymer film was characterized by cyclic voltammetry and a reversible current peak was obtained at +0.31 V. The sensitivity of the immunosensor was compared with the standard immunological tests ELISA and Western Blot. It was found that none of the negative human sera reacted to the positive immunosensor test showing a 100% specificity, while positive HCV-RNA were negative for the three cited antibodies used in the standard test. Therefore, due to the high sensitivity of the OF immunosensor, only E2 envelope protein was detected in RNA positive patients compared to the standard tests, which required the use of three cited antibodies.

Apart from sensing applications, OF electrodes have also gained popularity for imaging and the characterization of biological samples by scanning electrochemical microscopy (SECM) due to its non-invasive mode of operation. Takahashi and co-workers developed high resolution SECM using OF electrodes.[23] These electrodes play a significant role in SECM for characterization studies. Here, a conical shaped nanometer sized OF electrode was fabricated by pulling a single OF using a carbondioxide laser, which is later on sputter coated with Ti/Pt, followed by insulation with a layer of xylene polymer. Hot air at 450˚C was blown on this insulating layer to expose the electroactive area on the SECM tip. This conical OF electrode was used for the topographic and fluorescence near-field imaging of the green fluorescent protein (GFP), expressed in *E. coli* (Figure 2.12). The height of the *E. coli* was determined to be 490 nm with the cross section of the topography. These conical OF electrodes contributed immensely to the lateral resolution of the optical image, which surpassed the diffraction limit. Additionally, the authors used capillary electrode (glass capillary was pulled using a capillary puller followed by Pt film deposition and parylene C coating) in standing approach (STA; feedback mechanism adjusting the tip-to-substrate distance) mode SECM/OM for the simultaneous topographic and electrochemical imaging of

single rat adrenal medulla PC12 cells. (Figure 2.13 A-B) However, the topographic image of PC12 cells were noisy and showed a lower lateral resolution compared to the OF probe. Moreover, the cell was checked for any damages resulting from the STA imaging mode. The PC12 cells were stained with calcein AM for 15 minutes and fluorescence and optical images with no noticeable damage were obtained. The electrochemical imaging at -0.50 V showed reduction currents for the local oxygen at the center and exterior of the cell. (Figure 2.13 C-D) This facilitated the calculation of respiration rate of a single cell, which was calculated to be 7.8 $x10^{-18}$ mol s^{-1}.

It was observed that the sensitivity of these conical shaped OF/glass capillary electrode was low. Hence, Takahashi and co-workers went on to fabricate a disk- and ring-shaped nano-OF electrode for the simultaneous electrochemical, fluorescent and topographic imaging of gene transfected single HeLa cells.[24] The difference in the fabrication compared to the conical shaped probe was that the electroactive area of the OF probe was exposed by using a focused ion beam to form an optical aperture. These nano OF ring electrodes were used as probes in constant-distance and constant-height mode SECM/OM. It also facilitated the detection of two reporter proteins, SEAP secreted from the cell to the outside solution, and GFP expressed inside the cell. It was found that the constant-distance mode permits a higher contrast than the constant-height mode, because the concentration of SEAP was high near the transfected HeLa cell. The efficiency of constant-distance imaging over constant-height imaging was evident from the cross-sectional fluorescence signals. Thus, it was concluded that distance plays an important role in bio-imaging based on fluorescence emission.

OF probes with surface and geometrical modifications progressed immensely in the fields of bioelectrochemical sensing and topographical imaging applications. It is the study of live cell signaling and metabolic activities through locally monitoring and quantifying material flux that will make a significant contribution to understanding various biological mechanisms in living organisms. This can be achieved by designing high resolution OF based nanometer sized electrodes for SECM and SPECM.

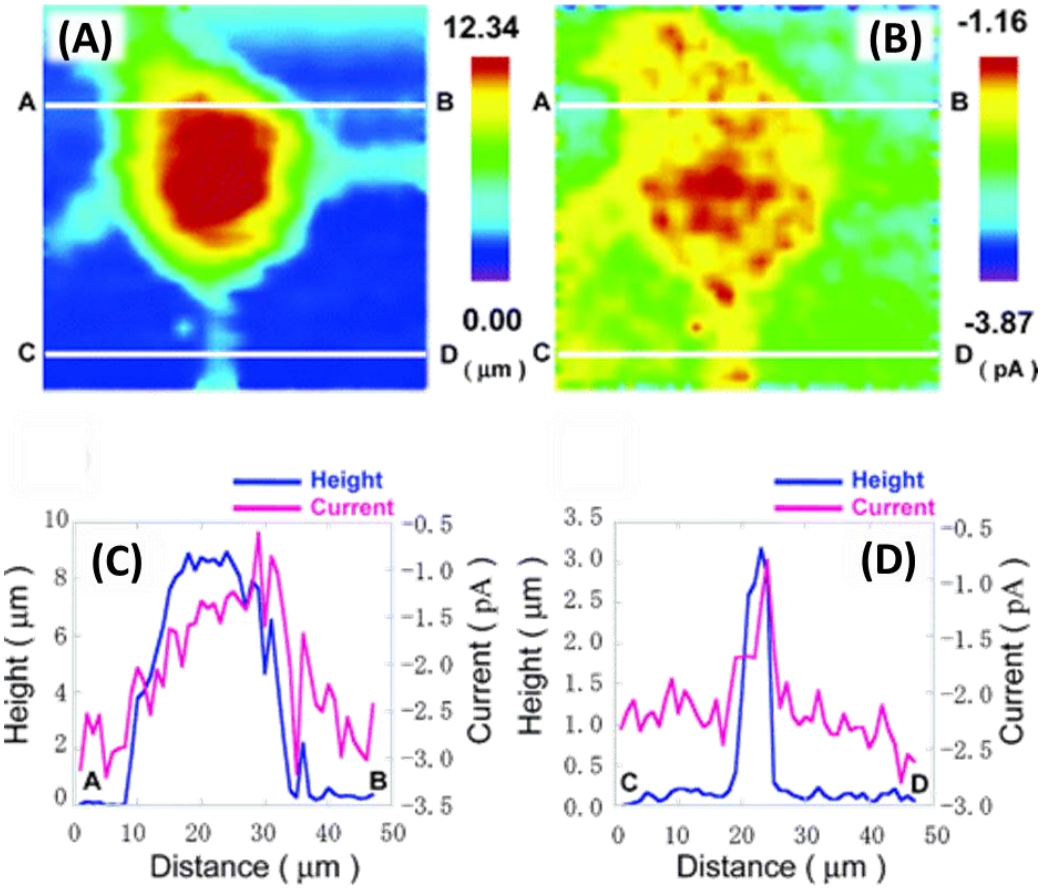

Figure 2.13 *Topography (a) and electrochemical (b) images of PC12 cells in a PBS solution in STA mode using a capillary electrode. The cross sections of the cell body (c) and axons (d) were shown for the topographic and electrochemical signals. The white lines in (a) and (b) indicate the position of the cross section.*[23]

Table 2.1 *Comprehensive overview of different OF probes used for various electrochemical applications.*

Probe Type	Probe Structure	Method of Fabrication	Size	Application	Ref
Disk	OF-Au-Nafion+RBITC	Sputter coating, Immobilization		Hydrogen peroxide imaging sensor	[19]

	OF-Epoxy-Au-MoS_2	Template transfer	200 µm	Methanol detection	[32]
	OF coupled to dual Pt microelectrode	Coupling		SPECM- PS1 characterization	[21]
	Xe lamp coupled to OF	Coupling	400 µm	SECM- Synthesis and Screening of ZnxCd1-xS ySe1-y photocatalyst	[117]
	OF Bundle	Sol-gel, coupling		Glucose determination	[118]
	Laser coupled OF	Commercial OF	50/125 µm	SPECM- PEC characterization	[119]
	OF coupled to Pt microelectrode	Coupling		SPECM- PS1 characterization	[65]
	PMMA POF		0.980 mm	Biofilm sensor	[97]
	Xe-lamp, OF-Pt	Coupling		SECM	[55]
	Au-OF	Elelctron beam evaporation	400 µm	SPR sensor	[120]
	Xe-lamp coupled OF	Coupling	200 µm	Screening of photo-electrocatalytic system	[48]
	Hg-Xe lamp coupled OF-Au UME	Thinning, sealing, pulling	50 µm	SECM- mapping of TiO_2 arrays	[121]

	OF tip	Layer-by-layer electrostatic	105/125 µm	Hydrogen peroxide sensing	[122]
	Xe-lamp coupled OF	Coupling		SECM-illumination	[123]
	Au mini grid		1 mm	ECL microoptoprobe	[124]
	OFs in Stainless		100 or 200 µm	Spectro-electrochemical	[49]
	OF	Mechanical stripping	1000 µm core	Biosensor	[113]
	OF	Chemical etching	3.7 µm	In-situ imaging of polycrystalline Ti	[27]
	Hg-Xe lamp coupled to OF	Coupling	~ 400 µm	SPECM-Photoanodes	[22]
	Tapered OF		400 and 100 µm	Sensor	[125]
	HeNe laser coupled to OF	Coupling	4 µm	Laser spot scanning	[58]
	OF		105 µm	SPECM probe	[126]
	OF	Capillary puller	270 µm	Scanning Droplet Cell Microscopy	[127]
	Xe lamp coupled OF		400 µm	SECM	[81,88,128,129]

	Xe lamp coupled OF Pt ring-Au-OF	Electrochemical plating	400 µm 200 µm	SECM	[80]
	Laser coupled OF	Coupling		SPECM-Rapid screening of photoanode materials	[87]
	Xe lamp coupled OF	Pulled	200 µm	Illumination of sample-SECM	[130]
	Xe lamp coupled OF		200 µm	SECM probe	[131]
	Lamp coupled OF			Illumination of sample-SECM	[20]
MORE	PAAH-Au-OF	Laser puller, vacuum evaporation, insulation	3.7/125 µm	SECM-Characterization of tapered tip probe	[37]
	PAAH-Au-OF	Selective chemical etching	25 µm	SECM-Characterization of conical probe	[39]
	PAAH-Au-OF (pencil-shaped)	Selective chemical etching,	27/125 µm	SECM imaging-PC12 cell	[40]
	Au-Ag/Sn particles-OF	Electroless plating		Probe characterization	[41]

	Au-OF	Thermal evaporation	2.5 x 10^{-4} m	Characterization of MORE	[35]
	Au-OF	Thermal evaporation	2.5 x 10^{-4} m	Transport limited steady state	[29]
	Au-OF	Thermal evaporation	2.5 x 10^{-4} m	Transient photocurrent studies	[36]
	Epoxy-Au-OF	Chemical treatment	200 µm	MORE tip on photocurrent	[132]
	Xe-lamp coupled OF	Coupling Commercial	400 µm	SECM- Screening of metal oxide	[133]
	Xylene polymer-Ti/Pt-OF	Laser puller, sputtering	SMF	Single cell imaging	[23,24]
	PAAH/Au-OF	Laser puller	3.7 µm	SECM/OM- EC	[15]
	Polyamide-Au- OF	Coating	50/125 µm	SECM- Characterization of Ti/TiO_2	[33]
	Polyamide-Au- OF	Coating	50 µm core	Corrosion film Characterization	[25,26,134]
	Au-OF	Sputtering	SMF	Electroative Biofilms	[99]
	Au-OF	Commercial electrode	200 µm	Probe characterization	[135]

	Epoxy-Au-OF	Chemical treatment	200 µm	Multiple actinide ion sensor	[136]
	Carbon deposited	Laser puller	1.2 mm	SPECM probe	[64]
	Al/Ag/Au film coated OF	Laser puller, focused ion beam milling	200 nm	Optical sensing	[137]
	TiO_2 film coated OF	Electrophoretic deposition	600 µm	Waste water treatment	[138]
	Xe-lamp coupled Au-OF	Coupling, sputtering		Photochemical processes	[139]
	Epoxy-Ti-Ag-OF	Mechanical stripping	4 µm	Electrode strain measurement	[140]
	Varnish-Au-OF	Chemical etching, sputtering	3.7/125 µm	EC microscopy	[141]
	Polyimide-Au- OF	Commercial		SECM and PEM	[34]
Lateral	Au mesh- OF	Commercial OF	200 µm	Spectroelectrochemical sensor	[30]
	ITO coated EA-FOC	Sputtering	SMF	Spectro-electrochemical characterization	[44]
	ITO-OF	Hexagonal barrel-sputtering	400 µm	Spectro-electrochemical sensor	[45]

	ITO-OF	Magnetron sputtering	400/840 µm	LMR sensor-Ketoprofen detection	[142]
	ITO coated LPG OF	Magnetron sputtering	SMF	Optical investigation of EC processes	[143]
	Fe-C alloy-Ag-OF	Chemical etching, electroplating	62.5/125	Corrosion sensor	[90]
	Fe-C alloy-Au-OF	Vacuum deposition	62.5/125 µm	Corrosion sensor	[94]
	Pd/Sn colloidal monolayer- Ni-P-OF	Electroless plating	400 µm	Corrosion sensor	[92]
	Chemical etching, sputtering	Al alloy-OF	< 150 µm	Corrosion sensor	[91]
	ITO-OF	Magnetron sputtering	400/730 µm	LMR sensor	[144]
	Graphene multilayers OF	Chemical vapour deposition	SMF	Fiber graphene devices studies	[145]
	Cu-OF	Mecahnical stripping,	400 µm	Corrosion sensor	[93]
	Acrylic-OF	Coating	8.2 µm	Corrosion sensor	[146]

	Pyrolytic carbon-OF	Pyrolysis, laser microablation	200 µm	Electrochemical detection of dopamine	[147]
	ITO-OF	Deposition	400/840 µm	LMR sensor	[148]
Array	Epoxy-Au-OF	Chemical etching	25 µm	Chemical imaging	[17]
	Epoxy-Au-OF	Electroless deposition	25µm	Fabrication of probe	[54]
	Photoresist coated-Au-OF	Chemical etching	3-4 µm	Spectro-electrochemical sensing	[46]
	OF imaging bundle coated with $Ru(bpy)^{2+}_3$ /Nafion/Au	Coating	3 µm	Chemical sensor	[149]
	Poly(methyl methacrylate) bifurcated		3.5 mm	Cholesterol biosensor	[150]
	Bifurcated fiber-optic bundles		200 and 600 µm	Immunosensor	[151]
	Au-OF	Magnetron sputtering	3-4 µm	ECL	[152]
	Pt wire woven - Fused silica Ofs		200 µm 12 Ofs	Chemiluminescence	[153]

	OF with cage Pt WE				
	Acrylic resin-AuNPs-OF	Chemical etching	3-4 µm	Electrochemical characterization	[154]
	Halogen lamp			Glucose sensor	[155]
	Ofs embedded in Torr-seal		200 µm	Spectro-electrochemistry	[156]
	Ni – OF	Laser puller, coating	20-30 µm	Photometric patch electrode	[157]
	Au-OF	Chemical etching, coating	3-4 µm	SECM	[158]
Others	Epoxy-Pt coated capillary	Heating and pulling		Probe fabrication	[50]
	Au-OF	Sputter coating	200 µm	Development, modeling	[51]
	OF embedded in cell electrode			Sensor	[159]
	OF encapsulated in lithium ion battery cell			Battery performance monitoring sensor	[160]
	U-shaped, double tapered OF	Chemical etching	105 µm	Biofilm sensor	[98]
Surface	Immobilized OF	Silanization, Immobilization	1 mm	Biosensor	[104]

modify-cation	Biotinalyed MBs immobilized OF	Chemical etching, immobilization	~ 60 µm	DNA Biosensor	[105]
	Bioluminescent cells immobilized OF	Immobilization OF tip	400 µm	Biosensor	[108]
	Antigen (Cholera toxin B) immobilized OF tip	Silanization, immobilization	1000 µm	Immunosensor	[109]
	GIPC-1 antigen immobilized OF tip	Mechanical stripping, immobilization	400 µm	Immunosensor	[114]
	WNV antigen immobilized OF	Mechanical stripping, silanization, immobilization	400 µm	Immunosensor	[112]
	Viral antigen immobilized poly-pyrrole-benzophenone	Sputtering	400 µm	Immunosensor	[115]
	Viral antigen immobilized poly-pyrrole-benzophenone	Sputtering, electro-polymerization	400 µm	Immunosensor	[116]
	Immobilized bacteria	Immobilization	0.3 mm	Biosensor	[107]

	Bacteria immobilized OF	Stripping, thinning	MMF	Biosensor	[106]
	Horseradish-peroxidase-labeled avidin-pyrrole-biotin-ITO-OF	Magnetron, sputtering	400 µm	Chemiluminescence characterization	[111]
	Pneumococcus polysaccharide conjugated OF	Chemical modification	400 µm	Immunosensor	[110]
	Oligonucleotide hybridized OF	Chemical treatment, hybridization	SMF	Biosensor	[105]

2.5 Conclusion and Future Prospects

This article reviews the development and advancement in the field of spectroelectrochemical probe fabrication and their applicable research areas, such as photoactive energy materials, surface corrosion, and single live cell imaging. A comprehensive summary is provided and tabulated in Table 2.1 Various methodologies, adopted and explored for the advancement of optical probes, ranging from single optical electrodes (disk-shaped, ring-shaped, lateral shaped) to multi-electrode (optical arrays) at the nanoscale are highlighted. Scanning probe techniques, such as SECM and SPECM have been proven useful to characterize surfaces of biological and non-biological nature. This review highlights the integration of OFs to scanning probe microscopy to advance SECM into a powerful imaging technique that can track electrochemical photoactive processes at the micro- and nanoscale.

Research efforts have focused on the down scaling of fiber electrodes to the nanometer level.[55] This is attractive, because nanoelectrodes offer the ability to carry out photoelectrochemistry in low volumes, as small as a drop, micro-emulsion, and single biological cells. Moreover, decreased

electric double layer capacitance results in a quick electrochemical response and enables the detection of short-lived intermediate species. As an example, the detection of reactive oxygen species (ROS) helps the scientific community to understand complex mechanisms, such as the photoelectrochemical splitting of water to oxygen under physiological conditions.[21] No doubt, OF probes of various shapes and sizes have been proven useful in the field of optical imaging. However, fabrication of probes with nanometer dimensions is still challenging. For example, the most commonly used laser-puller methodology adopted by the community to fabricate the ring- and disk-shaped electrode needs more optimization to approach the nanometer dimensions of probes for better understanding and tracing short lived species with high resolution. In this regard, the research team of Prof. M.V. Mirkin demonstrated the ability of this methodology by fabricating disk-shaped Pt-UME having diameter in the range of 40 nm, which was applied to understand the oxygen evolution reaction during SPECM.[55] Alternative methodology, such as selective chemical etching should be optimized by eliminating harsh etching conditions as much as possible.

The design the OF based electrodes and implementing them towards a mechanistic understanding of various energy related processes lead to the design of stable and highly efficient catalysts.[82,86] This is exemplified by OER activity enhancement upon incorporating an additional metal in the parent $BiVO_4$ by several orders of magnitude, established using the SPECM measurements. This process is only feasible when the sample was irradiated, and the generated photocurrent was monitored over the disk-shaped Pt-UME providing fundamental insights.

Optical arrays also provided significant advancement in the field of imaging using SPECM, owing to their ability to generate quantitatively higher current as compared to a single optical electrode and it therefore becomes possible to image the surface activity with enhanced resolutions. For example, nanostructured OF arrays are extensively researched for biochemical sensing and remote imaging of organs and tissues within their environments.[47] OF array imaging has made a significant contribution in medicine owing to its small size, versatility, multiplexing capability and remote detection.[47] Though, inter-electrode distance contributing to diffusional overlap remains one of the main challenges of OF arrays, it provides scope for future research in developing “ultra-high” density sensitive OF nano arrays.[17]

Based on recent advancements and the increasing attention by the electrochemical community over the past decade, it is anticipated that OF probes (single and multi-systems) will play a significant role in various scanning electrochemical tools, such as SECM, SPECM, SICM in future years. SPECM has the potential to witness metabolic activities within a single cell through high resolution imaging and quantifying biomolecules, which are markers of various diseases. Highly interesting studies emerged, applying OF electrodes to biology, as shown by studies on the electrochemical reactivity of electroactive biofilms (EABs) for environmental monitoring.[98]

OFs have contributed to the development of various corrosion monitoring sensors but, it is the *in-situ* corrosion monitoring, which requires advanced research and is benefiting industries. The feasibility of these corrosion monitoring sensors depends on various environmental as well as mechanical properties.[145] High resolution OF probes in analytical scanning electrochemical tools will enable not only the surface characterization of corrosion films but also facilitate the development of corrosion inhibitors. OF probe at the nanoscale along with its incredible properties of enhanced resolution, sensitivity and selectivity will enable us to study complex interfacial processes occurring at metallic surfaces.

Overall, the combination of electrochemistry and OFs has a tremendous potential to drive future research in various fields in analytical chemistry through the use of micro- and nanoscale OF electrodes with reliable selectivity, high sensitivity, sub-micron resolution and cost efficiency.

2.6 Acknowledgements

The authors acknowledge the Natural Sciences and Engineering Research Council of Canada (RGPIN-2019-05365) for its financial support. Research funding by the Canada Research Coordinating Committee through a New Frontiers in Research Fund (NFRFE-2018-00190) is also acknowledged.

2.7 References

(1) Leung, A.; Shankar, P. M.; Mutharasan, R. A Review of Fiber-Optic Biosensors. *Sens Actuators B Chem* **2007**, *125* (2), 688–703. https://doi.org/10.1016/j.snb.2007.03.010.

(2) Addanki, S.; Amiri, I. S.; Yupapin, P. Review of Optical Fibers-Introduction and Applications in Fiber Lasers. *Results Phys* **2018**, *10*, 743–750. https://doi.org/10.1016/j.rinp.2018.07.028.

(3) Maurer, R.; Keck, D.; Schlutz, P. Method of Producing Optical Waveguide Fibers, 1970. https://patents.google.com/patent/US3711262A/en%0Ahttps://patents.google.com/patent/US3711262. (accessed 2024-08-06).

(4) Bellis, M. *How fiber optics was invented*. ThoughtCo. https://www. thoughtco.com/birth-of-fiber-optics-4091837, (accessed 2024-08-06).

(5) Jupnik, H. Fiber Optics. Principles and Applications. N. S. Kapany. Academic Press, New York, 1967. 447 Pp.,. *Science (1979)* **1968**, *159* (3811), 183–183. https://doi.org/10.1126/science.159.3811.183.

(6) Lee, B. Review of the Present Status of Optical Fiber Sensors. *Optical Fiber Technology* **2003**, *9* (2), 57–79. https://doi.org/10.1016/S1068-5200(02)00527-8.

(7) Vo-dinh, T.; Scaffidi, J.; Gregas, M.; Zhang, Y. Applications of Fiber-Optics-Based Nanosensors to Drug Discovery Applications of Fiber-Optics-Based Nanosensors to Drug Discovery. **2009**, *0441*. https://doi.org/10.1517/17460440903085112.

(8) Leemput, L. E. C. van de; Kempen, H. van. Scanning Tunnelling Microscopy. *Reports on Progress in Physics* **1992**, *55* (8), 1165–1240. https://doi.org/10.1088/0034-4885/55/8/002.

(9) Betzig, E.; Chichester, R. J. Single Molecules Observed by Near-Field Scanning Optical Microscopy. *Science (1979)* **1993**, *262* (5138), 1422–1425. https://doi.org/10.1126/science.262.5138.1422.

(10) Marsh, T. C.; Vesenka, J.; Henderson, E. A New DNA Nanostructure, the G-Wire, Imaged by Scanning Probe Microscopy. *Nucleic Acids Res* **1995**, *23* (4), 696–700. https://doi.org/10.1093/nar/23.4.696.

(11) Engel, A.; Schoenenberger, C.-A.; Müller, D. J. High Resolution Imaging of Native Biological Sample Surfaces Using Scanning Probe Microscopy. *Curr Opin Struct Biol* **1997**, *7* (2), 279–284. https://doi.org/10.1016/S0959-440X(97)80037-1.

(12) Bard, A. J.; Fan, F. R. F.; Kwak, J.; Lev, O. Scanning Electrochemical Microscopy. Introduction and Principles. *Anal Chem* **1989**, *61* (2), 132–138. https://doi.org/10.1021/ac00177a011.

(13) Maus, R. G.; McDonald, E. M.; Wightman, R. M. Imaging of Nonuniform Current Density at Microelectrodes by Electrogenerated Chemiluminescence. *Anal Chem* **1999**, *71* (21), 4944–4950. https://doi.org/10.1021/ac9905827.

(14) Zu, Y.; Ding, Z.; Zhou, J.; Lee, Y.; Bard, A. J. Scanning Optical Microscopy with an Electrogenerated Chemiluminescent Light Source at a Nanometer Tip. *Anal Chem* **2001**, *73* (10), 2153–2156. https://doi.org/10.1021/ac001538q.

(15) Lee, Y.; Ding, Z.; Bard, A. J. Combined Scanning Electrochemical/Optical Microscopy with Shear Force and Current Feedback. *Anal Chem* **2002**, *74* (15), 3634–3643. https://doi.org/10.1021/ac015713u.

(16) Fan, F.-R. F.; Cliffel, D.; Bard, A. J. Scanning Electrochemical Microscopy. 37. Light Emission by Electrogenerated Chemiluminescence at SECM Tips and Their Application to Scanning Optical Microscopy. *Anal Chem* **1998**, *70* (14), 2941–2948. https://doi.org/10.1021/ac980107t.

(17) Szunerits, S.; Walt, D. R. The Use of Optical Fiber Bundles Combined with Electrochemistry for Chemical Imaging. *ChemPhysChem* **2003**, *4* (2), 186–192. https://doi.org/10.1002/cphc.200390029.

(18) Guo, T. Fiber Grating-Assisted Surface Plasmon Resonance for Biochemical and Electrochemical Sensing. *Journal of Lightwave Technology* **2017**, *35* (16), 3323–3333. https://doi.org/10.1109/JLT.2016.2590879.

(19) Khan, S. S.; Jin, E. S.; Sojic, N.; Pantano, P. A Fluorescence-Based Imaging-Fiber Electrode Chemical Sensor for Hydrogen Peroxide. *Anal Chim Acta* **2000**, *404* (2), 213–221. https://doi.org/10.1016/S0003-2670(99)00727-8.

(20) Zhao, F.; Hartmann, V.; Ruff, A.; Nowaczyk, M. M.; Rögner, M.; Schuhmann, W.; Conzuelo, F. Unravelling Electron Transfer Processes at Photosystem 2 Embedded in an Os-Complex Modified Redox Polymer. *Electrochim Acta* **2018**, *290*, 451–456. https://doi.org/10.1016/j.electacta.2018.09.093.

(21) Zhao, F.; Hardt, S.; Hartmann, V.; Zhang, H.; Nowaczyk, M. M.; Rögner, M.; Plumeré, N.; Schuhmann, W.; Conzuelo, F. Light-Induced Formation of Partially Reduced Oxygen Species Limits the Lifetime of Photosystem 1-Based Biocathodes. *Nat Commun* **2018**, *9* (1). https://doi.org/10.1038/s41467-018-04433-z.

(22) Conzuelo, F.; Sliozberg, K.; Gutkowski, R.; Grutzke, S.; Nebe, M.; Schuhmann, W. High-Resolution Analysis of Photoanodes for Water Splitting by Means of Scanning Photoelectrochemical Microscopy. *Anal Chem* **2017**, *89* (2), 1222–1228. https://doi.org/10.1021/acs.analchem.6b03706.

(23) Takahashi, Y.; Hirano, Y.; Yasukawa, T.; Shiku, H.; Yamada, H.; Matsue, T. Topographic, Electrochemical, and Optical Images Captured Using Standing Approach Mode Scanning Electrochemical/Optical Microscopy. *Langmuir* **2006**, *22* (25), 10299–10306. https://doi.org/10.1021/la0611763.

(24) Takahashi, Y.; Shiku, H.; Murata, T.; Yasukawa, T.; Matsue, T. Transfected Single-Cell Imaging by Scanning Electrochemical Optical Microscopy with Shear Force Feedback Regulation. *Anal Chem* **2009**, *81* (23), 9674–9681. https://doi.org/10.1021/ac901796r.

(25) Sosa, E.; Hernández, F.; Casillas, N.; Cabrera-Sierra, R.; Oropeza, T.; González, I. Homogeneity and Activity Characterization of Iron Sulfide Films after Immersion in Different Electrolytic Media. *J Electrochem Soc* **2003**, *150* (4), 237–243. https://doi.org/10.1149/1.1556051.

(26) Sosa, E.; Cabrera-Sierra, R.; Oropeza, M. T.; Hernández, F.; Casillas, N.; Tremont, R.; Cabrera, C.; González, I. Chemical Characterization of Corrosion Films Electrochemically Grown on Carbon Steel in Alkaline Sour Environment. *J Electrochem Soc* **2003**, *150* (11), 530–535. https://doi.org/10.1149/1.1617303.

(27) Garfias-Mesias, L. F.; Smyrl, W. H. High Resolution In-Situ Imaging of Reactive Heterogeneous Surfaces. *Electrochim Acta* **1999**, *44* (21), 3651–3657. https://doi.org/10.1016/S0013-4686(99)00068-7.

(28) Amphlett, J. L.; Denuault, G. Scanning Electrochemical Microscopy (SECM): An Investigation of the Effects of Tip Geometry on Amperometric Tip Response. *J Phys Chem B* **1998**, *102* (49), 9946–9951. https://doi.org/10.1021/jp982829u.

(29) Andrieux, F. P. L.; Boxall, C.; O'Hare, D. The Micro-Optical Ring Electrode Part 2: Theory for the Transport Limited, Steady-State Photocurrent. *Journal of Electroanalytical Chemistry* **2006**, *589* (2), 177–186. https://doi.org/10.1016/j.jelechem.2005.12.002.

(30) Imai, K.; Okazaki, T.; Hata, N.; Taguchi, S.; Sugawara, K.; Kuramitz, H. Simultaneous Multiselective Spectroelectrochemical Fiber-Optic Sensor: Demonstration of the Concept Using Methylene Blue and Ferrocyanide. *Anal Chem* **2015**, *87* (4), 2375–2382. https://doi.org/10.1021/ac504321u.

(31) Goss, C. A.; Charych, D. H.; Majda, Marcin. Application of (3-Mercaptopropyl)Trimethoxysilane as a Molecular Adhesive in the Fabrication of Vapor-Deposited Gold Electrodes on Glass Substrates. *Anal Chem* **1991**, *63* (1), 85–88. https://doi.org/10.1021/ac00001a018.

(32) Du, B.; Ruan, Y.; Ly, T. T.; Jia, P.; Sun, Q.; Feng, Q.; Yang, D.; Ebendorff-Heidepriem, H. MoS2-Enhanced Epoxy-Based Plasmonic Fiber-Optic Sensor for Selective and Sensitive Detection of Methanol. *Sens Actuators B Chem* **2020**, *305* (November 2019), 127513. https://doi.org/10.1016/j.snb.2019.127513.

(33) Casillas, N.; James, P.; Smyrl, W. H. A Novel Approach to Combine Scanning Electrochemical Microscopy and Scanning Photoelectrochemical Microscopy. *J Electrochem Soc* **1995**, *142* (1), L16–L18. https://doi.org/10.1149/1.2043970.

(34) James, P.; Casillas, N.; Smyrl, W. H. Simultaneous Scanning Electrochemical and Photoelectrochemical Microscopy by Use of a Metallized Optical Fiber. *J Electrochem Soc* **1996**, *143* (12), 3853–3865. https://doi.org/10.1149/1.1837308.

(35) Pennarun, G. I.; Boxalla, C.; O'Hare, D. Micro-Optical Ring Electrode: Development of a Novel Electrode for Photoelectrochemistry. *Analyst* **1996**, *121* (12), 1779–1788. https://doi.org/10.1039/an9962101779.

(36) Andrieux, F. P. L.; Boxall, C.; O'Hare, D. The Micro-Optical Ring Electrode. 3: Transient Photocurrent Studies of Photophysical-Electrochemical and Photophysical-Chemical-

Electrochemical Systems. *Journal of Physical Chemistry B* **2006**, *110* (32), 16148–16156. https://doi.org/10.1021/jp0622785.

(37) Lee, Y.; Bard, A. J. Fabrication and Characterization of Probes for Combined Scanning Electrochemical/Optical Microscopy Experiments. *Anal Chem* **2002**, *74* (15), 3626–3633. https://doi.org/10.1021/ac015705d.

(38) Bach, C. E.; Nichols, R. J.; Beckmann, W.; Meyer, H.; Schulte, A.; Besenhard, J. O.; Jannakoudakis, P. D. Effective Insulation of Scanning Tunneling Microscopy Tips for Electrochemical Studies Using an Electropainting Method. *J Electrochem Soc* **1993**, *140* (5), 1281–1284. https://doi.org/10.1149/1.2220971.

(39) Xiong, H.; Guo, J.; Kurihara, K.; Amemiya, S. Fabrication and Characterization of Conical Microelectrode Probes Templated by Selectively Etched Optical Fibers for Scanning Electrochemical Microscopy. *Electrochem commun* **2004**, *6* (6), 615–620. https://doi.org/10.1016/j.elecom.2004.04.016.

(40) Maruyama, K.; Ohkawa, H.; Ogawa, S.; Ueda, A.; Niwa, O.; Suzuki, K. Fabrication and Characterization of a Nanometer-Sized Optical Fiber Electrode Based on Selective Chemical Etching for Scanning Electrochemical/ Optical Microscopy. *Anal Chem* **2006**, *78* (6), 1904–1912. https://doi.org/10.1021/ac0502549.

(41) Wu, S.; Su, B. A Simple Approach for Fabrication of Microring Electrodes. *Journal of Electroanalytical Chemistry* **2013**, *694*, 12–16. https://doi.org/10.1016/j.jelechem.2013.01.018.

(42) Wang, Y.; Luo, J.; Chen, H.; He, Q.; Gan, N.; Li, T. A Microchip-Based Flow Injection-Amperometry System with Mercaptopropionic Acid Modified Electroless Gold Microelectrode for the Selective Determination of Dopamine. *Anal Chim Acta* **2008**, *625* (2), 180–187. https://doi.org/10.1016/j.aca.2008.07.030.

(43) Svir, I.; Oleinick, A.; Yunus, K.; Fisher, A. C.; Wadhawan, J. D.; Davies, T. J.; Compton, R. G. Theoretical and Experimental Study of the ECE Mechanism at Microring Electrodes. *Journal of Electroanalytical Chemistry* **2005**, *578* (2), 289–299. https://doi.org/10.1016/j.jelechem.2005.01.011.

(44) Beam, B. M.; Armstrong, N. R.; Mendes, S. B. An Electroactive Fiber Optic Chip for Spectroelectrochemical Characterization of Ultra-Thin Redox-Active Films. *Analyst* **2009**, *134* (3), 454–459. https://doi.org/10.1039/b814338b.

(45) Okazaki, T.; Shiokawa, E.; Orii, T.; Yamamoto, T.; Hata, N.; Taguchi, A.; Sugawara, K.; Kuramitz, H. Simultaneous Multiselective Spectroelectrochemical Fiber-Optic Sensor: Sensing with an Optically Transparent Electrode. *Anal Chem* **2018**, *90* (4), 2440–2445. https://doi.org/10.1021/acs.analchem.7b03957.

(46) Bombail, T.; Garrigue, P.; Goudeau, B.; Talaga, D.; Bouffier, L.; Bonhommeau, S.; Servant, L.; Zigah, D.; Arbault, S.; Sojic, N. Dual Microelectrodes Decorated with Nanotip Arrays: Fabrication, Characterization and Spectroelectrochemical Sensing. *Electrochim Acta* **2019**, *328*. https://doi.org/10.1016/j.electacta.2019.135105.

(47) Deiss, F.; Sojic, N.; White, D. J.; Stoddart, P. R. Nanostructured Optical Fibre Arrays for High-Density Biochemical Sensing and Remote Imaging. *Anal Bioanal Chem* **2010**, *396* (1), 53–71. https://doi.org/10.1007/s00216-009-3211-0.

(48) Yuan, D.; Xiao, L.; Jia, J.; Zhang, J.; Han, L.; Li, P.; Mao, B. W.; Zhan, D. Combinatorial Screening of Photoelectrocatalytic System with High Signal/Noise Ratio. *Anal Chem* **2014**, *86* (24), 11972–11976. https://doi.org/10.1021/ac503614h.

(49) Van Dyke, D. A.; Cheng, H. yuan. Fabrication and Characterization of a Fiber-Optic-Based Spectroelectrochemical Probe. *Anal Chem* **1988**, *60* (13), 1256–1260. https://doi.org/10.1021/ac00164a004.

(50) Macpherson, J. V.; Unwin, P. R. Radial Flow Microring Electrode: Development and Characterization. *Anal Chem* **1998**, *70* (14), 2914–2921. https://doi.org/10.1021/ac9801667.

(51) Bitziou, E.; Rudd, N. C.; Unwin, P. R. Microjet Ring Electrode (MJRE): Development, Modelling and Experimental Characterisation. *Journal of Electroanalytical Chemistry* **2007**, *602* (2), 263–274. https://doi.org/10.1016/j.jelechem.2007.01.014.

(52) Tiwari, A.; Singh, V.; Nagaiah, T. C. Tuning the MnWO4 Morphology and Its Electrocatalytic Activity towards Oxygen Reduction Reaction. *J Mater Chem A Mater* **2018**, *6* (6), 2681–2692. https://doi.org/10.1039/c7ta10380h.

(53) Tiwari, A.; Nagaiah, T. C.; Bordoloi, A. Electrocatalytic Activity of Tungsten Oxide Nanoclusters Grafted on Mesoporous Nitrogen-Rich Carbon Material in the Dioxygen Reduction Reaction. *Chempluschem* **2015**, *80* (11), 1666–1672. https://doi.org/10.1002/cplu.201500253.

(54) Szunerits, S.; Walt, D. R. Fabrication of an Optoelectrochemical Microring Array. *Anal Chem* **2002**, *74* (7), 1718–1723. https://doi.org/10.1021/ac010933t.

(55) Bae, J. H.; Nepomnyashchii, A. B.; Wang, X.; Potapenko, D. V.; Mirkin, M. V. Photo-Scanning Electrochemical Microscopy on the Nanoscale with Through-Tip Illumination. *Anal Chem* **2019**, *91* (20), 12601–12605. https://doi.org/10.1021/acs.analchem.9b03347.

(56) Lin, C. W.; Fan, F. F.; Bard, A. J. High Resolution Photoelectrochemical Etching of n-GaAs with the Scanning Electrochemical and Tunneling Microscope. *J Electrochem Soc* **1987**, *134* (4), 1038–1039. https://doi.org/10.1149/1.2100566.

(57) Eriksson, S.; Carlsson, P.; Holmström, B.; Uosaki, K. Scanning Tunneling Microscopy-Tip Current Voltammetry Studies of n-GaAs — Effect of Illumination, Doping Density and Potential. *Journal of Electroanalytical Chemistry* **1992**, *336* (1–2), 57–71. https://doi.org/10.1016/0022-0728(92)80262-3.

(58) Eriksson, S.; Carlsson, P.; Holmström, B.; Uosaki, K. Laser Spot Scanning in Photoelectrochemical Systems, Relation between Spot Size and Spatial Resolution of the Photocurrent. *J Appl Phys* **1991**, *69* (4), 2324–2327. https://doi.org/10.1063/1.348714.

(59) A, E. S. S.; Tyler, P. S.; Kozlowski, M. R.; Smyrl, W. H.; Atanasoski, R. T. Photoelectrochemical Microscopy as a Probe of Localized Properties of Thin TiO2 Films. **1987**, *231*, 295–302.

(60) Avalos-Martinez, J.; Villatoro, J.; Flores, J. L.; Garcia-Torales, G.; Barcena-Soto, M.; Casillas, N. Optimal Optical Fiber for High Spatial Resolution in Scanning Electrochemical and Photoelectrochemical Microscopy. *Infrared Spaceborne Remote Sensing XII* **2004**, *5543* (52), 350. https://doi.org/10.1117/12.561579.

(61) Mirkin, M. V.; Fan, F.-R. F.; Bard, A. J. Scanning Electrochemical Microscopy Part 13. Evaluation of the Tip Shapes of Nanometer Size Microelectrodes. *Journal of Electroanalytical Chemistry* **1992**, *328* (1–2), 47–62. https://doi.org/10.1016/0022-0728(92)80169-5.

(62) Laforge, F. O.; Velmurugan, J.; Wang, Y.; Mirkin, M. V. Nanoscale Imaging of Surface Topography and Reactivity with the Scanning Electrochemical Microscope. *Anal Chem* **2009**, *81* (8), 3143–3150. https://doi.org/10.1021/ac900335c.

(63) Zoski, C. G.; Liu, B.; Bard, A. J. Scanning Electrochemical Microscopy: Theory and Characterization of Electrodes of Finite Conical Geometry. *Anal Chem* **2004**, *76* (13), 3646–3654. https://doi.org/10.1021/ac049938r.

(64) Zhao, F.; Conzuelo, F.; Hartmann, V.; Li, H.; Stapf, S.; Nowaczyk, M. M.; Rögner, M.; Plumeré, N.; Lubitz, W.; Schuhmann, W. A Novel Versatile Microbiosensor for Local Hydrogen Detection by Means of Scanning Photoelectrochemical Microscopy. *Biosens Bioelectron* **2017**, *94* (December 2016), 433–437. https://doi.org/10.1016/j.bios.2017.03.037.

(65) Zhao, F.; Plumeré, N.; Nowaczyk, M. M.; Ruff, A.; Schuhmann, W.; Conzuelo, F. Interrogation of a PS1-Based Photocathode by Means of Scanning Photoelectrochemical Microscopy. *Small* **2017**, *13* (26), 1–8. https://doi.org/10.1002/smll.201604093.

(66) Landman, A.; Dotan, H.; Shter, G. E.; Wullenkord, M.; Houaijia, A.; Maljusch, A.; Grader, G. S.; Rothschild, A. Photoelectrochemical Water Splitting in Separate Oxygen and Hydrogen Cells. *Nat Mater* **2017**, *16* (6), 646–651. https://doi.org/10.1038/nmat4876.

(67) Jacobsson, T. J. Photoelectrochemical Water Splitting: An Idea Heading towards Obsolescence? *Energy Environ Sci* **2018**, *11* (8), 1977–1979. https://doi.org/10.1039/C8EE00772A.

(68) Miller, E. L. Photoelectrochemical Water Splitting. *Energy Environ Sci* **2015**, *8* (10), 2809–2810. https://doi.org/10.1039/C5EE90047F.

(69) Suryanto, B. H. R.; Wang, Y.; Hocking, R. K.; Adamson, W.; Zhao, C. Overall Electrochemical Splitting of Water at the Heterogeneous Interface of Nickel and Iron Oxide. *Nat Commun* **2019**, *10* (1), 5599. https://doi.org/10.1038/s41467-019-13415-8.

(70) Roger, I.; Shipman, M. A.; Symes, M. D. Earth-Abundant Catalysts for Electrochemical and Photoelectrochemical Water Splitting. *Nat Rev Chem* **2017**, *1* (1), 0003. https://doi.org/10.1038/s41570-016-0003.

(71) Jang, Y. J.; Lee, J. S. Photoelectrochemical Water Splitting with P-Type Metal Oxide Semiconductor Photocathodes. *ChemSusChem* **2019**, *12* (9), 1835–1845. https://doi.org/10.1002/cssc.201802596.

(72) Gao, D.; Liu, R.; Biskupek, J.; Kaiser, U.; Song, Y.; Streb, C. Modular Design of Noble-Metal-Free Mixed Metal Oxide Electrocatalysts for Complete Water Splitting. *Angewandte Chemie International Edition* **2019**, *58* (14), 4644–4648. https://doi.org/10.1002/anie.201900428.

(73) Chandrasekaran, S.; Yao, L.; Deng, L.; Bowen, C.; Zhang, Y.; Chen, S.; Lin, Z.; Peng, F.; Zhang, P. Recent Advances in Metal Sulfides: From Controlled Fabrication to Electrocatalytic, Photocatalytic and Photoelectrochemical Water Splitting and Beyond. *Chem Soc Rev* **2019**, *48* (15), 4178–4280. https://doi.org/10.1039/C8CS00664D.

(74) She, H.; Jiang, M.; Yue, P.; Huang, J.; Wang, L.; Li, J.; Zhu, G.; Wang, Q. Metal (Ni2+/Co2+) Sulfides Modified BiVO4 for Effective Improvement in Photoelectrochemical Water Splitting. *J Colloid Interface Sci* **2019**, *549*, 80–88. https://doi.org/10.1016/j.jcis.2019.04.038.

(75) Garcia-Torregrosa, I.; Wijten, J. H. J.; Zanoni, S.; Oropeza, F. E.; Hofmann, J. P.; Hensen, E. J. M.; Weckhuysen, B. M. Template-Free Nanostructured Fluorine-Doped Tin Oxide Scaffolds for Photoelectrochemical Water Splitting. *ACS Appl Mater Interfaces* **2019**, *11* (40), 36485–36496. https://doi.org/10.1021/acsami.9b05176.

(76) Shen, S.; Chen, J.; Cai, L.; Ren, F.; Guo, L. A Strategy of Engineering Impurity Distribution in Metal Oxide Nanostructures for Photoelectrochemical Water Splitting. *Journal of Materiomics* **2015**, *1* (2), 134–145. https://doi.org/10.1016/j.jmat.2015.02.003.

(77) Wang, S.; Chen, P.; Yun, J.; Hu, Y.; Wang, L. An Electrochemically Treated $BiVO_4$ Photoanode for Efficient Photoelectrochemical Water Splitting. *Angewandte Chemie International Edition* **2017**, *56* (29), 8500–8504. https://doi.org/10.1002/anie.201703491.

(78) Harati, M.; Jia, J.; Giffard, K.; Pellarin, K.; Hewson, C.; Love, D. A.; Lau, W. M.; Ding, Z. One-Pot Electrodeposition, Characterization and Photoactivity of Stoichiometric Copper Indium Gallium Diselenide (CIGS) Thin Films for Solar Cells. *Physical Chemistry Chemical Physics* **2010**, *12* (46), 15282–15290. https://doi.org/10.1039/c0cp00586j.

(79) Ye, H.; Park, H. S.; Bard, A. J. Screening of Electrocatalysts for Photoelectrochemical Water Oxidation on W-Doped BiVO4 Photocatalysts by Scanning Electrochemical Microscopy. *Journal of Physical Chemistry C* **2011**, *115* (25), 12464–12470. https://doi.org/10.1021/jp200852c.

(80) Jang, J. S.; Lee, J.; Ye, H.; Fan, F. R. F.; Bard, A. J. Rapid Screening of Effective Dopants for Fe 2o 3 Photocatalysts with Scanning Electrochemical Microscopy and Investigation of Their Photoelectrochemical Properties. *Journal of Physical Chemistry C* **2009**, *113* (16), 6719–6724. https://doi.org/10.1021/jp8109429.

(81) Park, H. S.; Kweon, K. E.; Ye, H.; Paek, E.; Hwang, G. S.; Bard, A. J. Factors in the Metal Doping of $BiVO_4$ for Improved Photoelectrocatalytic Activity as Studied by Scanning Electrochemical Microscopy and First-Principles Density-Functional Calculation. *The Journal of Physical Chemistry C* **2011**, *115* (36), 17870–17879. https://doi.org/10.1021/jp204492r.

(82) Gutkowski, R.; Khare, C.; Conzuelo, F.; Kayran, Y. U.; Ludwig, A.; Schuhmann, W. Unraveling Compositional Effects on the Light-Induced Oxygen Evolution in Bi(V-Mo-X)O4 Material Libraries. *Energy Environ Sci* **2017**, *10* (5), 1213–1221. https://doi.org/10.1039/c7ee00287d.

(83) Guo, S.-X.; Liu, Y.; Lee, C.-Y.; Bond, A. M.; Zhang, J.; Geletii, Y. V.; Hill, C. L. Graphene-Supported [{Ru4O4(OH)2(H2O)4}(γ-SiW10O36)2]10− for Highly Efficient Electrocatalytic Water Oxidation. *Energy Environ Sci* **2013**, *6* (9), 2654. https://doi.org/10.1039/c3ee41892h.

(84) Stracke, J. J.; Finke, R. G. Water Oxidation Catalysis Beginning with 2.5 MM $[Co_4(H_2O)_2(PW_9O_{34})_2]^{10-}$: Investigation of the True Electrochemically Driven Catalyst at ≥600 MV Overpotential at a Glassy Carbon Electrode. *ACS Catal* **2013**, *3* (6), 1209–1219. https://doi.org/10.1021/cs400141t.

(85) Kimmich, D.; Taffa, D. H.; Dosche, C.; Wark, M.; Wittstock, G. Combinatorial Screening of Photoanode Materials - Uniform Platform for Compositional Arrays and Macroscopic Electrodes. *Electrochim Acta* **2018**, *259*, 204–212. https://doi.org/10.1016/j.electacta.2017.10.147.

(86) Shinde, P. S.; Peng, X.; Wang, J.; Ma, Y.; McNamara, L. E.; Hammer, N. I.; Gupta, A.; Pan, S. Rapid Screening of Photoanode Materials Using Scanning Photoelectrochemical Microscopy Technique and Formation of Z-Scheme Solar Water Splitting System by Coupling p- and n-Type Heterojunction Photoelectrodes. *ACS Appl Energy Mater* **2018**, *1* (5), 2283–2294. https://doi.org/10.1021/acsaem.8b00381.

(87) Ye, H.; Lee, J.; Jang, J. S.; Bard, A. J. Rapid Screening of Bivo4-Based Photocatalysts by Scanning Electrochemical Microscopy (SECM) and Studies of Their Photoelectrochemical Properties. *Journal of Physical Chemistry C* **2010**, *114* (31), 13322–13328. https://doi.org/10.1021/jp104343b.

(88) Bohni, H.; Suter, T.; Assi, F. Micro-Electrochemical Techniques for Studies of Localized Processes on Metal Surfaces in the Nanometer Range. *Surf Coat Technol* **2000**, *130*, 80–86.

(89) Li, X. M.; Chen, W.; Huang, Z. Q.; Huang, S.; Bennett, K. D. <title>Fiber Optic Corrosion Sensor Fabricated by Electrochemical Method</Title>. *Smart Structures and Materials 1998: Sensory Phenomena and Measurement Instrumentation for Smart Structures and Materials* **1998**, *3330* (March 1998), 126–133. https://doi.org/10.1117/12.316965.

(90) Rutherford, P. S.; Ikegami, R.; Shrader, J.; Sherrer, D. W.; Zabaronick, N.; Zeakes, J. S.; Murphy, K. A.; Claus, R. O. Novel NDE Fiber Optic Corrosion Sensor. *Proceedings of SPIE - The International Society for Optical Engineering* **1996**, *2718*, 158–169.

(91) Abderrahmane, S.; Himour, A.; Kherrat, R.; Chailleux, E.; Jaffrezic-Renault, N.; Stremsdoerfer, G. An Optical Fibre Corrosion Sensor with an Electroless Deposit of Ni-P. *Sens Actuators B Chem* **2001**, *75* (1–2), 1–4. https://doi.org/10.1016/S0925-4005(00)00677-8.

(92) Benounis, M.; Jaffrezic-Renault, N.; Stremsdoerfer, G.; Kherrat, R. Elaboration and Standardization of an Optical Fibre Corrosion Sensor Based on an Electroless Deposit of Copper. *Sens Actuators B Chem* **2003**, *90* (1–3), 90–97. https://doi.org/10.1016/S0925-4005(03)00050-9.

(93) Dong, S.; Liao, Y.; Tian, Q.; Luo, Y.; Qiu, Z.; Song, S. Optical and Electrochemical Measurements for Optical Fibre Corrosion Sensing Techniques. *Corros Sci* **2006**, *48* (7), 1746–1756. https://doi.org/10.1016/j.corsci.2005.05.025.

(94) Szunerits, S.; Pust, S. E.; Wittstock, G. Multidimensional Electrochemical Imaging in Materials Science. *Anal Bioanal Chem* **2007**, *389* (4), 1103–1120. https://doi.org/10.1007/s00216-007-1374-0.

(95) Subramanian, S.; Huiszoon, R. C.; Chu, S.; Bentley, W. E.; Ghodssi, R. Microsystems for Biofilm Characterization and Sensing – A Review. *Biofilm* **2020**, *2* (September 2019), 100015. https://doi.org/10.1016/j.bioflm.2019.100015.

(96) Philip-Chandy, R.; Scully, P. J.; Eldridge, P.; Kadim, H. J.; Grapin, M. G.; Jonca, M. G.; D'Ambrosio, M. G.; Colin, F. Optical Fiber Sensor for Biofilm Measurement Using Intensity Modulation and Image Analysis. *IEEE Journal on Selected Topics in Quantum Electronics* **2000**, *6* (5), 764–772. https://doi.org/10.1109/2944.892616.

(97) Zhong, Nianbing; Zhao, Mingfu; Li, Y. U-Shaped, Double-Tapered, Fiber-Optic Sensor for Effective Biofilm Growth Monitoring. *Biomed Opt Express* **2016**, *7* (2), 352. https://doi.org/10.1364/boe.7.000352.

(98) Yuan, Y.; Guo, T.; Qiu, X.; Tang, J.; Huang, Y.; Zhuang, L.; Zhou, S.; Li, Z.; Guan, B.-O.; Zhang, X.; Albert, J. Electrochemical Surface Plasmon Resonance Fiber-Optic Sensor: *In Situ* Detection of Electroactive Biofilms. *Anal Chem* **2016**, *88* (15), 7609–7616. https://doi.org/10.1021/acs.analchem.6b01314.

(99) Keiser, G. *Biophotonics Concepts to Applications*.

(100) Bosch, M. E.; Sánchez, A. J. R.; Rojas, F. S.; Ojeda, C. B. Recent Development in Optical Fiber Biosensors. *Sensors* **2007**, *7* (6), 797–859. https://doi.org/10.3390/s7060797.

(101) Martin, M.; Olives, A.; Castillo, B.; Menendez, J. Trends in the Design and Application of Optical Chemosensors in Pharmaceutical and Biomedical Analysis. *Curr Pharm Anal* **2008**, *4* (3), 106–117. https://doi.org/10.2174/157341208785161236.

(102) Trettnak, W.; Wolfbels, O. S. A Fiber Optic Cholesterol Biosensor with an Oxygen Optrode as the Transducer. *Anal Lett* **1989**, *22* (9), 2191–2197. https://doi.org/10.1080/00032718908051247.

(103) Abel, A. P.; Weller, M. G.; Duveneck, G. L.; Ehrat, M.; Widmer, H. M. Fiber-Optic Evanescent Wave Biosensor for the Detection of Oligonucleotides. *Anal Chem* **1996**, *68* (17), 2905–2912. https://doi.org/10.1021/ac960071+.

(104) Liu, X.; Tan, W. A Fiber-Optic Evanescent Wave DNA Biosensor Based on Novel Molecular Beacons. *Anal Chem* **1999**, *71* (22), 5054–5059. https://doi.org/10.1021/ac990561c.

(105) Pilevar, S.; Davis, C. C.; Portugal, F. Tapered Optical Fiber Sensor Using Near-Infrared Fluorophores to Assay Hybridization. *Anal Chem* **1998**, *70* (10), 2031–2037. https://doi.org/10.1021/ac9709965.

(106) Ikariyama, Y.; Nishiguchi, S.; Koyama, T.; Kobatake, E.; Aizawa, M.; Tsuda, M.; Nakazawa, T. Fiber-Optic-Based Biomonitoring of Benzene Derivatives by Recombinant E. Coli Bearing Luciferase Gene-Fused TOL-Plasmid Immobilized on the Fiber-Optic End. *Anal Chem* **1997**, *69* (13), 2600–2605. https://doi.org/10.1021/ac961311o.

(107) Polyak, B.; Bassis, E.; Novodvorets, A.; Belkin, S.; Marks, R. S. Bioluminescent Whole Cell Optical Fiber Sensor to Genotoxicants: System Optimization. *Sens Actuators B Chem* **2001**, *74* (1–3), 18–26. https://doi.org/10.1016/S0925-4005(00)00707-3.

(108) Marks, R. S. Chemiluminescent Optical Fiber Immunosensor for Detecting Cholera Antitoxin. *Optical Engineering* **1997**, *36* (12), 3258. https://doi.org/10.1117/1.601560.

(109) Marks, R. S.; Margalit, A.; Bychenko, A.; Bassis, E.; Porat, N.; Dagan, R. Development of a Chemiluminescent Optical Fiber Immunosensor to Detect Streptococcus Pneumoniae Antipolysaccharide Antibodies. *Applied Biochemistry and Biotechnology - Part A Enzyme Engineering and Biotechnology* **2000**, *89* (2–3), 117–126. https://doi.org/10.1385/ABAB:89:2-3:117.

(110) Marks, R. S.; Novoa, A.; Konry, T.; Krais, R.; Cosnier, S. Indium Tin Oxide-Coated Optical Fiber Tips for Affinity Electropolymerization. *Materials Science and Engineering C* **2002**, *21* (1–2), 189–194. https://doi.org/10.1016/S0928-4931(02)00085-1.

(111) Herrmann, S.; Leshem, B.; Landes, S.; Rager-Zisman, B.; Marks, R. S. Chemiluminescent Optical Fiber Immunosensor for the Detection of Anti-West Nile Virus IgG. *Talanta* **2005**, *66* (1), 6–14. https://doi.org/10.1016/j.talanta.2004.10.013.

(112) Magrisso, M.; Etzion, O.; Pilch, G.; Novodvoretz, A.; Perez-Avraham, G.; Schlaeffer, F.; Marks, R. Fiber-Optic Biosensor to Assess Circulating Phagocyte Activity by Chemiluminescence. *Biosens Bioelectron* **2006**, *21* (7), 1210–1218. https://doi.org/10.1016/j.bios.2005.05.006.

(113) Salama, O.; Herrmann, S.; Tziknovsky, A.; Piura, B.; Meirovich, M.; Trakht, I.; Reed, B.; Lobel, L. I.; Marks, R. S. Chemiluminescent Optical Fiber Immunosensor for Detection of Autoantibodies to Ovarian and Breast Cancer-Associated Antigens. *Biosens Bioelectron* **2007**, *22* (7), 1508–1516. https://doi.org/10.1016/j.bios.2006.07.003.

(114) Petrosova, A.; Konry, T.; Cosnier, S.; Trakht, I.; Lutwama, J.; Rwaguma, E.; Chepurnov, A.; Mühlberger, E.; Lobel, L.; Marks, R. S. Development of a Highly Sensitive, Field Operable Biosensor for Serological Studies of Ebola Virus in Central Africa. *Sens Actuators B Chem* **2007**, *122* (2), 578–586. https://doi.org/10.1016/j.snb.2006.07.005.

(115) Konry, T.; Novoa, A.; Shemer-Avni, Y.; Hanuka, N.; Cosnier, S.; Lepellec, A.; Marks, R. S. Optical Fiber Immunosensor Based on a Poly(Pyrrole-Benzophenone) Film for the Detection of Antibodies to Viral Antigen. *Anal Chem* **2005**, *77* (6), 1771–1779. https://doi.org/10.1021/ac048569w.

(116) Liu, G.; Liu, C.; Bard, A. J. Rapid Synthesis and Screening of ZnxCd1-XS YSe1-y Photocatalysts by Scanning Electrochemical Microscopy. *Journal of Physical Chemistry C* **2010**, *114* (49), 20997–21002. https://doi.org/10.1021/jp1058116.

(117) Zhu, L.; Li, Y.; Tian, F.; Xu, B.; Zhu, G. Electrochemiluminescent Determination of Glucose with a Sol-Gel Derived Ceramic-Carbon Composite Electrode as a Renewable Optical Fiber Biosensor. *Sens Actuators B Chem* **2002**, *84* (2–3), 265–270. https://doi.org/10.1016/S0925-4005(02)00035-7.

(118) Rincón, M. E.; Trujillo, M. E.; Ávalos, J.; Casillas, N. Photoelectrochemical Processes at Interfaces of Nanostructured TiO 2/Carbon Black Composites Studied by Scanning Photoelectrochemical Microscopy. *Journal of Solid State Electrochemistry* **2007**, *11* (9), 1287–1294. https://doi.org/10.1007/s10008-007-0288-2.

(119) Jung, C. C.; Saban, S. B.; Yee, S. S.; Darling, R. B. Chemical Electrode Surface Plasmon Resonance Sensor. *Sens Actuators B Chem* **1996**, *32* (2), 143–147. https://doi.org/10.1016/0925-4005(96)80123-7.

(120) Badets, V.; Loget, G.; Garrigue, P.; Sojic, N.; Zigah, D. Combined Local Anodization of Titanium and Scanning Photoelectrochemical Mapping of TiO2 Spot Arrays. *Electrochim Acta* **2016**, *222*, 84–91. https://doi.org/10.1016/j.electacta.2016.10.151.

(121) Botero-Cadavid, J. F.; Brolo, A. G.; Wild, P.; Djilali, N. Detection of Hydrogen Peroxide Using an Optical Fiber-Based Sensing Probe. *Sens Actuators B Chem* **2013**, *185*, 166–173. https://doi.org/10.1016/j.snb.2013.04.068.

(122) Jang, J. S.; Yoon, K. Y.; Xiao, Y.; Fan, F. R. F.; Bard, A. J. Development of a Potential Fe2O3-Based Photocatalyst Thin Film for Water Oxidation by Scanning Electrochemical Microscopy: Effects of Ag-Fe2O3 Nanocomposite and Sn Doping. *Chemistry of Materials* **2009**, *21* (20), 4803–4810. https://doi.org/10.1021/cm901056c.

(123) Wang, H.; Xu, G.; Dong, S. Electrochemiluminescent Microoptoprobe with Mini-Grid Working Electrode and Self-Contained Sample Container. *Electrochem commun* **2002**, *4* (3), 214–217. https://doi.org/10.1016/S1388-2481(02)00252-7.

(124) Keirsse, J.; Boussard-Plédel, C.; Loréal, O.; Sire, O.; Bureau, B.; Leroyer, P.; Turlin, B.; Lucas, J. IR Optical Fiber Sensor for Biomedical Applications. *Vib Spectrosc* **2003**, *32* (1), 23–32. https://doi.org/10.1016/S0924-2031(03)00044-4.

(125) Kimmich, D.; Taffa, D. H.; Dosche, C.; Wark, M.; Wittstock, G. Photoactivity and Scattering Behavior of Anodically and Cathodically Deposited Hematite Photoanodes - A Comparison by Scanning Photoelectrochemical Microscopy. *Electrochim Acta* **2016**, *202*, 224–230. https://doi.org/10.1016/j.electacta.2016.03.187.

(126) Kollender, J. P.; Gasiorowski, J.; Sariciftci, N. S.; Mardare, A. I.; Hassel, A. W. Photoelectrochemical and Electrochemical Characterization of Sub-Micro-Gram Amounts of Organic Semiconductors Using Scanning Droplet Cell Microscopy. *Journal of Physical Chemistry C* **2014**, *118* (30), 16919–16926. https://doi.org/10.1021/jp500423a.

(127) Bhattacharya, C.; Lee, H. C.; Bard, A. J. Rapid Screening by Scanning Electrochemical Microscopy (SECM) of Dopants for Bi2WO6 Improved Photocatalytic Water Oxidation with Zn Doping. *Journal of Physical Chemistry C* **2013**, *117* (19), 9633–9640. https://doi.org/10.1021/jp308629q.

(128) Lee, J.; Ye, H.; Pan, S.; Bard, A. J. Screening of Photocatalysts by Scanning Electrochemical Microscopy. *Anal Chem* **2008**, *80* (19), 7445–7450. https://doi.org/10.1021/ac801142g.

(129) Li, F.; Unwin, P. R. Scanning Electrochemical Microscopy (SECM) of Photoinduced Electron Transfer Kinetics at Liquid/Liquid Interfaces. *Journal of Physical Chemistry C* **2015**, *119* (8), 4031–4043. https://doi.org/10.1021/jp510333d.

(130) Weng, Y. C.; Hsiao, K. T.; Chiu, K. C.; Su, Y. F. The Identification and Characterization of Ptx-Zn1−xO Photocatalysts for Photoelectrochemical Water Splitting Applications. *Int J Hydrogen Energy* **2016**, *41* (48), 22997–23006. https://doi.org/10.1016/j.ijhydene.2016.11.023.

(131) Linnett, G.; Andrieux, F.; Atherton, N.; Poteau, X. The Micro-Optical Ring Electrode: Surface Finish and Photocurrent Magnitude. *ECS Trans* **2018**, *85* (13), 1135–1143. https://doi.org/10.1149/08513.1135ecst.

(132) Liu, W.; Ye, H.; Bard, A. J. Screening of Novel Metal Oxide Photocatalysts by Scanning Electrochemical Microscopy and Research of Their Photoelectrochemical Properties. *Journal of Physical Chemistry C* **2010**, *114* (2), 1201–1207. https://doi.org/10.1021/jp909470f.

(133) Sosa, E.; Cabrera-Sierra, R.; Oropeza, M. T.; Hernández, F.; Casillas, N.; Tremont, R.; Cabrera, C.; González, I. Electrochemically Grown Passive Films on Carbon Steel (SAE 1018) in Alkaline Sour Medium. *Electrochim Acta* **2003**, *48* (12), 1665–1674. https://doi.org/10.1016/S0013-4686(03)00145-2.

(134) Weber, A.; Kuhn, L. S.; Weber, S. G. Microring Electrode/Optical Waveguide: Electrochemical Characterization and Application to Electrogenerated Chemiluminescence. *Anal Chem* **1990**, *62* (15), 1631–1636. https://doi.org/10.1021/ac00214a019.

(135) Linnett, G.; Andrieux, F. The Micro-Optical Ring Electrode: A Sensor for Multiple Actinide Ions Monitoring. *ECS Meeting Abstracts* **2018**, *MA2018-02* (52), 1782–1782. https://doi.org/10.1149/MA2018-02/52/1782.

(136) Zhang, Y.; Dhawan, A.; Vo-Dinh, T. Design and Fabrication of Fiber-Optic Nanoprobes for Optical Sensing. *Nanoscale Res Lett* **2010**, *6* (1), 18. https://doi.org/10.1007/s11671-010-9744-5.

(137) Esquivel, K.; Arriaga, L. G.; Rodríguez, F. J.; Martínez, L.; Godínez, L. A. Development of a TiO2 Modified Optical Fiber Electrode and Its Incorporation into a

Photoelectrochemical Reactor for Wastewater Treatment. *Water Res* **2009**, *43* (14), 3593–3603. https://doi.org/10.1016/j.watres.2009.05.035.

(138) Bitziou, E.; Rudd, N. C.; Szunerits, S.; Unwin, P. R. Microelectrode Systems for the Study of Photochemical Processes in Solution. *Journal of Electroanalytical Chemistry* **2010**, *646* (1–2), 60–67. https://doi.org/10.1016/j.jelechem.2010.01.009.

(139) Butler, M. A.; Ginley, D. S. New Technique for Measurement of Electrode Strain during Electrochemical Reactions. *J Electrochem Soc* **1988**, *135* (1), 45–51. https://doi.org/10.1149/1.2095586.

(140) Shi, G.; Garfias-Mesias, L. F.; Smyrl, W. H. Preparation of a Gold-Sputtered Optical Fiber as a Microelectrode for Electrochemical Microscopy. *J Electrochem Soc* **1998**, *145* (6), 2011–2016. https://doi.org/10.1149/1.1838591.

(141) Bogdanowicz, R.; Niedziałkowski, P.; Sobaszek, M.; Burnat, D.; Białobrzeska, W.; Cebula, Z.; Sezemsky, P.; Koba, M.; Stranak, V.; Ossowski, T.; Śmietana, M. Optical Detection of Ketoprofen by Its Electropolymerization on an Indium Tin Oxide-Coated Optical Fiber Probe. *Sensors (Switzerland)* **2018**, *18* (5), 1–15. https://doi.org/10.3390/s18051361.

(142) Janczuk-Richter, M.; Piestrzyńska, M.; Burnat, D.; Sezemsky, P.; Stranak, V.; Bock, W. J.; Bogdanowicz, R.; Niedziółka-Jönsson, J.; Śmietana, M. Optical Investigations of Electrochemical Processes Using a Long-Period Fiber Grating Functionalized by Indium Tin Oxide. *Sens Actuators B Chem* **2019**, *279* (April 2018), 223–229. https://doi.org/10.1016/j.snb.2018.10.001.

(143) Niedziałkowski, P.; Białobrzeska, W.; Burnat, D.; Sezemsky, P.; Stranak, V.; Wulff, H.; Ossowski, T.; Bogdanowicz, R.; Koba, M.; Śmietana, M. Electrochemical Performance of Indium-Tin-Oxide-Coated Lossy-Mode Resonance Optical Fiber Sensor. *Sens Actuators B Chem* **2019**, *301* (June), 127043. https://doi.org/10.1016/j.snb.2019.127043.

(144) Lee, E. J.; Choi, S. Y.; Jeong, H.; Park, N. H.; Yim, W.; Kim, M. H.; Park, J.-K.; Son, S.; Bae, S.; Kim, S. J.; Lee, K.; Ahn, Y. H.; Ahn, K. J.; Hong, B. H.; Park, J.-Y.; Rotermund, F.; Yeom, D.-I. Active Control of All-Fibre Graphene Devices with Electrical Gating. *Nat Commun* **2015**, *6* (1), 6851. https://doi.org/10.1038/ncomms7851.

(145) Fan, L.; Bao, Y.; Chen, G. Feasibility of Distributed Fiber Optic Sensor for Corrosion Monitoring of Steel Bars in Reinforced Concrete. *Sensors* **2018**, *18* (11), 3722. https://doi.org/10.3390/s18113722.

(146) Vasudevan, S.; Kajtez, J.; Bunea, A. I.; Gonzalez-Ramos, A.; Ramos-Moreno, T.; Heiskanen, A.; Kokaia, M.; Larsen, N. B.; Martínez-Serrano, A.; Keller, S. S.; Emnéus, J. Leaky Optoelectrical Fiber for Optogenetic Stimulation and Electrochemical Detection of Dopamine Exocytosis from Human Dopaminergic Neurons. *Advanced Science* **2019**, *1902011*. https://doi.org/10.1002/advs.201902011.

(147) Smietana, M.; Sobaszek, M.; Michalak, B.; Niedzialkowski, P.; Bialobrzeska, W.; Koba, M.; Sezemsky, P.; Stranak, V.; Karczewski, J.; Ossowski, T.; Bogdanowicz, R. Optical Monitoring of Electrochemical Processes With ITO-Based Lossy-Mode Resonance Optical Fiber Sensor Applied as an Electrode. *Journal of Lightwave Technology* **2018**, *36* (4), 954–960. https://doi.org/10.1109/JLT.2018.2797083.

(148) Jin, E. S.; Norris, B. J.; Pantano, P. An Electrogenerated Chemiluminescence Imaging Fiber Electrode Chemical Sensor for NADH. *Electroanalysis* **2001**, *13* (15), 1287–1290. https://doi.org/10.1002/1521-4109(200110)13:15<1287::AID-ELAN1287>3.0.CO;2-I.

(149) Trettnak, W.; Wolfbeis, O. S. A Fiber Optic Lactate Biosensor with an Oxygen Optrode as the Transducer. *Anal Lett* **1989**, *22* (9), 2191–2197. https://doi.org/10.1080/00032718908051247.

(150) Bright, F. V.; Betts, T. A.; Litwiler, K. S. Regenerable Fiber-Optic-Based Immunosensor. *Anal Chem* **1990**, *62* (10), 1065–1069. https://doi.org/10.1021/ac00209a019.

(151) Li, H.; Garrigue, P.; Bouffier, L.; Arbault, S.; Kuhn, A.; Sojic, N. Double Remote Electrochemical Addressing and Optical Readout of Electrochemiluminescence at the Tip of an Optical Fiber. *Analyst* **2016**, *141* (14), 4299–4304. https://doi.org/10.1039/c6an00652c.

(152) VanDyke, D. A.; Cheng, H. Y. Electrochemical Manipulation of Fluorescence and Chemiluminescence Signals at Fiber-Optic Probes. *Anal Chem* **1989**, *61* (6), 633–636. https://doi.org/10.1021/ac00181a029.

(153) Szunerits, S.; Garrigue, P.; Bruneel, J. L.; Servant, L.; Sojic, N. Fabrication of a Sub-Micrometer Electrode Array: Electrochemical Characterization and Mapping of an

Electroactive Species by Confocal Raman Microspectroscopy. *Electroanalysis* **2003**, *15* (5–6), 548–555. https://doi.org/10.1002/elan.200390068.

(154) Gunasingham, H.; Tan, C. H.; Seow, J. K. L. Fiber-Optic Glucose Sensor with Electrochemical Generation of Indicator Reagent. *Anal Chem* **1990**, *62* (7), 755–759. https://doi.org/10.1021/ac00206a022.

(155) Schwab, S. D.; McCreery, R. L.; Gamble, F. T. Normal and Resonance Raman Spectroelectrochemistry with Fiber Optic Light Collection. *Anal Chem* **1986**, *58* (12), 2486–2492. https://doi.org/10.1021/ac00125a029.

(156) Ohmori, H. Photometric Patch Electrode to Simultaneously Measure Neural Electrical Activity and Optical Signal in the Brain Tissue; 2020; pp 131–153. https://doi.org/10.1007/978-1-4939-9944-6_6.

(157) Adam, C.; Kanoufi, F.; Sojic, N.; Etienne, M. Shearforce Positioning of Nanoprobe Electrode Arrays for Scanning Electrochemical Microscopy Experiments. *Electrochim Acta* **2015**, *179*, 45–56. https://doi.org/10.1016/j.electacta.2015.04.140.

(158) Raghavan, A.; Kiesel, P.; Wilko, L.; Schwartz, J.; Lochbaum, A.; Hegyi, A.; Schuh, A.; Arakaki, K.; Saha, B.; Ganguli, A.; Ho, K.; Kim, C.; Jin, H.; Kim, S.; Hwang, G.; Chung, G.; Choi, B.; Alamgir, M. Embedded Fi Ber-Optic Sensing for Accurate Internal Monitoring of Cell State in Advanced Battery Management Systems Part 1 : Cell Embedding Method and Performance. *J Power Sources* **2017**, *341*, 466–473. https://doi.org/10.1016/j.jpowsour.2016.11.104.

(159) Alemohammad, H.; Ghannoum, A.; Zdravkova, L.; Iyer, K.; Nieva, P.; Yu, A.; Khajepour, A. Embedded Fiber Optic Sensors for Battery Performance Monitoring in Lithium Ion Battery Cells. *NSTI: Advanced Materials - TechConnect Briefs 2015* **2015**, *4*, 308–311.

(160) Ivask, A.; Green, T.; Polyak, B.; Mor, A.; Kahru, A.; Virta, M.; Marks, R. Fibre-Optic Bacterial Biosensors and Their Application for the Analysis of Bioavailable Hg and As in Soils and Sediments from Aznalcollar Mining Area in Spain. *Biosens Bioelectron* **2007**, *22* (7), 1396–1402. https://doi.org/10.1016/j.bios.2006.06.

Chapter 3

Temperature Effect on the Electrochemical Current Response during Scanning Electrochemical Microscopy of Living Cells

As discussed in Chapters 1 and 2, SECM and SPECM has a wide range of applications in mammalian cells, making it crucial to understand the impact of temperature variation on the electrochemical response of living cells. To ensure the reliability of experimental results, it is important for the cells to be maintained under physiological conditions. Temperature is a key physiological parameter that affects cell viability and metabolic function. This chapter highlights the significance of maintaining the physiological temperature during SECM of living cells.

Prior to conducting SECM studies with HeLa cells, the effect of temperature on the diffusion coefficient of $FcCH_2OH$ was investigated by performing cyclic voltammetry (CV) on a Pt UME within a temperature range of 25 to 37 ℃. The experimental data aligned with numerical simulations, showing that the diffusion coefficient of $FcCH_2OH$ increases with rising temperature. For the presented work, an SECM setup with a temperature-controlled stage was used. HeLa cell imaging was performed at different temperature zones within a petri dish, where the temperature ranged from 31 to 37 ℃. This study demonstrated that a temperature variation of 2℃ or more can influence the electrochemical reaction kinetics of cells.

The research presented in this chapter has been published in *Analytical Chemistry* and is reprinted with permission from: *Thomas, N., Lima, D., Trinh, D., & Kuss, S. (2023). Temperature Effect on the Electrochemical Current Response during Scanning Electrochemical Microscopy of Living Cells.Analytical Chemistry, 95(49), 17962-17967. https://doi.org/10.1021/acs.analchem.3c03716*. The supplementary information for this chapter can be found in Appendix 1.

All experiments, data analysis, discussions, writing, and manuscript editing were conducted by NT. DL contributed scientific insights, discussions, and manuscript editing. DT performed numerical simulations and contributed to the manuscript. SK provided guidance and contributed to the manuscript.

3.1 Abstract

Scanning Electrochemical Microscopy (SECM) is being used increasingly to monitor electrochemical processes at the interface of living cells and electrodes. This allows the detection and quantification of biomarkers that further the understanding of various diseases. Rapid SECM experiments are often carried out without monitoring the analyte solution temperature or are performed at room temperature. The reported research demonstrates that temperature control is crucial during SECM imaging of living cells to obtain reliable data. In this study, an SECM-integrated thermostatic ring on the sample stage enabled imaging of living biological cells in constant height mode at various temperatures. Two-dimensional line scans were conducted while scanning single *Adenocarcinoma Cervical* cancer (HeLa) cells. Numerical modeling was carried out to evaluate the effect of temperature on the electrochemical current response of living cells to compare the apparent heterogeneous rate constant (k_0), representing cellular reaction kinetics. This study reveals that even small temperature variations of approximately 2ºC affect the reaction kinetics of single living cells, altering the measured current during SECM.

3.2 Introduction

Scanning Electrochemical Microscopy (SECM) has gained increasing popularity since its conceptualization and application by Royce C. Engstrom in 1986 and Allen J. Bard in 1989.[1–3] Over the last two decades, it has been used for various biological applications, including studies to understand protein expression,[4–6] enzymatic activity,[7,8] DNA mismatches,[9,10] antigen-antibody immune response,[11–13] and to image living cells in general.[14,15] The main component of an SECM applied to biological samples is a movable ultramicroelectrode (UME). This UME is positioned above a substrate in a solution containing a redox mediator and is biased at a potential exceeding the standard potential of the redox species. The recorded electrochemical current carries information about a sample's electrochemical properties. In the case of living cells, SECM enables the non-invasive imaging of cellular kinetics, k_0, with a high spatial resolution by quantifying the flux of molecules to and from cells.[16] Experimental parameters that are commonly adjusted to the scale of living cells include tip-to-substrate distance, scan velocity, electrolyte concentration, and scan time.[17] An experimental parameter that is often considered, but rarely monitored closely and throughout an experiment, during SECM imaging of biological cells, is the solution temperature.

The temperature of the cell environment is an important parameter to maintain cell viability and integrity. It plays an important role in the chemical and biochemical cellular mechanisms, thereby affecting the efflux rate of cell metabolites.[18] For instance, biological reactions and enzymes associated with the respiratory chain, and redox signaling pathways function ideally at physiological temperature.[19] Cell permeability and fluidity are also significantly affected by temperature. At high temperatures, membrane fluidity increases allowing the diffusion of more species through the membrane whereas at low temperatures cell membrane gets rigid constricting the movement of molecules.[18] Physical phenomena such as electron transfer, chemical reactions, and mass transport occurring during electrochemical processes are also temperature dependent, thereby affecting diffusion coefficients and cell kinetics.[20] Therefore, the temperature is an essential parameter that must be controlled during live-cell imaging, monitoring the transmembrane transport of molecules. Various research groups conducted non-biological temperature-related studies using SECM, which demonstrates the importance of integrating temperature control units into SECM apparatus and understanding the effect of temperature on SECM sample resolution.[21–23] Researchers have also discussed the importance of convective heat transfer during SECM and how SECM data are influenced by temperature by using numerical modeling.[20,24–26] Other groups have proposed the use of hot-tip SECM[27,28] and hot-wire electrochemistry with SECM[29] to perform temperature-dependent studies. Biological SECM studies for live cells have been conducted by numerous researchers at room/ambient temperature[5,30–42] as well as physiological temperature (37°C)[43–50], whereby it is not always clear whether the temperature was monitored throughout an experiment or just at the beginning of the imaging procedure.

In the presented study, we use an SECM setup with a temperature-controlled thermostatic ring, incorporated on the sample stage to fit in a 35 mm petri dish. This arrangement results in a maximum temperature at the sides of the petri dish and a decreasing temperature gradient towards the center. This results in 5 distinguishable temperature zones with different temperature ranges.

The presented research quantifies changes in the electrochemical current measured across living cells due to solution temperature changes. Quantitative SECM imaging of living cells requires the decoupling of cell topography from cellular reactivity.[51] In the literature, numerical modeling enabled the extraction of an apparent heterogeneous rate constant (k_0) at slow scan velocities by

means of forced convection.[52] Using this methodology, the bulk steady state current at platinum (Pt) UMEs with varying temperatures was evaluated. SECM line scan imaging of living cells was then conducted at three different temperature ranges to understand the effect of temperature on the cells' apparent heterogeneous rate constant, k_0.

3.3 Materials and Methods

3.3.1 Chemicals

Potassium chloride (KCl, ≥ 99.9%) was purchased from Fisher Chemical (Belgium). Hydroxymethyl ferrocene ($FcCH_2OH$, $C_{11}H_{12}FeO$, > 95.0%) was obtained from TCI (USA). Solutions were prepared using nanopure water with a resistivity of no less than 18.2 MΩ cm at 25 °C. MicroPolish Alumina (1.0, 0.3 and 0.05 μm) and MicroCloth Polishing Cloth were from Buehler (USA).

3.3.2 Cell Culture

HeLa cells were gently provided by Dr. Sean McKenna (Department of Chemistry, University of Manitoba, Winnipeg, MB). Cells were cultured in HyClone Dubelcco's Modified Eagle Medium/High Glucose (4.00 mM L-Glutamine, 4500 mg/L Glucose and sodium pyruvate) purchased from Cytiva (USA) which was supplemented with 10% v/v heat inactivated fetal bovine serum (Gibco/Invitrogen, ON, Canada). Cells were cultured in T-75 flasks (Fisher Scientific, USA) at 37°C and 5% CO_2. On reaching a confluency of 70-90%, cells were washed with phosphate buffered saline (Cytiva, USA) and harvested using 0.05% Trypsin-EDTA solution (Gibco, USA). This was followed by seeding the cells onto 35 mm petri dishes (Thermo Fisher) and incubation for ~24 hours prior SECM experiments. The 35-mm petri dishes were marked using a divider and compass ruler on the outside of the petri dish prior to cell seeding, to create different temperature zones. The radii were based on the temperature variation throughout the ring temperature groove on the sample stage of the SECM.

3.3.3 Electrochemical Measurements

SP-200 BioLogic potentiostat was used to carry out cyclic voltammetry (CV) measurements using a 10 μm Pt microelectrode (BASi) working electrode, a Pt counter electrode and Ag/AgCl pseudo

reference electrode. A digital thermometer (Fischer Scientific) was used for monitoring the temperature of the electrochemical cell during CV measurements. A heating plate (Thermo Scientific) was used for temperature control during diffusion coefficient studies.

SECM measurements were conducted using a ElPROScan-3 workstation with POTMASTER software and a 25-µm Pt UME (HEKA Elektronik GmbH, Harvard Bioscience Inc). The electrochemical setup was integrated with a CL-100 Biopolar Temperature Controller acquired from Warner Instruments. Line scans were performed using an Ag/AgCl pseudo reference and a Pt counter electrode.

3.3.4 Numerical Simulations

The experimental dynamic viscosity of water is calculated using the semi-empirical Vogel-Fulcher-Tammann equation. The data is interpolated using the *Interpolation* function of Wolfram Mathematica. The theoretical value of the diffusion coefficient as a function of temperature is then computed. High-speed scanning electrochemical measurements are simulated using the Finite Element Method (FEM) with COMSOL Multiphysics. The heterogeneous reaction rate of the sample is adjusted within the range of $k_0 = 10^{-8}$ m/s to 10 m/s. The normalized current of the tip is subsequently plotted against Ps on a logarithmic scale. The experimental data is normalized. Data analysis is carried out using Wolfram Mathematica for multiple scanning lines, considering temperature, velocity, and zone as variables. The heterogeneous reaction rate is determined by fitting the experimental data (normalized tip current as a function of k_0 and Ps) with simulation curves. The fitting process is executed in Wolfram Mathematica using the *NMinimize* function.

3.4 Results and Discussion

In this section, we first discuss the effect of temperature on the steady state current measured at Pt UMEs to consider changes in the diffusion coefficient of the redox mediator ferrocenemethanol ($FcCH_2OH$). After the diffusion coefficient changes were integrated into the numerical model for individual temperatures, HeLa cells were investigated by SECM.

3.4.1 Effect of temperature on the steady state current and diffusion coefficient

The steady state equation for microelectrodes (1) describes the proportionality of the diffusion coefficient (*D*) with the steady state current[3,53].

$$i_{ss} = 4nFDcr \tag{3.1}$$

where i_{ss} (A) is the steady state current, *n* is the number of electrons of the redox reaction under investigation, *F* (sA/mol) is the Faraday constant, *D* (cm^2/s) is the diffusion coefficient, *c* (M) is the concentration of the redox mediator and *r* (cm) is the radius of the disk UME. As a fundamental variable in the mass transfer equation, *D* represents the amount of substance that diffuses per second towards a unit area cm^2 of an electrode.

To understand the dependence of the steady state current on temperature changes, cyclic voltammograms were recorded with a 10-µm (diameter) Pt microelectrode in 0.1 M KCl containing 1 mM $FcCH_2OH$. As shown in Figure 3.1A, the experimental steady state current (solid lines) and theoretical current (dotted lines) increases with increasing temperature from 25 to 37ºC, indicating that the current is directly proportional to the temperature. This was confirmed by comparing experimental data to theoretical current values at 50 mV/s (Figure 2.1 A), which was in good agreement.

Herein, the *D* value for $FcCH_2OH$ was calculated based on the steady state current for each tested temperature, with a measurable linear increase (Figure 3.1 B). The simulation values are calculated by using equation (3.2). The effect of temperature on the diffusion coefficient are shown in the Stokes-Einstein equation below.

$$\frac{D_{T_1}}{D_{T_2}} = \frac{T_1}{T_2}\frac{\mu_{T_1}}{\mu_{T_2}} \tag{3.2}$$

In this equation, D_T is the temperature dependent diffusion coefficient, *T* is the temperature and μ is the electrical mobility. The dynamic viscosity of water as a function of temperature (in K) can be calculated by using the semi-empirical Vogel-Fulcher-Tammann (VFT) equation (3.3):

$$\log(|\eta|) = A + B / (T - T_o) \tag{3.3}$$

where η is the viscosity, A and B are empirical material-dependent parameters, T and T_o are the temperature, empirical fitting temperature which is below the glass transition temperature, respectively.

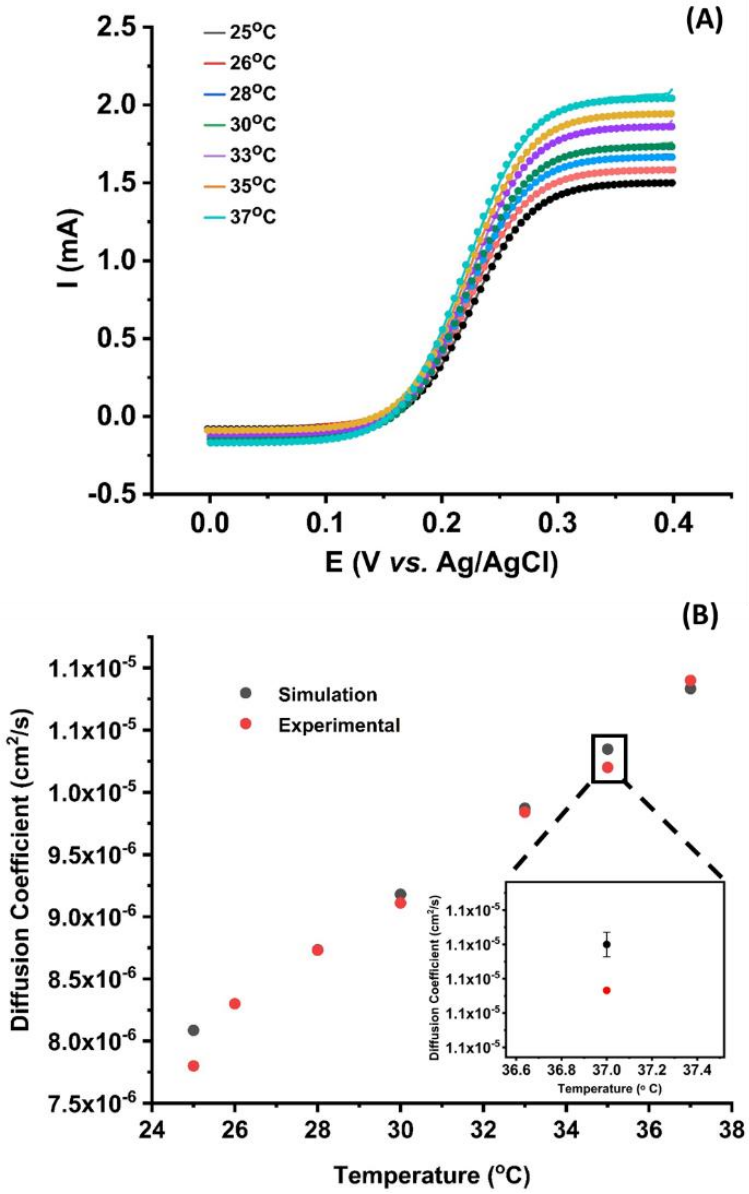

Figure 3.1 *Effect of temperature on the electrochemical current. A) Experimental (solid lines) currents compared to theoretical (dotted lines) current signals obtained during cyclic voltammetry in 1 mM $FcCH_2OH$ at varying temperatures. B) Diffusion coefficients based on experimental (red) data compared to simulation-based (black) diffusion coefficients as a function of temperature. Experimental error bars are too small to be visible. A zoom view is provided for the experimental data at 37°C.*

The three-parameter from the VFT equation forms the foundation for analyzing viscous systems, providing the capability to characterize the viscosity within a broad range of temperatures for numerous glass-forming liquids. The calculation using the VFT equation becomes necessary due to the intriguing nature of viscosity changes in the supercooled regime – a temperature range just before the glass transition occurs.

The calculations confirmed that the increase in the solution temperature was accompanied by a viscosity decrease (Figure A1.1). As the viscosity and the temperature are inversely proportional parameters, the *D* value was theoretically calculated for $FcCH_2OH$ for different temperatures (Figure 3.1 B, red dots), which is in good agreement with the theory (Figure 3.1B). Thus, the increase in the steady state current measured at the Pt UME is attributed to an increased diffusion of the redox species in solution at higher temperatures. A reliable analysis of the influence of temperature on the redox activity of living biological cells must take this change in diffusion behavior of $FcCH_2OH$ into account. Temperature has a significant effect on the metabolic activity of living cells, since it affects not only intracellular mechanisms but also cellular response to external stimuli.[18]

3.4.2 SECM imaging of HeLa cells at various temperatures

SECM measurements were performed across single living adenocarcinoma cervical cancer (HeLa) cells adherend to 35-mm diameter petri dishes. As shown in Figure 3.2 A and Figure A1.2**,** petri dishes were marked with different temperature ring-zones, as follows: Zone A (r = 0.4 cm): 31.5-33.1 ºC, Zone B (r = 0.7 cm): 33.9- 34.8 ºC, Zone C (r = 1. 0 cm): 35.6-36.0 ºC, Zone D (r = 1.3 cm): 36.2-37.2 ºC and Zone E (r = 1.6 cm): 37.7-38.0 ºC (r = petri dish radius). The temperature in each zone was maintained using a temperature controller integrated into the SECM, equipped with a sensor thermistor probe for sample temperature monitoring. This setup functions based on heating and cooling cycles for specific periods of time, which allows the system to maintain the set temperature with high stability. The temperature of a particular zone was continuously monitored using a sensor probe placed inside the Petri dish during the SECM measurements.

Zones A (pink), B (blue), and D (green) were chosen as the ring-zones of interest because they represent realistic temperature fluctuations within ±1.0 ℃, if the temperature is not continuously

monitored during SECM imaging experiments. 2D-line scans were performed across HeLa cells in different temperature zones using a 25-µm diameter Pt UME, which is close to the size of living Hela cells (20-40 µm),[54] enabling the collection of all chemical species released by the cells at the UME surface. The Pt UME was biased at a potential of 0.4 V to drive the oxidation of $FcCH_2OH$. Figure 3.2 B schematically illustrates the experiment. $FcCH_2OH$ diffuses into cells, whereby it is also constantly converted to $[FcCH_2OH]^+$ at the tip of the UME. The presence of $FcCH_2OH$ promotes the intracellular formation of reduced glutathione (GSH), which promotes the regeneration of $FcCH_2OH$, as published previously.[6] Because of the regeneration of $FcCH_2OH$, an increase in electrochemical current is recorded every time the UME crosses a living cell. The uptake of $FcCH_2OH$ by cells and its regeneration by GSH is dependent on the redox state of the cell and reduced/oxidized intracellular glutathione ratios (GSH/GSSG). $FcCH_2OH$, being cell permeable, enters cells through passive diffusion.[4,6] As cell permeability as well as the efflux rate of cell metabolites are known to be dependent on cell environmental factors,[18] such as the temperature, it is expected that the electrochemical current signal will be affected by changes in the temperature.

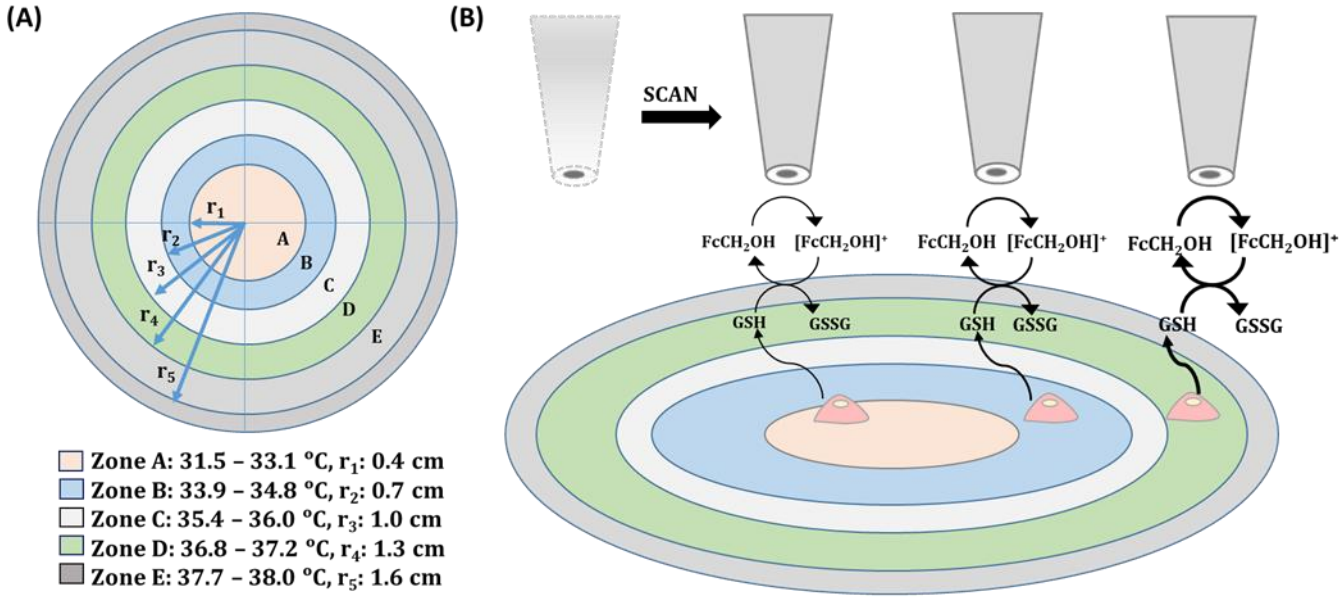

Figure 3.2 *Experimental setup. A) Schematic representation of a 35 mm petri dish with respective temperature ring-zones and their radii. B) Illustration of SECM scans across single HeLa cells in Zone A, Zone B and Zone D in the presence of 1 mM $FcCH_2OH$.*

The UME was initially positioned over a bare region of the Petri dish at a tip-to-substrate distance greater than the height of the cells (approximately 12 μm) by conducting an approach curve (Figure A1.4).[4,6] During 2D-scans across single HeLa cells in each temperature zone (each zone n=6) (Figure 3.3), the peak currents were monitored and compared. When the solution temperature dropped by approximately 2 ºC, drastic current variations were observed between cells (Figure 3.3 A and B), whereas the cellular current response remained homogeneous between 36.8 ºC and 37.2 ºC (Figure 3.3 C). This result demonstrates that even slight temperature variations of approximately 2 ºC affect the electrochemical response of living cells.

To confirm that the current variations are statistically significant, the apparent heterogenous rate constant k_0, representing cellular kinetics, was extracted. In this study, cell kinetics are defined as the cell's ability to regenerate $FcCH_2OH$. The current monitored during SECM cell imaging is influenced by cell topography and the electrochemical cellular reactivity.[48,51] The successful decoupling of cell topography from reactivity using numerical simulations, which consider the effect of geometry of substrate, based on tip velocity enables the extraction of k_0.[48]

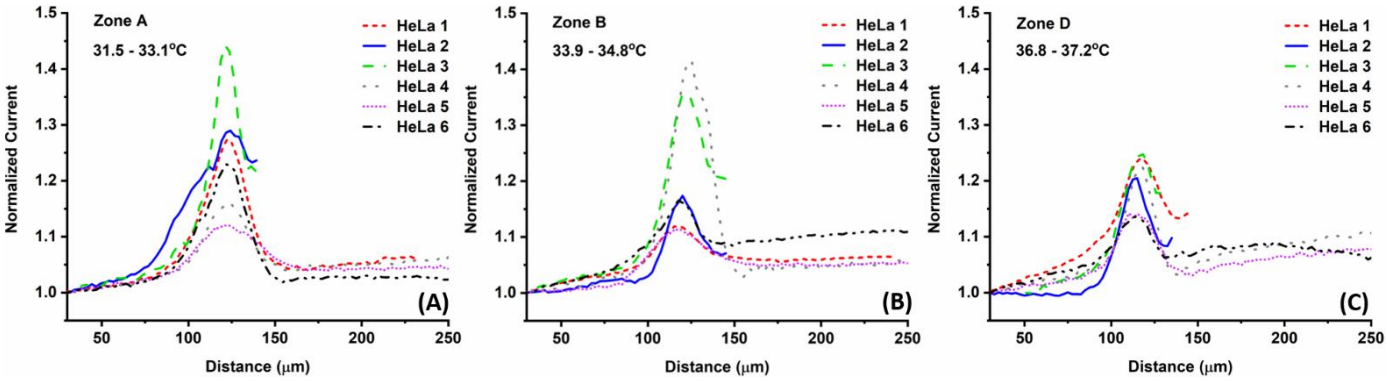

Figure 3.3 *2D-line scans of across single living HeLa cells. (A) Zone A with a temperature range of 31.5- 33.1ºC. (B) Zone B with a temperature range of 33.9-34.8ºC and (C) Zone D with a temperature range of 36.8-37.2ºC. Normalized current presents measured current divided by electrode current at full scan speed (first measurement point in graph).*

3.4.3 Influence of temperature on cellular reactivity during SECM

The electrochemical kinetics of HeLa cells was numerically simulated using the mass transport and the Butler-Volmer equation, as described previously.[52] The SECM experiments for numerical simulation were conducted using a 25-µm Pt UME, in the presence of 1 mM $FcCH_2OH$, with the UME scanning HeLa cells at velocities varying from 50 to 150 µm/s. As the scan velocity was increased, an increase in the tip current was observed over the cell irrespective of the temperature zone (Figure A1.3). The peak current at each scan velocity was then used to calculate k_0 for each living cell[52].

Figure 3.4 B reports k_0 values of HeLa cells located in different temperature ring-zones as a function of normalized current and as shear Peclet number (P_s). Details on normalization and shear Peclet number have been reported previously.[48] In short, we utilized COMSOL Multiphysics to generate SECM line scans as a function of P_s and k_0. Several values of k_0, ranging from 10^{-8} to 10^{1}, were employed to generate multiple line scan profiles. The experimental k_0 values were subsequently extracted through a fitting process applied to the experimental line scans. Compared to the substrate kinetics of the petri dish, which remain constant at varying temperatures (Figure 3.4 A, A1.5A and D), HeLa cells demonstrated a differential behavior. Living cells showed maximum k_0 values in zone D (Figure 3.4 C, green), which is in the physiological temperature range. This indicates that the ability to regenerate $FcCH_2OH$ by living HeLa cells depends on the temperature of their surroundings and decreases with decreasing temperature. Additional data sets are shown in Figure A1.5.

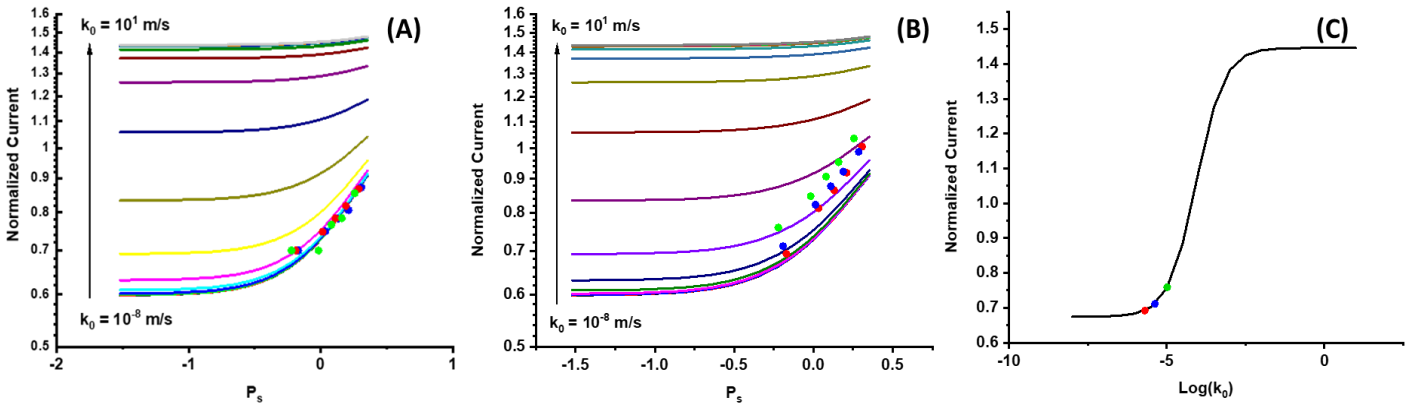

Figure 3.4 *Influence of temperature on cellular reactivity. Representative data set. A) Substrate kinetics of the petri dish B) Hela cell kinetics in varying temperature zones A (red), B (Blue) and D (green). C) Comparison of average cell kinetics in temperature zones A, B and D.*

3.5 Conclusions

This study provides scientific evidence for temperature-induced changes in cellular responses during SECM imaging of living HeLa cells. After compensating for changes in the diffusion coefficient *D*, an existing numerical model was adapted to include temperature as a variable factor, which enabled the successful extraction of the heterogeneous reaction rate, k_0. The reaction kinetics for the regeneration of $FcCH_2OH$ by HeLa cells was found to vary markedly with the temperature, showing a decrease rate at temperatures below the physiological range. The solution temperature is an experimental parameter, which is often considered, but may not be monitored strictly. This study confirms that for example the sole preheating of the solution prior to experiments would be insufficient, as even slight temperature changes will alter the cellular response during an SECM experiment. A thermostated and closely monitored electrochemical cell is crucial to provide reliable data on molecule exchange between cells and electrodes.

3.6 Acknowledgements

SK acknowledges the Natural Sciences and Engineering Research Council of Canada (RGPIN-2019-05365) for its financial support. NT acknowledges funding through an NSERC-PGS-D.

3.7 References

(1) Engstrom, R. C.; Weber, M.; Wunder, D. J.; Burgess, R.; Winquist, S. Measurements within the Diffusion Layer Using a Microelectrode Probe. *Analytical Chemistry* **1986**, *58* (4), 844–848. https://doi.org/10.1021/ac00295a044.

(2) Engstrom, R. C.; Pharr, C. M. Scanning Electrochemical Microscopoy. *Anal. Chem.* **1989**, *61* (19), 1099A-1104A.

(3) Bard, A. J.; Fan, F. R. F.; Kwak, J.; Lev, O. Scanning Electrochemical Microscopy. Introduction and Principles. *Analytical Chemistry* **1989**, *61* (2), 132–138. https://doi.org/10.1021/ac00177a011.

(4) Kuss, S.; Polcari, D.; Geissler, M.; Brassard, D.; Mauzeroll, J. Assessment of Multidrug Resistance on Cell Coculture Patterns Using Scanning Electrochemical Microscopy. *Proceedings of the National Academy of Sciences of the United States of America* **2013**, *110* (23), 9249–9254. https://doi.org/10.1073/pnas.1214809110.

(5) Takahashi, Y.; Miyamoto, T.; Shiku, H.; Asano, R.; Yasukawa, T.; Kumagai, I.; Matsue, T. Electrochemical Detection of Epidermal Growth Factor Receptors on a Single Living Cell Surface by Scanning Electrochemical Microscopy. *Analytical Chemistry* **2009**, *81* (7), 2785–2790. https://doi.org/10.1021/ac900195m.

(6) Kuss, S.; Cornut, R.; Beaulieu, I.; Mezour, M. A.; Annabi, B.; Mauzeroll, J. Assessing Multidrug Resistance Protein 1-Mediated Function in Cancer Cell Multidrug Resistance by Scanning Electrochemical Microscopy and Flow Cytometry. *Bioelectrochemistry* **2011**, *82* (1), 29–37. https://doi.org/10.1016/j.bioelechem.2011.04.008.

(7) Zhou, Y.; Takahashi, Y.; Fukuma, T.; Matsue, T. Scanning Electrochemical Microscopy for Biosurface Imaging. *Current Opinion in Electrochemistry* **2021**, *29*, 100739. https://doi.org/10.1016/j.coelec.2021.100739.

(8) Morkvenaite-Vilkonciene, I.; Ramanaviciene, A.; Kisieliute, A.; Bucinskas, V.; Ramanavicius, A. Scanning Electrochemical Microscopy in the Development of Enzymatic Sensors and Immunosensors. *Biosensors and Bioelectronics* **2019**, *141* (May), 111411. https://doi.org/10.1016/j.bios.2019.111411.

(9) Diakowski, P. M.; Kraatz, H. B. Detection of Single-Nucleotide Mismatches Using Scanning Electrochemical Microscopy. *Chemical Communications* **2009**, *7345* (10), 1189–1191. https://doi.org/10.1039/b819876d.

(10) Moradi, N.; Noori, A.; Mehrgardi, M. A.; Mousavi, M. F. Scanning Electrochemical Microscopy for Electrochemical Detection of Single-Base Mismatches by Tagging

Ferrocenecarboxylic Acid as a Redox Probe to DNA. *Electroanalysis* **2016**, *28* (4), 823–832. https://doi.org/10.1002/elan.201500598.

(11) Sciutto, G.; Prati, S.; Mazzeo, R.; Zangheri, M.; Roda, A.; Bardini, L.; Valenti, G.; Rapino, S.; Marcaccio, M. Localization of Proteins in Paint Cross-Sections by Scanning Electrochemical Microscopy as an Alternative Immunochemical Detection Technique. *Analytica Chimica Acta* **2014**, *831*, 31–37. https://doi.org/10.1016/j.aca.2014.04.058.

(12) Wittstock, G.; Yu, K. jia; Halsall, H. B.; Ridgway, T. H.; Heineman, W. R. Imaging of Immobilized Antibody Layers with Scanning Electrochemical Microscopy. *Analytical Chemistry* **1995**, *67* (19), 3578–3582. https://doi.org/10.1021/ac00115a030.

(13) Kasai, S.; Shiku, H.; Torisawa, Y. suke; Nagamine, K.; Yasukawa, T.; Watanabe, T.; Matsue, T. Cytokine Assay on a Cellular Chip by Combining Collagen Gel Embedded Culture with Scanning Electrochemical Microscopy. *Analytica Chimica Acta* **2006**, *566* (1), 55–59. https://doi.org/10.1016/j.aca.2006.02.061.

(14) Conzuelo, F.; Schulte, A.; Schuhmann, W. Biological Imaging with Scanning Electrochemical Microscopy. *Proceedings of the Royal Society A: Mathematical, Physical and Engineering Sciences* **2018**, *474* (2218). https://doi.org/10.1098/rspa.2018.0409.

(15) Amemiya, S.; Guo, J.; Xiong, H.; Gross, D. A. Biological Applications of Scanning Electrochemical Microscopy: Chemical Imaging of Single Living Cells and Beyond. *Analytical and Bioanalytical Chemistry* **2006**, *386* (3), 458–471. https://doi.org/10.1007/s00216-006-0510-6.

(16) Filice, F. P.; Ding, Z. Analysing Single Live Cells by Scanning Electrochemical Microscopy. *Analyst* **2019**, *144* (3), 738–752. https://doi.org/10.1039/c8an01490f.

(17) Bard, A. J.; Mirkin, M. V. *Scanning Electrochemical Microscopy*, Third.; Taylor& Francis.

(18) Knapp, B. D.; Huang, K. C. The Effects of Temperature on Cellular Physiology. *Annual Review of Biophysics* **2022**, *51*, 499–526. https://doi.org/10.1146/annurev-biophys-112221-074832.

(19) Holmström, K. M.; Finkel, T. Cellular Mechanisms and Physiological Consequences of Redox-Dependent Signalling. *Nature Reviews Molecular Cell Biology* **2014**, *15* (6), 411–421. https://doi.org/10.1038/nrm3801.

(20) Pan, H.; Zhang, H.; Lai, J.; Gu, X.; Sun, J.; Tang, J.; Jin, T. Integration of Thermocouple Microelectrode in the Scanning Electrochemical Microscope at Variable Temperatures: Simultaneous Temperature and Electrochemical Imaging and Its Kinetic Studies. *Scientific Reports* **2017**, *7* (July 2016), 1–6. https://doi.org/10.1038/srep43685.

(21) Sode, A.; Nebel, M.; Pinyou, P.; Schmaderer, S.; Szeponik, J.; Plumeré, N.; Schuhmann, W. Determination of Temperature Gradients with Micrometric Resolution by Local Open Circuit Potential Measurements at a Scanning Microelectrode. *Electroanalysis* **2013**, *25* (9), 2084–2091. https://doi.org/10.1002/elan.201300258.

(22) Schäfer, D.; Puschhof, A.; Schuhmann, W. Scanning Electrochemical Microscopy at Variable Temperatures. *Physical Chemistry Chemical Physics* **2013**, *15* (14), 5215–5223. https://doi.org/10.1039/c3cp43520b.

(23) Clausmeyer, J.; Schäfer, D.; Nebel, M.; Schuhmann, W. Temperature-Induced Modulation of the Sample Position in Scanning Electrochemical Microscopy. *ChemElectroChem* **2015**, *2* (7), 946–948. https://doi.org/10.1002/celc.201500087.

(24) Novev, J. K.; Compton, R. G. Convective Heat Transfer in a Measurement Cell for Scanning Electrochemical Microscopy. *Physical Chemistry Chemical Physics* **2016**, *18* (43), 29836–29846. https://doi.org/10.1039/c6cp06121d.

(25) Novev, J. K.; Compton, R. G. Thermal Convection in Electrochemical Cells. Boundaries with Heterogeneous Thermal Conductivity and Implications for Scanning Electrochemical Microscopy. *Physical Chemistry Chemical Physics* **2017**, *19* (20), 12759–12775. https://doi.org/10.1039/c7cp01797a.

(26) Zhang, H.; Xiao, X.; Su, T.; Gu, X.; Jin, T.; Du, L.; Tang, J. A Novel Thermocouple Microelectrode for Applications in SECM and Variable Temperature Electrochemistry. *Electrochemistry Communications* **2014**, *47*, 71–74. https://doi.org/10.1016/j.elecom.2014.06.027.

(27) Boika, A.; Zhao, Z. First Principles of Hot-Tip Scanning Electrochemical Microscopy: Differentiating Substrates According to Their Thermal Conductivities. *Electrochemistry Communications* **2016**, *68*, 36–39. https://doi.org/10.1016/j.elecom.2016.04.017.

(28) Zhao, Z.; Leonard, K. C.; Boika, A. Hot-Tip Scanning Electrochemical Microscopy: Theory and Experiments Under Positive and Negative Feedback Conditions. *Analytical Chemistry* **2019**, *91* (4), 2970–2977. https://doi.org/10.1021/acs.analchem.8b05192.

(29) Wert, S.; Fußstetter, A.; Iffelsberger, C.; Matysik, F. M. Scanning Electrochemical Microscopy of Electrically Heated Wire Substrates. *Molecules* **2020**, *25* (5), 1–10. https://doi.org/10.3390/molecules25051169.

(30) Henderson, J. D.; Filice, F. P.; Li, M. S. M.; Ding, Z. Tracking Live-Cell Response to Hexavalent Chromium Toxicity by Using Scanning Electrochemical Microscopy. *ChemElectroChem* **2017**, *4* (4), 856–863. https://doi.org/10.1002/celc.201600783.

(31) Zhao, X.; Zhang, M.; Long, Y.; Ding, Z. Redox Reactions of Reactive Oxygen Species in Aqueous Solutions as the Probe for Scanning Electrochemical Microscopy of Single Live T24 Cells. *Canadian Journal of Chemistry* **2010**, *88* (6), 569–576. https://doi.org/10.1139/V10-051.

(32) Filice, F. P.; Li, M. S. M.; Wong, J. M.; Ding, Z. The Effects of Long Duration Chronic Exposure to Hexavalent Chromium on Single Live Cells Interrogated by Scanning Electrochemical Microscopy. *Journal of Inorganic Biochemistry* **2018**, *182* (January), 222–229. https://doi.org/10.1016/j.jinorgbio.2018.02.009.

(33) Zhang, M. M. N.; Long, Y. T.; Ding, Z. Filming a Live Cell by Scanning Electrochemical Microscopy: Label-Free Imaging of the Dynamic Morphology in Real Time. *Chemistry Central Journal* **2012**, *6* (1), 1–6. https://doi.org/10.1186/1752-153X-6-20.

(34) Diakowski, P. M.; Ding, Z. Interrogation of Living Cells Using Alternating Current Scanning Electrochemical Microscopy (AC-SECM). *Physical Chemistry Chemical Physics* **2007**, *9* (45), 5966–5974. https://doi.org/10.1039/b711448f.

(35) Kaya, T.; Torisawa, Y. S.; Oyamatsu, D.; Nishizawa, M.; Matsue, T. Monitoring the Cellular Activity of a Cultured Single Cell by Scanning Electrochemical Microscopy

(SECM). A Comparison with Fluorescence Viability Monitoring. *Biosensors and Bioelectronics* **2003**, *18* (11), 1379–1383. https://doi.org/10.1016/S0956-5663(03)00083-6.

(36) Takahashi, Y.; Hirano, Y.; Yasukawa, T.; Shiku, H.; Yamada, H.; Matsue, T. Topographic, Electrochemical, and Optical Images Captured Using Standing Approach Mode Scanning Electrochemical/Optical Microscopy. *Langmuir* **2006**, *22* (25), 10299–10306. https://doi.org/10.1021/la0611763.

(37) Takahashi, Y.; Shevchuk, A. I.; Novak, P.; Murakami, Y.; Shiku, H.; Korchev, Y. E.; Matsue, T. Simultaneous Noncontact Topography and Electrochemical Imaging by SECM/SICM Featuring Ion Current Feedback Regulation. *Journal of the American Chemical Society* **2010**, *132* (29), 10118–10126. https://doi.org/10.1021/ja1029478.

(38) Liu, B.; Rotenberg, S. A.; Mirkin, M. V. Scanning Electrochemical Microscopy of Living Cells: Different Redox Activities of Nonmetastatic and Metastatic Human Breast Cells. *Proceedings of the National Academy of Sciences of the United States of America* **2000**, *97* (18), 9855–9860. https://doi.org/10.1073/pnas.97.18.9855.

(39) Feng, W.; Rotenberg, S. A.; Mirkin, M. V. Scanning Electrochemical Microscopy of Living Cells. 5. Imaging of Fields of Normal and Metastatic Human Breast Cells. *Analytical Chemistry* **2003**, *75* (16), 4148–4154. https://doi.org/10.1021/ac0343127.

(40) Rotenberg, S. A.; Mirkin, M. V. Scanning Electrochemical Microscopy: Detection of Human Breast Cancer Cells by Redox Environment. *Journal of Mammary Gland Biology and Neoplasia* **2004**, *9* (4), 375–382. https://doi.org/10.1007/s10911-004-1407-7.

(41) Nebel, M.; Grützke, S.; Diab, N.; Schulte, A.; Schuhmann, W. Visualization of Oxygen Consumption of Single Living Cells by Scanning Electrochemical Microscopy: The Influence of the Faradaic Tip Reaction. *Angewandte Chemie - International Edition* **2013**, *52* (24), 6335–6338. https://doi.org/10.1002/anie.201301098.

(42) Skaanvik, S. A.; Stephens, L. I.; Gateman, S. M.; Geissler, M.; Mauzeroll, J. Quantitative Feedback Referencing for Improved Kinetic Fitting of Scanning Electrochemical

Microscopy Measurements. *Analytical Chemistry* **2022**, *94* (40), 13852–13859. https://doi.org/10.1021/acs.analchem.2c02498.

(43) Zhang, M. N.; Ding, Z.; Long, Y. T. Sensing Cisplatin-Induced Permeation of Single Live Human Bladder Cancer Cells by Scanning Electrochemical Microscopy. *Analyst* **2015**, *140* (17), 6054–6060. https://doi.org/10.1039/c5an01148e.

(44) Zhang, M. M. N.; Long, Y. T.; Ding, Z. Cisplatin Effects on Evolution of Reactive Oxygen Species from Single Human Bladder Cancer Cells Investigated by Scanning Electrochemical Microscopy. *Journal of Inorganic Biochemistry* **2012**, *108*, 115–122. https://doi.org/10.1016/j.jinorgbio.2011.11.010.

(45) Li, M. S. M.; Filice, F. P.; Henderson, J. D.; Ding, Z. Probing Cd2+-Stressed Live Cell Membrane Permeability with Various Redox Mediators in Scanning Electrochemical Microscopy. *Journal of Physical Chemistry C* **2016**, *120* (11), 6094–6103. https://doi.org/10.1021/acs.jpcc.6b00453.

(46) Filice, F. P.; Li, M. S. M.; Henderson, J. D.; Ding, Z. Mapping Cd2+-Induced Membrane Permeability Changes of Single Live Cells by Means of Scanning Electrochemical Microscopy. *Analytica Chimica Acta* **2016**, *908*, 85–94. https://doi.org/10.1016/j.aca.2015.12.027.

(47) Zhao, X.; Lam, S.; Jass, J.; Ding, Z. Scanning Electrochemical Microscopy of Single Human Urinary Bladder Cells Using Reactive Oxygen Species as Probe of Inflammatory Response. *Electrochemistry Communications* **2010**, *12* (6), 773–776. https://doi.org/10.1016/j.elecom.2010.03.030.

(48) Kuss, S.; Trinh, D.; Mauzeroll, J. High-Speed Scanning Electrochemical Microscopy Method for Substrate Kinetic Determination: Application to Live Cell Imaging in Human Cancer. *Analytical Chemistry* **2015**, *87* (16), 8102–8106. https://doi.org/10.1021/acs.analchem.5b01269.

(49) Filice, F. P.; Li, M. S. M.; Ding, Z. Simulation Assisted Nanoscale Imaging of Single Live Cells with Scanning Electrochemical Microscopy. *Advanced Theory and Simulations* **2019**, *2* (2), 1–8. https://doi.org/10.1002/adts.201800124.

(50) Zhao, Y.; Li, Y.; Kuermanbayi, S.; Liu, Y.; Zhang, J.; Ye, Z.; Guo, H.; Qu, K.; Xu, F.; Li, F. In Situ and Quantitatively Monitoring the Dynamic Process of Ferroptosis in Single Cancer Cells by Scanning Electrochemical Microscopy. *Analytical Chemistry* **2022**. https://doi.org/10.1021/acs.analchem.2c04179.

(51) Kuss, S.; Trinh, D.; Danis, L.; Mauzeroll, J. High-Speed Scanning Electrochemical Microscopy Method for Substrate Kinetic Determination: Method and Theory. *Analytical Chemistry* **2015**, *87* (16), 8096–8101. https://doi.org/10.1021/acs.analchem.5b01268.

(52) Kuss, S.; Kuss, C.; Trinh, D.; Schougaard, S. B.; Mauzeroll, J. Forced Convection during Scanning Electrochemical Microscopy Imaging over Living Cells: Effect of Topographies and Kinetics on the Microelectrode Current. *Electrochimica Acta* **2013**, *110*, 42–48. https://doi.org/10.1016/j.electacta.2013.03.149.

(53) Pons, S.; Fleischmann, M. The Behavior of Microelectrodes. *Analytical Chemistry* **1987**, *59* (24), 1391A-1399A.

(54) Beaulieu, I.; Kuss, S.; Mauzeroll, J.; Geissler, M. Biological Scanning Electrochemical Microscopy and Its Application to Live Cell Studies. *Analytical Chemistry* **2011**, *83* (5), 1485–1492. https://doi.org/10.1021/ac101906a.

Chapter 4

Effects of Media Composition and Light Exposure on the Electrochemical Current Response during Scanning Electrochemical Microscopy Live Cell Imaging

While Chapter 3 discusses the importance of temperature during SECM studies, this chapter focuses on how experimental parameters such as media composition and light exposure contribute to the electrochemical current signal during SECM imaging of HeLa cells. Physiological temperature was maintained while analyzing HeLa cells in PBS, DMEM, and DMEM+10% FBS.

Prior to cell scanning, cyclic voltammetry (CV) was performed in these three media using $FcCH_2OH$ as the redox mediator to assess their effects on the steady state current of the Pt UME. SECM imaging of HeLa cells in the different media showed increased cellular kinetics in DMEM compared to PBS and $DMEM^{FBS}$. Additionally, HeLa cells were kept at relevant physiological temperature in DMEM to analyse the effect of light on the cellular electrochemical reaction kinetics. The experimental data showed that stable illumination results in consistent electrochemical current, while fluctuating light caused variations in the current.

The research on experimental parameters such as temperature, media composition, and light exposure signifies the importance of maintaining relevant physiological conditions to obtain reliable electroanalytical data from living entities.

This chapter has been published in the Analyst and is reprinted with permission from:
Thomas, N., Lyu, M., Khouv, J., Lima, D., Kuss, S. (2024). Effects of Media Composition and Light Exposure on the Electrochemical Current Response during Scanning Electrochemical Microscopy Live Cell Imaging, 149 (22), 5555–5562. https://doi.org/10.1039/d4an01075b.
Additional information for this chapter is provided in Appendix 2.

NT conducted the experimental work, data analysis, writing, editing, figure preparation, and discussion. ML performed experiments, data analysis, writing, and discussion. JK contributed to experiments and data analysis. DL reviewed and edited the manuscript. SK supervised, reviewed, and edited the manuscript.

4.1 Abstract

Scanning Electrochemical Microscopy (SECM) has been used as a non-invasive electrochemical technique for studying cellular processes. SECM enables the quantification of cellular metabolites in real-time providing a deeper understanding of cellular responses to external stimuli. SECM imaging of living cells requires maintaining an ideal physiological environment to ensure reliable data collection on cellular reactivity. The cellular response can be directly influenced by physicochemical parameters including cell media composition, temperature and light exposure. This research demonstrates the effect of media composition on the electrochemical current signal of adenocarcinoma cervical cancer (HeLa) cells during SECM measurements using ferrocenemethanol as a redox mediator. Investigated media that are commonly used as electrolyte, are phosphate buffered saline (PBS), and Dulbecco's Modified Eagle's Medium (DMEM) in the absence and presence of fetal bovine serum (FBS). In addition, this research demonstrates that fluctuating light illumination impacts the stability of the cellular electrochemical current response. Our findings reveal that media composition and illumination are important parameters that must be carefully considered and monitored during SECM live cell imaging.

4.2 Introduction

With more than three decades, scanning electrochemical microscopy (SECM) has been used successfully for a wide range of studies involving living cells.[1–12] SECM imaging involves the movement of an ultramicroelectrode (UME) biased at a constant potential over a substrate of interest, probing surface reactivity or metabolism of living cells often utilizing a redox mediator in solution. [13] The resulting electrochemical current signal from a living cell reflects the flux of molecules from cells towards the electrode tip.[13] Experimental parameters such as scan velocity, tip-to-substrate distance, electrolyte concentration and analysis time are commonly adapted for different cell types.[14,15] As maintaining an environment that is close to physiological conditions is crucial for reliable living cell studies with SECM, parameters including cell media type, temperature, and cell adhesion to the substrate are essential factors to be considered in order to preserve cellular homeostasis.[16] Literature on SECM research applied to mammalian cells over the past five years (2019-2024) reports inconsistent selections of temperature and cell media

parameters for various applications. In fact, as shown in Figure 4.1 (a) and (b), 62% of research studies were performed at room temperature. Other studies do not specifically mention how and to what extent temperature fluctuations were controlled over the course of the experiment. Similarly, 42% of studies employed buffer solutions as electrolytes. No studies were found that studied the effects of light exposure settings during SECM imaging of living cells. With the increasing popularity of SECM, understanding how experimental parameters contribute towards the cellular electrochemical current signal is crucial for analytical data evaluation.

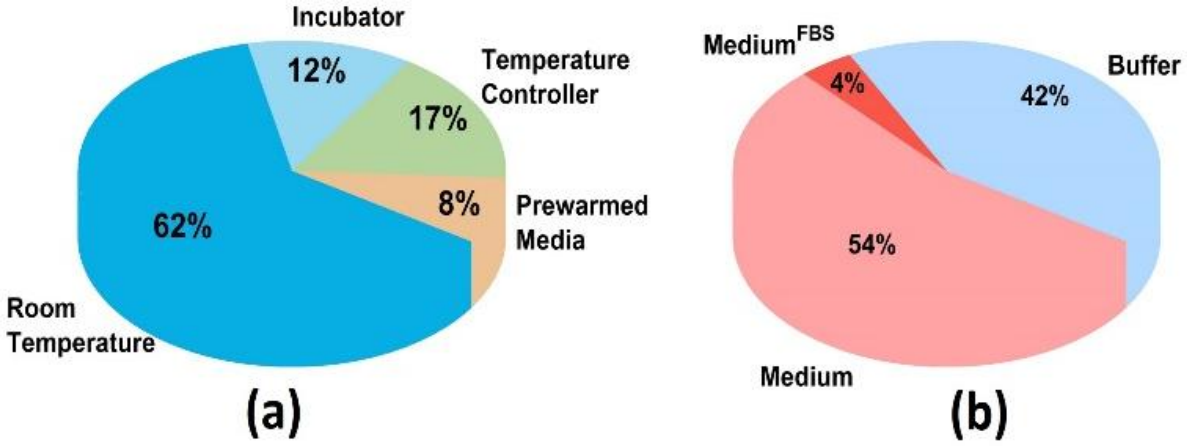

Figure 4.1 *Representation of experimental parameters reported in the literature. (a) Temperature and (b) electrolyte used during SECM mammalian cell research applications from 2019 to 2024.*

SECM measurements for living cell applications require conducting an approach curve to bring the electrode near the biological entity, followed by electrochemical analysis to quantify the flux of molecules locally.[13] The analysis time from approach curve to the end of 2D- or 3D-imaging usually takes up to 40 minutes depending on the instrumental setup. During this time cellular morphology and behaviour is often monitored by optical microscopy to visually assess cell viability during the experimental procedure. Live cell imaging by SECM often employs phosphate-buffered saline (PBS) as the electrolyte. [17] PBS, composed of sodium chloride (NaCl, 137 mM/L), potassium chloride (KCl, 2.7 mM/L), sodium hydrogen phosphate (Na_2HPO_4, 10 mM/L) and potassium dihydrogen phosphate (KH_2PO_4, 1.8 mM/L) is classified as non-toxic and isotonic, aiding in pH balance.[18–20] It is also regularly used for short time intervals in cell culture for cell washes. [19] However, literature has shown that prolonged *in vitro* exposure of cells to PBS results

in their detachment from surface, shrivelling and even rupture of the cell membrane,[21] because of deteriorated biochemical pathways involved in the cellular metabolism. To avoid these undesired effects on the cellular electrochemical response, studies have reported the use of cell culture medium during SECM imaging of living cells. Cell culture media consist of a buffering system and a mixture of nutrients including carbohydrates, amino acids, vitamins, and minerals, which ensures cell maintenance, growth and proliferation *in vitro*.[22] Cell media are often supplemented with foetal bovine serum (FBS) to facilitate attachment, growth and proliferation.[23] However, due to the complexity of the medium, the possibility of non-specific electrochemical interference, and anticipated electrode fouling, researchers may rely on PBS or cell media without FBS for electrochemical measurements with living cells.[24] Electrode fouling in FBS-supplemented cell media has been studied for different electrode materials, but it is mostly significant to applications where electrodes are placed in physiological environments for periods longer than 10 minutes. [25]

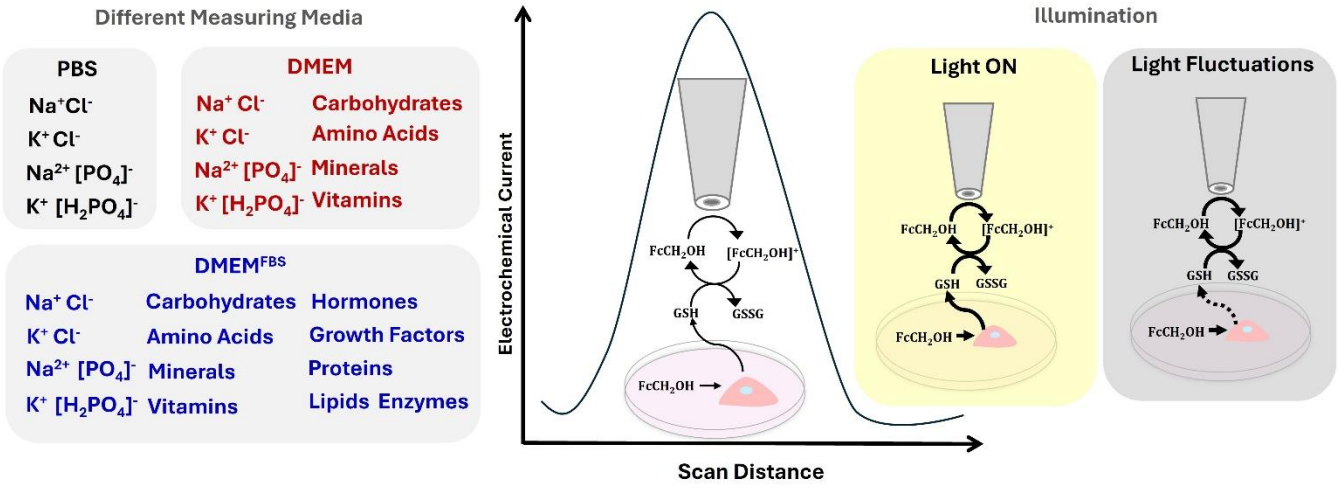

Scheme 4.1 *Composition of most commonly used cell media as SECM electrolytes and illustration of light exposure effect on the electrochemical current signal of HeLa cells.*

In addition to the medium, the exposure of cells to light is another parameter that could potentially affect cell homeostasis. For instance, studies have shown that different luminous intensities can affect metabolic processes in living cells. [26,27] In SECM living cell analysis, the light exposure is directly through the lighting system integrated into the electrochemical setup. While our previous research demonstrated the effect of temperature on the electrochemical current from living

adenocarcinoma cervical cancer (HeLa) cells and highlighted the importance of maintaining a physiological temperature (37 °C) for attaining reliable SECM data, [28] the present study reports the effect of media composition and light exposure on the electrochemical current during SECM analysis of HeLa cells. SECM has been applied to mammalian cells in the past, whereby HeLa cells have been proven particularly useful to explore cellular processes of cell metabolism[29–33], respiration[34–36], membrane permeability[37,38], and multidrug resistance.[13,39,40] Because Hela cells are robust they are model organisms for SECM live cell imaging revealing extracellular and intracellular processes. Due to their popularity, HeLa cells were herein chosen as model system to understand the effects of experimental parameters.

Herein, an SECM setup with a temperature-controlled sample stage and integrated lighting sytem is used for understanding the differences in the current signal from HeLa cells in different cell media used as electrolytes and under constant and fluctuating light conditions (Scheme 4.1). Initially, cyclic voltammetry (CV) was performed in 1X PBS, DMEM, and DMEM with 10% FBS ($DMEM^{FBS}$) containing 1 mM ferrocenemethanol ($FcCH_2OH$), a commonly employed redox mediator to quantify glutathione efflux from cells during SECM. Two-dimensional (2D) SECM line scans were then conducted across HeLa cells in different electrolyte media to evaluate possible variations in the electrochemical cell current response. Finally, 2D-line scans were performed on HeLa cells under constant and fluctuating light.

4.3 Experimental

4.3.1 Cell Culture

Adenocarcinoma cervical cancer (HeLa) cells were used for living cell experiments and were provided by Dr. Sean McKenna (Department of Chemistry, University of Manitoba, Winnipeg, MB). HyClone Dulbecco's Modified Eagle Medium/High Glucose (4.00 mM L-Glutamine, 4500 mg/L Glucose and sodium pyruvate) was purchased from Cytiva (USA) and supplemented with 10% v/v heat inactivated fetal bovine serum (Gibco/Invitrogen, ON, Canada). T-75 flasks (Fisher Scientific, USA) were used for culturing HeLa cells at 37°C and 5% CO_2. After attaining a confluency of 70-90%, phosphate-buffered saline (Cytiva, USA) was used to wash cells. Trypsin-EDTA (0.05%) solution (Gibco, USA) was used for cell detachment and harvesting. Cells were

then seeded onto 35 mm petri dishes (Thermo Fisher) and incubated for ~24 hours at 37 °C and 5% CO_2 prior to SECM experiments

4.3.2 Electrochemical Measurements

An SP-200 BioLogic potentiostat was used to perform cyclic voltammetry (CV) measurements with a 25 μm Pt ultramicroelectrode (HEKA) as the working electrode, a Pt wire as the counter electrode and an Ag/AgCl as a pseudo reference electrode. A digital thermometer (Fischer Scientific) was used for monitoring the temperature of the electrochemical cell during all CV measurements. A heating plate (Thermo Scientific) was used for temperature control during CV measurements in different media (PBS, DMEM or $DMEM^{FBS}$) containing 1mM $FcCH_2OH$ (TCI, USA)[28].

SECM measurements were conducted using an ElPROScan-3 workstation with POTMASTER software and a 25-μm Pt UME (HEKA Elektronik GmbH, Harvard Bioscience, Inc). The Pt UME was polished using a HEKA MHK 1A micro polisher using a MHK fine polishing pad (895057). The electrochemical setup was integrated with a CL-100 Biopolar Temperature Controller acquired from Warner Instruments. Line scans were performed using an Ag/AgCl pseudo reference and a Pt counter electrode. The SECM illumination set up consists of a ring light (Brightfield S80-25) from SCHOTT consisting of 80 high brightness LEDs with a color temperature of 5600K along with a visiLED controller MC 1000 from SCHOTT. The visiLED controller enables the ring light to be illuminated in different segment patterns such as full circle, semi-circle, quarter circle, 2-segment, and 4-segment mode, and the intensity of light can be set from 1 to 10. During constant light illumination during experiments with HeLa cells, the ring light was illuminated at full circle and an intensity of 10 providing 360 klx at 30 mm working distance from the substrate surface, which is the distance of the living cell from the light source. This working distance prevents significant buffer heating, which was confirmed through a temperature sensor placed inside the media during measurements. During fluctuations of light, HeLa cells were exposed to regular room light during transport from the incubator to the sample stage, and during exchange of the culture media. Cells were exposed to SECM LED-illumination while performing approach curves and in between the dark time intervals of 10, 20, 30, and 40 minutes to check the position and morphology of the HeLa cells. The room light was maintained as usual during the

entirety of the experiment. The conditions of full light exposure and fluctuating light were selected as they present the most common and likely scenarios in SECM live cell imaging.

4.4 Results and discussion

In this section, we initially discuss the electrochemical currents recorded at a 25-μm Pt UME in solutions of 1 mM $FcCH_2OH$ prepared in PBS, DMEM, and $DMEM^{FBS}$ through CV. This is followed by SECM imaging of HeLa cells in different media. Finally, we investigate the effect of illumination on HeLa cells during SECM.

4.4.1 Effect of media composition on the steady state current

The CV of a disk UME in the presence of the redox mediator $FcCH_2OH$ shows a steady state current at approximately 0.2 V *vs.* Ag/AgCl. [41,42] According to the steady state current equation (1), the steady state current (i_{ss}, *A*) is dependent on the number of electrons involved in the redox reaction (*n*), the Faraday constant (*F, sA/mol*), the diffusion coefficient of the redox mediator (*D, cm^2/s*), the concentration of the redox mediator (*c, M*), and the radius of the UME (*r, cm*).

$$i_{ss} = 4nFDcr \tag{4.1}$$

To assess the influence of media-electrolytes on the steady state current of 1 mM $FcCH_2OH$ cyclic voltammograms were recorded at a 25-μm Pt UME at 50 mV/s. The temperature was controlled to 37 °C as this is the common temperature parameter requirement for the analyses of most mammalian cells. The redox mediator was dissolved in PBS, DMEM and $DMEM^{FBS}$, respectively. Fifty voltammetric sweeps were recorded in each electrolyte (Figure A2.1.). While we observe a characteristic steady state behavior of $FcCH_2OH$ at Pt UME, the reduction current at the negative potential of PBS is attributed to the onset of the oxygen or ferrocenium reduction reaction.[43] A higher oxidation steady state current was observed in PBS and DMEM compared to $DMEM^{FBS}$. A decrease in overall current observed in $DMEM^{FBS}$ (Figure 4.2 a and b, blue) is attributed to the presence of FBS. This additive consists of a complex mixture of biomolecules such as growth

factors, proteins, lipids, and hormones. Proteins are highly adsorptive resulting in the accumulation of their oxidation products on the electrode surface.[25]

While it is important to provide living cells with nutrients over long incubation times, the presence of these biomolecules affects the solution viscosity, therefore impacting the diffusion and mass transport of the analyte towards the electrode. The Stokes-Einstein equation (2) states that the diffusion coefficient ($D(x)$) is inversely proportional to the viscosity (η) of the solution.[44]

$$D(x) = \frac{k_B T}{3\pi\eta x} \tag{4.2}$$

In this equation, k_B is the Boltzmann constant, T is the temperature, and x is the hydrodynamic particle diameter. Among the three media analyzed in this study, PBS is known to have a lower viscosity followed by DMEM and $DMEM^{FBS}$.[45] This would indicate PBS having a higher i_{ss}, however, from Figure 3.2 b, it is observed that the overall i_{ss} was the highest in DMEM compared to $DMEM^{FBS}$ and PBS. Although $DMEM^{FBS}$ presented a lower current, which is attributed to the FBS-blocked electrode surface, DMEM generated higher currents without causing electrode fouling. The lower current in $DMEM^{FBS}$ is due to the exposure of the metal surface to FBS containing hormones, growth factors, and proteins over extended periods of time is known to block or foul their surface.[25] The higher currents observed for $FcCH_2OH$ in DMEM can be ascribed to the medium composition, which consists of amino acids, vitamins and inorganic salts such as $CaCl_2$, $MgSO_4$ and $Fe(NO_3)_3$ in addition to the buffering system.[46]

The calculated diffusion coefficient D of $FcCH_2OH$ in PBS, DMEM and $DMEM^{FBS}$ at 37 °C are 1.20×10^{-5}, 1.36×10^{-5}, and 1.16×10^{-5} cm^2s^{-1}, respectively. The diffusion coefficient of $FcCH_2OH$ in DMEM is higher than that in PBS although the viscosity is lower in PBS. This can be explained by the hydrodynamic particle diameter changing as a function of complexation in different solution media.[47]

As demonstrated in this study, the composition of cell media as the electrolyte plays a crucial role on the intensity and stability of the steady state current over time. Investigating the influence of

the media composition on the electrochemical current during SECM live cell studies is also important because the cellular metabolism is greatly dependent on culture media.

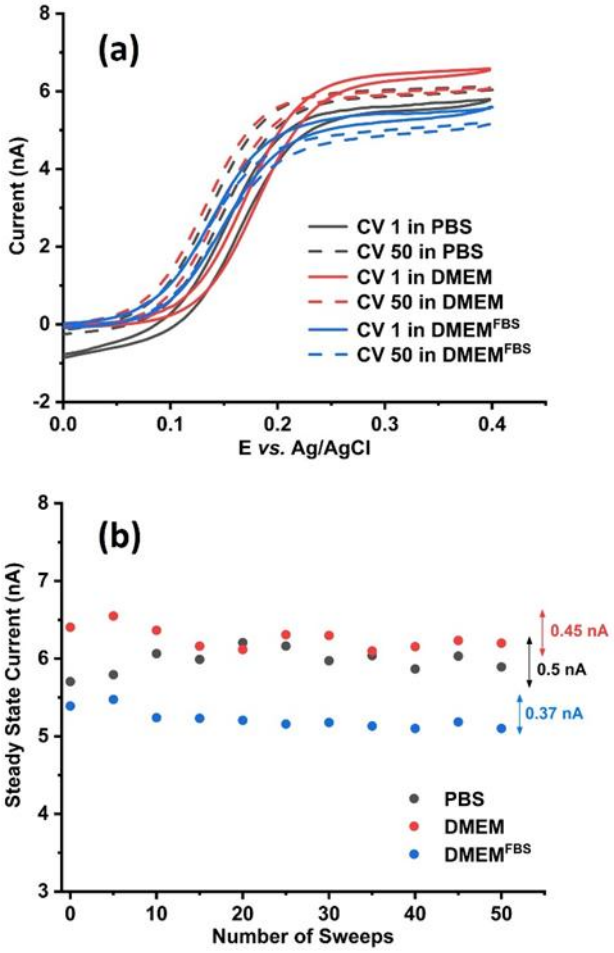

Figure 4.2 *Effect of different media on the steady state current at a Pt UME. (a) 1st, and 50th sweeps of cyclic voltammograms in 1 mM $FcCH_2OH$ dissolved in PBS (black), DMEM (red) and $DMEM^{FBS}$ (blue) at 50 mV/s. (b) Variation in the steady state current over the course of 50 sweeps*

4.4.2 SECM cell imaging in different cell-media-electrolytes

To assess how different electrolyte media affect cellular redox activity using SECM, HeLa cells were measured in PBS, DMEM and $DMEM^{FBS}$ containing 1 mM $FcCH_2OH$ employing a Pt UME at scan rates ranging from 10 µm/s to 100 µm/s (Figure 4.3). Cells were maintained at a constant temperature of 37.0 ± 0.2 °C throughout the experiment, as reported in our previous study.[28] Herein, the Pt UME was biased at 0.4 V (*vs.* Ag/AgCl), which ensured the constant oxidation of $FcCH_2OH$ to $[FcCH_2OH]^+$ at the electrode tip. Reduced glutathione (GSH), which is expelled by the cells, reacts with $[FcCH_2OH]^+$ and regenerates $FcCH_2OH$.[13] As a result, an increased

electrochemical current is observed when a UME is scanned across living cells during SECM measurements. Fig 4.3a visualizes the cellular electrochemical response as a 3D scan, which is composed of multiple line scans. The diffusion intensity of GSH away from the cell is illustrated by the colours in Fig 3a. The cellular metabolism plays a major role in the rate of $FcCH_2OH$ regeneration by the GSH-GSSG redox couple.[13] Since the resulting current signal is dependent on the redox state of the cell, it is crucial to understand how changes in the composition of the cell-media-electrolyte will affect the cellular electrochemical activity. An approach curve was performed near living cells and the UME was retracked to a tip-to-substrate distance greater than the height of a cell (12 µm) during the SECM line scans. The peak currents across two HeLa cells in PBS (n = 8) (Fig 4.3a & Fig A2.2), DMEM (n = 8) (Figure 4.3b & Figure A2.3) and $DMEM^{FBS}$ (n = 8) (Figure 4.3c & Figure A2.4) at velocities of 10, 30, 50, 80 and 100 µm/s were recorded and compared. Depending on how close cells are positioned next to one another, either a prominent single peak (Figure 3.3b-c) or two separate peaks (Figure 4.3d) are visible during line scans. The current decreases over cells at a scan velocity of 10 µm/s due to hindered diffusion. In this case, the ability of the cell to regenerate $FcCH_2OH$ is not able to overcompensate the hindered diffusion by the physical body of the cell.[15] The normalized peak currents of different groups of cells in each media were plotted against the corresponding scan velocity.

Scanning the electrode at various scan velocities, enables the use of a so-called “convection effect” to determine the cellular kinetics, which represents the ability of cells to regenerate the redox mediator $FcCH_2OH$. An apparent heterogeneous rate constant (cell kinetics) is derived from the slope that originates from the dependence of the peak current on the scan velocity.[15,48,49] Herein, although cell kinetics are not calculated, the experimental slopes are used to determine relative changes in cell kinetics. Furthermore, this approach has been shown to be useful to reduce the overall analysis time.

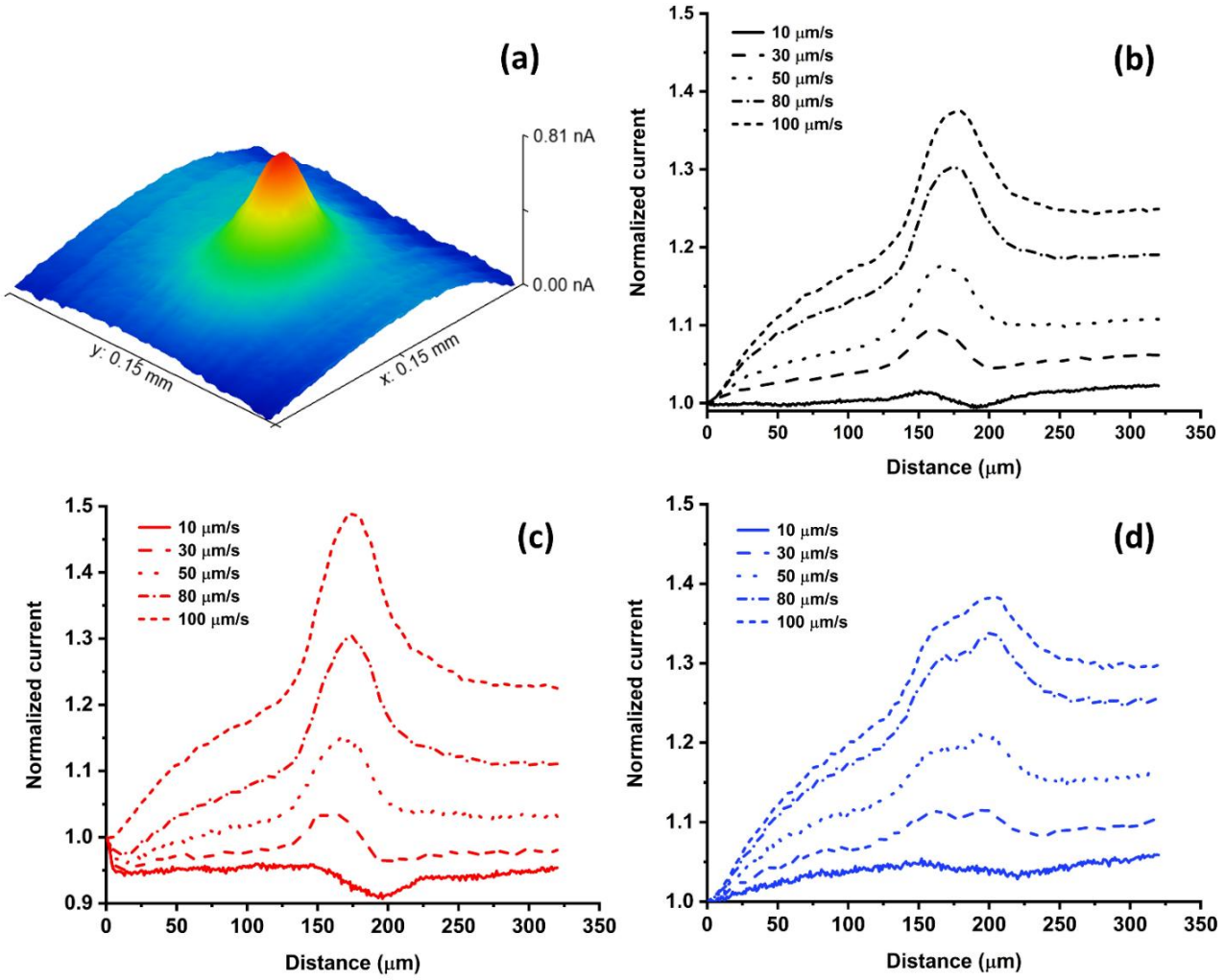

Figure 4.3 *HeLa cell imaging. a) 3D imaging across a single HeLa cell at 100 µm/s. 2D line scans obtained at scan velocities ranging from 10 to 100 µm/s in (b) PBS (c) DMEM and (d) DMEM with 10% FBS used as electrolyte. All solutions contain 1 mM* $FcCH_2OH$*. Normalized current is the electrochemical current divided by the initial current value of the line scan. An increase in the baseline current is observed due to a slope of the substrate surface.*

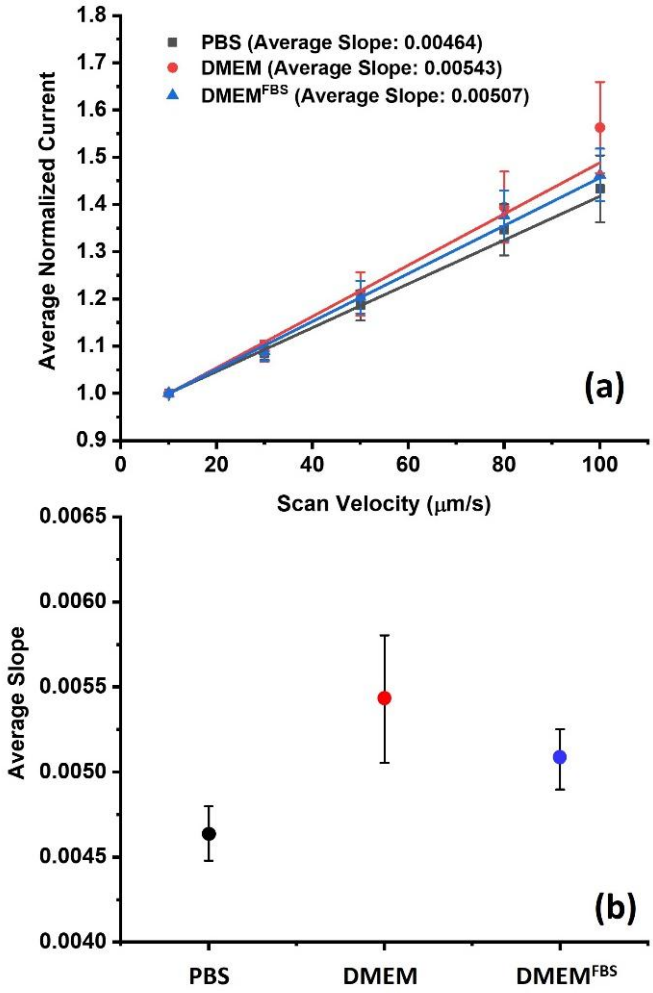

Figure 4.4. *Effect of different media on the electrochemical current response of HeLa cells. (a) Linear dependency of the average normalized peak current with respect to the scan velocity in PBS (black), DMEM (red), and DMEM^{FBS} (blue) (b) Comparison of average slope in different media indicating higher electrochemical cell response in DMEM.*

A linear relationship was observed between the normalized peak currents and the scan velocity for each media, and their respective slopes are shown in Figure A2.5. The observed increase is due to the enhanced mass transport of electroactive species caused by forced convection.[48] In this approach, a cell's ability to regenerate $FcCH_2OH$ (cell kinetics) and its topography are reflected by the slope.[15,49] Monitoring changes in slope can function as an indicator of the influence of media solution on the cellular metabolism, as long as all instrumental parameters and the solution

temperature are maintained constantly throughout the experiments. When performing line scans across multiple groups of cells on different days, outliers were identified by the Grubb's test (α = 0.05). Fig 4.4a presents the average correlations and standard deviations for the different media. The mean value of slopes in PBS, DMEM, and $DMEM^{FBS}$ were 0.00464 ± 0.00016, 0.00543± 0.00037 and 0.00507 ± 0.00018 s/µm, respectively. Interestingly, the highest average slope was achieved in experiments conducted in DMEM without FBS, which suggests the highest rate of regeneration of $FcCH_2OH$ in this medium. An effect on the cellular metabolic integrity cannot be excluded in the case of PBS (Figure 4.4b). It is thought that cells potentially reduce their metabolic rate when not exposed to sufficient minimal nutrients, minerals, glucose, and other factors, as it is the case in PBS. However, slope test performed among the average slopes of the three media showed no significant statistical difference at the 95% confidence interval. (Appendix 2 for details) It is concluded that DMEM or cell media without FBS in general provides best electron transfer efficiency, low viscosity, but sufficient supplements for maintaining regular cell metabolic rates, while avoiding electrode fouling during biological SECM analyses.

4.4.3 Influence of light exposure

It was reported that living cells exposed to different wavelengths of light for extended periods of time, e.g. 20-24 hours, display effects on their proliferation and attachment. [50,51] In contrast to standard optical microscopy, which is designed to examine the growth of cells or to analyze fixed samples, SECM is an electrochemical technique that measures molecule exchange between living cells and an electrode. Due to the sensitive nature of SECM, it is not clear whether short-term light exposure or light fluctuations could affect the measured electrochemical signals. Herein, the effect of illumination on the cellular response of living HeLa cells during SECM imaging was examined. Line scans were conducted over the cells at time intervals of 10, 20, 30 and 40 minutes in the presence of white light and under fluctuating light conditions in 1 mM $FcCH_2OH$ dissolved in DMEM (Figure 4.5, A2.6, and A2.7). Cells were scanned at a fixed velocity of 50 µm/s. It was observed that the normalized peak current fluctuated in the absence of light (Figure 4.5a) and under light exposure (Figure 4.5b) similarly during the first 10 minutes. Under illumination, the electrochemical current response of cells stabilized over the course of 40 minutes (Figure 4.5c). When white light fluctuated, e.g. when cells were removed from the incubator (dark), moved to the SECM (light), were shielded from light until the experiment began (dark), were illuminated

during an approach curve for UME positioning (light), and scanned without illumination from the microscope (room light), the current response varied significantly over 40 min. It must be noted that conditions in total darkness were not studied here, as it is practically impossible to conduct all steps of SECM live cell imaging in complete darkness. Light fluctuations and consistent light exposure after culturing are the most realistic experimental conditions that researchers will likely apply. Importantly, the literature on SECM live cell imaging does not report details on light exposure or fluctuating conditions. This demonstrates that there is a lack of awareness about the importance of this parameter. To assess the statistical significance of the current variability in the presence and absence of illumination, a student's t-test was performed showing no significant difference in the electrochemical current response among the different time intervals at the 95% confidence interval ($p > 0.05$). Although the statistical difference was found to be non-significant at time intervals of up to 40 minutes, the effects of illumination on some cells' electrochemical response is clearly visible (Figure 4.5c). [52] This becomes a problem when analysing single cells and relying on data originating from small data sets. It is recommended to keep white light exposure throughout SECM live cell imaging experiments constant to provide most stable conditions for cell analysis.

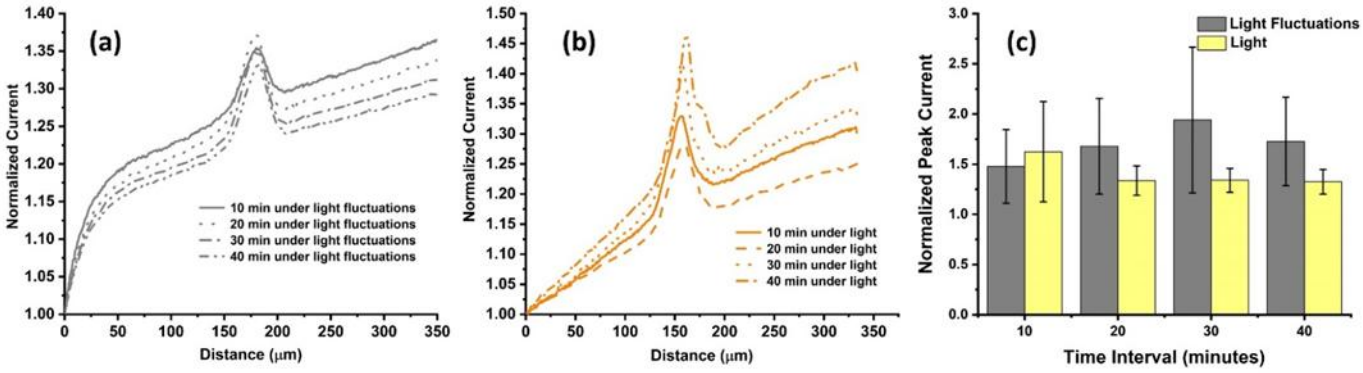

Figure 4.5 *Effect of light exposure on the electrochemical current signal of HeLa cells. 2D line scans were performed under fluctuating (a) or under full light (b) conditions at time intervals of 10, 20, 30 and 40 minutes. (c) Graph displays the variation in average normalized peak current (n=3) at 10, 20, 30, and 40 minutes in fluctuating (grey) and in full light (yellow) conditions.*

4.5 Conclusions

This study provides insight into the importance of experimental parameters of cell media composition and light exposure during SECM imaging of living cells. The effect of different cell-media-electrolytes on HeLa cells was evaluated by monitoring the electrochemical current response during cell analysis. SECM imaging of HeLa cells demonstrated the highest cellular current response in DMEM in the absence of FBS. Although PBS provides high ionic strength and conductivity for electrochemical measurements, SECM analysis involving fast and real-time monitoring of biological entities mimicking their physiological environment [7] requires the use of minimal cell medium, as it provides crucial nutrient for cells to maintain a normal metabolism and avoiding artifacts in current changes. It should be noted that HeLa is a model cancer cell line that is known to be robust, being able to cope with stress better than other cell lines.[53] The effects shown in this study may be more pronounced in more sensitive samples, such as Chinese Hamester Ovary[21] and Acute Myeloid Leukaemia[19]. These cell lines have been shown to be less viable in PBS, resulting in their rupture and disintegration during prolonged incubation times. Therefore, it is recommended to use serum-free cell media for any SECM cell studies for reliable bioelectrochemical measurements. This study also shows that the electrochemical current signal from HeLa cells was most stable during constant light illumination compared to conditions where light exposure fluctuates. Thus, the impact of light on the cellular current response of living cells must not be neglected.

The maintenance of cells under close to physiological conditions through media and consistent light illumination, in combination with closely monitored temperature conditions, are essential for reliable bioelectrochemical cell studies. Respecting and controlling these parameters will lead to more reliable and accurate data collection for mammalian cell SECM applications.

4.6 Acknowledgements

SK acknowledges funding by the Natural Sciences and Engineering Research Council of Canada (RGPIN-2024-05454) for its financial support. We thank Harvard Bioscience and HEKA Electronics for continuing support.

4.7 References

(1) Polcari, D.; Dauphin-Ducharme, P.; Mauzeroll, J. Scanning Electrochemical Microscopy: A Comprehensive Review of Experimental Parameters from 1989 to 2015. *Chem Rev* **2016**, *116* (22), 13234–13278. https://doi.org/10.1021/acs.chemrev.6b00067.

(2) Amemiya, S.; Guo, J.; Xiong, H.; Gross, D. A. Biological Applications of Scanning Electrochemical Microscopy: Chemical Imaging of Single Living Cells and Beyond. *Anal Bioanal Chem* **2006**, *386* (3), 458–471. https://doi.org/10.1007/s00216-006-0510-6.

(3) Zoski, C. G. Review—Advances in Scanning Electrochemical Microscopy (SECM). *J Electrochem Soc* **2016**, *163* (4), H3088–H3100. https://doi.org/10.1149/2.0141604jes.

(4) Conzuelo, F.; Schulte, A.; Schuhmann, W. Biological Imaging with Scanning Electrochemical Microscopy. *Proceedings of the Royal Society A: Mathematical, Physical and Engineering Sciences* **2018**, *474* (2218). https://doi.org/10.1098/rspa.2018.0409.

(5) Zhou, Y.; Takahashi, Y.; Fukuma, T.; Matsue, T. Scanning Electrochemical Microscopy for Biosurface Imaging. *Curr Opin Electrochem* **2021**, *29*, 100739. https://doi.org/10.1016/j.coelec.2021.100739.

(6) Poderyte, M.; Ramanavicius, A.; Valiūnienė, A. Exploring the Living Cell: Applications and Advances of Scanning Electrochemical Microscopy. *Crit Rev Anal Chem* **2024**, 1–12. https://doi.org/10.1080/10408347.2024.2328135.

(7) Beaulieu, I.; Kuss, S.; Mauzeroll, J.; Geissler, M. Biological Scanning Electrochemical Microscopy and Its Application to Live Cell Studies. *Anal Chem* **2011**, *83* (5), 1485–1492. https://doi.org/10.1021/ac101906a.

(8) Kuss, S.; Polcari, D.; Geissler, M.; Brassard, D.; Mauzeroll, J. Assessment of Multidrug Resistance on Cell Coculture Patterns Using Scanning Electrochemical Microscopy. *Proc Natl Acad Sci U S A* **2013**, *110* (23), 9249–9254. https://doi.org/10.1073/pnas.1214809110.

(9) Bard, A. J.; Mirkin, M. V. *Scanning Electrochemical Microscopy*, Third.; Taylor& Francis.

(10) Verma, A.; Verma, M.; Singh, A. Animal Tissue Culture Principles and Applications. In *Animal Biotechnology: Models in Discovery and Translation*; Elsevier, 2020; pp 269–293. https://doi.org/10.1016/B978-0-12-811710-1.00012-4.

(11) Liu, B.; Rotenberg, S. A.; Mirkin, M. V. Scanning Electrochemical Microscopy of Living Cells: Different Redox Activities of Nonmetastatic and Metastatic Human Breast Cells. *Proc Natl Acad Sci U S A* **2000**, *97* (18), 9855–9860. https://doi.org/10.1073/pnas.97.18.9855.

(12) Phosphate Buffer. *Cold Spring Harb Protoc* **2006**, *2006* (1), pdb.rec8543. https://doi.org/10.1101/pdb.rec8543.

(13) Lichtenauer, M.; Nickl, S.; Hoetzenecker, K.; Mangold, A.; Moser, B.; Zimmermann, M.; Hacker, S.; Niederpold, T.; Mitterbauer, A.; Ankersmit, H. J. Phosphate Buffered Saline Containing Calcium and Magnesium Elicits Increased Secretion of Interleukin-1 Receptor Antagonist. *Lab Med* **2009**, *40* (5), 290–293. https://doi.org/10.1309/LMBMG5A7NOVQBXWD.

(14) Wangen, R.; Aasebø, E.; Trentani, A.; Døskeland, S. O.; Bruserud, Ø.; Selheim, F.; Hernandez-Valladares, M. Preservationmethod and Phosphate Buffered Salinewashing Affect the Acutemyeloid Leukemia Proteome. *Int J Mol Sci* **2018**, *19* (1). https://doi.org/10.3390/ijms19010296.

(15) Chen, A.; Leith, M.; Tu, R.; Tahim, G.; Sudra, A.; Bhargava, S. Effects of Diluents on Cell Culture Viability Measured by Automated Cell Counter. *PLoS One* **2017**, *12* (3). https://doi.org/10.1371/journal.pone.0173375.

(16) Arora, M. Cell Culture Media: A Review. *Materials and Methods* **2013**, *3*. https://doi.org/10.13070/mm.en.3.175.

(17) Liu, S.; Yang, W.; Li, Y.; Sun, C. Fetal Bovine Serum, an Important Factor Affecting the Reproducibility of Cell Experiments. *Sci Rep* **2023**, *13* (1). https://doi.org/10.1038/s41598-023-29060-7.

(18) Harris, A. R.; Newbold, C.; Stathopoulos, D.; Carter, P.; Cowan, R.; Wallace, G. G. Comparison of the In Vitro and In Vivo Electrochemical Performance of Bionic Electrodes. *Micromachines (Basel)* **2022**, *13* (1). https://doi.org/10.3390/mi13010103.

(19) Harris, A. R.; Carter, P.; Cowan, R.; Wallace, G. G. Impact of Protein Fouling on the Charge Injection Capacity, Impedance, and Effective Electrode Area of Platinum Electrodes for Bionic Devices. *ChemElectroChem* **2021**, *8* (6), 1078–1090. https://doi.org/10.1002/celc.202001574.

(20) Sun, D.; Zhang, Z.; Chen, F. Effects of Light Intensity, Light Quality, and Illumination Period on Cell Growth, TFA Accumulation, and DHA Production in Crypthecodinium Sp. SUN. *J Appl Phycol* **2018**, *30* (3), 1495–1502. https://doi.org/10.1007/s10811-017-1379-9.

(21) Walter, B.; Peters, J.; van Beusekom, J. E. E. The Effect of Constant Darkness and Short Light Periods on the Survival and Physiological Fitness of Two Phytoplankton Species and Their Growth Potential after Re-Illumination. *Aquat Ecol* **2017**, *51* (4), 591–603. https://doi.org/10.1007/s10452-017-9638-z.

(22) Thomas, N.; Lima, D.; Trinh, D.; Kuss, S. Temperature Effect on the Electrochemical Current Response during Scanning Electrochemical Microscopy of Living Cells. *Anal Chem* **2023**. https://doi.org/10.1021/acs.analchem.3c03716.

(23) Stulik, K.; Amatore, C.; Holub, K.; Marecek, V.; Kutner, W. Microelectrodes.Definitions, Characterization, and Applications. *Pure and Applied Chemistry* **2000**, *72* (8), 1483–1492. https://doi.org/10.1016/S0022-0728(02)00745-3.

(24) Montenegro, M. I. ; Queiros, M. A. ;; Daschbach, J. L. ; *Microelectrodes: Theory and Applications*; 1991. https://doi.org/10.1007/978-94-011-3210-7.

(25) Zmpitas, J.; Gross, J. Modified Stokes-Einstein Equation for Molecular Self-Diffusion Based on Entropy Scaling. *Ind Eng Chem Res* **2021**, *60* (11), 4453–4459. https://doi.org/10.1021/acs.iecr.0c06090.

(26) Poon, C. Measuring the Density and Viscosity of Culture Media for Optimized Computational Fluid Dynamics Analysis of in Vitro Devices. https://doi.org/10.1101/2020.08.25.266221.

(27) Miao, W.; Ding, Z.; Bard, A. J. Solution Viscosity Effects on the Heterogeneous Electron Transfer Kinetics of Ferrocenemethanol in Dimethyl Sulfoxide-Water Mixtures. *Journal of Physical Chemistry B* **2002**, *106* (6), 1392–1398. https://doi.org/10.1021/jp013451u.

(28) Kuss, S.; Kuss, C.; Trinh, D.; Schougaard, S. B.; Mauzeroll, J. Forced Convection during Scanning Electrochemical Microscopy Imaging over Living Cells: Effect of Topographies and Kinetics on the Microelectrode Current. *Electrochim Acta* **2013**, *110*, 42–48. https://doi.org/10.1016/j.electacta.2013.03.149.

(29) Kuss, S.; Trinh, D.; Danis, L.; Mauzeroll, J. High-Speed Scanning Electrochemical Microscopy Method for Substrate Kinetic Determination: Method and Theory. *Anal Chem* **2015**, *87* (16), 8096–8101. https://doi.org/10.1021/acs.analchem.5b01268.

(30) Kuss, S.; Trinh, D.; Mauzeroll, J. High-Speed Scanning Electrochemical Microscopy Method for Substrate Kinetic Determination: Application to Live Cell Imaging in Human Cancer. *Anal Chem* **2015**, *87* (16), 8102–8106. https://doi.org/10.1021/acs.analchem.5b01269.

(31) Stockley, J. H.; Evans, K.; Matthey, M.; Volbracht, K.; Agathou, S.; Mukanowa, J.; Burrone, J.; Káradóttir, R. T. Surpassing Light-Induced Cell Damage in Vitro with Novel Cell Culture Media. *Sci Rep* **2017**, *7* (1). https://doi.org/10.1038/s41598-017-00829-x.

(32) Waldchen, S.; Lehmann, J.; Klein, T.; Van De Linde, S.; Sauer, M. Light-Induced Cell Damage in Live-Cell Super-Resolution Microscopy. *Sci Rep* **2015**, *5*. https://doi.org/10.1038/srep15348.

(33) Golovynska, I.; Golovynskyi, S.; Qu, J. Comparing the Impact of NIR, Visible and UV Light on ROS Upregulation via Photoacceptors of Mitochondrial Complexes in Normal, Immune and Cancer Cells. *Photochem Photobiol* **2023**, *99* (1), 106–119. https://doi.org/10.1111/php.13661.

(34) Chandra Jagetia, G.; Nayak, V. *Effect of Doxorubicin on Cell Survival and Micronuclei Formation in HeLa Cells Exposed to Different Doses of Gamma-Radiation*; 2000; Vol. 176.

Chapter 5

Single Cell Scanning Photoelectrochemical Microscopy using Micro-Optical-Ring Electrodes

While chapters 3 and 4 discuss the significance of experimental parameters in living cell SECM, and Chapter 2 provided an understanding, comparison, interdisciplinary applicability and fabrication methodologies of different optical fiber (OF) probes. This chapter focuses on Micro-Optical Ring Electrodes (MOREs), emphasizing their advantages over microelectrodes and their multifunctionality as both electrochemical light guide and spectroelectrochemical probes. A user-friendly fabrication procedure for MOREs is described, and their repeatability and reproducibility are evaluated through CV, numerical modeling, and SEM.

After successful characterization, MOREs were integrated into SECM, and the spectroscopic and spectroelectrochemical properties of SPECM were explored using the colored and redox nature of N, N, N', N'-Tetramethyl-p-phenylenediamine (TMPD). The applicability of SPECM to living cells was studied using a light-sensitive biological model system. The oxygen production/consumption of the algae *Eremosphaera viridis* was investigated under local illumination with simultaneous electrochemical detection. This chapter demonstrates the potential of SPECM as a multifaceted tool for analyzing biomolecule flux in living entities.

The work presented in this chapter has been published in *Biosensors and Bioelectronics* and is reprinted from: *Thomas, N.; Singh, V.; Ahmed, N.; Trinh, D.; Kuss, S. (2022) Single-Cell Scanning Photoelectrochemical Microscopy Using Micro-Optical-Ring Electrodes. Biosensors and Bioelectronics, 217.* *https://doi.org/10.1016/j.bios.2022.114658*.
Appendix 3 contains the supplementary information for this chapter.
As specified by the journal's rights and permissions, authors do not need permission to include their respective article in the thesis.

The writing, experimental work, review, editing, and discussion were carried out by NT. VS contributed to the investigation, writing, editing, and discussions. NA participated in the experimental work and writing. Numerical modeling and analysis were performed by DT. SK provided supervision, guidance, and reviewing of the manuscript.

5.1 Abstract

Microelectrodes as analytical sensing tools have gained immense popularity in a wide range of applications, ranging from probe design advancement to single live cell imaging. Micro-Optical-Ring Electrodes (MOREs) are micro-scale electrodes offering multi-functionality, enabled through an optical fiber core, which is surrounded by metal coating and an insulating epoxy/capillary layer. The optical fiber centre enables the MORE to function either as a light guide or as a remote spectrophotometer while also acquiring an electrochemical current signal. Herein, we present a user-friendly and cost-effective method to fabricate MOREs for Scanning Photoelectrochemical Microscopy (SPECM) applications. MOREs were characterized by electrochemistry, numerical modelling, and Scanning Electron Microscopy (SEM), ensuring reproducibility in terms of a well-defined geometry and functionality. In this study, the integration of MOREs into scanning probe microscopy enabled the spectro-electrochemical detection of N, N, N, N'- Tetramethyl-p-phenyl-enediamine (TMPD) and its oxidized radical cation counterpart. To demonstrate the applicability of MOREs to electrochemical single live cell imaging, oxygen production was detected in living algae (Eremosphaera viridis) by local illumination and concurrent electrochemical measurements.

5.2 Introduction

Microelectrodes are well-characterized tools for the detection of electroactive analytes and entities of interest at the microscopic scale.[1–7] With advantages including small size, low-current measurements and increased species flux towards the electroactive surface[4,8,9], the applicability of these electrodes include, but are not limited to the electrochemical characterization of semiconductor materials in energy applications[10–13], analyzing surface homogeneities/heterogeneities of metallic surfaces for corrosion studies[14–16], and the electrochemical detection and quantification of material flux and/or biomarkers at the single cell level.[4,17–19] In combination with optical fibers, these electrodes become multi-functional sensors, facilitating the understanding of photoelectrochemical reactions with micro-scale resolution. The integration of optical fibers into electrochemical devices has attracted immense attention over the past decade. [20] The approach to incorporate optical fibers into a working electrode is particularly interesting, as it enables the combination of electrochemical imaging and spectroscopy. Micro-

Optical-Ring Electrodes (MOREs) are electrodes with an optical fiber center, coated by a metal layer, and surrounded by an insulating layer of epoxy or glass for stability. MOREs were initially discussed by Kuhn and Webber in 1990 and applied to study electro-generated chemiluminescence.[21] It was also used to sense and characterize photo-generated species of short lifetimes to understand the kinetics of a chemical reaction and to analyze mass transport processes of photoelectrochemical systems.[18,22–24] Although these probes were successfully applied to scanning probe applications to characterize materials for energy and corrosion applications, as well as biological imaging, their applicability towards the local detection of species flux from living cells is yet to be explored.

Fabrication methodologies developed for optical fiber containing electrodes have been proposed based on a procedure reported by Bard et al.[25] This procedure included heating, pulling and metallic coating of the optical fiber, followed by insulation and electrode tip exposition. Apart from heating, pulling and spin metal coating, etching of the optical fiber was necessary, followed by sputter coating to achieve different tip shapes.[26,27] Furthermore, electro-less gold coating of the optical fiber [28] and photolithographic deposition of gold on optical fibers was also demonstrated in the literature.[29] Unfortunately, these fabrication methods were not only time consuming and expensive, they also required immense precision making its reproducibility difficult. Especially during electrochemical imaging of complex sample, such as biological cells, a well-defined geometry of the electrode as a sensor is crucial to understand and interpret the recorded data accurately. As bioelectrochemical measurements require time and a statistical assessment of cellular responses, it is often necessary to complete studies with several electrodes. To assure accuracy and reproducibility it is important to be able to rely on sensors identical in parameters, such as size, shape, and ratio of electroactive and insulating surface area.

Herein, we present the design, development and fabrication of a cost-effective, time-efficient, and user-friendly method to fabricate MOREs with a well-defined geometry and reproducible functionality. This fabrication procedure enables qualitative and quantitative electrochemical analysis of molecule transport across membranes in single living cells by scanning photoelectrochemical microscopy (SPECM). Multi-functional MOREs were employed as a light

guide, as a spectroscopic probe, and as an electrochemical sensor to non-invasively detect electroactive species released from single biological cells.

5.3 Materials and Methods

5.3.1 Materials and Chemicals

Gold coated optical fibers (OD: 155 ± 16 μm) were received from Fiber guide (NJ, USA) and used as received. Epoxy resin and hardener were obtained from Pace Technologies (USA). Soda lime glass capillary (OD: 0.9 mm) were purchased from Hilgenberg (Germany), and copper wire (diameter: 0.25 mm) was received from Goodfellow (England). Epoxy silver was obtained from World Precision Instruments (USA). Diamond polishing pads (0.1, 6.0 and 9.0 μm) were purchased from Struers (USA).

Solutions were prepared using nanopure water with a resistivity of no less than 18.2 MΩ cm at 25 °C. Potassium chloride (KCl, ≥ 99.9%) was received from Fisher Chemical (Belgium). Hydroxymethyl ferrocene (C11H12FeO, > 95.0%) was obtained from TCI (USA) and N, N, N, N'- Tetramethyl-p-phenyl-enediamine (TMPD, 99.0%) was purchased from Sigma Aldrich (USA). MicroPolish Alumina (1.0, 0.3 and 0.05 μm) and MicroCloth Polishing Cloth were from Buehler (USA).

5.3.2 Numerical Simulations

Numerical simulations in 3D were performed to quantify the MORE current dependence on the geometry of microelectrode. Electrochemical current was coupled with the mass transport of the electroactive species. The electrochemical kinetics observed at the MORE surface were modeled using the Butler-Volmer equation. The parameters were taken from the experimental conditions: the MORE geometry, redox concentration of 1 mM $FcCH_2OH$, scan rate of 30 mV/s, diffusion coefficient $D = 8 \times 10^{-6}$ cm^2/s, standard rate constants $k_0 = 0.03$ cm/s. The PDE (Partial Differential Equations) were solved using the FEM methods of the Comsol Multiphysics© software. The mesh quality was optimized to obtain a very high accuracy with a relative error of about 0.1%.

5.3.3 SPECM Measurements

All spectroscopic measurements were performed using a fiber-coupled spectrophotometer module (High-Performance QEPro from Ocean Insight, FL, USA), coupled to a scanning electrochemical microscope setup with a customized control software (HEKA Elektronik GmbH, Harvard Bioscience Inc.). MOREs were interfaced with the system through a custom-made opto-electrode holder, which was connected to the spectrophotometer unit via a SMA fiber with a 400 µm core diameter and a UV-Vis-NIR light source (DH-2000-BAL). A 35 mm petri dish was filled to a volume of 4 ml with 0.1 mM TMPD prepared in 0.1 M KCl. A bottom spot illumination was carried out towards the petri dish and a MORE was prepositioned at a tip-to-substrate distance of 150 µm. A MORE was aligned with the illumination spot to maximize the signals during absorbance measurements in TMPD/TMPD+•. For better comparison and quantitative analysis, the obtained absorbance values of the UV-Vis spectra were processed using the data analysis software OriginLab. Absorbance readings were normalized by calculating the average of the first ten data points. All data points of the spectrum were then divided using this average to illustrate the change in absorbance during the optimization studies. The obtained normalized absorbance was plotted as a function of the wavelength (nm).

5.3.4 Cell culture

Ready to use, sterile 100% Bold's Basal Medium and *Eremosphaera viridis* (CPCC 127) were acquired from Canadian Phycological Culture Centre, ON, Canada. E. viridis (size: 144 µm) were cultured in Erlenmeyer flasks with cool white LED illumination for 12-hours in light and dark periods.

5.3.5 Oxygen production recognition in bulk solution

Electrochemical measurements were obtained using a SP-200 potentiostat from BioLogic (France). After attaining dense growth of *E. viridis* in the culture flask, 4 ml of uniformly distributed *E. viridis* solution was transferred to a vial for linear sweep voltammetry measurements at 50 mVs-1 using a 3-mm gold working electrode (BASi, USA), Pt counter electrode and Ag/AgCl pseudo reference electrode. The same vial was placed in darkness for three hours, before LSV measurements were repeated.

5.3.6 Single Cell SPECM measurements

All SPECM measurements were performed using the ElProScan-3 with POTMASTER software (HEKA Elektronik GmbH, Harvard Bioscience Inc.). The SPECM included an integrated inverted optical microscope (with objectives 4×, 10×, 40×, 100×). 35-mm petri dishes (Thermo fischer, USA) were coated with PLL (poly-L-lysine 0.01 % (PLL)) obtained from Sigma.) for E. viridis attachment. 1 mL of PLL was added to the petri dish, which was gently swirled to achieve a uniform coating of the petri dish surface. After 5 minutes PLL was aspirated, the surface was rinsed with nano-pure water three times. The petri dish was then left to dry for 2 hours. PLL coating steps were repeated 2 times. Eremosphaera Viridis was harvested, seeded into the petri dishes, and then incubated at room temperature overnight to ensure attachment to the petri dish. The petri dish with attached algae were taken for SPECM measurements. The algae were imaged in a constant height mode and measurements were performed using a Ag/AgCl reference electrode and a platinum wire as auxiliary electrode in Bold's Basal Medium. Since the PLL coated petri dish is non-conductive, an approach curve was performed to position the electrode in close proximity to the algal sample. Light illumination was realized through the MORE's optical fiber, connected to a 3-mm LED white light. The MORE was positioned 140 µm above the petri dish to the left of the identified target algal cell. Line scan was performed across the living algal cell at a velocity of 10 µm/s with the light switched OFF. After retracting the MORE to its initial position, the light was turned ON and the line scan was repeated. The 3D scan of a single algal cell was performed at -0.6 V, 50 µm/s with a scan area of 1000 x 1000 µm and step size of 25 µm in the X-Y direction.

5.4 Results and Discussion

5.4.1 Fabrication and Characterization of MOREs

The fabrication of MOREs is schematically shown in Scheme 5.1. To assess the MORE assembly and geometry closely, the fabricated electrodes were characterized at different stages of the fabrication process using Scanning Electron Microscopy (SEM) imaging (Figure 5.1a to d). MORE fabrication was carried out by filling the front end of a soda-lime glass capillary (OD: 0.9 mm, L: 70 mm) with an insulating epoxy (resin: hardener = 5:1 ratio). The construct was placed in a hot air oven at 55 °C for 10 to 15 minutes (Scheme 5. 1 a, step 1). When partial curing of the epoxy mixture occurred, a gold coated optical fiber was inserted through the rear end of the

capillary until it protruded at the front end (Scheme 5.1 a, step 2). This assembly was placed in a hot air oven at 55 °C for 2 hours to achieve complete curing of the epoxy resin. Electrical contact was established by attaching a copper wire to the gold with conductive silver epoxy. The optical fiber protruding at the front end was cut with a blade to ensure that the glass capillary, epoxy and optical fiber was exposed in the same plane. After cutting the protruding tip, an unpolished tip of the probe revealed a dragging of the gold coating from the center outwards and into the epoxy surface, as shown in Figure 5.1c. The electrode was polished using diamond polishing pads of decreasing grain sizes (9.0, 6.0 and 0.1 µm) to obtain a planar and smooth surface (Scheme 5.1 a, step 3, Figure 5.1 d). Final one-minute sonication in ethanol removed any dust residues from the electroactive surface and the optical fiber. The fabricated MOREs were then characterized visually and electrochemically and with the help of numerical simulations to assure a defined geometry and proper functionality. The aspect of a defined and controlled geometry of the working electrode is especially important when investigating complex biological samples, as diffusion processed and related changes in the electrochemical signal must be understood in order to draw conclusions about the origin of the signal. Reproducibility in terms of geometry and functionality is crucial, so that signals taken from different electrodes can be compared, if necessary.

The electrochemical characterization of MOREs was achieved by cyclic voltammetry in the presence of a known redox mediator, ferrocenemethanol ($FcCH_2OH$), to assess whether the fabricated electrodes function properly and in agreement with literature. $FcCH_2OH$ is an electroactive iron-complex that is commonly used for electrochemical and bioelectrochemical characterization studies[30,31] and exhibits well-defined oxidation and reduction potentials in aqueous solutions.[32,33] In the presence of $FcCH_2OH$, cyclic voltammograms were performed at various scan rates ranging from 30 mV s^{-1} to 150 mV s^{-1} to validate the diffusion behavior of $FcCH_2OH$ towards the electrode surface. As shown in Figure 5.1 e and f, an increase in the electrochemical current signal was observed with increasing scan rates. The shape of the cyclic voltammograms appears to be a combination of one to be expected from a macro- and a micro-electrode (Figure 5.1 e).[34] The duck-shaped voltammogram profile of a macro-electrode becomes more prominent as the scan rate increases from 80 mV s^{-1} to 150 mV s^{-1}. A linear relationship was observed between the peak current and the square root of the scan rate (Figure 5.1 f). This result was expected and confirms a diffusional behavior of $FcCH_2OH$ at the electrode and validates the

functionality of the fabricated MOREs. A shift in the redox potential during scan rate variations is attributed to the sluggish kinetics of $FcCH_2OH$ oxidation at the gold ring of the MORE.

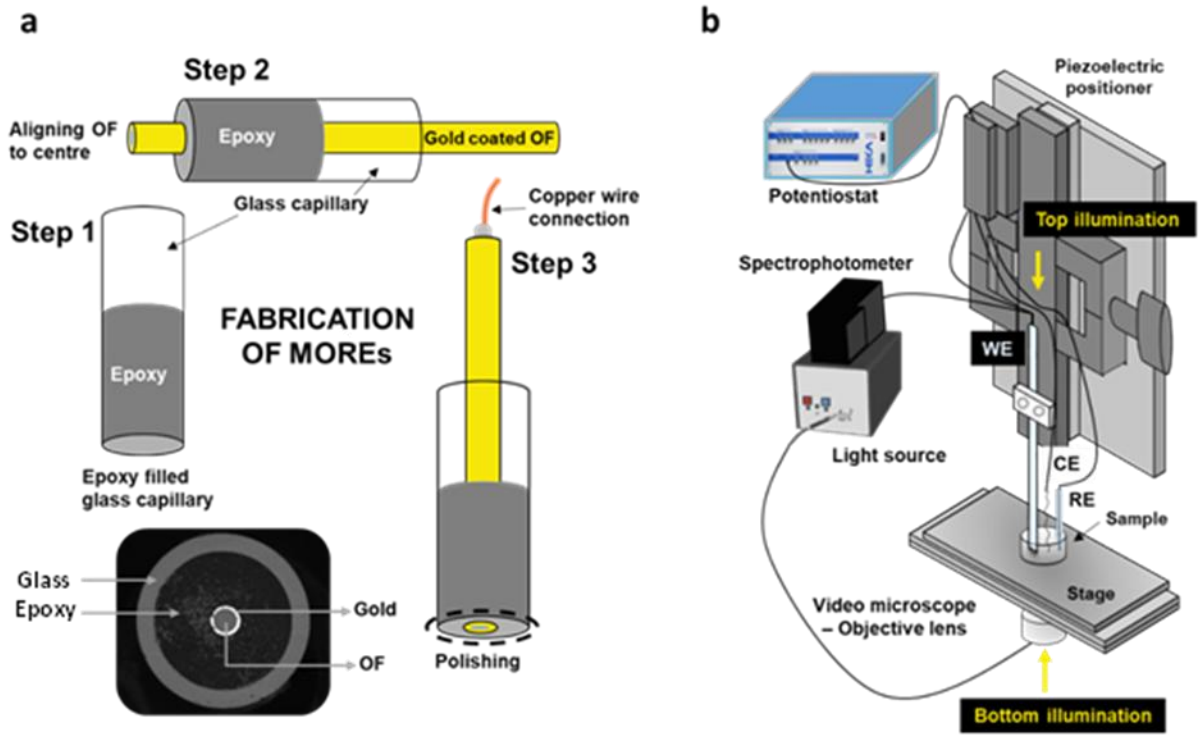

Scheme 5.1 *Schematic representation of MORE fabrication and instrumental setup. (a) Stepwise fabrication procedure of MOREs. (b) Scanning Photoelectrochemical Microscopy (SPECM) setup used in the present study.*

Although the electrode surface of the fabricated MOREs after polishing is nearly flawless, a slight offset of optical fiber and gold ring from the center can be seen in some probes (Figure 5.1 d and 5.2 a inset). To understand if this offset influences the obtained electrochemical current signal, experimental data for cyclic voltammetry in 1 mM $FcCH_2OH$ of three MOREs was compared to the theoretical current obtained by numerical simulations, based on the electrode parameters, such as electroactive material, electrode size and solution composition. Figure 5.2a and Figure A3.1 a-b shows the experimental (black curve) and the theoretical (red dotted line) current profile for three individual MOREs under the same experimental conditions. As experimental and theoretical data are in good agreement, a slight offset of the gold-coated optical fiber from the center of the

capillary excludes an effect on the electrochemical current signal, ensuring robust functionality of these sensors.

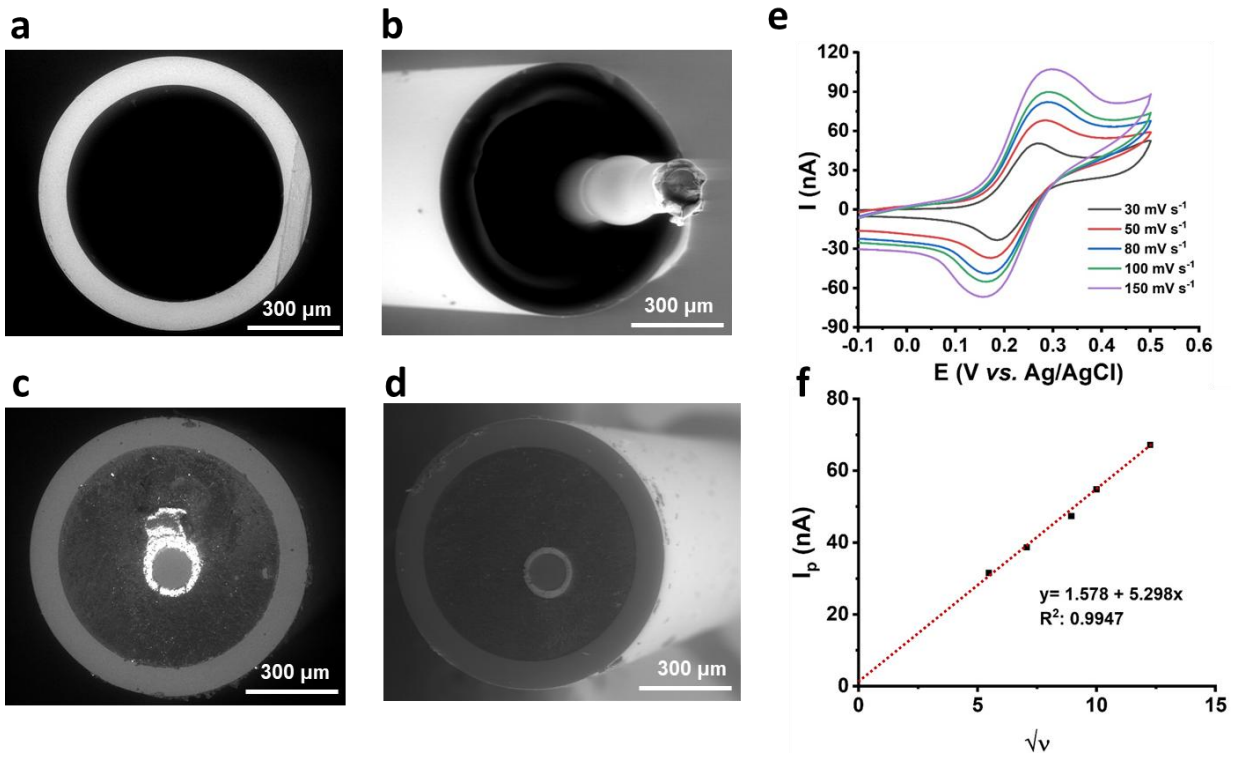

Figure 5.1 *Optical and electrochemical characterization of MOREs. SEM images of (a) an empty glass capillary, (b) the optical fiber protruding from the epoxy filled glass capillary, (c) an unpolished MORE, and (d) a polished MORE as the final product. (e-f) Electrochemical characterization of the MORE functionality. (e) Scan rate variation during cyclic voltammetry of 1 mM $FcCH_2OH$ in a 0.1 M KCl solution reveals an expected linear relationship between peak current and square root of the scan rate (f).*

Having fabricated and characterized fully electrochemically functional MOREs, their combination with sample illumination and spectroscopy is presented in the following. To irradiate a sample through the optical fiber end of a MORE was mounted into a custom-made opto-electrode holder (HEKA-Electronics/ Harvard Bioscience), which was connected to a spectrophotometer unit via an SMA fiber with a 400µm core diameter. This combination allows the guiding of light through the optical fiber at any given wavelength, as it is shown for white light in Figure A3.2.

Figure 5.2 b shows a schematic representation of the SPECM setup, including a MORE to irradiate a sample. To highlight the applicability of the fabricated probes in SPECM, the organic compound TMPD was chosen to obtain information about both spectroscopy and electrochemistry (Figure 5. 2 b-d). TMPD offers two consecutive electron transfer reactions during its oxidation. The first electron transfer step (reaction (1)) was chosen, as it is a reversible process.[35]

$$TMPD \rightleftharpoons TMPD^{+\bullet} + e^{-} \tag{5.1}$$

When applying a potential of 200 mV, TMPD is oxidized to $TMPD^{\bullet+}$, which exhibits a characteristic blue color in solution.[35–37] An absorption spectrum of a partially oxidized solution of TMPD/$TMPD^{+\bullet}$, collected through a bare optical fiber (Figure 5.2 c) shows two distinct absorption peaks at the wavelengths of 580 and 620 nm.[38] This result was reproduced when the spectrum was collected through a fabricated MORE (Figure 5.2 d), which shows a comparatively higher value of absorbance intensity, and slightly higher noise features. To minimize the noise, the tip-to-substrate distance of the MORE, and thereby its relative position to the bottom illumination focus point, was optimized by retracting the electrode from the surface while stepwise recording UV-Vis spectra of TMPD/$TMPD^{+\bullet}$. The absorption intensity reached a maximum value at 200 µm tip-to-substrate distance, decreased again from 200 to 350 µm and reached a second maximum at 650 µm, where the signal is prominent, and noise could be minimized (Figure 5.3 a and b). A discussion of this behavior is provided in Appendix 3. Further increase in the distance shows a subsequent decrease in the absorption intensity until 1050 µm, where it remains constant. To assess the capability of MOREs to monitor changes in solution composition at the immediate electrode interface, cyclic voltammetry was collected in a TMPD/$TMPD^{+\bullet}$ solution, as shown in the inset of Figure 5.3c. Based on this CV, reduction (-300 mV) and oxidation (200 mV) potentials were selected for chronoamperometric measurements. Different time intervals for electro-oxidation and reduction of TMPD were applied by holding the potential at 200 mV or -300 mV, respectively for intervals of 40 s, 90 s, and 180 s. An absorption spectrum through the fabricated MORE was recorded immediately after electro-oxidation and reduction. Figure 5.3c shows spectra obtained after 180 s of chronoamperometric measurements, where an increase in the absorption intensity was observed when the potential was held at oxidation conditions. This reflects the color change of the solution at the interface of the electrode, as more $TMPD^{+\bullet}$ is formed. At shorter durations of chronoamperometry (40 s and 90 s, Figure 5.3 d), a similar, less pronounced effect was recorded. Collecting spectro-electrochemical information simultaneously to electrochemical data has the

potential to be a game changer for live cell studies by scanning probe microscopy techniques, as it potentially allows the identification of electroactive species released from living organisms. Redox potentials and control studies are commonly used to correlate electrochemical signals with species of interest. Including information about absorption properties of analytes in solution will thereby confirm the accuracy of measurements but also detect and maybe even identify potential current-interfering species.

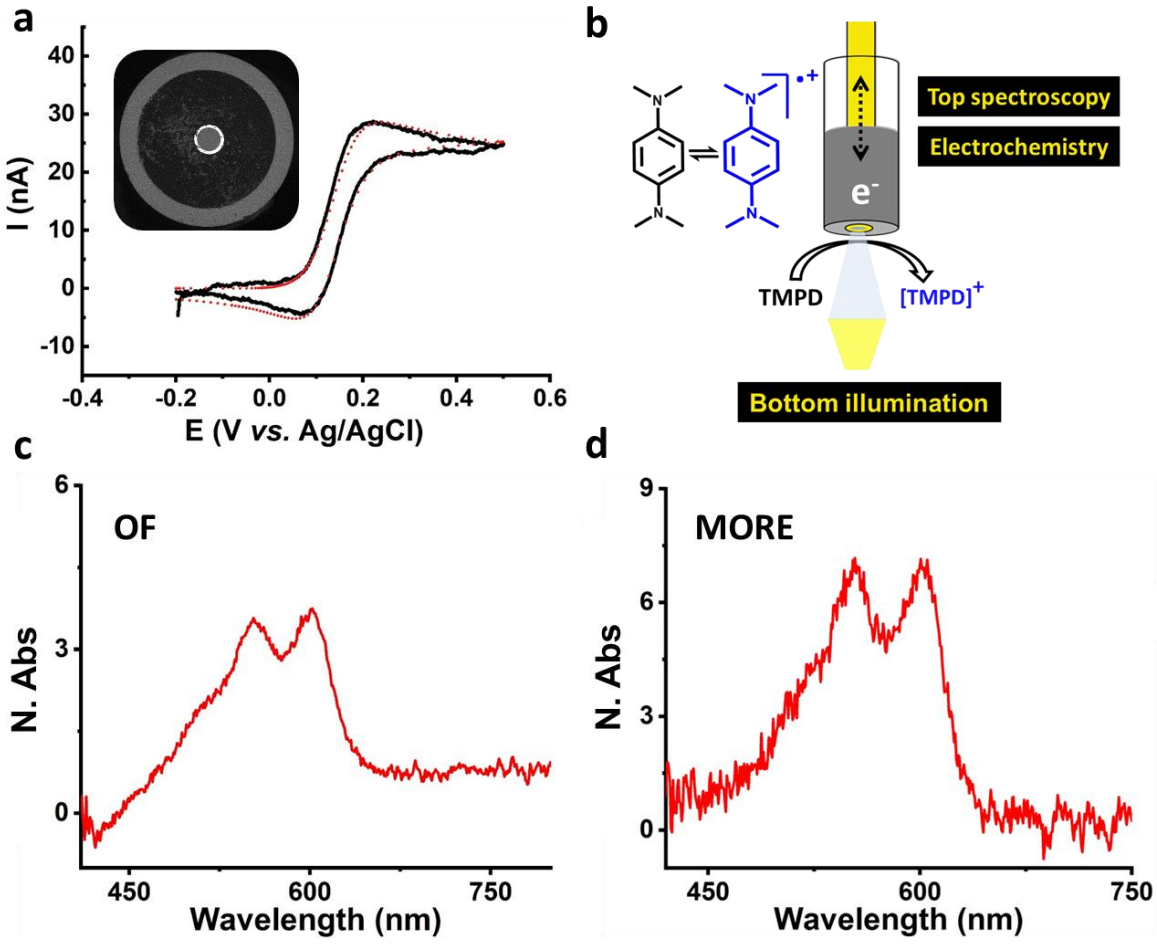

Figure 5.2 *Numerical simulation of MORE and UV-Vis spectroscopy performed through the SPECM. (a) Cyclic voltammograms recorded in 1 mM $FcCH_2OH$ in 0.1 M KCl at a scan rate of 30 mV s^{-1} are shown for an individual MORE. Experimental data (black) is in agreement with the numerical simulations (red). (b) Schematic representation of SPECM setup, including bottom illumination and spectra-tip-collection, as well as electrochemical monitoring of TMPD through a MORE. (c) UV-Vis spectra collected in 0.1 mM TMPD using an optical fiber, and (d) a MORE. Absorbance normalized to the average of the first 10 data points.*

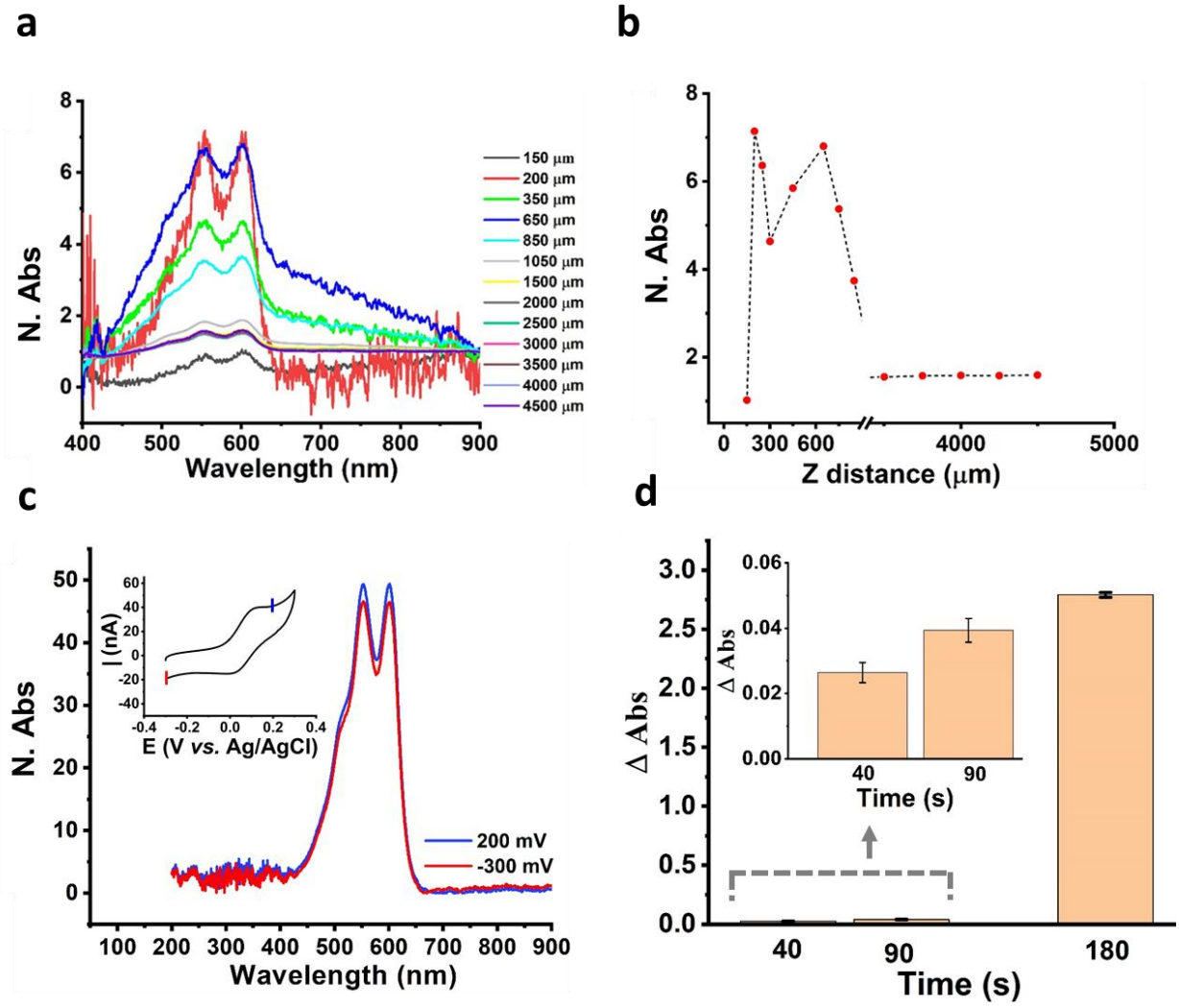

Figure 5.3 *Spectro-electrochemical investigation of TMPD. (a) UV-Vis spectra collected at various tip-substrate distances ranging from 150 to 4500 µm. (b) Absorbance signal dependence on tip-to-substrate distance. Absorbance normalized to the average of the first 10 data points. (c) Collection of UV-Vis spectra following chronoamperometry at a MORE in TMPD for 180 seconds. cyclic voltammetry of TMPD/TMPD$^{+\bullet}$(inset) (d) Absorbance difference following chronoamperometry visualized at 40, 90 and 180 seconds (inset: enlargement of times of 40 and 90 sec).*

5.4.2 Single cell SPECM measurements

Micrometer-scale MOREs, which can be reproducibly fabricated, are ideal tools to measure the electrochemical response of light sensitive substrates. Especially when investigating complex samples, such as living cells, a well-defined geometry and reproducible fabrication is crucial to be able to compare obtained signals between measurements, that often require extended time periods and polishing of the electrode surface. The applicability of the fabricated MORE to single cell measurements was explored by studying the evolution of oxygen from living biological algae cells. The overall diameter of the gold ring is approximately 150 µm, which is convenient for the analysis of large biological cells, as demonstrated below for algae *Eremosphaera viridis* (~140 µm in diameter). Algae were chosen as a model organism, because of their ability to produce oxygen in response to light.[39] *E. viridis* offers next to its light sensitivity a convenient cell size for easy localization of biological entities. Here, the electroactive area of the MORE is in line with the size of *E. viridis*. To confirm oxygen production by *E. viridis* prior to single cell analysis, linear sweep voltammograms (LSV) were collected at 50 mV s^{-1} in a cell suspension using a 3-mm gold macro-electrode as the working electrode (Figure 5.4a, inset). LSV presented in Figure 5.4a, demonstrates the response of algae after exposure to 3 hours of darkness (light off) conditions (black curve), where a significant decrease in oxygen reduction current was observed compared to signals obtained when algae were exposed to light (red curve). This experiment confirms oxygen production occurring depending on light-exposure in these organisms.

Combining cell irradiation and simultaneous current measurements, oxygen production was monitored while scanning a MORE across a single living cell of *E. viridis* (Figure 5.4b, c and d). A MORE was brought in contact with the poly-l- lysine coated plastic surface of the petri dish in close proximity to a single algae entity. Electrode positioning was realized through an approach curve next to the cell and retracted to a tip-to-substrate distance of 140 µm. During this experiment the SPECM setup was positioned in a dark-room, therefore light guided through the optical fiber can trigger oxygen production locally on the micrometer scale. Under dark conditions, the MORE was scanned across the surface where one *E. viridis* entity was located in undiluted Bold's Basal Medium, functioning as an electrolyte. A potential of -0.6 V was applied at the MORE to recognize oxygen through its electrochemical reduction. Since the reduction of oxygen is a kinetically slow phenomenon and involves two steps: initial formation of H_2O_2 by accepting 2e- and then

converting into the final product, H_2O_2 by further 2e- reduction.[40] Thus a higher negative potential enables complete reduction of O_2 to water. As shown in Figure 5.4d (red curve), a lower current is recorded when the MORE passes the cell, indicating the hindered diffusion of oxygen towards the electrode by the body of the cell, because the small amounts of oxygen produced by the algae were not able to overcompensate the hindered diffusion under these conditions. After the line scan was completed, the MORE was retracted to its initial position and light was irradiated through the optical fiber. During a second line scan under light exposure through the MORE (black curve), a pronounced reduction peak was observed, which corresponds to the electrochemical reduction of oxygen released by the living cell. The amount of generated oxygen is sufficient to overcompensate the hindering of diffusion by the body of the cell, resulting in an electrochemical increase of ~ 0.70 nA current when the electrode passes the cell. A 3D scan of a single algal cell was performed to observe the oxygen production during illumination (Fig 5.4e & f). A distinction in the current profile was observed when the MORE with the light OFF and ON scanned over a single algal cell. Overall, a reduction current was seen when the top illuminated MORE scans over the algal cell. This experiment demonstrates that MORE electrodes can be used for the local irradiation of a biological sample and simultaneous electrochemical monitoring. Though, the present work discusses the detection of oxygen released from living cells, other cell metabolites, such as glutathione or reactive oxygen species are potential future targets. The capability to irradiate a single cell by light opens the door for cell communication studies, where only one single light sensitive entity is stimulated by light exposure, and the effect on neighboring cells could be studied by SPECM. The wavelength of irradiation can thereby be selected ranging from infrared to UV-light exposure.

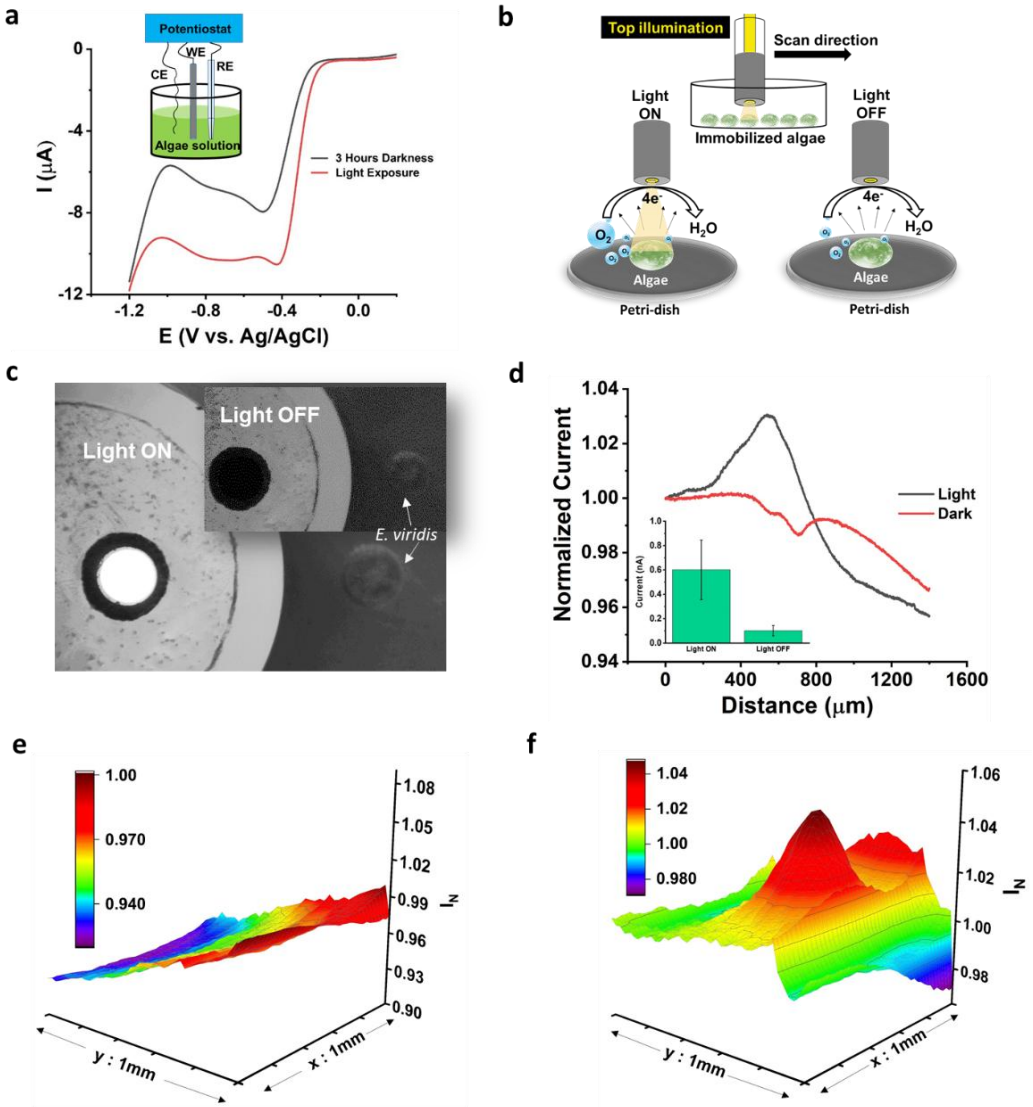

Figure 5.4 *Single cell SPECM investigation in algae. (a) Linear sweep voltammetry collected in the presence of E. viridis under light conditions and after three hours of darkness at a scan rate of 50 mVs^{-1}. (b) Schematic representation of the experimental setup used to study oxygen production in E. viridis in the presence and absence of light, (c) optical images with the MORE light ON (left) and OFF (right) at the SPECM with the targeted algal cell for SPECM measurement (d) the electrochemical current recorded during line scans across E. viridis at a scan rate of 10 μm s^{-1} when the light was switched ON (black) and OFF (red). Current difference with the MORE light switched ON and OFF (inset). Three-dimensional scan image of a single algal cell under (e) dark and (f) light at a scan range and step size of of 1000 x 1000 μm and 25 μm. Signals are plotted as normalized current by dividing all measurement points by the initial signal obtained at origin.*

5.5 Conclusions

Conclusively, we have successfully demonstrated a highly reproducible and user-friendly method of fabricating MOREs, that are able to irradiate light, collect spectroscopic information, and record electrochemical current signals. The fabricated MOREs were thoroughly characterized using visual, simulation and electrochemical methods, which confirm tip geometry and functionality. As a proof of concept, the optical spectra of TMPD was recorded and optimized in terms of tip-to-substrate distance. MOREs were able to detect oxygen production in a single living algae cell, depending on local irradiation through the MORE-integrated optical fiber. This work successfully demonstrates the potential of MOREs towards the local detection of species flux from biological entities, and future applications to living bacteria and cancer cells.

5.6 Acknowledgements

The authors thank Drs. Christian Heinemann and Frank Wang from HEKA Elektronik GmbH for the technical support on the SPECM instrument and software integrations. The authors also thank Frank Wang for helpful discussions.

5.7 References

(1) Armstrong-James, M.; Millar, J. Carbon Fibre Microelectrodes. *J Neurosci Methods* **1979**, *1* (3), 279–287. https://doi.org/10.1016/0165-0270(79)90039-6.

(2) Davies, P. W.; Brink, F. Microelectrodes for Measuring Local Oxygen Tension in Animal Tissues. *Review of Scientific Instruments* **1942**, *13* (12), 524–533. https://doi.org/10.1063/1.1769961.

(3) Kita, Justin M.; Wightman, R. M. Microelectrodes for Studying Neurobiology. *Curr Opin Chem Biol* **2008**, *12* (5), 491–496. https://doi.org/10.1016/j.cbpa.2008.06.035.Microelectrodes.

(4) Moussa, S.; Mauzeroll, J. Review—Microelectrodes: An Overview of Probe Development and Bioelectrochemistry Applications from 2013 to 2018. *J Electrochem Soc* **2019**, *166* (6), G25–G38. https://doi.org/10.1149/2.0741906jes.

(5) Stulik, K.; Amatore, C.; Holub, K.; Marecek, V.; Kutner, W. Microelectrodes.Definitions, Characterization, and Applications. *Pure and Applied Chemistry* **2000**, *72* (8), 1483–1492. https://doi.org/10.1016/S0022-0728(02)00745-3.

(6) Suter, T.; Böhni, H. Microelectrodes for Studies of Localized Corrosion Processes. *Electrochim Acta* **1998**, *43* (19–20), 2843–2849. https://doi.org/10.1016/S0013-4686(98)00025-5.

(7) Szunerits, S.; Walt, D. R. The Use of Optical Fiber Bundles Combined with Electrochemistry for Chemical Imaging. *ChemPhysChem* **2003**, *4* (2), 186–192. https://doi.org/10.1002/cphc.200390029.

(8) Montenegro, M. I. ; Queiros, M. A. ;; Daschbach, J. L. ; *Microelectrodes: Theory and Applications*; 1991. https://doi.org/10.1007/978-94-011-3210-7.

(9) Pons, S.; Fleischmann, M. The Behavior of Microelectrodes. *Anal Chem* **1987**, *59* (24), 1391A-1399A.

(10) Bae, J. H.; Nepomnyashchii, A. B.; Wang, X.; Potapenko, D. V.; Mirkin, M. V. Photo-Scanning Electrochemical Microscopy on the Nanoscale with Through-Tip Illumination. *Anal Chem* **2019**, *91* (20), 12601–12605. https://doi.org/10.1021/acs.analchem.9b03347.

(11) Conzuelo, F.; Sliozberg, K.; Gutkowski, R.; Grutzke, S.; Nebe, M.; Schuhmann, W. High-Resolution Analysis of Photoanodes for Water Splitting by Means of Scanning Photoelectrochemical Microscopy. *Anal Chem* **2017**, *89* (2), 1222–1228. https://doi.org/10.1021/acs.analchem.6b03706.

(12) Jang, J. S.; Yoon, K. Y.; Xiao, Y.; Fan, F. R. F.; Bard, A. J. Development of a Potential Fe2O3-Based Photocatalyst Thin Film for Water Oxidation by Scanning Electrochemical Microscopy: Effects of Ag-Fe2O3 Nanocomposite and Sn Doping. *Chemistry of Materials* **2009**, *21* (20), 4803–4810. https://doi.org/10.1021/cm901056c.

(13) Liu, G.; Liu, C.; Bard, A. J. Rapid Synthesis and Screening of ZnxCd1-XS YSe1-y Photocatalysts by Scanning Electrochemical Microscopy. *Journal of Physical Chemistry C* **2010**, *114* (49), 20997–21002. https://doi.org/10.1021/jp1058116.

(14) Bohni, H.; Suter, T.; Assi, F. Micro-Electrochemical Techniques for Studies of Localized Processes on Metal Surfaces in the Nanometer Range. *Surf Coat Technol* **2000**, *130*, 80–86.

(15) Garfias-Mesias, L. F.; Smyrl, W. H. High Resolution In-Situ Imaging of Reactive Heterogeneous Surfaces. *Electrochim Acta* **1999**, *44* (21), 3651–3657. https://doi.org/10.1016/S0013-4686(99)00068-7.

(16) Sosa, E.; Cabrera-Sierra, R.; Oropeza, M. T.; Hernández, F.; Casillas, N.; Tremont, R.; Cabrera, C.; González, I. Electrochemically Grown Passive Films on Carbon Steel (SAE 1018) in Alkaline Sour Medium. *Electrochim Acta* **2003**, *48* (12), 1665–1674. https://doi.org/10.1016/S0013-4686(03)00145-2.

(17) Bergner, S.; Wegener, J.; Matysik, F. M. Simultaneous Imaging and Chemical Attack of a Single Living Cell within a Confluent Cell Monolayer by Means of Scanning Electrochemical Microscopy. *Anal Chem* **2011**, *83* (1), 169–174. https://doi.org/10.1021/ac1021375.

(18) Bitziou, E.; Rudd, N. C.; Szunerits, S.; Unwin, P. R. Microelectrode Systems for the Study of Photochemical Processes in Solution. *Journal of Electroanalytical Chemistry* **2010**, *646* (1–2), 60–67. https://doi.org/10.1016/j.jelechem.2010.01.009.

(19) Santos, C. S.; Kowaltowski, A. J.; Bertotti, M. Single Cell Oxygen Mapping (SCOM) by Scanning Electrochemical Microscopy Uncovers Heterogeneous Intracellular Oxygen Consumption. *Sci Rep* **2017**, *7* (1), 2–8. https://doi.org/10.1038/s41598-017-11956-w.

(20) Thomas, N.; Singh, V.; Kuss, S. Optical Fibers in Analytical Electrochemistry: Recent Developments in Probe Design and Applications. *TrAC Trends in Analytical Chemistry* **2021**, *136*, 116–196. https://doi.org/10.1016/j.trac.2021.116196.

(21) Weber, A.; Kuhn, L. S.; Weber, S. G. Microring Electrode/Optical Waveguide: Electrochemical Characterization and Application to Electrogenerated Chemiluminescence. *Anal Chem* **1990**, *62* (15), 1631–1636. https://doi.org/10.1021/ac00214a019.

(22) Andrieux, F. P. L.; Boxall, C.; O'Hare, D. The Micro-Optical Ring Electrode Part 2: Theory for the Transport Limited, Steady-State Photocurrent. *Journal of Electroanalytical Chemistry* **2006**, *589* (2), 177–186. https://doi.org/10.1016/j.jelechem.2005.12.002.

(23) Andrieux, F. P. L.; Boxall, C.; O'Hare, D. The Micro-Optical Ring Electrode. 3: Transient Photocurrent Studies of Photophysical-Electrochemical and Photophysical-Chemical-Electrochemical Systems. *Journal of Physical Chemistry B* **2006**, *110* (32), 16148–16156. https://doi.org/10.1021/jp0622785.

(24) Pennarun, G. I.; Boxalla, C.; O'Hare, D. Micro-Optical Ring Electrode: Development of a Novel Electrode for Photoelectrochemistry. *Analyst* **1996**, *121* (12), 1779–1788. https://doi.org/10.1039/an9962101779.

(25) Lee, Y.; Bard, A. J. Fabrication and Characterization of Probes for Combined Scanning Electrochemical/Optical Microscopy Experiments. *Anal Chem* **2002**, *74* (15), 3626–3633. https://doi.org/10.1021/ac015705d.

(26) Maruyama, K.; Ohkawa, H.; Ogawa, S.; Ueda, A.; Niwa, O.; Suzuki, K. Fabrication and Characterization of a Nanometer-Sized Optical Fiber Electrode Based on Selective Chemical Etching for Scanning Electrochemical/ Optical Microscopy. *Anal Chem* **2006**, *78* (6), 1904–1912. https://doi.org/10.1021/ac0502549.

(27) Xiong, H.; Guo, J.; Kurihara, K.; Amemiya, S. Fabrication and Characterization of Conical Microelectrode Probes Templated by Selectively Etched Optical Fibers for Scanning Electrochemical Microscopy. *Electrochem commun* **2004**, *6* (6), 615–620. https://doi.org/10.1016/j.elecom.2004.04.016.

(28) Wu, S.; Su, B. A Simple Approach for Fabrication of Microring Electrodes. *Journal of Electroanalytical Chemistry* **2013**, *694*, 12–16. https://doi.org/10.1016/j.jelechem.2013.01.018.

(29) Svir, I.; Oleinick, A.; Yunus, K.; Fisher, A. C.; Wadhawan, J. D.; Davies, T. J.; Compton, R. G. Theoretical and Experimental Study of the ECE Mechanism at Microring Electrodes. *Journal of Electroanalytical Chemistry* **2005**, *578* (2), 289–299. https://doi.org/10.1016/j.jelechem.2005.01.011.

(30) Kuss, S.; Polcari, D.; Geissler, M.; Brassard, D.; Mauzeroll, J. Assessment of Multidrug Resistance on Cell Coculture Patterns Using Scanning Electrochemical Microscopy. *Proc Natl Acad Sci U S A* **2013**, *110* (23), 9249–9254. https://doi.org/10.1073/pnas.1214809110.

(31) Kuss, S.; Cornut, R.; Beaulieu, I.; Mezour, M. A.; Annabi, B.; Mauzeroll, J. Assessing Multidrug Resistance Protein 1-Mediated Function in Cancer Cell Multidrug Resistance by Scanning Electrochemical Microscopy and Flow Cytometry. *Bioelectrochemistry* **2011**, *82* (1), 29–37. https://doi.org/10.1016/j.bioelechem.2011.04.008.

(32) Cannes, C.; Kanoufi, F.; Bard, A. J. Cyclic Voltammetry and Scanning Electrochemical Microscopy of Ferrocenemethanol at Monolayer and Bilayer-Modified Gold Electrodes. *Journal of Electroanalytical Chemistry* **2003**, *547* (1), 83–91. https://doi.org/10.1016/S0022-0728(03)00192-X.

(33) Lovelock, K. R. J.; Ejigu, A.; Loh, S. F.; Men, S.; Licence, P.; Walsh, D. A. On the Diffusion of Ferrocenemethanol in Room-Temperature Ionic Liquids: An Electrochemical Study. *Physical Chemistry Chemical Physics* **2011**, *13* (21), 10155–10164. https://doi.org/10.1039/c1cp20392d.

(34) Brookes, B. A.; Gavaghan, D. J.; Compton, R. G. Microring Electrodes: A Computational Study of Transport-Limited Processes. **2002**, 4886–4896.

(35) Moressi, M. B.; Zón, M. A.; Fernández, H. Electrochemical and Spectroscopic Studies of the TMPD/TMPD.+ Redox Couple in Non-Aqueous Binary Solvent Mixtures by Using Ultramicroelectrodes. Role of the Preferential Solvation Phenomenon. *Electrochim Acta* **1997**, *42* (2), 303–314. https://doi.org/10.1016/0013-4686(96)00186-7.

(36) Kuss, S.; Compton, R. G. Electrocatalytic Detection of Ascorbic Acid Using N,N,N',N'-Tetramethyl-Para-Phenylene-Diamine (TMPD) Mediated Oxidation at Unmodified Gold Electrodes; Reaction Mechanism and Analytical Application. *Electrochim Acta* **2017**, *242*, 19–24. https://doi.org/10.1016/j.electacta.2017.05.003.

(37) Kuss, S.; Tanner, E. E. L.; Ordovas-Montanes, M.; Compton, R. G. Electrochemical Recognition and Quantification of Cytochrome c Expression in: Bacillus Subtilis and

Aerobe/Anaerobe Escherichia Coli Using N, N, N ′, N ′-Tetramethyl- Para -Phenylene-Diamine (TMPD). *Chem Sci* **2017**, *8* (11), 7682–7688. https://doi.org/10.1039/c7sc03498a.

(38) Kao, S. Y.; Kawahara, Y.; Nakatsuji, S.; Ho, K. C. Achieving a Large Contrast, Low Driving Voltage, and High Stability Electrochromic Device with a Viologen Chromophore. *J Mater Chem C Mater* **2015**, *3* (14), 3266–3272. https://doi.org/10.1039/c5tc00456j.

(39) Shuler, R. L.; Affens, W. A. Effect of Light Intensity and Thickness of Culture Solution on Oxygen Production by Algae. *Appl Microbiol* **1970**, *19* (1), 76–86. https://doi.org/10.1128/am.19.1.76-86.1970.

(40) Singh, V.; Adhikary, S. D.; Tiwari, A.; Mandal, D.; Nagaiah, T. C. Sustainable Non-Noble Metal Bifunctional Catalyst for Oxygen-Depolarized Cathode and Cl2 Evolution in HCl Electrolysis. *Chemistry of Materials* **2017**, *29* (10), 4253–4264.

Chapter 6

SECM and SPECM applied to skin cells

Building on the conclusions of chapters 2 and 3 on experimental parameters, along with the feasibility of performing SPECM on living cells as demonstrated in chapter 5, the present chapter focuses on applying the determined ideal experimental conditions during SPECM measurements of human skin cell lines. This chapter specifically investigates Human Epidermal Keratinocytes (HEKa), Human Epidermal Melanocytes (HEMa), and Melanoma (SK-MEL-28) cells. These cell lines were selected because of their sensitivity to external stimuli, such as UV radiation, making them suitable candidates for SPECM analysis. The primary objective of the research is to investigate differences in reactive oxygen species (ROS) production among these three cell lines. Additionally, this study explores melanin production in melanoma cells electrochemically, both in the presence and absence of localized UV radiation, Overall, this work demonstrates a strong potential for the applications of SPECM to study mammalian cells.

6.1 Abstract

Melanoma is one of the deadliest forms of skin cancer. Over the years, various detection methodologies and targeted therapies have been developed.[1] However, fast and real- time detection of skin cancer remains an area of ongoing research.[2] Although many groups have developed biosensors specific to various protein and biomarker pathways, the accuracy of these instruments still needs to be optimized to reduce false positives.[2,3] This study focuses on using scanning electrochemical microscopy (SECM) for examining reactive oxygen species (ROS) production in Human Epidermal Keratinocytes (HEKa), Human Epidermal Melanocyte (HEMa), and melanoma cell line (SK-MEL-28). Furthermore, melanin production in SK-MEL-28 is analyzed electrochemically, both in the absence and presence of localized UV radiation, using scanning photoelectrochemical microscopy (SPECM) equipped with a micro-optical ring electrode (MORE). This research aims to demonstrate the potential benefits of developing optical sensors towards skin cancer detection.

6.2 Introduction

Among the different types of skin cancers (Basal Cell Carcinoma (BCC), Squamous Cell Carcinoma (SCC), and Melanoma), melanoma, being metastatic, is the most aggressive and dangerous form of cancer.[4,5] The developments in the understanding, detection, and treatment of skin cancer date back to the 1800s.[6] Advancements in skin cancer research include the development of commercial digital photographic imaging systems such as Mole Max, Vectra, Dermoscan, DermEngine, FotoFinder etc.[5] Several specialized imaging technologies, such as Raman spectroscopy,[7–9] electrical impedance spectroscopy,[10–12] multispectral imaging,[13,14] ultrasound,[15,16] fluorescence,[17] and confocal microscopy,[18] have also emerged to aid in the screening of skin cancers. Further, AI machine learning and convolutional neural networks have been incorporated to improve the effectiveness of skin cancer classification.[5]

Although significant progress has been made in the diagnosis and detection of skin cancer over the past four decades, biopsy remains the gold standard.[5] At least 20 biopsies are typically required for a definitive skin cancer diagnosis.[19,20] In addition to biopsies, physicians use non- and semi-

invasive techniques such imaging and spectroscopy, as mentioned above. Another non-invasive technique is tape stripping,[20] which leads to genetic and protein analyses of skin cells, though it can be time consuming in terms of data analyses. Studies have shown that non-invasive methods for detecting skin cancer include point-of-care devices like electrochemical biosensors.[21–25] Electrochemical techniques such as voltammetry, amperometry, and impedance are employed by these biosensors which are highly specific and efficient, leading to increased accuracy and fewer false positives compared to biopsies. These biosensors can aid in early detection and may also serve as a precursor to biopsy for confirmed positives.[20]

Here, an advanced electrochemical technique known as Scanning Photoelectrochemical Microscopy (SPECM) is used to investigate skin cancer. SPECM offers increased specificity due to its multifunctional ability to perform simultaneous electrochemistry, spectroscopy, and radiation. The characteristic feature of SPECM is its specialized optical probes. This study uses a Micro-Optical Ring Electrode (MORE) which consists of an optical fiber center with a gold coating insulated with epoxy in a glass capillary. The introduction of SPECM dates back to 1995, when the research group of William H. Smyrl, combined SECM and Photoelectrochemical Microscopy (PEM) to form SPECM integrating a gold coated OF as the probe.[26,27] This led to its widespread use for understanding various light sensitive semiconductor materials and solar cells,[28–31] becoming popular in materials sciences and energy applications. For living cell applications, a ring optical electrode is more advantageous than a disk optical electrode, as the OF center allows for not only localized irradiation but also spectroscopy and fluorescence measurements. For instance, Takahashi *et al* demonstrated the measurement of electrochemical and fluorescent signals from transfected HeLa cells through a Pt-coated OF ring electrode in SPECM.[32] While the ring OF electrodes fabricated by Takahashi provided high resolution imaging at nanoscale, the reproducibility and ease of fabrication of these probes were challenging. As demonstrated in chapter 5, we developed a cost efficient and user-friendly fabrication of MORE which was integrated into SPECM to study the oxygen consumption in light-sensitive algal cells.[33]

Building on this proof-of-concept study, the applicability of SPECM is extended to Human Epidermal Keratinocytes (HEKa), Human Epidermal Melanocytes (HEMa), and melanoma (SK-MEL) cells, all of which are sensitive to external stimuli such as UV irradiation. This research

aims to understand the reactive oxygen species (ROS) production in cancerous melanoma versus non-cancerous keratinocytes and melanocytes. We also examine the difference in melanin production in the presence and absence of UV light.

6.3 Experimental Methods

6.3.1 Cell Culture

Human Epidermal Keratinocytes (HEKa, PCS-200-011), Human Epidermal Melanocytes (HEMa, PCS-200-013) and malignant melanoma cells SK-MEL-28 (HTB-72) were obtained from ATCC, USA. Dermal Cell Basal Medium (PCS-200-300) supplemented with keratinocyte growth kit (PCS-200-040) and melanocyte growth kit (PCS-200-042) obtained from ATCC, were used for culturing HEKa and HEMa, respectively. The media were also supplemented with phenol red (PCS-999-001) and Penicillin-Streptomycin-Amphotericin B solution (PCS-999-002), purchased from ATCC, USA. Eagle's Minimum Essential Medium (EMEM, 30-2003) obtained from ATCC, USA, was supplemented with with 10% v/v heat-inactivated fetal bovine serum (Gibco/Invitrogen, ON, Canada) and was used as the culture medium for SK-MEL-28 cells. T-75 flasks (Fisher Scientific, USA) were used for culturing HEKa, HEMa, and SK-MEL-28 cells at 37°C and 5% CO_2. On reaching 70-90% confluency, Dulbecco's Phosphate-Buffered Saline (D-PBS) 1X from ATCC, USA, was used to wash cells. Trypsin-EDTA (0.05%) solution (Gibco, USA) was used for cell detachment and harvesting of SK-MEL-28 cells, whereas Trypsin-EDTA for Primary cells (PCS-999-003) and Trypsin Neutralizing Solution (PCS-999-004) from ATCC, USA, were used for detaching and harvesting HEKa and HEMa. The cells were then seeded onto 35 mm petri dishes (Thermo Fisher) and incubated for approximately 24 hours at 37 °C and 5% CO_2 prior to SECM/ SPECM/ Fluorescence experiments.

6.3.2 Fluorescence Microscopy

Fluorescence images were obtained using the EVOS FL Auto Imaging System (Thermo Fisher Scientific). ROS detection through fluorescence was performed using the Image-iT LIVE Green Reactive Oxygen Species Detection Kit (I36007, Molecular Probes) from Thermo Fisher Scientific. The assay employed 5-(and-6)-carboxy-2′,7′-dichlorodihydrofluorescein diacetate

(carboxy-H_2DCFDA), a proven green-fluorescent dye, to detect ROS in live cells (Ex/Em: 495/529 nm). After washing the cells with 1X PBS, an appropriate volume of 25µM carboxy-H_2DCFDA solution was added to serum and phenol red free medium in the petri dish containing adherent cells. The petri dish was then incubated at 37°C for 40 minutes followed by fluorescence imaging.

6.3.3 Electrochemical Measurements

SECM measurements were conducted on an ElPROScan-3 workstation integrated with POTMASTER software and a 10-µm Au UME (HEKA Elektronik GmbH, Harvard Bioscience, Inc.). The SPECM experiments were conducted with the same setup, but with an in-house fabricated MORE. A Pt wire was used as the counter electrode and an Ag/AgCl electrode was used as a pseudo reference electrode during line scans. This setup was integrated with a CL-100 Biopolar Temperature Controller acquired from Warner Instruments. The light source consisted of a ring of white light-emitting diodes (LEDs), which was positioned above the sample stage. The UV light source was the deuterium lamp of Ocean Optics DH-2000 UV-Vis-NIR light source. For cell scanning, 1 mM hexaammineruthenium (III) chloride ($[Ru(NH_3)_6]Cl_3$, RuHex, Sigma-Aldrich) in serum-free medium was used to scan the cells at -0.4 V. After the initial scan, the cells were washed three times with PBS, followed by ROS or melanin SECM/SPECM imaging in PBS.

6.4 Results and Discussion

This section investigates the ROS production in HEKa, HEMa, and SK-MEL-28. Followed by the impact of localized radiation on melanin synthesis in melanoma.

6.4.1 ROS detection in Skin Cells

Reactive oxygen species (ROS) are highly reactive molecules found in trace amounts in the human body.[34,35] ROS are radicals, ions or molecules having single unpaired electron in the outermost electron shell. Some examples of ROS include superoxide ($O_2•^-$), hydroxy radical ($^•OH$), singlet oxygen (O_2), and hydrogen peroxide (H_2O_2). Among these, H_2O_2, •OH, and $O_2•^-$ are the most widely explored ROS in literature in the context of tumor progression.[34,35] H_2O_2, a small and stable ROS molecule, is produced by cells both intracellularly and extracellularly, and serves as an indicator of the pathological or physiological status of the cell.[36]

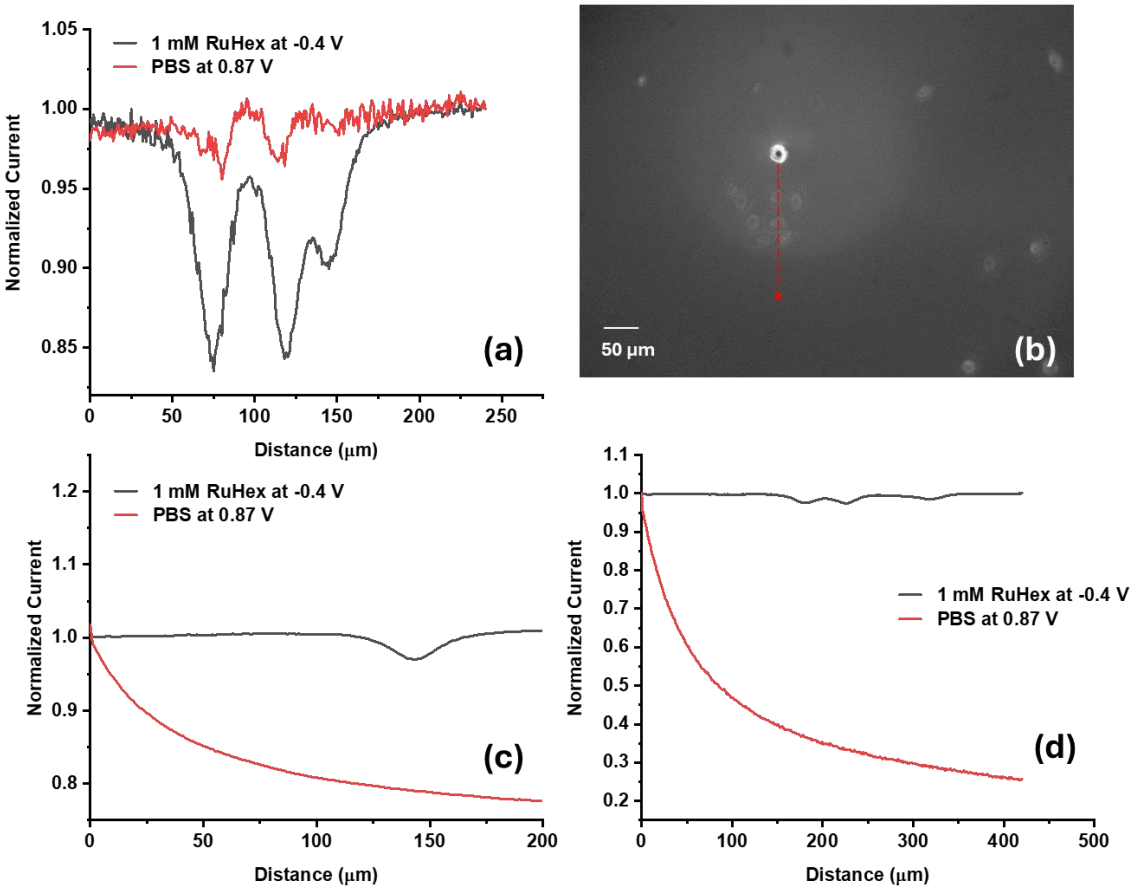

Figure 6.1 *H_2O_2 detection in skin cells. SECM scans across (a) HEKa and the corresponding (b) optical micrograph (c) HEMa (d) SK-MEL-28 at -0.4 V, 10 µm/s in 1 mM RuHex (black) and at 0.87 V, 10 µm/s in PBS (red).*

H_2O_2 being redox active, can undergo oxidation at +0.87 V *vs.* Ag/AgCl at neutral pH.[37] H_2O_2 also has a lifetime on the order of seconds to minutes *in-vivo*, making it favorable for electrochemical stimulation and detection.[38] A 10 µm Au UME biased at 0.87 V was used in SECM feedback mode to scan over HEKa, HEMa and SK-MEL28 cells. An approach curve above plastic was performed prior to cell studies in 1 mM RuHex to position the electrode. Figure 6.1 a, c, and d (in black) shows line scans over HEKa, HEMa, and SK-MEL-28, respectively at -0.4 V. This was followed by aspirating the RuHex media, washing the cells with PBS and placing them in their respective serum free media. Cell scans with RuHex resulted in a decrease in current as the electrode scanned over cells because RuHex does not interacting with the cells, and the measured current therefore pertains to the topography of the cell. When the cells were scanned at a potential of 0.87 V, a less

intense decrease, or even a slight increase in the current was observed for HEKa (Figure 6.1 a, red) cells compared to HEMa (Figure 6.1 c, red) and SK-MEL-28 (Figure 6.1 d, red), where a signal was not observed. This enhanced current signal corresponds to the presence of H_2O_2. These results agree with the literature where the H_2O_2 levels in HEKa cells are higher than melanocytes. Keratinocytes are found on the outermost layer of the skin and are biochemically wired to produce more ROS.[39] Although some studies report cancer cells are known to produce higher levels of ROS, this could not be observed in the melanoma cell lines.[40] This can be attributed to the fact that melanin, which is produced by both melanocyte and melanoma acts as ROS scavenger.[41–44] A qualitative measurement of ROS was also obtained by fluorescence microscopy as shown in Figure 6.2. Higher carboxy H_2DCFDA intensity was observed with HEKa cells (figure 6.2 a) compared to HEMa (Figure 6.2 b) or SKMEL-28 (Figure 6,2 c), which validates the electrochemical data. This study demonstrates the ability of SECM to track the presence of H_2O_2 in living cells.

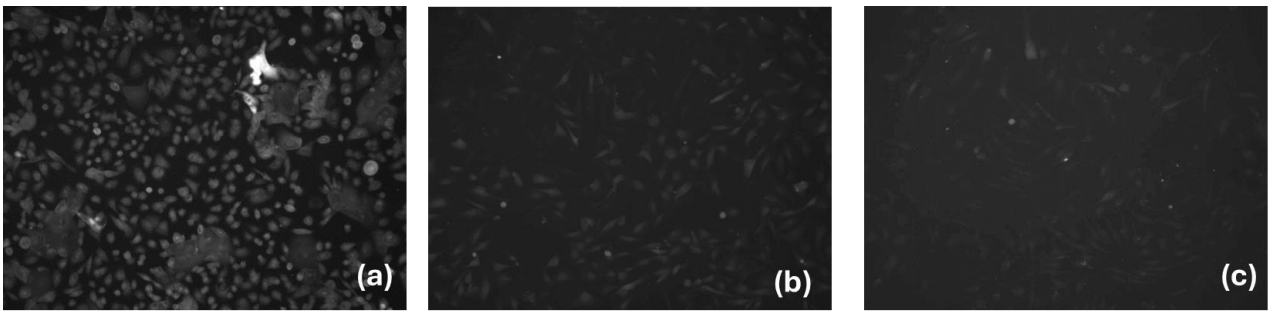

Fig 6.2 *Fluorescence microscopy images for ROS detection. (a) HEKa, (b) HEMa, and (c) SK-MEL-28.*

6.4.2 Melanin Detection- Melanocytes *vs.* Melanoma

Melanin is a naturally occurring macromolecule responsible for pigmentation in animals, plants, fungi and bacteria.[45] It is long known to give pigmentation to skin, hair, and the iris in mammalian cells.[45] In addition to this, melanin is also known for its photoprotective properties against harmful UV radiation and melanoma metastasis.[46] Melanoma is known to produce increased amounts of melanin compared to normal melanocytes through melanogenesis.[47] Melanin can be measured at a negative potential of -0.8 V owing to the presence of Na^+ and K^+ cations in the serum free media solution.[48] Initially, the cell position was determined using 1 mM RuHex as shown in Figure 6.3 a and c, (black) for HEMa and SK-MEL-28 cells, respectively. Optical micrographs (Figure 6.3 b

and d) present electrode and cell locations as well as scan directions. A less negative and an increase in current was observed when the cells were scanned at the potential of -0.8 V, confirming the oxidation of melanin produced by HEMa Figure 6.3 a, red) and SK-MEL-28 (Figure 6.3 c, red). The melanin production in SK-MEL-28 was analyzed in the presence and absence of UV radiation (Figure 6.3 e). For this purpose, UVA radiation in the range of 320-400 nm was chosen, as UVA exposure can trigger both immediate pigment darkening (IPD) and persistent pigment darkening (PPD), particularly in darker skin.[46] Additionally, UVA is known to cause pigmentation through the oxidation or redistribution of existing melanin, [46] which is relevant given that melanoma produces melanin in excess.[49] Experimental analysis showed that, in the absence of UV radiation (Figure 6.3 e, black) a more prominent reduction peak is observed indicating the topography of the cells scanned. In contrast, in the presence of UV radiation through the OF of a MORE, an increase in current signal was observed (Figure 6.3 e, red), indicating the oxidation of the melanin released by cancerous SK-MEL-28.

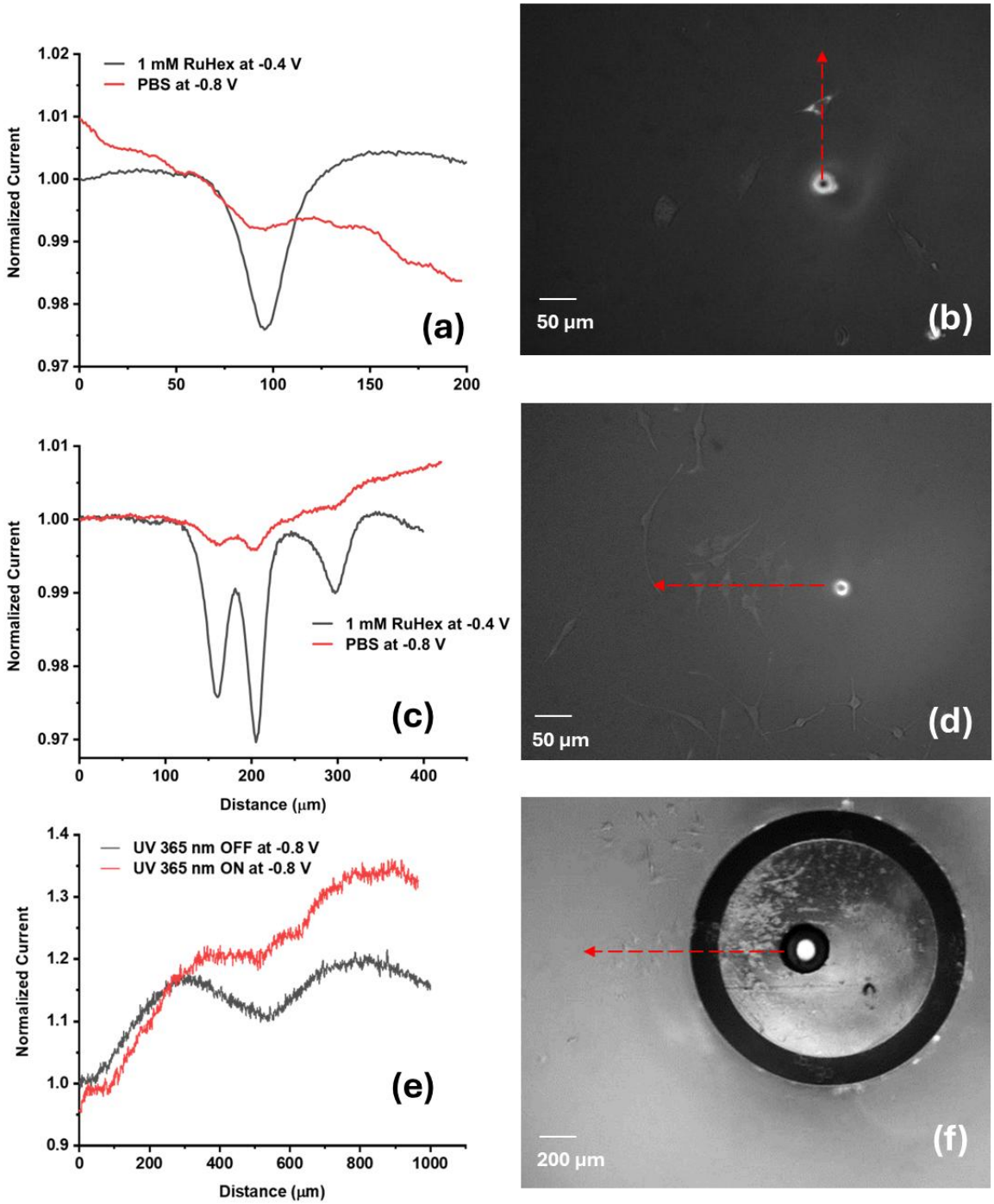

Fig 6.3 *Electrochemical detection of melanin in (a) HEMa, (c) and SK-MEL-28 using a Au UME in 1 mM RuHex at -0.4 V, 10 µm/s (black) and in PBS at -0.8 V, 10 µm/s (red). (b) and (d) are the corresponding optical images respectively. (e) SK-MEL-28 in the absence (black) and presence (red) of UV with MORE biased at -0.8 V, (f) the corresponding optical micrograph.*

6.5 Conclusion

This work provides valuable insight into how an electrochemical technique like SPECM can be used to investigate the impact of localized irradiation on electrochemical current signals. It was confirmed that ROS production in adherent cells, such as keratinocytes, is significantly higher than in cancerous melanoma cells. Furthermore, it was observed that UV irradiation affects melanin production in melanoma cells. One potential direction for future research is the quantification of the ROS and melanin produced by cells under varying conditions.

A current limitation of this study is the size of the Micro-Optical Ring Electrode (MORE), which requires scanning groups of cells rather than individual cells. This introduces variability, as it may not be possible to scan every cell in the group or provide uniform irradiation across all cells. Despite this limitation, this research lays the groundwork for applying SPECM to study mammalian cell lines. Overcoming these challenges will be crucial for enabling more precise and quantifiable experiments in the future.

6.6 References

(1) Chatzilakou, E.; Hu, Y.; Jiang, N.; Yetisen, A. K. Biosensors for Melanoma Skin Cancer Diagnostics. *Biosens Bioelectron* **2024**, *250*, 116045. https://doi.org/10.1016/j.bios.2024.116045.

(2) Galarneau, A. Biosensor Technology for Melanoma Biomarker Detection. *J Biosens Bioelectron* **2022**. https://doi.org/10.4172/2155-6210.2022.13.337.

(3) Jayanthi, V. S. P. K. S. A.; Das, A. B.; Saxena, U. Recent Advances in Biosensor Development for the Detection of Cancer Biomarkers. *Biosens Bioelectron* **2017**, *91*, 15–23. https://doi.org/10.1016/j.bios.2016.12.014.

(4) Hasan, N.; Nadaf, A.; Imran, M.; Jiba, U.; Sheikh, A.; Almalki, W. H.; Almujri, S. S.; Mohammed, Y. H.; Kesharwani, P.; Ahmad, F. J. Skin Cancer: Understanding the Journey of Transformation from Conventional to Advanced Treatment Approaches. *Molecular*

Cancer. BioMed Central Ltd December 1, 2023. https://doi.org/10.1186/s12943-023-01854-3.

(5) Chatzilakou, E.; Hu, Y.; Jiang, N.; Yetisen, A. K. Biosensors for Melanoma Skin Cancer Diagnostics. *Biosensors and Bioelectronics*. Elsevier Ltd April 15, 2024. https://doi.org/10.1016/j.bios.2024.116045.

(6) The History of Skin Cancer. *J Am Acad Dermatol* **2015**, *72* (5), AB27. https://doi.org/10.1016/j.jaad.2015.02.121.

(7) Zhao, J.; Zeng, H.; Kalia, S.; Lui, H. Using Raman Spectroscopy to Detect and Diagnose Skin Cancer In Vivo. *Dermatol Clin* **2017**, *35* (4), 495–504. https://doi.org/10.1016/j.det.2017.06.010.

(8) Lui, H.; Zhao, J.; McLean, D.; Zeng, H. Real-Time Raman Spectroscopy for In Vivo Skin Cancer Diagnosis. *Cancer Res* **2012**, *72* (10), 2491–2500. https://doi.org/10.1158/0008-5472.CAN-11-4061.

(9) Bratchenko, I. A.; Bratchenko, L. A.; Moryatov, A. A.; Khristoforova, Y. A.; Artemyev, D. N.; Myakinin, O. O.; Orlov, A. E.; Kozlov, S. V.; Zakharov, V. P. In Vivo Diagnosis of Skin Cancer with a Portable Raman Spectroscopic Device. *Exp Dermatol* **2021**, *30* (5), 652–663. https://doi.org/10.1111/exd.14301.

(10) Braun, R. P.; Mangana, J.; Goldinger, S.; French, L.; Dummer, R.; Marghoob, A. A. Electrical Impedance Spectroscopy in Skin Cancer Diagnosis. *Dermatol Clin* **2017**, *35* (4), 489–493. https://doi.org/10.1016/j.det.2017.06.009.

(11) Zhang, F.; Jin, T.; Hu, Q.; He, P. Distinguishing Skin Cancer Cells and Normal Cells Using Electrical Impedance Spectroscopy. *Journal of Electroanalytical Chemistry* **2018**, *823*, 531–536. https://doi.org/10.1016/j.jelechem.2018.06.021.

(12) Sarac, E.; Meiwes, A.; Eigentler, T.; Forchhammer, S.; Kofler, L.; Häfner, H.; Garbe, C. Diagnostic Accuracy of Electrical Impedance Spectroscopy in Non-Melanoma Skin Cancer. *Acta Dermato Venereologica* **2020**, *100* (18), adv00328. https://doi.org/10.2340/00015555-3689.

(13) Kuzmina, I.; Diebele, I.; Jakovels, D.; Spigulis, J.; Valeine, L.; Kapostinsh, J.; Berzina, A. Towards Noncontact Skin Melanoma Selection by Multispectral Imaging Analysis. *J Biomed Opt* **2011**, *16* (6), 060502. https://doi.org/10.1117/1.3584846.

(14) Farina, B.; Bartoli, C.; Bono, A.; Colombo, A.; Lualdi, M.; Tragni, G.; Marchesini, R.; Farina, B.; Bartoli, C.; Bono, A.; Colombo, A.; Lualdi, M.; Tragni, G. Multispectral Imaging Approach in the Diagnosis of Cutaneous Melanoma: Potentiality and Limits. *Phys Med Biol* **2000**, *45* (5), 1243–1254. https://doi.org/10.1088/0031-9155/45/5/312.

(15) Kia, S.; Setayeshi, S.; Pouladian, M.; Ardehali, S. H. Early Diagnosis of Skin Cancer by Ultrasound Frequency Analysis. *J Appl Clin Med Phys* **2019**, *20* (11), 153–168. https://doi.org/10.1002/acm2.12671.

(16) Catalano, O.; Roldán, F. A.; Varelli, C.; Bard, R.; Corvino, A.; Wortsman, X. Skin Cancer: Findings and Role of High-Resolution Ultrasound. *J Ultrasound* **2019**, *22* (4), 423–431. https://doi.org/10.1007/s40477-019-00379-0.

(17) Liu, L.; Yang, Q.; Zhang, M.; Wu, Z.; Xue, P. Fluorescence Lifetime Imaging Microscopy and Its Applications in Skin Cancer Diagnosis. *J Innov Opt Health Sci* **2019**, *12* (05). https://doi.org/10.1142/S1793545819300040.

(18) Ahlgrimm-Siess, V.; Laimer, M.; Rabinovitz, H. S.; Oliviero, M.; Hofmann-Wellenhof, R.; Marghoob, A. A.; Scope, A. Confocal Microscopy in Skin Cancer. *Curr Dermatol Rep* **2018**, *7* (2), 105–118. https://doi.org/10.1007/s13671-018-0218-9.

(19) Rivers, J. K.; Copley, M. R.; Svoboda, R.; Rigel, D. S. Non-Invasive Gene Expression Testing to Rule Out Melanoma. *Skin Therapy Lett* **2018**, *23* (5), 1–4.

(20) Darvishi, S.; Pick, H.; Lin, T. E.; Zhu, Y.; Li, X.; Ho, P. C.; Girault, H. H.; Lesch, A. Tape-Stripping Electrochemical Detection of Melanoma. *Anal Chem* **2019**, *91* (20), 12900–12908. https://doi.org/10.1021/acs.analchem.9b02819.

(21) Macovei, D.-G.; Irimes, M.-B.; Hosu, O.; Cristea, C.; Tertis, M. Point-of-Care Electrochemical Testing of Biomarkers Involved in Inflammatory and Inflammatory-Associated Medical Conditions. *Anal Bioanal Chem* **2023**, *415* (6), 1033–1063. https://doi.org/10.1007/s00216-022-04320-z.

(22) Pour, S. R. S.; Calabria, D.; Emamiamin, A.; Lazzarini, E.; Pace, A.; Guardigli, M.; Zangheri, M.; Mirasoli, M. Electrochemical vs. Optical Biosensors for Point-of-Care Applications: A Critical Review. *Chemosensors* **2023**, *11* (10), 546. https://doi.org/10.3390/chemosensors11100546.

(23) Hasan, M. R.; Ahommed, M. S.; Daizy, M.; Bacchu, M. S.; Ali, M. R.; Al-Mamun, M. R.; Saad Aly, M. A.; Khan, M. Z. H.; Hossain, S. I. Recent Development in Electrochemical Biosensors for Cancer Biomarkers Detection. *Biosens Bioelectron X* **2021**, *8*, 100075. https://doi.org/10.1016/j.biosx.2021.100075.

(24) Fu, L.; Karimi-Maleh, H. Leveraging Electrochemical Sensors to Improve Efficiency of Cancer Detection. *World J Clin Oncol* **2024**, *15* (3), 360–366. https://doi.org/10.5306/wjco.v15.i3.360.

(25) Kim, J.; Jeong, J.; Ko, S. H. Electrochemical Biosensors for Point-of-Care Testing. *Biodes Manuf* **2024**. https://doi.org/10.1007/s42242-024-00301-6.

(26) Casillas, N.; James, P.; Smyrl, W. H. A Novel Approach to Combine Scanning Electrochemical Microscopy and Scanning Photoelectrochemical Microscopy. *J Electrochem Soc* **1995**, *142* (1), L16–L18. https://doi.org/10.1149/1.2043970.

(27) James, P.; Casillas, N.; Smyrl, W. H. Simultaneous Scanning Electrochemical and Photoelectrochemical Microscopy by Use of a Metallized Optical Fiber. *J Electrochem Soc* **1996**, *143* (12), 3853–3865. https://doi.org/10.1149/1.1837308.

(28) A, E. S. S.; Tyler, P. S.; Kozlowski, M. R.; Smyrl, W. H.; Atanasoski, R. T. Photoelectrochemical Microscopy as a Probe of Localized Properties of Thin TiO2 Films. **1987**, *231*, 295–302.

(29) Zhao, F.; Conzuelo, F.; Hartmann, V.; Li, H.; Stapf, S.; Nowaczyk, M. M.; Rögner, M.; Plumeré, N.; Lubitz, W.; Schuhmann, W. A Novel Versatile Microbiosensor for Local Hydrogen Detection by Means of Scanning Photoelectrochemical Microscopy. *Biosens Bioelectron* **2017**, *94* (December 2016), 433–437. https://doi.org/10.1016/j.bios.2017.03.037.

(30) Conzuelo, F.; Sliozberg, K.; Gutkowski, R.; Grutzke, S.; Nebe, M.; Schuhmann, W. High-Resolution Analysis of Photoanodes for Water Splitting by Means of Scanning Photoelectrochemical Microscopy. *Anal Chem* **2017**, *89* (2), 1222–1228. https://doi.org/10.1021/acs.analchem.6b03706.

(31) Zhao, F.; Plumeré, N.; Nowaczyk, M. M.; Ruff, A.; Schuhmann, W.; Conzuelo, F. Interrogation of a PS1-Based Photocathode by Means of Scanning Photoelectrochemical Microscopy. *Small* **2017**, *13* (26), 1–8. https://doi.org/10.1002/smll.201604093.

(32) Takahashi, Y.; Hirano, Y.; Yasukawa, T.; Shiku, H.; Yamada, H.; Matsue, T. Topographic, Electrochemical, and Optical Images Captured Using Standing Approach Mode Scanning Electrochemical/Optical Microscopy. *Langmuir* **2006**, *22* (25), 10299–10306. https://doi.org/10.1021/la0611763.

(33) Thomas, N.; Singh, V.; Ahmed, N.; Trinh, D.; Kuss, S. Single-Cell Scanning Photoelectrochemical Microscopy Using Micro-Optical-Ring Electrodes. *Biosens Bioelectron* **2022**, *217*. https://doi.org/10.1016/j.bios.2022.114658.

(34) Liou, G. Y.; Storz, P. Reactive Oxygen Species in Cancer. *Free Radical Research*. 2010, pp 479–496. https://doi.org/10.3109/10715761003667554.

(35) Kumari, S.; Badana, A. K.; Murali Mohan, G.; Shailender, G.; Malla, R. R. Reactive Oxygen Species: A Key Constituent in Cancer Survival. *Biomark Insights* **2018**, *13*. https://doi.org/10.1177/1177271918755391.

(36) Gough, D. R.; Cotter, T. G. Hydrogen Peroxide: A Jekyll and Hyde Signalling Molecule. *Cell Death and Disease*. October 2011. https://doi.org/10.1038/cddis.2011.96.

(37) Gerlache, M.; Senturk, Z.; Quarin, G.; Kauffmann, J. M. Electrochemical Behavior of H2O2 on Gold. *Electroanalysis* **1997**, *9* (14), 1088–1092. https://doi.org/10.1002/elan.1140091411.

(38) Gulaboski, R.; Mirčeski, V.; Kappl, R.; Hoth, M.; Bozem, M. Review—Quantification of Hydrogen Peroxide by Electrochemical Methods and Electron Spin Resonance Spectroscopy. *J Electrochem Soc* **2019**, *166* (8), G82–G101. https://doi.org/10.1149/2.1061908jes.

(39) Pelle, E.; Mammone, T.; Maes, D.; Frenkel, K. Keratinocytes Act as a Source of Reactive Oxygen Species by Transferring Hydrogen Peroxide to Melanocytes. *Journal of Investigative Dermatology* **2005**, *124* (4), 793–797. https://doi.org/10.1111/j.0022-202X.2005.23661.x.

(40) Ros, E.; Cell, C. Reactive Oxygen Species in Cancer Cells : Live by the Sword , Die by the Sword. No., 175–176. https://doi.org/10.1016/j.ccr.2006.08.015.

(41) Bustamante, J.; Bredeston, L.; Malanga, G.; Mordoh, J. Role of Melanin as a Scavenger of Active Oxygen Species. *Pigment Cell Res* **1993**, *6* (5), 348–353. https://doi.org/10.1111/j.1600-0749.1993.tb00612.x.

(42) Fu, W.; Wu, Z.; Zheng, R.; Yin, N.; Han, F.; Zhao, Z.; Dai, M.; Han, D.; Wang, W.; Niu, L. Inhibition Mechanism of Melanin Formation Based on Antioxidant Scavenging of Reactive Oxygen Species. *Analyst* **2022**, *147* (12), 2703–2711. https://doi.org/10.1039/D2AN00588C.

(43) Różanowska, M.; Sarna, T.; Land, E. J.; Truscott, T. G. Free Radical Scavenging Properties of Melanin. *Free Radic Biol Med* **1999**, *26* (5–6), 518–525. https://doi.org/10.1016/S0891-5849(98)00234-2.

(44) Tada, M.; Kohno, M.; Niwano, Y. Scavenging or Quenching Effect of Melanin on Superoxide Anion and Singlet Oxygen. *J Clin Biochem Nutr* **2010**, *46* (3), 224–228. https://doi.org/10.3164/jcbn.09-84.

(45) El-Naggar, N. E.-A.; Saber, W. I. A. Natural Melanin: Current Trends, and Future Approaches, with Especial Reference to Microbial Source. *Polymers (Basel)* **2022**, *14* (7). https://doi.org/10.3390/polym14071339.

(46) Maddodi, N.; Jayanthy, A.; Setaluri, V. Shining Light on Skin Pigmentation: The Darker and the Brighter Side of Effects of UV Radiation. In *Photochemistry and Photobiology*; 2012; Vol. 88, pp 1075–1082. https://doi.org/10.1111/j.1751-1097.2012.01138.x.

(47) Brożyna, A. A.; Jóźwicki, W.; Roszkowski, K.; Filipiak, J.; Slominski, A. T. *Melanin Content in Melanoma Metastases Affects the Outcome of Radiotherapy*; 2016; Vol. 7. www.impactjournals.com/oncotarget/.

(48) Tian, Z.; Hwang, W.; Kim, Y. J. Mechanistic Understanding of Monovalent Cation Transport in Eumelanin Pigments. *J Mater Chem B* **2019**, *7* (41), 6355–6361. https://doi.org/10.1039/c9tb01211g.

(49) Saud, A.; Sagineedu, S.; Ng, H.-S.; Stanslas, J.; Lim, J. Melanoma Metastasis: What Role Does Melanin Play? (Review). *Oncol Rep* **2022**, *48* (6), 217. https://doi.org/10.3892/or.2022.8432.

Chapter 7

Conclusion and Future and Directions

The main goal of this thesis is to understand the importance of experimental parameters and advance SECM to SPECM for mammalian cell applications. This was accomplished through four main objectives: (1) Assessment of experimental parameters during SECM of living cells (2) Fabrication of MORE to advance SECM to SPECM (3) Detection of cell metabolite through SPECM (4) Application of SPECM to skin cells. The following chapter provides a comprehensive summary of the conclusions achieved and discusses the impact on the scientific community. Suggestions for future research directions are proposed.

7.1 Summary and Discussion of Impact

Understanding the ideal conditions to carry out living cell measurements with SECM/ SPECM is indispensable in experimental analysis. The first objective of this thesis, addressed in chapters 2 and 3, focused on this aspect. In chapter 2, the impact of temperature on the electrochemical current was investigated. It was found that the diffusion coefficient of the redox mediator, $FcCH_2OH$, increased with temperature, which was confirmed through numerical simulations. Using a temperature-controlled SECM workstation, the electrochemical current in HeLa cells was analyzed, providing insights into how cellular kinetics change with temperature variations. It was determined that the cellular electrochemical reactivity was more consistent under physiological temperatures. This finding is significant for future studies involving mammalian cells, as temperature plays a critical role in ensuring optimal cellular metabolism and obtaining reliable electrochemical data.

In addition to the influence of temperature, Chapter 3 examined how experimental parameters such as media composition and light exposure affected the electrochemical current signal. The impact of different electrolytes - PBS, DMEM, and $DMEM^{FBS}$ on the steady state current at Pt UME

revealed that PBS and DMEM produced higher steady state currents compared to $DMEM^{FBS}$. This result confirmed that FBS, containing proteins, growth factors and lipids tends to adsorb on to the electrode surface. When performing SECM with HeLa cells in various media, it was observed that the cellular electrochemical current was highest in DMEM, highlighting the need for nutrient media in electrochemical analyses. It was also found that due to the fouling effect of FBS, DMEM without FBS is preferred for 2D or 3D line scans involving living cells. Additionally, the effect of light exposure on living cell SECM demonstrated that fluctuations in light intensity can lead to unstable electrochemical current signals. Therefore, consistent light conditions are essential for obtaining stable electrochemical data from cells.

Chapters 2 and 3 provide fundamental insights that are crucial for achieving consistent electrochemical output during SECM studies with mammalian cells across different research groups. These findings enable the validation of comparable data and drive the advancement of the field. This work underscores the importance of conducting SECM experiments not only at room temperature or in pre-warmed solutions but under well-maintained physiological conditions. Furthermore, it highlights to the scientific community that media composition, particularly the absence of serum, and consistent illumination are essential for reliable SECM applications. Prior to this thesis, no other work in the literature thoroughly investigated or reflected on the impact of experimental parameters during SECM studies on living cells. Therefore, the work of this thesis will guide various bioelectrochemical research groups, specializing in biological SECM (as introduced in chapter 1), in their future research.

Achieving objective two required the development of specialized probes, a key instrumental advancement in SECM. This upgrade also involves coupling SECM with other techniques and establishment of different operational modes.[1] In the literature, the fabrication of specialized SECM probes with various geometries and sizes has been achieved using advanced methods such as laser pulling, chemical etching, sputter coating, electroless coating, and photolithography. To advance SECM to SPECM through probe development, Chapter 4 reviews the fabrication methodologies and applications of different types of optical electrodes. This chapter brings together more than 100 research articles over 40 decades, providing a comprehensive literature review on the design, fabrication, and applicability of optical fiber probes in electroanalysis.

In this study, electroanalysis with SPECM utilizes an optical ring electrode (MORE), which serves not only for electrochemical measurements but also for irradiation and spectroscopy. A user-friendly, cost-effective, and time-efficient fabrication methodology for MORE was developed. The fabricated MORE featured an optical fiber (OF) with a diameter of ~125 µm and a gold ring thickness of ~30 µm, resulting in an overall active diameter of ~155 µm. This design enabled coupling the optical fiber with a spectrophotometer for absorption measurements or with a light source for localized irradiation. Chapter 5 offers a comprehensive overview of the characteristics of MOREs. It was found that electrochemically, MOREs behaved as an intermediate between macro- and microelectrodes. Furthermore, for precise absorption measurements, optimizing the height of the MORE tip relative to the light source was critical. This optimization enabled spectroelectrochemical analysis, where the specific oxidation and reduction potentials of TMPD produced their respective absorption spectra.

With the development of these versatile MOREs, objective three was achieved by using *Eremosphaera viridis*, an algae species, as a model system for detecting cell metabolites. SPECM, integrated with MORE, was employed for localized irradiation and to measure oxygen production from algae. This approach offers significant advantages over most SPECM setups, which typically use a single optical electrode where light passes through the glass capillary surrounding the metal disc electrode. The MORE design overcomes the scattering of light from the lateral surface of the capillary and eliminates the need for coating to prevent light loss. Due to its highly reproducible fabrication process, which enables the preparation of fully functional probes in just two hours, MOREs effectively demonstrate the feasibility of single cell photoelectrochemistry using SPECM. The application of SPECM in this context opens new opportunities for real-time measurement of species flux in living cells, offering a more efficient alternative to existing, time-consuming assays.

To accomplish objective 4, the principles of temperature, media composition, and light exposure were applied to analyze the ROS output from skin cells in both cancerous and non-cancerous morphologies. SPECM, performed under optimal physiological conditions, enabled the detection of enhanced H_2O_2 production in keratinocytes whereas increased melanin production was found in melanoma cells in the presence of UV irradiation. Chapter 6 highlights the advancements of

SPECM for mammalian cell applications. While SPECM has demonstrated the localized, non-invasive detection of species flux from mammalian cells, the ability to quantify these species, particularly those at low concentrations or in complex environments, requires electrodes with significantly decreased dimensions, ideally in the nanoscale range.

Quantitative studies are a hallmark of SECM, where the use of UMEs with electroactive areas on the scale of the mammalian cell or even smaller allows for high-resolution measurements. Previous research has demonstrated the ability of SECM to detect and quantify ROS, providing valuable data on cellular stress, metabolic changes, and redox reactions.[2–8] These advancements indicate that nanoscale electrodes can indeed facilitate the precise electrochemical characterization of cellular processes in real-time, which is crucial for understanding changes in the cellular microenvironment. This reduction in electrode size is essential for improving the spatial resolution of measurements and enhancing the detection of molecular species at the cellular level.

An exciting prospect is the combination of SPECM with electrodes in the nanometer range, which would enhance both spatial and temporal resolution, allowing for even more precise electrochemical measurements. This could in turn pave the way for simultaneous quantification through electrochemistry, paired with complementary spectroscopic techniques. For instance, spectroelectrochemistry, which integrates optical measurements with electrochemical data could enable the validation and cross-referencing of electrochemical data, improving the accuracy of molecular detection.

However, challenges remain, particularly with respect to the size and performance of the MOREs. While these multifunctional electrodes show promise, their miniaturization and optimization for high-resolution measurements on living cells are still areas of active research. Though MOREs integrated into SPECM would require optimization in terms of tip to substrate distance for spectroscopic measurements and experimental parameters across various living cells, due to differences in cell dimensions and microenvironment, SPECM with nanoscale electrodes holds great promise for advancing the quantification of disease pathologies, enabling early detection and monitoring of therapeutic interventions. Furthermore, the combination of electrochemical and

spectroscopic methods could reveal deeper insights into the behavior of photosensitive compounds and other molecular species involved in key biological processes.

In conclusion, while SECM along with optimized experimental parameters have already proven invaluable in molecular electrochemical analysis, SPECM with the development of nanoscale electrodes and multifunctional probes will enable the next generation of quantitative studies. This research lays the foundation for future research focused on improving disease diagnosis, understanding cellular responses to external stimuli, and investigating redox-active species in cellular systems.

7.2 Future Research Prospectives

Suggestions for future research focus on SPECM probe development, extension of SPECM applicability to different operating modes, other cell lines, and electrochemiluminescence, and SPECM in other areas of research.

7.2.1 Probe Development

Probe advancement mainly emphasizes methods for improving signal to noise ratio and specificity in detection. This involves reduction of the MORE size and surface modification of the MORE metallic ring through polymerization or nano particles (NPs).

7.2.1.1 MORE size reduction

The current MOREs used in our SPECM setup have an active area diameter of 155 µm, which includes both the optical fiber (OF) core and the surrounding gold ring. Reducing the active area diameter to 100 µm—by using a 50 µm diameter OF and a 50 µm diameter metallic ring—will improve the resolution of electrochemical and absorption measurements in living cell studies. Since most mammalian cells range in size from 10 to 100 µm, adjusting the diameters of the OF and metallic ring to match the cell size will address the challenge of obtaining accurate measurements of cell metabolite efflux in the pico- and femtomolar concentration ranges.

Fabricating a MORE with smaller tip dimensions is achievable by adjusting the pulling parameters for the optical fibers. Laser pullers designed for optical fibers can be used to produce tapered tips,[9] (Figure 7.1 a) which can then be coated with thin films of platinum or gold through sputter coating[10–12] (Figure 7.1 b). Sputter coating is a physical vapor deposition technique that applies a uniform functional coating to the substrate using high-energy plasma generated by electrically charging the sputtering cathode.[13] Alternatively, commercially available metallic-coated optical fibers can be adapted for this purpose by optimizing the laser pulling parameters.

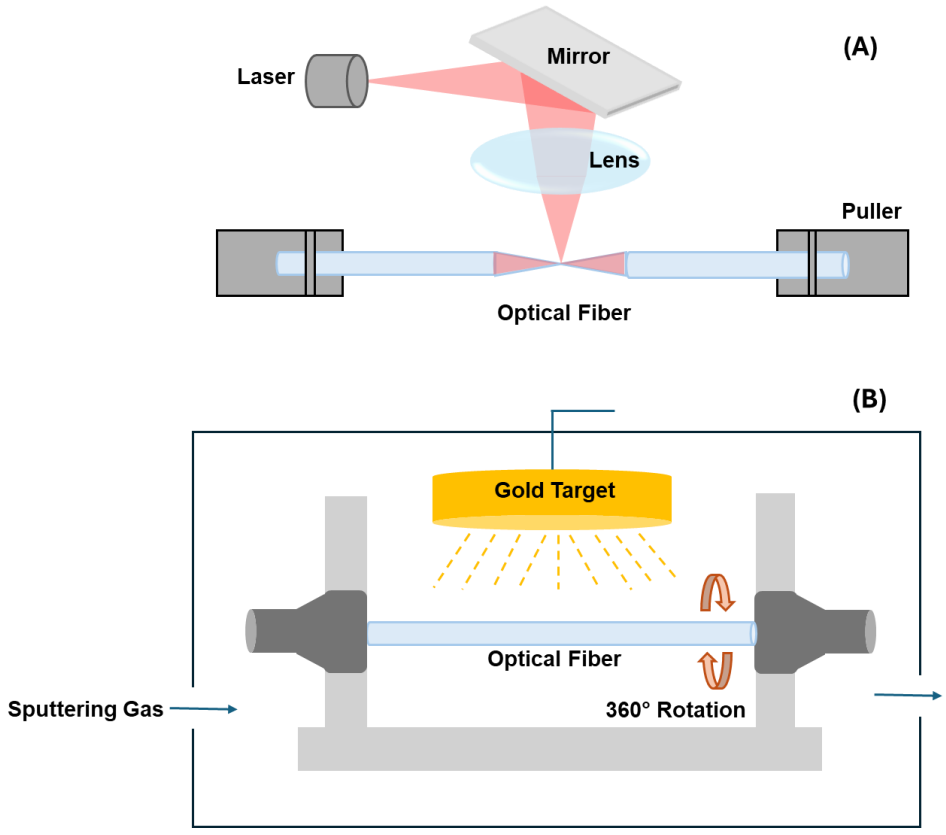

Figure 7.1 *OF size reduction by (A) laser puller and coating by (B) sputter coating*

While reducing the size of the optical fiber is feasible, one challenge remains in coupling the smaller fiber with the spectrophotometer. Multimode fiber (MMF) cables, commonly used for spectroscopy, have diameters ranging from 200 to 600 µm,[14] which could result in loss of the absorption signal when coupled with a MORE featuring an optical fiber diameter of less than 100 µm. This issue can be mitigated by adjusting the spectrophotometer's aperture to accommodate

MMF fibers with diameters in the 50-100 µm range, or by using single-mode fiber (SMF) cables, which have diameters as small as 6 µm,[15] particularly when the experimental setup employs a defined light mode.

7.2.1.2 MORE tip modification

Modification of electrode tips is commonly achieved through NP[16] or polymer deposition[17], which can be performed by physical adsorption, chemical binding and electrodeposition.[18] (Figure 7.2) Using NPs and polymers for electrode modification has offers several advantages such as improved mass transport, high surface to volume ratio and enhanced current signal.[16,18] Electrodeposition of NPs or conducting polymers (CPs) is particularly suitable for ring electrodes, as it avoids blocking the center of the optical fiber (OF) (Figure 7.2 c).

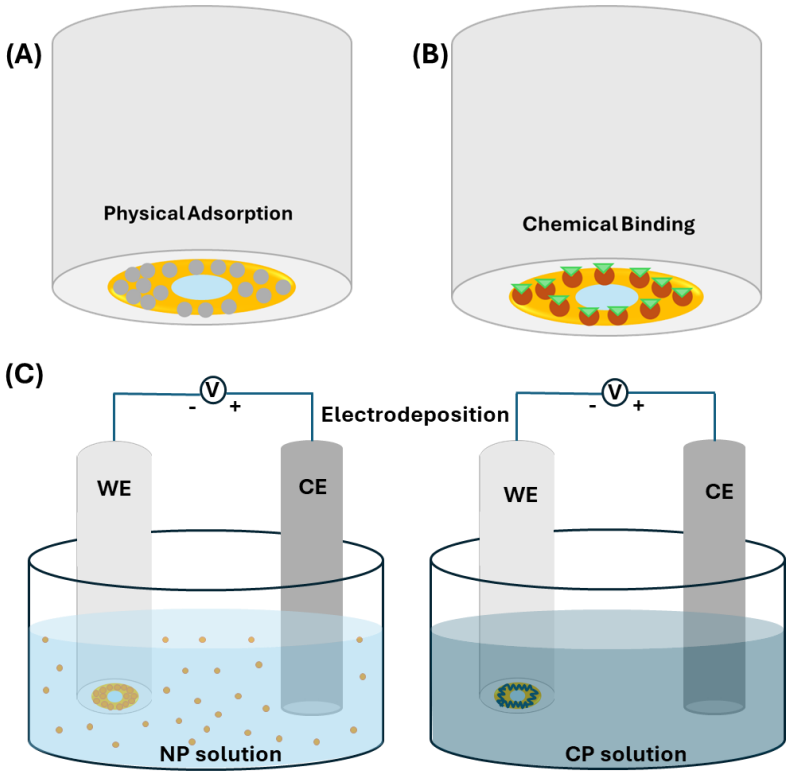

Figure 7.2 *Illustration of MORE tip modification by (A) physical adsorption of microparticles on the gold ring (B) chemical binding of biomolecules or compounds (green) on the gold ring through a recognition element (brown) and (C) electrodeposition of NPs or CP.*

CPs such as polypyrrole (PPy) and its derivatives, polythiophene and its derivatives, poly (3,4-ethylenedioxythiphene) (PEDOT) and its derivatives, polyaniline (PANI) and its derivatives, and polycarbazole, and their composites with nanoparticles or ionic liquids are known to have improved sensitivity and selectivity.[19] These enhancements are achieved through biomolecule immobilization or enzyme active sites specific to the analyte of interest. Electrodeposition also improves the specificity of attachment to the metallic ring. Furthermore, the use of Pt, Cu, and carbon NPs or nanomaterials can improve the selective detection of ROS,[20–22] and these modifications could be explored for use with MORE. Additionally, the gold ring surface of the MORE can undergo aptamer functionalization for targeting specific biomarkers. Aptamer functionalization has been shown to enhance the specificity of detection for protein biomarkers.[23]

7.2.2. Extended applications of SPECM

This section provides a broad overview on the application of SPECM to different cell lines, in different operating modes and towards electrochemiluminescence.

7.2.2.1 Other cell lines

SPECM can be applied to various cancerous and non-cancerous cell lines, such as ovarian, lung, and fibroblast cells, to investigate how exposure to specific wavelengths of irradiation affects these cells. Given that cancer treatments often involve exposing patients to radiation, such as x-rays and gamma rays,[24] SPECM could be utilized to study, in real time, the impact of these radiations and the development of chemoresistance over time.

7.2.2.2 Operating modes

The feedback mode of SPECM/SECM has been the primary operating mode used throughout this thesis. However, it would be interesting to explore the SG/TC mode with cell lines, where cells continuously release metabolites or biomarkers. These could be detected at the ring electrode in the presence of a specific stimulant, such as localized irradiation.

7.2.2.3 Electrochemiluminescence

Electrochemiluminescence (ECL) can be explored for detecting ROS in various cell lines[25–27] using SPECM. This can be achieved by using ECL probes, such as tris (2,2’-bipyridyl) ruthenium

(II) (Ru(bpy))[28] and luminol (L012)[29] in measuring solutions. Notably, the OF of the electrode can be coupled to a photomultiplier tube (PMT) or an electron multiplying charge coupled device (EMCCD), which amplifies the ECL signal generated at the electrode surface.[30] The electrochemical signal from the cell can be measured by biasing the electrode at potentials specific to the ROS being produced extracellularly.[29] These ECL probes are known to emit luminescence in the presence of ROS, allowing both electrochemical signals and luminescence to be detected at single cell level using the MORE integrated with SPECM.

7.2.3. Other applications of SPECM

7.2.3.1 Biomaterials or Biodegradables

The popularity of various biomaterials such as metallic, polymeric, ceramic, inorganic, and regenerative glass materials, has grown significantly due to their wide-ranging applications in biomedicine, including tissue repair, drug delivery, medical devices, and sutures. One of the most challenging aspects of biomaterial research is their detailed characterization.[31] SPECM offers an efficient approach for real-time, chemical analysis of surface homogeneities and heterogeneities through electrochemical techniques, enabling rapid and comprehensive evaluation. In addition, SPECM can be used to assess the biological compatibility of biomaterials in vitro.

For ocular tissue engineering applications, SPECM can investigate the photosensitivity of biomaterials by applying localized irradiation with different wavelengths. Furthermore, SPECM can be employed to test biodegradable packaging materials, commonly used in the food industry, for their reactivity to environmental stimuli, such as temperature, light, and liquids, as well as their interaction with various food ingredients. Another potential application is in evaluating the UV/radiation curing properties of materials, whether biodegradable or not, which is crucial for industries that rely on curing technologies, such as coatings or adhesives.

7.2.3.2 Agriculture

In agriculture, SPECM can be used to study the impact of pesticides on *in-vitro* plant and animal cells. Photodegradation of pesticides is a critical area of research aimed at improving food safety and security.[32–34] Pesticides, when applied, are constantly exposed to sunlight which contains harmful UV rays. Pesticides such as dimethoate, parathion, glyphosate, chloroaniline, and atrazine

are known to undergo photodegradation, producing toxic byproducts.[35] The properties of these pesticides when irradiated with UV light can be investigated through SPECM to analyze their transformation into other potentially harmful compounds.

7.2.4 Conclusion

The future of SPECM holds immense potential for advancing our understanding of not only cellular processes and disease mechanisms but also in investigating material or chemical interactions at the micro-scale.

Continued development of MOREs particularly through techniques such as size reduction and surface modification, will enhance the resolution, sensitivity, and specificity of measurements, allowing for more precise detection and quantification of molecular species at the single-cell level. By refining these probes, researchers will be able to investigate cellular efflux and metabolic processes with unprecedented accuracy, opening new avenues for understanding complex biological systems.

The integration of ECL and the exploration of alternative operating modes, such as SG/TC mode, will further broaden the capabilities of SPECM, enabling studies on dynamic cellular responses to various stimuli under conditions of desired experimental setting. These advancements will allow SPECM to provide real-time, non-invasive insights into cellular behavior and offer powerful tools for monitoring disease progression and treatment effects.

Moreover, the applications of SPECM extend far beyond cellular studies. Its ability to perform real-time, chemical analysis will be invaluable in biomaterials research, particularly in assessing the biocompatibility of new materials in fields like ocular tissue engineering and biodegradable packaging, where environmental factors like temperature play a significant role in material behavior. In agriculture, SPECM could play a key role in monitoring the photodegradation of pesticides, contributing to safer food production practices and environmental sustainability.

Ultimately, the continued development of MOREs and SPECM will drive innovation across multiple disciplines, from medicine to material science to environmental research. As these technologies evolve, SPECM will offer researchers a more powerful and precise technique for

understanding complex biological phenomena, testing new materials, and improving safety and efficacy in a wide range of applications.

7.3 References

(1) Polcari, D.; Dauphin-Ducharme, P.; Mauzeroll, J. Scanning Electrochemical Microscopy: A Comprehensive Review of Experimental Parameters from 1989 to 2015. *Chem Rev* **2016**, *116* (22), 13234–13278. https://doi.org/10.1021/acs.chemrev.6b00067.

(2) Liu, B.; Rotenberg, S. A.; Mirkin, M. V. Scanning Electrochemical Microscopy of Living Cells: Different Redox Activities of Nonmetastatic and Metastatic Human Breast Cells. *Proc Natl Acad Sci U S A* **2000**, *97* (18), 9855–9860. https://doi.org/10.1073/pnas.97.18.9855.

(3) Hu, K.; Li, Y.; Rotenberg, S. A.; Amatore, C.; Mirkin, M. V. Electrochemical Measurements of Reactive Oxygen and Nitrogen Species inside Single Phagolysosomes of Living Macrophages. *J Am Chem Soc* **2019**, *141* (11), 4564–4568. https://doi.org/10.1021/jacs.9b01217.

(4) Li, Y.; Hu, K.; Yu, Y.; Rotenberg, S. A.; Amatore, C.; Mirkin, M. V. Direct Electrochemical Measurements of Reactive Oxygen and Nitrogen Species in Nontransformed and Metastatic Human Breast Cells. *J Am Chem Soc* **2017**, *139* (37), 13055–13062. https://doi.org/10.1021/jacs.7b06476.

(5) Zhao, X.; Lam, S.; Jass, J.; Ding, Z. Scanning Electrochemical Microscopy of Single Human Urinary Bladder Cells Using Reactive Oxygen Species as Probe of Inflammatory Response. *Electrochem commun* **2010**, *12* (6), 773–776. https://doi.org/10.1016/j.elecom.2010.03.030.

(6) Zhao, X.; Zhu, R.; Anikovskiy, M.; Wu, Q.; Ding, Z. Profiling H2O2 from Single COS-7 Cells by Means of Scanning Electrochemical Microscopy. *Biosens Bioelectron* **2023**, *227*. https://doi.org/10.1016/j.bios.2023.115123.

(7) Vaneev, A. N.; Gorelkin, P. V.; Garanina, A. S.; Lopatukhina, H. V.; Vodopyanov, S. S.; Alova, A. V.; Ryabaya, O. O.; Akasov, R. A.; Zhang, Y.; Novak, P.; Salikhov, S. V.;

Abakumov, M. A.; Takahashi, Y.; Edwards, C. R. W.; Klyachko, N. L.; Majouga, A. G.; Korchev, Y. E.; Erofeev, A. S. In Vitro and in Vivo Electrochemical Measurement of Reactive Oxygen Species after Treatment with Anticancer Drugs. *Anal Chem* **2020**, *92* (12), 8010–8014. https://doi.org/10.1021/acs.analchem.0c01256.

(8) Salamifar, S. E.; Lai, R. Y. Use of Combined Scanning Electrochemical and Fluorescence Microscopy for Detection of Reactive Oxygen Species in Prostate Cancer Cells. *Anal Chem* **2013**, *85* (20), 9417–9421. https://doi.org/10.1021/ac402367f.

(9) Hidayat, N.; Aziz, M. S.; Krishnan, G.; Johari, A. R.; Nur, H.; Taufiq, A.; Mufti, N.; Mukti, R. R.; Bakhtiar, H. Tapered Optical Fibers Using CO2laser and Their Sensing Performances. In *Journal of Physics: Conference Series*; Institute of Physics, 2023; Vol. 2432. https://doi.org/10.1088/1742-6596/2432/1/012013.

(10) Shukla, S. K.; Kushwaha, C. S.; Guner, T.; Demir, M. M. Chemically Modified Optical Fibers in Advanced Technology: An Overview. *Optics and Laser Technology*. Elsevier Ltd July 1, 2019, pp 404–432. https://doi.org/10.1016/j.optlastec.2019.02.025.

(11) Wang, X. D.; Wolfbeis, O. S. Fiber-Optic Chemical Sensors and Biosensors (2015-2019). *Analytical Chemistry*. American Chemical Society January 7, 2020, pp 397–430. https://doi.org/10.1021/acs.analchem.9b04708.

(12) Wang, X. D.; Wolfbeis, O. S. Fiber-Optic Chemical Sensors and Biosensors (2013-2015). *Analytical Chemistry*. American Chemical Society January 5, 2016, pp 203–227. https://doi.org/10.1021/acs.analchem.5b04298.

(13) Gulbiński, W. Deposition of Thin Films by Sputtering. In *Chemical Physics of Thin Film Deposition Processes for Micro- and Nano-Technologies*; Springer Netherlands: Dordrecht, 2002; pp 309–333. https://doi.org/10.1007/978-94-010-0353-7_13.

(14) *Fiber Optic Cable Selection: How to Select the Best Fiber Optic Cable for High Performance Spectroscopic Analysis*. Process Insights. https://guided-wave.com/how-to-select-the-best-fiber-optic-cable/ (accessed 2024-11-11).

(15) *Single-Mode vs. Multimode Fiber Cable: A Direct Comparison of Features and Cost*. Omnitron Systems. https://www.omnitron-systems.com/blog/single-mode-vs-multimode-

fiber-cable-a-direct-comparison-of-features-and-cost#:~:text=Single%2Dmode%20fiber%20is%20preferred,cost%2Deffectiveness%20is%20a%20priority. (accessed 2024-11-11).

(16) Bozal-Palabiyik, B.; Selcuk, O.; Uslu, B. Development of Nanoparticle-Modified Ultramicroelectrodes and Their Electroanalytical Application. In *Handbook of Nanobioelectrochemistry: Application in Devices and Biomolecular Sensing*; Springer, 2023; pp 861–879. https://doi.org/10.1007/978-981-19-9437-1_39.

(17) Bone, J. M.; Jenkins, J. L. Understanding Polymer Electrodeposition and Conducting Polymer Modified Electrodes Using Electrochemistry, Spectroscopy, and Scanning Probe Microscopy. *J Chem Educ* **2023**, *100* (10), 4062–4071. https://doi.org/10.1021/acs.jchemed.3c00656.

(18) Baig, N.; Sajid, M.; Saleh, T. A. Recent Trends in Nanomaterial-Modified Electrodes for Electroanalytical Applications. *TrAC - Trends in Analytical Chemistry*. Elsevier B.V. February 1, 2019, pp 47–61. https://doi.org/10.1016/j.trac.2018.11.044.

(19) Biallozor, S.; Kupniewska, A. Conducting Polymers Electrodeposited on Active Metals. *Synth Met* **2005**, *155* (3), 443–449. https://doi.org/10.1016/j.synthmet.2005.09.002.

(20) Liu, Y.; Shang, T.; Liu, Y.; Liu, X.; Xue, Z.; Liu, X. Highly Sensitive Platinum Nanoparticles-Embedded Porous Graphene Sensor for Monitoring ROS from Living Cells upon Oxidative Stress. *Sens Actuators B Chem* **2018**, *263*, 543–549. https://doi.org/10.1016/j.snb.2018.02.135.

(21) Liu, T.; Xiao, B.; Xiang, F.; Tan, J.; Chen, Z.; Zhang, X.; Wu, C.; Mao, Z.; Luo, G.; Chen, X.; Deng, J. Ultrasmall Copper-Based Nanoparticles for Reactive Oxygen Species Scavenging and Alleviation of Inflammation Related Diseases. *Nat Commun* **2020**, *11* (1), 2788. https://doi.org/10.1038/s41467-020-16544-7.

(22) Huynh, G. T.; Kesarwani, V.; Walker, J. A.; Frith, J. E.; Meagher, L.; Corrie, S. R. Review: Nanomaterials for Reactive Oxygen Species Detection and Monitoring in Biological Environments. *Front Chem* **2021**, *9*. https://doi.org/10.3389/fchem.2021.728717.

(23) Oberhaus, F. V; Frense, D.; Beckmann, D. Immobilization Techniques for Aptamers on Gold Electrodes for the Electrochemical Detection of Proteins: A Review. *Biosensors (Basel)* **2020**, *10* (5). https://doi.org/10.3390/bios10050045.

(24) Baskar, R.; Dai, J.; Wenlong, N.; Yeo, R.; Yeoh, K. W. Biological Response of Cancer Cells to Radiation Treatment. *Frontiers in Molecular Biosciences*. Frontiers Media S.A. November 17, 2014. https://doi.org/10.3389/fmolb.2014.00024.

(25) He, X.; Deng, Y.; Jiang, D.; Fang, D. Electrochemiluminescence Detection and Imaging of Biomolecules at the Single-Cell Level. *Chemosensors*. Multidisciplinary Digital Publishing Institute (MDPI) October 1, 2023. https://doi.org/10.3390/chemosensors11100538.

(26) Liu, G.; Ma, C.; Jin, B. K.; Chen, Z.; Zhu, J. J. Direct Electrochemiluminescence Imaging of a Single Cell on a Chitosan Film Modified Electrode. *Anal Chem* **2018**, *90* (7), 4801–4806. https://doi.org/10.1021/acs.analchem.8b00194.

(27) Electrochemiluminescence Single-Cell Analysis_ Intensity- and Imaging-Based Methods _ Enhanced Reader.

(28) Hesari, M.; Ding, Z. Spooling Electrochemiluminescence Spectroscopy: Development, Applications and Beyond. *Nat Protoc* **2021**, *16* (4), 2109–2130. https://doi.org/10.1038/s41596-020-00486-x.

(29) Zhong, W.; Fu, Y.; Chen, X.; Lu, C. Understanding Reactive Oxygen Species in Potential-Resolved Electrochemiluminescence of Luminol-Dissolved O2. *Journal of Physical Chemistry C* **2024**. https://doi.org/10.1021/acs.jpcc.4c03871.

(30) Li, H.; Garrigue, P.; Bouffier, L.; Arbault, S.; Kuhn, A.; Sojic, N. Double Remote Electrochemical Addressing and Optical Readout of Electrochemiluminescence at the Tip of an Optical Fiber. *Analyst* **2016**, *141* (14), 4299–4304. https://doi.org/10.1039/c6an00652c.

(31) *Characterization of Biomaterials*; Bandyopadhyay, A., Bose, S., Eds.; Elsevier, 2013.

(32) Fenoll, J.; Flores, P.; Hellín, P.; Martínez, C. M.; Navarro, S. Photodegradation of Eight Miscellaneous Pesticides in Drinking Water after Treatment with Semiconductor Materials

under Sunlight at Pilot Plant Scale. *Chemical Engineering Journal* **2012**, *204–206*, 54–64. https://doi.org/10.1016/j.cej.2012.07.077.

(33) Xi, N.; Li, Y.; Xia, X. A Review of Pesticide Phototransformation on the Leaf Surface: Models, Mechanism, and Influencing Factors. *Chemosphere* **2022**, *308*, 136260. https://doi.org/10.1016/j.chemosphere.2022.136260.

(34) Katagi, T. Photodegradation of Pesticides on Plant and Soil Surfaces. *Rev Environ Contam Toxicol* **2004**, *182*, 1–189. https://doi.org/10.1007/978-1-4419-9098-3_1.

(35) Cui, G.; Lartey-Young, G.; Chen, C.; Ma, L. Photodegradation of Pesticides Using Compound-Specific Isotope Analysis (CSIA): A Review. *RSC Adv* **2021**, *11* (41), 25122–25140. https://doi.org/10.1039/d1ra01658j.

Appendix 1

Temperature Effect on the Electrochemical Current Response during Scanning Electrochemical Microscopy of Living Cells

```
SetDirectory[NotebookDirectory[]];
muWater = Import["viscosity of water.txt", "Table"];
muWaterf = Interpolation[muWater]
```

```
InterpolatingFunction
```

Domain: {{0.01, 99.6}}
Output: scalar

```
Show[ListPlot[muWater, Frame → True, FrameLabel → {"T (C)", "μ Water (mPas.s)"}], Plot[muWaterf[t], {t, 1, 80}]]
```

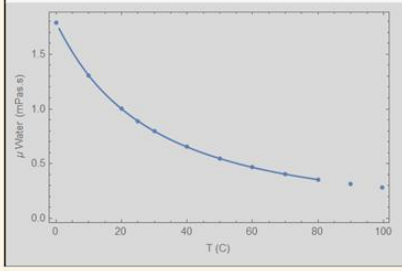

Figure A1.1 *Viscosity of water as a function of temperature.*

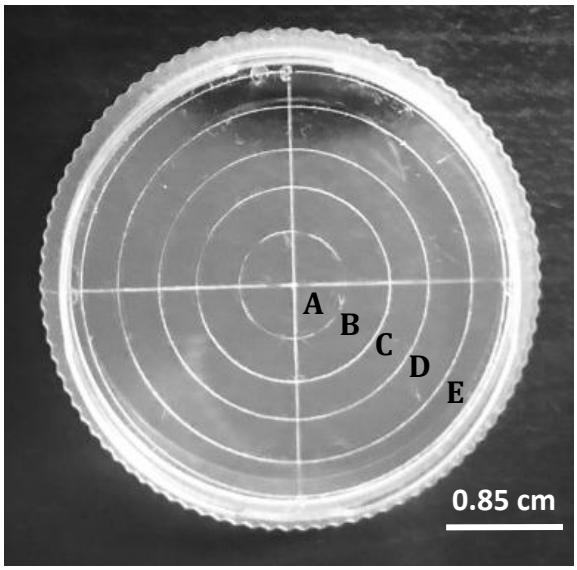

Figure A1.2 *Optical micrograph of a 35-mm petri dish with labelled temperature ring-zones.*

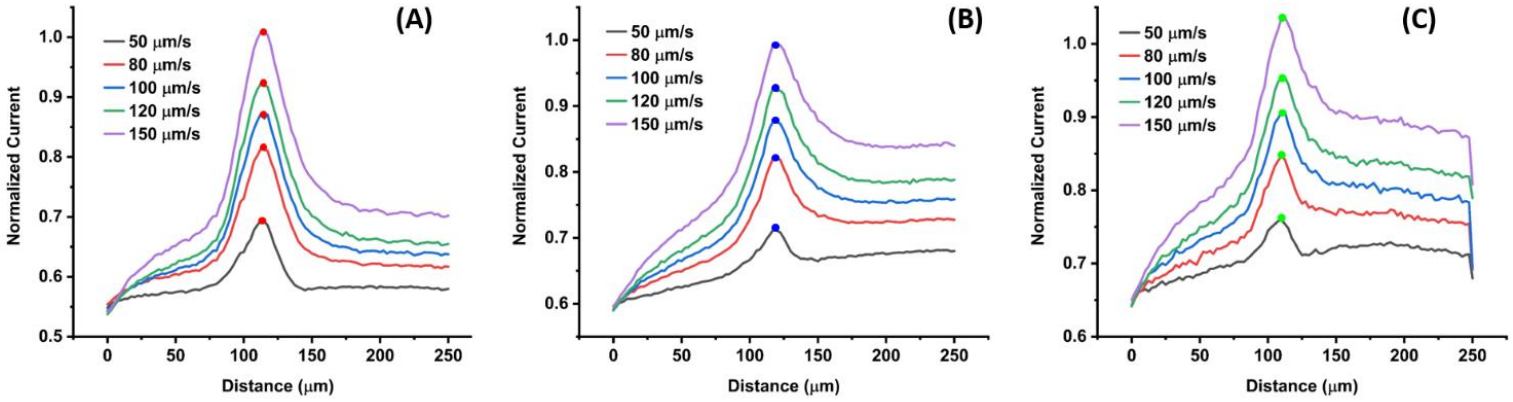

Figure A1.3 *2D-line scans over single HeLa cells. (A) Zone A with a temperature range of 31.5-33.1 ℃ (B) Zone B with a temperature range of 33.9-34.8°C and (C) Zone D with a temperature range of 36.8-37.2 ℃. Normalized current presents the measured current divided by the current far from the substrate.*

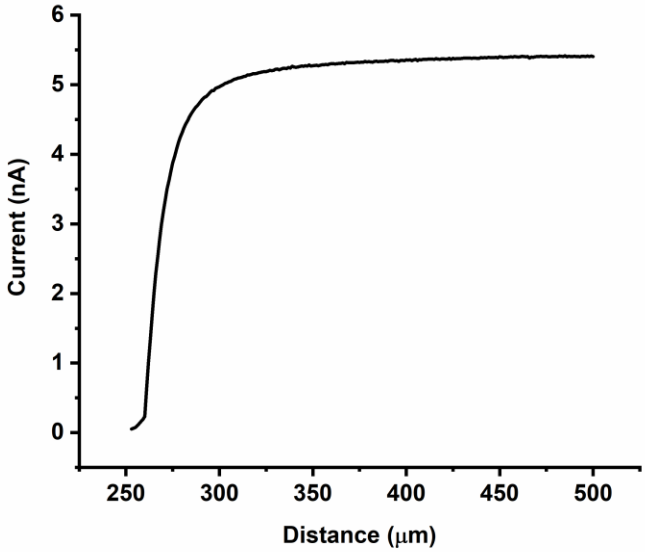

Figure A1.4 *Negative feedback shown by a 25 μm Pt UME as it is approaching the plastic surface of the Petri dish.*

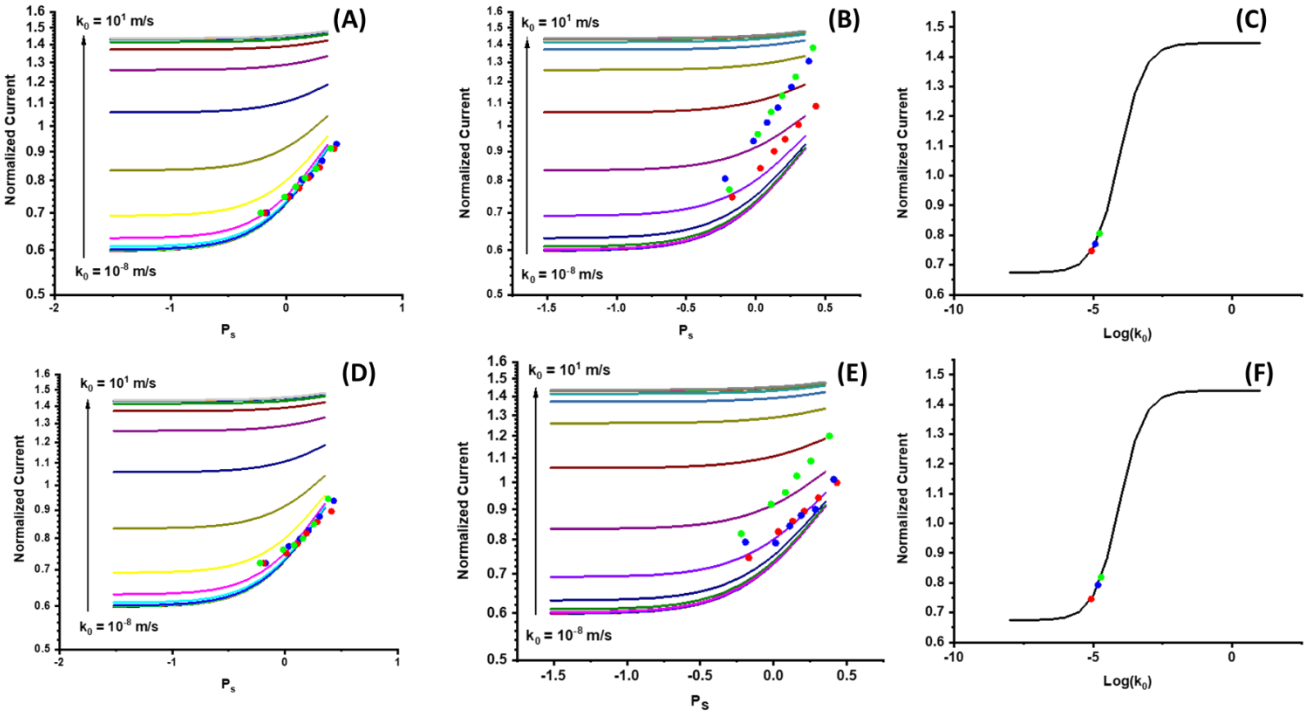

Figure A1.5 *Additional data sets. (A) and (D) showing kinetics across an insulating petri dish in Zone A: 31.5- 33.1ºC (red), Zone B: 33.9-34.8ºC (blue), and Zone D: 36.8-37.2ºC (green). (B) and (E) present kinetics across HeLa cells in Zone A: 31.5- 33.1ºC (red), Zone B: 33.9-34.8ºC (blue), and Zone D: 36.8-37.2ºC (green). (C) and (F) Comparison of cellular kinetics.*

Appendix 2

Effect of Media Composition and Light Exposure on the Electrochemical Current Response during Scanning Electrochemical Microscopy Live Cell Imaging

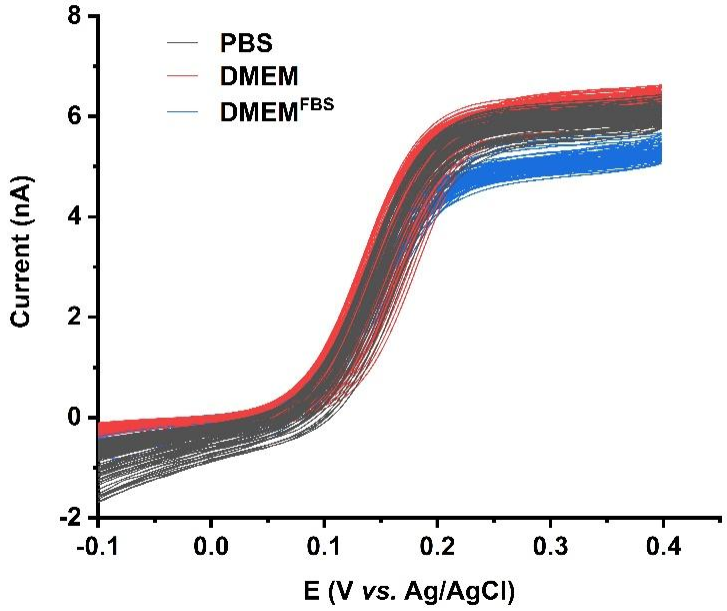

Figure A2.1 *50 cyclic voltammetry sweeps in 1 mM $FcCH_2OH$ dissolved in PBS (black), DMEM (red) and $DMEM^{FBS}$ (blue) at 50 mV/s.*

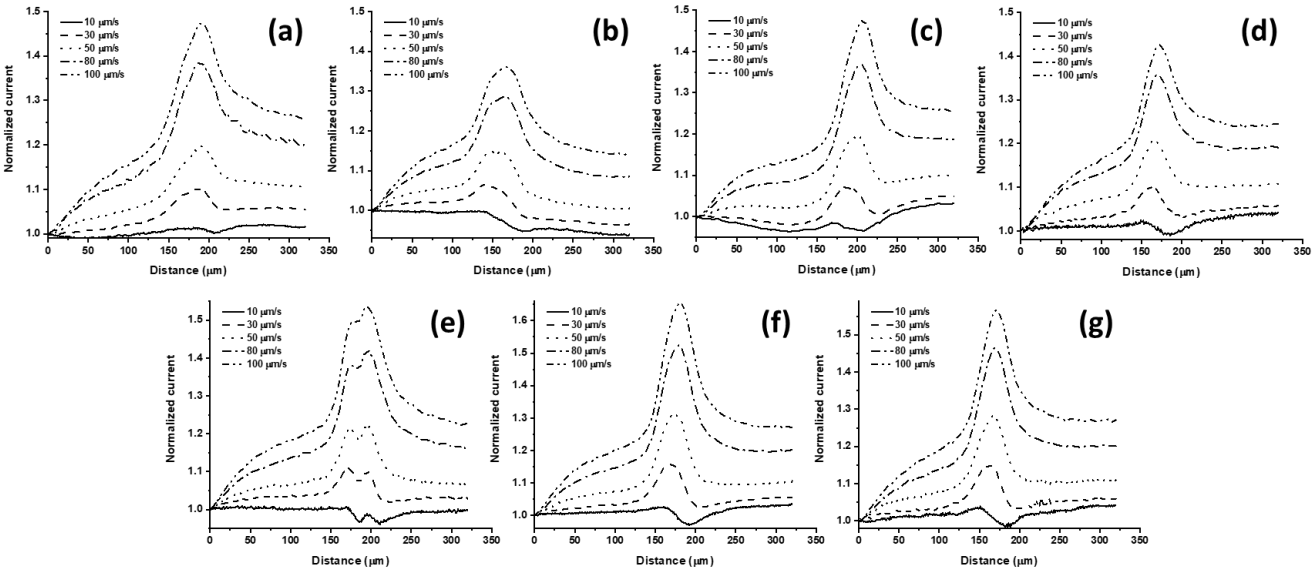

Figure A2.2 *(a-g) Line scans across HeLa cells in PBS solution with 1 mM $FcCH_2OH$.*

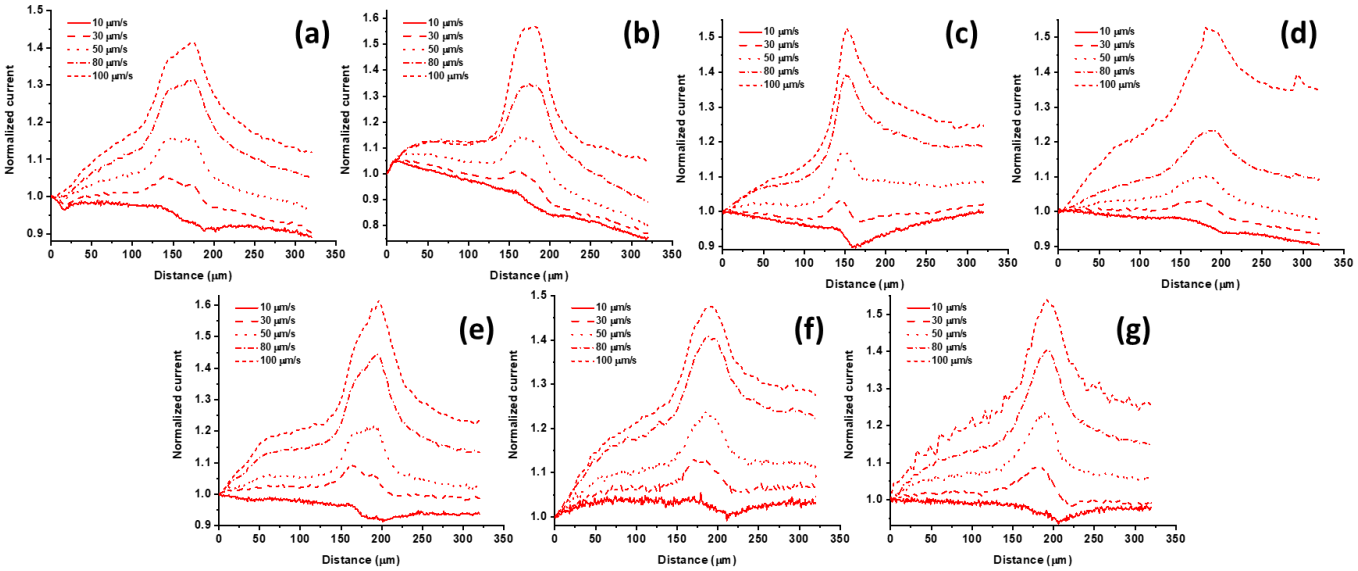

Figure A2.3 *(a-g) Line scans across HeLa cells in 1 mM $FcCH_2OH$ in DMEM*

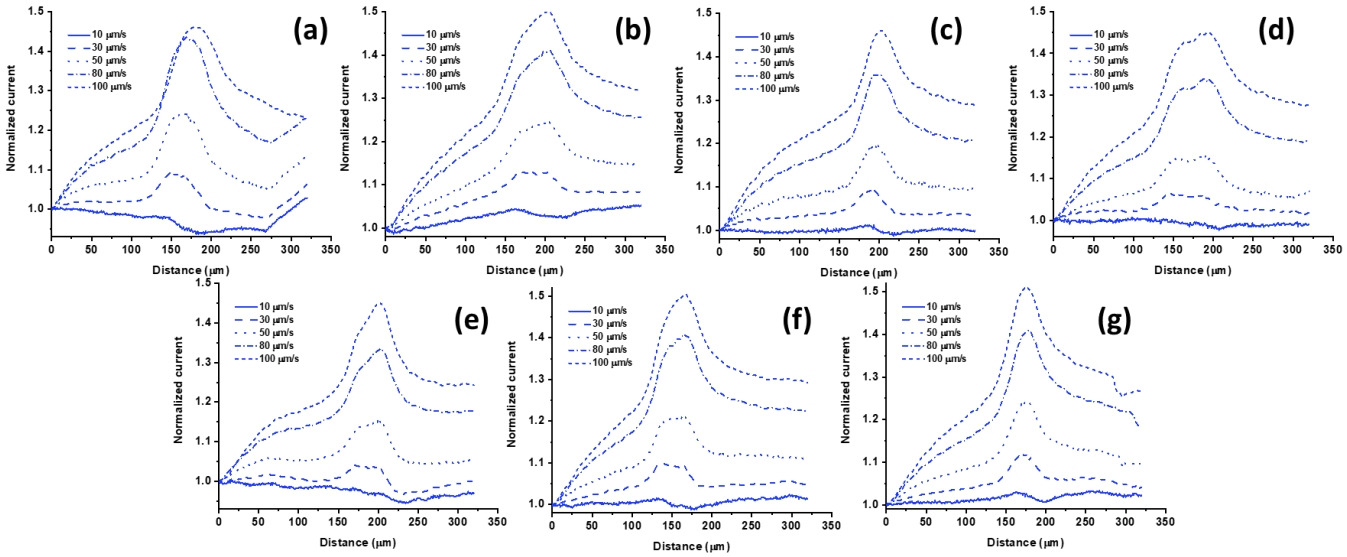

Figure A2.4 *(a-g) Line scans across HeLa cells in 1 mM $FcCH_2OH$ in DMEM with 10% FBS.*

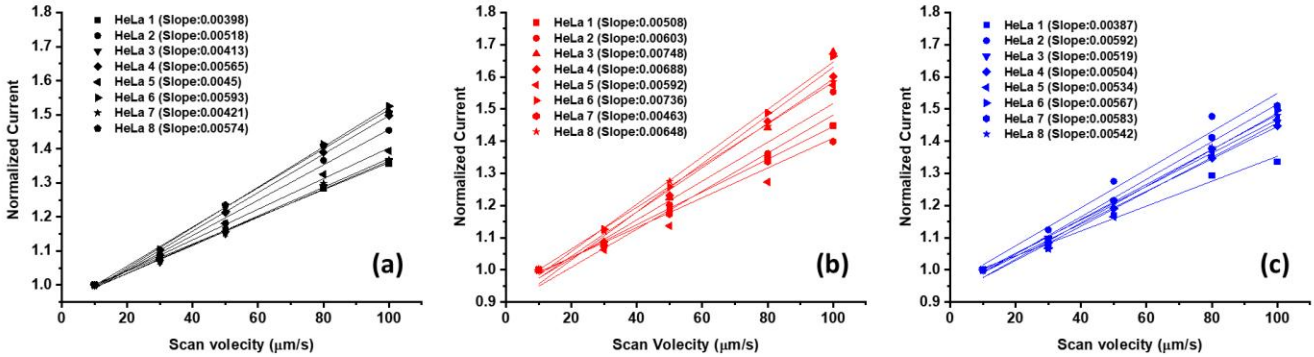

Figure A2.5 *Linear relationships of normalized peak current with scan velocity for HeLa cells in 1 mM $FcCH_2OH$ dissolved in (a) PBS b), DMEM (c) $DMEM^{FBS}$*

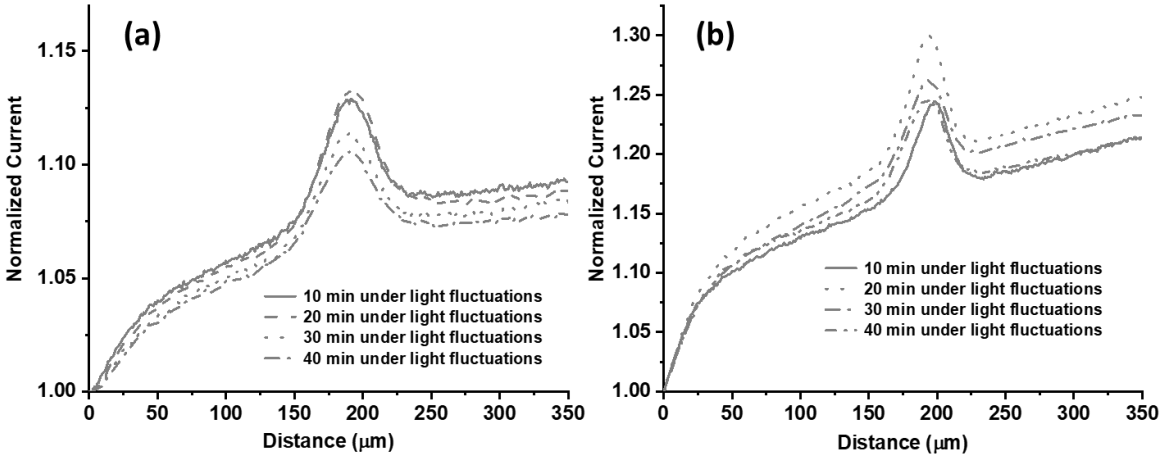

Figure A2.6 *Additional data. (a-b) 2D line scans across HeLa cells under fluctuating light at 10,20,30,and 40 minute time intervals .*

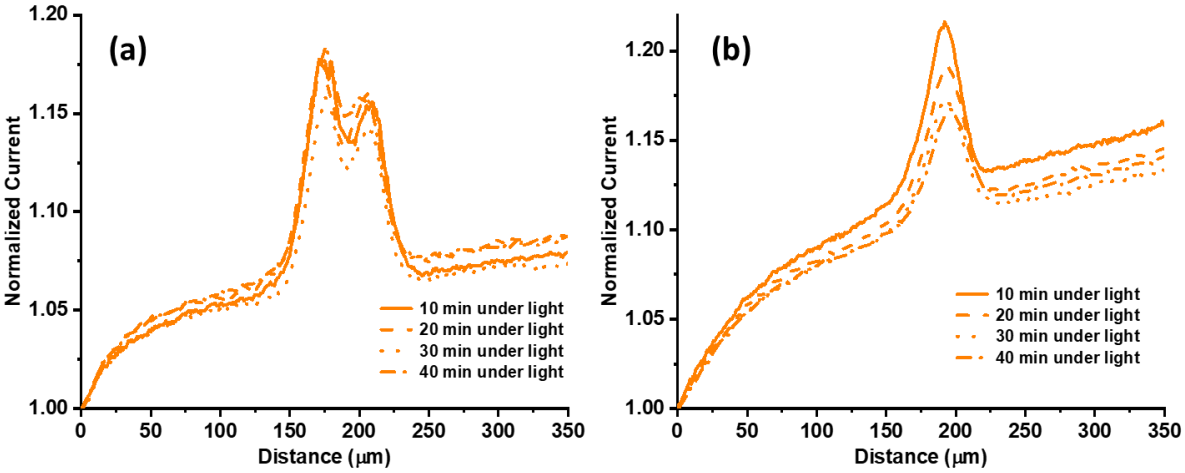

Figure A2.7 *Additional data. (a-b) 2D line scans across HeLa cells in full light at 10,20,30,and 40 minute time intervals*

Slope Test

SE: Standard Error S: Slope

$x = \sqrt{(SE1)^2 + (SE2)^2}$

$y = \frac{S_1 - S_2}{x}$

	Slope	Error
PBS	0.00464	1.59E-04
DMEM	0.00543	3.75E-04
DMEM FBS	0.00507	1.77E-04

PBS & DMEM	
x	y
0.00041	1.940504535
PBS & DMEM FBS	
x	y
0.00024	1.803003006
DMEM & DMEM FBS	
x	y
0.00041	0.86864141

y < critical value of 2.365 at df=7 and 95% confidence interval for the three combinations.

Appendix 3

Single Cell Scanning Photoelectrochemical Microscopy using Micro-Optical-Ring Electrodes

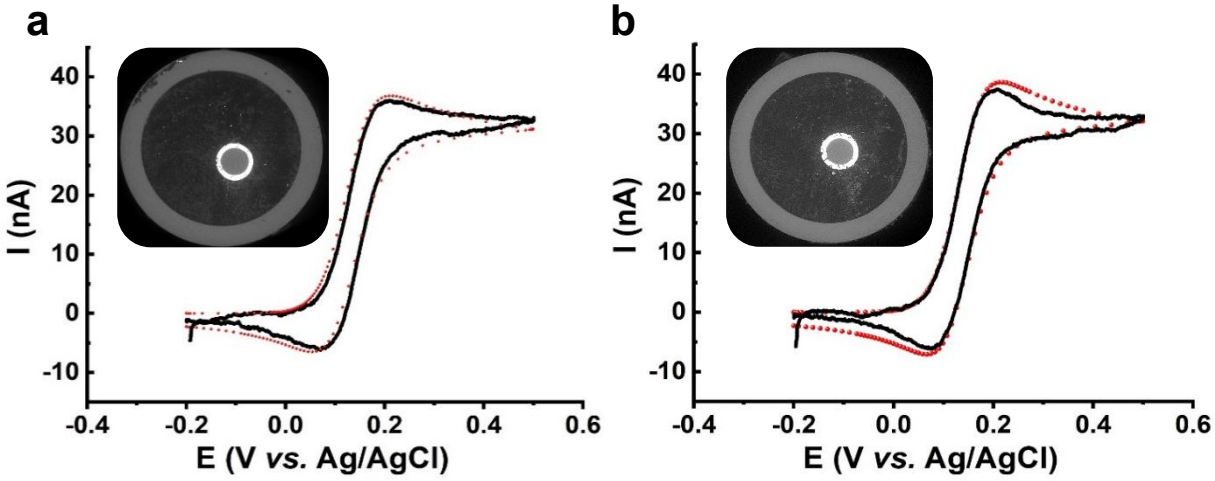

Figure A3.1 *Cyclic voltammograms recorded in 1 mM FcCH2OH in 0.1 M KCl at a scan rate of 30 mV s-1 are shown for two individual MOREs comparing the experimental data (black) and expected numerical simulation (red) independent of a slight offset of the optical fiber from the center of the epoxy containing glass capillary.*

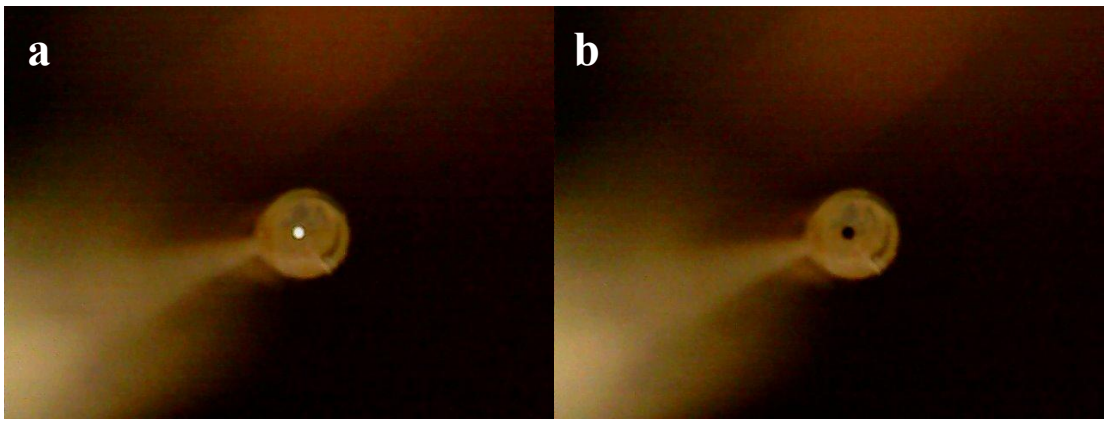

Figure A3.2 *Optical micrographs of (a) MORE light ON and (b) MORE light OFF*

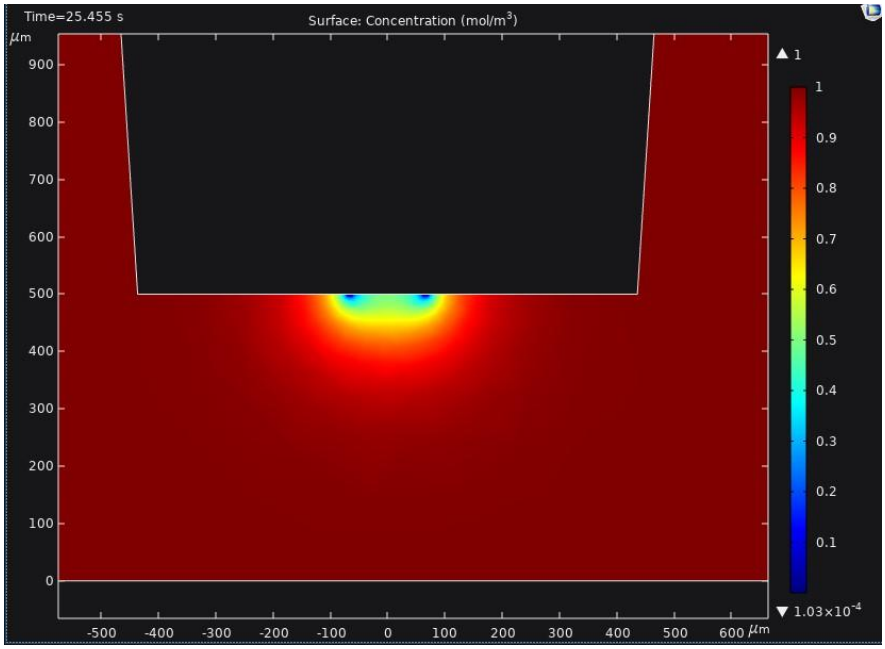

Figure A3.3 *Solution concentration profile calculated by COMSOL of the electroactive species $FcCH_2OH$ for MORE functionality assessment. Concentration of bulk solution shown in dark red.*

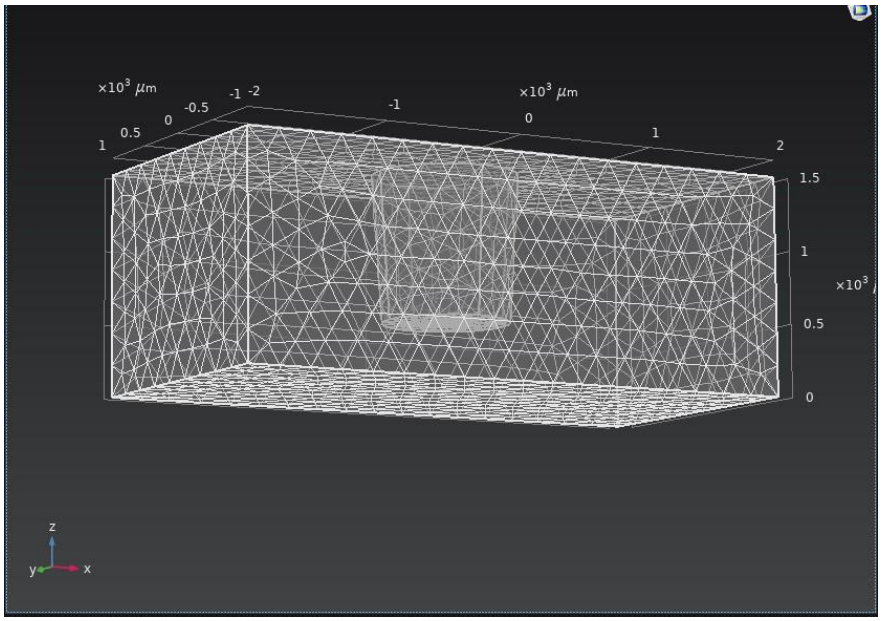

Figure A3.4 *Dimension boundary conditions and measurement point mesh of a theoretical MORE in solution as set in COMSOL for MORE functionality assessment.*

A3.1 Discussion

During optimization studies of absorbance readings collected through MOREs, the tip-to-substrate distance was consecutively increased. It was observed that the absorption intensity reached a maximum value at 200 µm tip-to-substrate distance, decreased again from 200 to 350 µm, and reached a second maximum at 650 µm, where the signal is prominent, and noise could be minimized (Figure 5.3 a and b). This effect is thought to originate due to two aspects: A) A diverging effect of the light beam, and B) tradeoff effect between the loss of light-intensity due to the divergent effect and the Beer-Lambert law.

(A) The inverted excitation light beam has a spot size that is defined as

$$\left(\frac{Inverted\ Fiber\ Diameter}{Objective\ Magnification}\right) 1.8 \tag{A3.1}$$

In this instrumental setup, the number 1.8 is an optics constant of the SPECM (ELP-3) system. If the inverted fiber diameter is 400 µm, and the objective magnification equals 10x, then the focused beam spot size will be 72 µm in diameter, which is smaller than the fiber diameter of the MORE. It is thought that at any distance that is past the focus point, the light beam could become diverged. This could explain the evidence that once the distance is greater than 650 µm (Supplementary Scheme A3.1 B), the incident light power starts to decrease due too much diverged light or loss of light intensity collected at the MORE. In other words, the extreme situation shown in part C considers the light to be a "point source" that emits an unparalleled divergent light beam.

(B) The absorbance value measured in the Potmaster software is a Log-based unit-less value, and it follows the Beer-Lambert law (equation A3.2).

$$log_{10}\frac{I_o}{I} = A = \varepsilon cl \tag{A3.2}$$

where A is the absorbance, ε is the molar absorption coefficient ($M^{-1}cm^{-1}$), c is the molar concentration (M) and l is the optical path length (cm). In this experimental setup, the tip-to-substrate distance equals the optical path length l, which initially should be proportional to the absorbance value A. However, if the tip-to-substrate distance is too large, the light-diverging effect makes the incident light become weaker, so the absorbance value A stops following a linear relationship with the increasing optical path length. This behavior explains the maximum absorbance value seen at 200 µm tip-to-substrate distance. The behavior seen between the tip-to-substrate distances of 200 µm and 650 µm might be a tradeoff effect between the loss of light-intensity due to divergent effect and the Beer-Lambert law, where A is proportional to l. The experimental setup will be further engineered to minimize these effects on absorbance measurements. For the presented study, this behavior is not thought to be problematic, as long as the tip-to-substrate distance is optimized prior to photoelectrochemical studies.

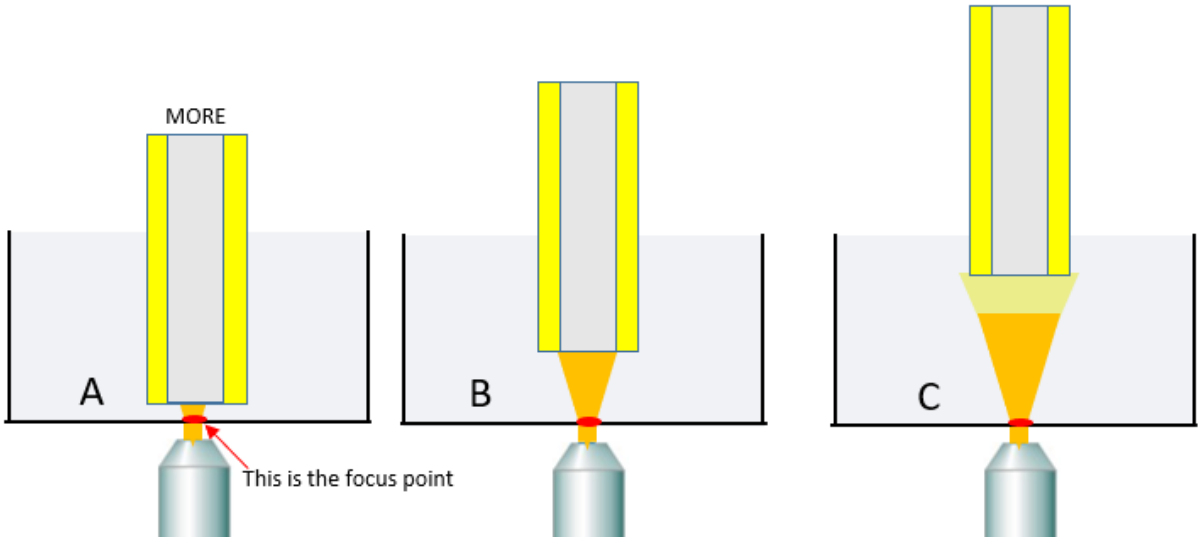

Scheme A3.1 *Diverging effect influencing the absorbance readings through MOREs between a tip-to-substrate distance of 200 µm and 650 µm.*